"Re-aeration of Rivers and Channels"

by

David Proctor, A.H.W.C.

Thesis presented for the Degree of Doctor of Philosophy of University of Edinburgh in the Faculty of Science.

October, 1968.

Frontispiece R. Almond

C O N T E N T S.

Chapter 1.

INTRODUCTION.

The impetus for this research programme came from a desire to throw light on the problem of reaeration in rivers and channels and if possible to suggest a way of increasing the rate of oxygen uptake of a given river. From the Water Pollution Research Laboratories it was learned that there was an unsatisfied need to predict accurately the mass transfer coefficient for atmospheric oxygen dissolving into flowing water. The W.P.R.L. have themselves put a great deal of effort into solving this problem between 1954 and 1964, as have many workers in the U.S.A. and elsewhere. No satisfactory solution has yet emerged, however.

(1.1) Justification for further research.

The practical problem of re-oxygenating polluted rivers has become of urgent importance in all highly industrialised countries. In Britain, as far back as 1949, it was becoming obvious that river pollution was going to become a by-product of the post-war industrial expansion. A case attracting wide attention in 1949 was that of the Thames Estuary, which during the hot, dry summer went anaerobic over a twenty to thirty mile stretch. Conditions were such that "a malodorous gas, hydrogen sulphide, was given off to such an extent as to occasion many complaints from the public, shipowners and manufacturers with premises on the bank of the estuary" (1). A similar state of pollution now exists in Lake Erie in North America.

The Thames situation was alleviated by drastically

controlling the quantity and quality of the effluent discharged into the river. This type of control can in the long term only have maximum effectiveness if accurate estimates can be made in advance of the permissible limits of the quality and quantity of effluent which may be discharged. The water demand from industry for process and cooling water, and from agriculture for irrigation, is increasing rapidly and as a consequence more and more water is drawn from rivers to meet the demand. Thus the diluting effect of rivers on the effluent released from treatment plants is constantly diminishing. Also the amount of effluent is itself continually increasing as a result of industrial expansion. It is therefore increasingly necessary to have means of estimating accurately how much effluent a given river may safely accommodate, so that the permissible limits of exploitation of a given river may be forecast and legislated for.

Before such estimates can be made, the two parts of the problem must be understood: the nature and estimation of the pollutants added to rivers; and the nature and quantitative effect of the factors governing the uptake of atmospheric oxygen by rivers.

(1.2) Pollutants and the law.

The words "polluted river" conjure up a mental picture of a foul coloured and evilsmelling stretch of flowing water, but this is only half the picture. A river can also be considered polluted when the natural animal-vegetable balance has been altered in favour of the vegetable side usually, by, say, fertiliser washed off fields. Most fertilisers are legally

considered as non-polluting matter. Such a "biologically" polluted river may eventually "die" from oxygen starvation within five to ten years from the time the balance was upset.

In Britain, the tests carried out on a sample of effluent are usually aimed at ascertaining the effects of the pollutant on a water-course rather than identifying all the components present. These tests are given in two booklets, one by H.M.S.O. (2) and the other by the Society for Analytical Chemistry (3).

The worst types of industrial plant for river pollution, and their pollutants, are in order (4)

(i)	Pulpmills	Suspended solids
		Carbohydrates
		Lignins
		Sulphates
(ii)	Smokeless Fuel Producers	Phenols
(iii)	Gasworks	Cyanides
		Thiocyanates
		Thiosulphates
		Ammonia
(iv)	Starch reduction in flour mills	Suspended Solids
		Carbohydrates
		Protein
(v)	Meat Canneries	Suspended solids
		Fats
		Protein

(vi)	Resin manufacturers	Phenols
		Formaldehyde
		Urea
(vii)	Distilleries	Suspended solids
		Carbohydrates
		Protein

All matter deposited in a river or stream will directly or indirectly cause deoxygenation of the water-course. Direct deoxygenation is self explanatory. Indirect deoxygenation occurs when the delicate natural plant-animal oxygen balance is upset by the promotion or elimination of one of the living species in the water-course.

There are basically five types of deposited matter that are classified as river pollutants. The first two cause deoxygenation directly, the third deoxygenates both directly and indirectly and the last two cause deoxygenation indirectly.

(i) Living micro-organism. These use up the dissolved oxygen whilst they are digesting part of the effluent.

(ii) Chemical reducing agents. Some substances can easily oxidise in water, giving rise to a chemical oxygen demand from the effluent.

(iii) Suspended solids. These usually interfere with the flow of the water and the plant and animal life of the river. Suspended solids can settle on the river bed as a blanket of "mud" which is lethal to animals and plants; or they may float on the surface, due to the evolution of gases or to natural buoyancy, thus cutting out the sunlight necessary for the plants

and animals.

(iv) Hot effluents. If the temperature of the effluent is too high, this will cause a much higher rate of oxygen usage by the micro-organisms and also speed up the chemical reduction reactions. Furthermore in streams which contain fish, a rise in temperature can be detrimental and can even result in fish mortality. On the other hand if the temperature rise is not too severe there will be an increase in the size and quantity of the plants and fish which will in turn cause an increase in the oxygen demand.

(v) Acid and alkalies. Any effluent which alters the pH of the stream outside the range 6 to 9 will cause the death of insects and fish.

It is interesting to note how the laws concerning the control of river pollution have changed over the years. The first Act of Parliament on Rivers was brought out in 1876; it prohibited the dumping of obnoxious matter into rivers and streams. This act gave little or no control over river pollution because no one was given the authority to enforce the act, and as a result it was left to the consciences of individual firms whether they did or did not pollute rivers. 1948 saw the next act on the subject. This was the "River Boards" Act, 1948, which set up River Purification Boards whose areas covered complete watersheds of rivers. Their duties were land drainage, prevention of pollution and improvement of fisheries, i.e. someone now had the power to impliment the 1876 Act. These Boards were no doubt set up in readiness for the 1951 "Rivers

(Prevention of Pollution) Act". This act gave River Boards the power to take to court and fine firms or individuals the sum of £50 for causing or knowingly permitting poisonous, noxious or polluting matter to enter a stream. This 1951 act was merely a warning shot to industry and town council alike to get their effluent disposal problems rectified in a manner acceptable to the River Boards. In 1960 the scope of the River Boards was enlarged to take in estuaries via the "Clean Rivers (Estuaries and Tidal Waters) Act".

In 1961 the controls were tightened by the "Rivers (Prevention of Pollution) Act", 1961, to include all discharges previously exempted by the 1951 act and that failure to comply with the new act could now result in a £100 fine.

Three things soon became apparent after 1961. Firstly many firms had ignored the "warning shot" of the 1951 act, and secondly there was no way of legally imposing restrictions on how much water could be extracted from a river. Thus if the abstractions kept on increasing at the rate of 1961-62 there was going to be reduced dilution for any particular discharge and so the effect of a polluted discharge will be more serious. Lastly, despite the stringent conditions laid down for firms by River Boards, rivers were still being seriously polluted at times.

In order to combat the defects in the 1961 act, a further "Rivers (Prevention of Pollution) Act" was passed in 1965 and eventually became law in February 1967. The main effect of this act was that firms could be shut down (and indeed have been)

until their effluent problems were corrected in accordance with the legal requirements, and/or the directors of the offending firm could be sent to jail. This last act caused some panic in certain quarters.

There have been some beneficial and unforseen effects of these acts. Firstly, there was a vast improvement during the early sixties in effluent plants, notably in the following spheres: oil recovery from drainage water (5); wool scour treatment (for Paton and Baldwins) (6); Activated Sludge and Aerator Plants (4,7,8); treatment of town sewage by mixing it with brine and electrolysing the solution (9) and the replacement of conventional filter beds by I.C.I. Plastics lightweight packing which has a very high surface area to volume ratio (10).

Secondly, there have been substantial changes in process materials. Due to the high cost of effluent treatment now required for the original process materials used in a particular process, it has been found cheaper in the long run to use a more expensive raw material e.g. (11)

(a) Hydrochloric acid is replacing sulphuric acid in ferrous metal pickling.

(b) Hydrogen peroxide is used in place of sodium hypochlorite or chlorine for cotton bleaching.

(c) A change in some of the ingredients used in detergents.

Thirdly, it has been found profitable to obtain useful by-products from effluents. Distilleries usually throw away into rivers the grain and maize residues from the fermentation tanks. D.C.L. at Cambus, Stirlingshire, now spray-dry this residue to

give a high quality animal food and pure water (10).

Lastly, the effluent treatment plant has often been found useful as a management tool. Where an effluent plant is installed and completely supervised, it is possible to monitor material losses from the works without the need for working with small differences of large numbers. It may be difficult to detect with certainty an avoidable loss of raw materials from a raw materials/product balance; effluent analysis will often show it up immediately (11).

Despite the 1965 act it is still possible for rivers to become polluted, as shown in the frontispiece. This picture was taken in November 1967, of the River Almond (Midlothian). In Chapter 7 it will be shown how pollution can still occur. Thus it is essential that a method for predicting the mass transfer coefficient for oxygen dissolving in water be found if the River Purification Boards are to do their work effectively and if public health hazards and eyesores are to be removed.

(1.3) Review of previous work on reaeration in rivers.

Previous researches were carried out by three groups, in Britain by W.P.R.L. (12,13,14,15,16,19) and in America by O'Connor and Dobbins (17) and Churchill et.al.(18) in the Tennessee Valley. These workers between them have investigated 19 rivers and channels whose widths, depths, velocities and mass transfer coefficients vary considerably. Unfortunately each group had its own way of expressing their findings. Since most of them have expressed their results in terms of a reaeration coefficient k_2, defined as:

$$\frac{\partial C_B}{\partial t} = k_2 (C_S - C_B) \qquad (1)$$

Where: C_B is the bulk concentration of the dissolved oxygen

C_S is the dissolved oxygen concentration at the free surface

t is time

rather than in terms of a mass transfer coefficient k_L, defined as:

$$\frac{\partial C_B}{\partial t} = \frac{k_L A}{V} (C_S - C_B) \qquad (2)$$

Where: A is the free surface area

V is the volume of liquid being aerated

and $k_L = k_2 d$ (13,17) (3)

where d is the liquid depth.

their results will be compared on this basis first of all.

All workers, bar one set of workers in Britain, postulate that the reaeration coefficient is a function of the depth and velocity, U . The functions obtained by various workers are summarised below:

$$k_2 = \frac{10.09\ U_{av}^{0.75}}{d^{1.75}} \qquad (4)$$ from all W.P.R.L. data (12,13,14, 15) by Olwens et.al. (16)

$$k_2 = \frac{9.41\ U_{av}^{0.67}}{d^{1.85}} \qquad (5)$$ from sources (12,13,16,18) by Owens et.al. (16)

$$k_2 = \frac{10.8\ U_{av}^{0.749}}{d^{1.613}} \qquad (6)$$ Owens et.al. own results (16)

$$k_2 = \frac{5.026\ U^{0.969}}{d^{1.673}} \qquad (7)$$ Churchill et.al own results (18)

$$k_2 = \frac{D_m^{0.5} U_{av}^{0.5}}{d^{1.5}} \qquad (8)$$ O'connor and Dobbins (17)

$$k_2 = \frac{14\, U_{av}^{0.8} (1 - e^{-30d})}{d^{2.1} (1 + 18w^{1.3})} \qquad (9)$$ from all W.P.R.L. data (19)

Where: D_m is the molecular diffusivity of oxygen in water

W is the river width

Equation (8) is obtained from an application of surface renewal theory; the others are empirical. It will be noticed that all the empirical equations are dimensionally incorrect. Equations (4) (5) (6) (7) (9) only hold for particular rivers. In order to make them applicable to other rivers they must be made dimensionally correct by the inclusion of variables. It must be pointed out that these empirical equations were obtained, from data in which there was a four to fivefold scatter (see figure (i)). The line extending from a hydraulic depth Reynold's Number Re_{HD}, of 3000 to 10^7 represents O'Connor and Dobbins' equation (8), since it can be manipulated into the dimensionless form:

$$\frac{k}{U_{av}} = \left(\frac{D_m \rho}{\mu}\right)^{0.5} \left(\frac{U_{av}\, d \rho}{\mu}\right)^{-0.5} \qquad (10)$$

where ρ is the density of water

μ is the viscosity of water.

Normally in open channel work the hydraulic depth d_{HD} is used in preference to the actual depth, d, where

$$d_{HD} = \frac{wd}{(2d + w)} \qquad (11)$$

*"the Reynolds number is based on the hydraulic depth. The Reynolds number in equation (10) can be considered as a hydraulic depth"

channel, although all values of $\frac{w}{d}$ greater than 10 give (to

$$k_2 = \frac{D_m^{0.5} U_{av}^{0.5}}{d^{1.5}} \qquad (8)$$ O'connor and Dobbins (17)

$$k_2 = \frac{14\, U_{av}^{0.8} (1 - e^{-30d})}{d^{2.1} (1 + 18w^{1.3})} \qquad (9)$$ from all W.P.R.L. data (19)

Where: D_m is the molecular diffusivity of oxygen in water

W is the river width

Equation (8) is obtained from an application of surface renewal theory; the others are empirical. It will be noticed that all the empirical equations are dimensionally incorrect. Equations (4) (5) (6) (7) (9) only hold for particular rivers. In order to make them applicable to other rivers they must be made dimensionally correct by the inclusion of variables. It must be pointed out that these empirical equations were obtained, from data in which there was a four to fivefold scatter (see figure (i)). The line extending from a hydraulic depth Reynold's Number Re_{HO}, of 3000 to 10^7 represents O'Connor and Dobbins' equation (8), since it can be manipulated into the dimensionless form:

$$\frac{k}{U_{av}} = \left(\frac{D_m \rho}{\mu}\right)^{0.5} \left(\frac{U_{av}\, d \rho}{\mu}\right)^{-0.5} \qquad (10)$$

where ρ is the density of water

μ is the viscosity of water.

Normally in open channel work the hydraulic depth d_{HD} is used in preference to the actual depth, d, where

$$d_{HD} = \frac{wd}{(2d + w)} \qquad (11)$$

(and w is the width of the channel)

Thus in this work* the Reynolds Number for an infinitely wide channel, although all values of $\frac{w}{d}$ greater than 10 give (to

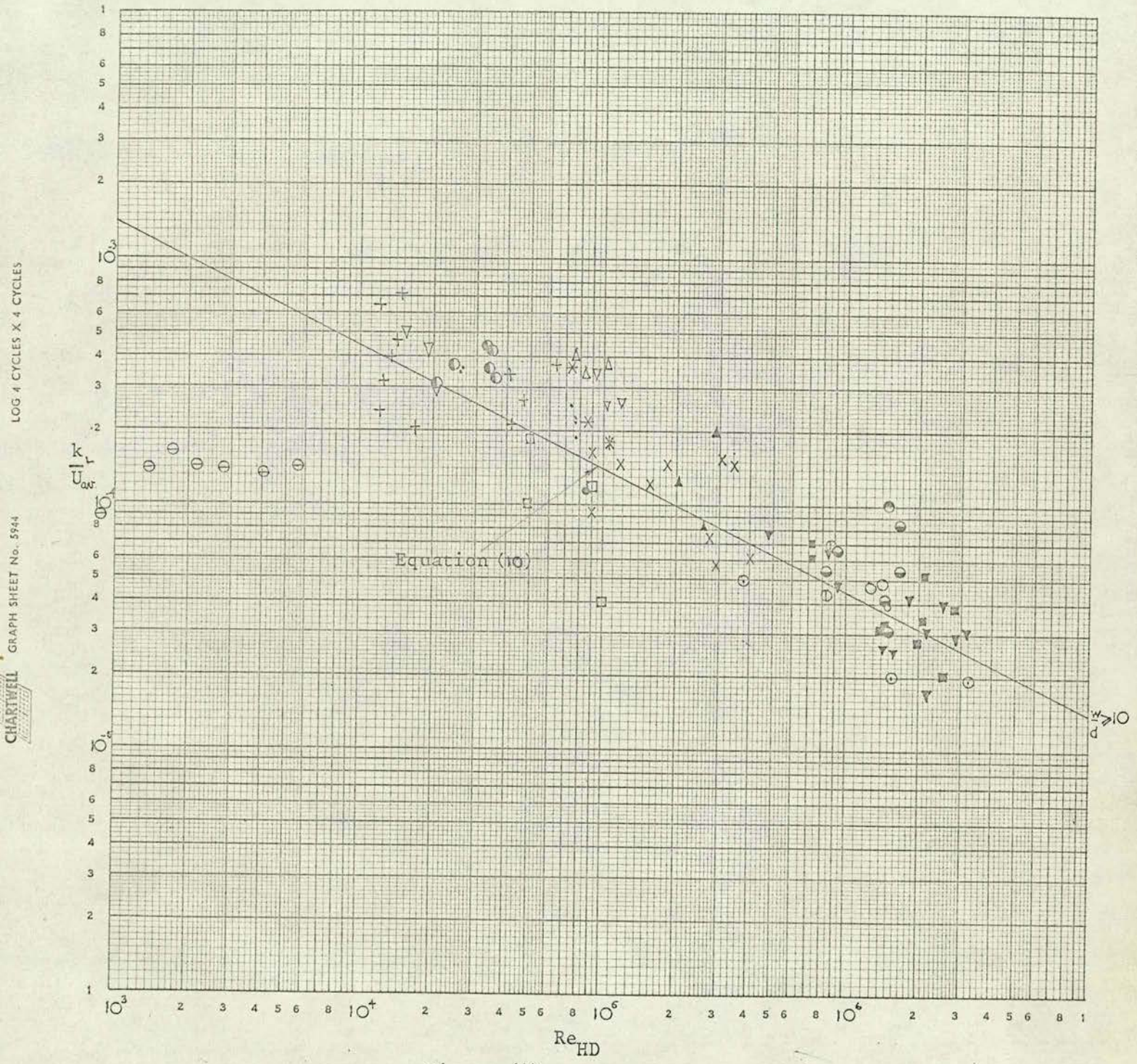
LOG 4 CYCLES X 4 CYCLES
CHARTWELL GRAPH SHEET No. 5944
$\frac{k_r}{U_{av}}$
Equation (10)
$d/r_p \geq 10$
Re_{HD}

Figure (i)

within 9%);

$$(Re_d)^{0.5} = (Re_{HD})^{0.5} \qquad (12)$$

From equation (10) the temperature correction for the mass transfer coefficient can be obtained, viz:

$$k_{LT} = k_{L20} \left(\frac{D_{mT}}{D_{m20}} \right)^{0.5} \qquad (13)$$

which gives the same temperature correction over the range 10 C to 30 C as the dimensionally incorrect equation of Streeter et.al.(20) viz:

$$k_{LT} = k_{L20} (1.016)^{T-20} \qquad (14)$$

Figure (i) was obtained by applying equation (13) to all the experimental results and then plotting $\frac{k_L}{\bar{U}_{av}}$ versus Re_{HD} and comparing the result with equation (10). The data used for the plot of figure (i) are contained in table (i) of Appendix VI. From figure (i) it is easily seen that equation (10), and hence equation (8), represents all the data in general but with an average scatter of the data of $\pm$ 200% about the line representing equation (10).

If the following variables alone are considered to affect the situation, it can be shown that the dimensionless groups involved are those of equation (10):

k_L	- mass transfer coefficient.	LT^{-1}
U_{av}	- average velocity of the river.	LT^{-1}
d_{HD}	- hydraulic depth of the river.	L
D_m	- Molecular diffusivity of oxygen in water.	L^2T^{-1}
μ	- viscosity of water.	$ML^{-1}T^{-1}$
ρ	- density of water.	ML^{-3}

Since there are 6 variables and 3 primary quantities there will

be 3 dimensionless groups relating the 6 variables. Thus from the Buckingham π Theorem:

$$\frac{k_L}{U_{av}} = \phi\left(\frac{U_{av}\, d_{HD}\, \rho}{\mu}, \frac{\mu}{D\rho}\right) \qquad (15)$$

If this is expressed as a power function of the π s, then:

$$\frac{k_L}{U_{av}} = A_1\left(\frac{U_{av}\, d_{HD}\, \rho}{\mu}\right)^{\beta}\left(\frac{D\rho}{\mu}\right)^{\alpha} \qquad (16)$$

From figure (i) (β) is equal to - 0.5. The value of α in equation (16) has yet to be ascertained. O'Connor and Dobbins have taken it as 0.5 since their equation was based on the surface renewal theory of Danckwerts.

(1.4) Explanation of why the exponent is 0.5 in the term involving the molecular diffusivity.

It has been tacitly assumed that the mass transfer coefficient depends on the molecular diffusivity raised to the power 0.5. By considering some of the models for mass transfer, in order of development, the exponent 0.5 can be seen to be most probably correct:

(a) Lewis - Whitman (21) film theory in which

$$k_L = \frac{D_M}{\delta} \qquad (17)$$

where δ is the fictive film thickness and is a function of D

(b) Hignie's penetration theory (22):

$$k_L \propto \sqrt{\frac{D_M}{t}} \qquad (18)$$

(c) Danckwerts' renewal theory (23):

$$k_L \propto \sqrt{D_M s} \qquad (19)$$

where s is the rate of surface renewal

(d) O'Connor and Dobbins (17) variation on Danckwerts' renewal theory with s replaced by ratio of the rootmean

square local velocity, $\sqrt{\overline{v^2}}$, to the scale of turbulence L (defined as (24):

$$L = \sqrt{\overline{v^2}} \int_0^\infty R(\theta)\, d\theta \qquad (20)$$

where $R(\theta)$ is the Lagrangian correlation coefficient and θ is the time scale

i.e. $$k_L \propto \left(\frac{D_m \sqrt{\overline{v^2}}}{L}\right)^{0.5} \qquad (21)$$

(e) Toor and Marchello's Film-penetration model (25) in which $k \propto D_m$ to $D_m^{0.5}$ depending on the Schmidt number.

(f) Harriot's random eddy modification of the penetration theory (26) which amounts to a restatement of Toor and Marchello's work except that the upper limit of the exponent on the molecular diffusivity is reduced from 1.0 to 0.9, and

(g) King's general model (27) in which

$$k_L \propto D_m^{1-\frac{1}{n}}$$

From the work of Krenkel and Orlob (28), King finds that for rivers and channels n is 2

$$\text{i.e. } k_L \propto D_m^{0.5} \qquad (22)$$

All except (a) (e) and (f) indicate that the exponent on the molecular diffusivity should be 0.5, and (e) and (f) include 0.5 in their range of exponent values. It would appear that the model of Toor and Marchello covers all the other models. From the figure in their paper in which they plot $\frac{k_L}{\bar{U}_{av}}$ against the Schmidt number, $\frac{k_L}{\bar{U}_{av}}$ is proportional to $\left(\frac{\mu}{\rho D_m}\right)^{0.5}$ at Schmidt numbers higher than 300. In the case of oxygen dissolving in water the Schmidt number is about 5000 i.e.:

$$\frac{k_L}{\bar{U}_{av}} \propto \left(\rho \frac{D_m}{\mu}\right)^{0.5}$$

for the oxygen-water system. Hence exponent 0.5 on the Schmidt

number in equation (10) is probably correct.

(1.5) What causes the scatter in figure (i)?

There appears to be five possible explanations:

(i) Errors in measuring the oxygen concentration in water.

(ii) Error in measuring the depth.

(iii) Error in measuring the velocity.

(iv) Omission of some chemical variable causing alteration in the properties of the water, e.g. due to dissolved materials.

(v) Omission of some physical variable not previously considered.

(i) The method used to measure the oxygen concentration was some form of the Winkler method, except in the case of Owens et.al. (16) who used a Mackereth Electrode system which measured the oxygen concentration directly without the need for taking samples. This system measured the dissolved oxygen concentration to within $\pm$ 0.1% although some cell systems will only measure the dissolved oxygen concentration to within $\pm$ 2% of the saturated dissolved oxygen concentration.

A D.S.I.R. report (29) has shown that errors of the order of 0.14 to 0.26 ppm in the dissolved oxygen concentration can be introduced by using modified Winkler Methods, though the modifications are designed to lower the inherent errors. On top of these errors there is a small sampling error caused by reaeration taking place as the sample is collected. The total error in the measured dissolved oxygen concentration is of the order of + 3% of the saturated dissolved oxygen concentration. The calculation of the mass transfer coefficient involves the

concentration in a term of the form $\ln \left(\frac{C_s - C_{s1}}{C_s - C_{s2}}\right)$,

where C_{s1} and C_{s2} are the measured bulk fluid dissolved oxygen concentrations at stations 1 and 2. The net error in this term is going to be between about + 3% and + 36% (mainly around + 14%) i.e. not enough to account for the + 200% variation in the data. The data from Owens et.al., whose maximum error in the dissolved oxygen concentration was $\pm$ 2%, shows the same scatter as that from the other workers, and thus it is not dissolved oxygen concentration measurement errors which are responsible for the scatter.

(ii) and (iii) can be taken together. An error of $\pm$ 100% in either the depth or the velocity or both is not capable of producing the observed scatter. At any rate, it is doubtful if the errors in these quantities would be greater than $\pm$ 10%.

(iv) Most of the British work was carried out in rivers free from pollution. In order to deoxygenate the rivers, sodium sulphite plus cuppric or cobalt salt as a catalyst, was added to the rivers. Yagi and Inoue (30) have suggested that the solubility of oxygen in saturated sodium sulphite-sulphate solution is about 30% less than it is in water, and that the molecular diffusivity of oxygen in sodium sulphite-sulphate solution increases slightly with increase in sulphite concentration. In the case of rivers the solubility of oxygen in the "water" is not going to be lowered by as much as 30% since there will be very dilute concentrations of sodium sulphite-sulphate in the river; e.g. in reference (13) a strong aqueous solution of sodium sulphite was used which was diluted a thousand fold by

the river. Even if it were 30% lower the error in the mass transfer coefficient would be at the most - 60% i.e. not enough to account for the - 200% part of the scatter.

In the case of a polluted river there will be surfactants present. Hickmann et.al. (31,32,33) have found that there are minute traces of surfactants in all but the most extraordinarily carefully prepared water. The effect of surfactants at a gas-liquid interface, a highly debatable subject at present, is reported to cause a damping of any waves present and to increase the interfacial resistance (34,35,36,37,38) which is appreciable under "normal" conditions in the case of absorption of oxygen by water (39). Duda et.al. (40,41) on the other hand show that the addition of surfactants to flowing systems can cause changes in the hydrodynamics resulting in a decrease in the mass transfer rate which has sometimes been incorrectly attributed to changes in the interfacial resistances.

Since the magnitude of these effects is unknown for rivers an idea of how they affect the mass transfer rate can be obtained by comparing unpolluted rivers with polluted ones. The Ivel and Lark rivers were known to be polluted and they show the same degree of scatter of the data as do the other rivers.

According to prevailing theories on the effects of surfactants on mass transfer, these could only cause a lowering of the mass transfer coefficient. The same is true of the influence of agents lowering the oxygen solubility. Hence these would not explain why some rivers show anomalously high reaeration rates. Furthermore, the effects of solubility

changes and surfactants can be ruled out in the work of Churchill et.al. (18). They were able to abstract naturally deoxygenated water from reservoirs for their work. (It is known that water in reservoirs exists in strata according to its oxygen content and it was a deoxygenated stratum that Churchill et.al. were able to tap). Comparing the scatter from their results with those of the Ohio and British rivers, it will be seen that there is no difference in the amount of scatter between the three groups.

This only leaves possibility (5) to explain the scatter. The most likely cause is the omission of a parameter describing the turbulence e.g. the intensity or scale of turbulence or the eddy diffusivity. Brow et.al. (42) have shown that the mass transfer coefficient of water into air from a porous sphere can be increased by increasing the upstream intensity of the turbulence of the air flowing past the sphere. On the other hand, in the case of smooth pipes there is evidence (43) that upstream turbulence promoters have little in influence on downstream transfer, the flow soon reverting to an equilibrium turbulence level determined by the flow Reynolds number. This seems to be generally true for flows in closed conduits in the absence of a pressure gradient. But of course the case may well be different for flows with a free surface.

As it is the local motions of the fluid in the direction perpendicular to the free surface (hereafter called y-direction) which mainly determine the rate at which reaeration takes place then attention need only be paid to the magnitude of quantities,

such as turbulent intensity, scale of turbulence and eddy diffusivity, in the y-direction, without worrying whether the turbulence is isotropic or non-isotropic. Evidence suggests that it is only in deep broad rivers that the turbulence at the free surface is isotropic (17). In the case of rivers the intensity and scale of turbulence and eddy diffusivity would have to be measured very close to the free surface, since it is the flow conditions in this area that are going to determine the mass transfer rates.

The intensity of turbulence in the y-direction is given by the ratio $\frac{\sqrt{\overline{v^2}}}{\bar{U}}$, where $\sqrt{\overline{v^2}}$ is the root mean square velocity in the transverse direction and U is the overall velocity at the point at which $\sqrt{\overline{v^2}}$ is measured. The scale of turbulence, L, is defined in equation (22). The eddy diffusivity, D_E, is the product of the root mean square velocity mentioned above and the scale of turbulence.

The effect of wind on water has also to be considered. There will exist different types of waves depending on the gas flow rate past the water surface (44). These initial experiments carried out by Hanratty and Engen (44) were with thin liquid films, but the results have been shown to hold for deeper liquids (45,46,47,48,49,50,51,52). The conditions at the liquid surface can be classified into five distinct types viz:

(a) smooth surface

(b) two-dimensional waves

(c) squalls

(d) roll waves, and

(e) dispersed flow.

Plate I R. Almond

Cohen and Hanratty (45) and Miles (52) have shown that two-dimensional waves do not occur in deep liquids until the gas is flowing at a fairly high velocity, hence the reason that wind generated waves are not usually seen on rivers except under unusual conditions and then the waves are two-dimensional. Thus there is little likelihood that wind generated waves cause the anomalies in the measured reaeration coefficients.

There are of course other causes of surface waves in rivers e.g. obstacles in rivers such as tree trunks, boulders (see plate (i)) and an undulating bottom or a hydraulic jump. Boyd and Marchello (53) have carried out experiments involving the absorption of carbon dioxide into water under the influence of surface waves, generated by the reciprocating movement of a blade extending from the surface of the liquid to the bottom and find that the mass transfer rate increases when waves are present. Similarly, gravity roll waves in wetted wall columns may increase the mass transfer rate by some 200% (54,55,56,57). The increase in interfacial area only accounts for 10% of this 200% rise.

Waves, if they are present, can at any rate be taken into account by the y-direction intensity of turbulence term since the waves will predominantly affect the local variations in the velocity perpendicular to the free surface. Thus it appears that the possible omission is the transverse turbulent intensity term, which in itself is a dimensionless term. Hence the correlation which has to be established will be of the form

$$\frac{k_L}{\bar{U}_{aw}} = A_1 \left(\frac{D_w \rho}{\mu}\right)^{0.5} \left(\frac{U_{aw}\, d_{H_2O}\, \rho}{\mu}\right)^{-0.5} \left(\frac{\sqrt{\overline{v^2}}}{\bar{U}}\right)_{ss}^{\alpha} \qquad (23)$$

where ss refers to the sub surface layers of luid.

(1.5) Choice of method for studying reaeration in rivers and channels.

Essentially what is required is a system in which the two dimensionless groups $\left(\frac{U_{av} d_{HD} \rho}{\mu}\right)$ and $\left(\frac{\sqrt{\tau}}{U}\right)$ can be varied over a sufficient range of values of each group to yield the values of A and α in equation (23). It appeared that a suitably chosen channel to which turbulence promoters or suppressors could be fitted would provide the answer.

For this work a channel was designed and constructed to cover a range of Reynolds numbers (based on the hydraulic depth) from 3000 to 1,000,000 and a twenty fold variation in the intensity of turbulence. In the next chapter an outline is given of some of the problems which became apparent when the channel was designed.

Chapter 2.

INTRODUCTION TO THIS WORK.

(2.1) Restrictions imposed on the channel design.

The major restriction on the channel design was the size in relation to the available laboratory space. Due to the shortage of laboratory space the system was built in the form of a closed loop.

The closed loop apparatus had to be made compact to fit into the available space. When deciding what the minimum length the open channel should be it was necessary to consider what measurements were going to be made. In this connection it was perceived that the accuracy of measuring the bulk liquid dissolved oxygen concentration, C_B, at the entrance and exit of the open channel in some situations was going to determine the accuracy of the mass transfer coefficient measurement. The minimum length for the maximum permissible error in the mass transfer coefficient was estimated to be about 1 foot.

The open channel plus an entrance and exit nozzle together made up a straight section 3.5 feet long. Each nozzle was just over a foot long giving an open channel of 13.25 inches. The outer radius of the inlet and outlet bends to the straight section was 1 foot.

(2.2) Materials of construction.

All the pipework was in rigid P.V.C. The inlet and outlet bends and squinches were made from 14G copper sheet. The choice of copper was made primarily on the grounds that it would not introduce corrosion contamincuits into the water, and

secondly the ease of manufacturing the bends and squinches out of copper sheet.

Originally it was decided to make the open channel section out of P.V.C. and perspex sheets welded together, but this was overruled on the grounds of cost. The alternative suggestion was to build it out of marine ply wood (58) coated with an Epoxy resin, with perspex windows.

When the wooden channel was tested to water tightness, it very soon became apparent that there were major leaks in the structure. The cause of the leaks was eventually traced; the Epoxy resin was found to permeable to water probably due to the fact that the resin had been sprayed on to the wood. Once the water got inside the marine ply it flowed along the very open pore structure, eventually coming out at the end grain in the flanges and side walls.

Further attempts by the makers of the channel to solve the seepage problem proved fruitless. The problem was finally solved by using polyurethane paint, which is impervious to water. Advantages of this paint are the hard smooth finish, which can be obtained very easily, and because it is chip-proof it can be machined where necessary. The paints used were Furinglass P.V.15 exterior grade, for the inside walls and narrowing sections and Kingston-Diamond polyurethane paint for the outside walls.

In the light of present experience gained in this work, future work should be carried out in channels made from welded P.V.C. and perspex or copper sheet.

(2.3) Entrance and exit problems posed by the closed loop system.

If the water in the supply duct were abruptly caused to enter an open channel, there would be an appreciable lag before the velocity profile in the open section attained that characteristic of open channel flow. This is a highly undesirable situation in this work since such a short open channel is being used. Furthermore, this changing velocity profile pattern would have to be taken into account when calculating the mass transfer coefficient, as was done by Fortesque (59,60). These complications can be eliminated by designing a nozzle which will produce a reasonably close approximation to the velocity profile normally obtained far from the entrance of a uniform open channel at the entrance to the open section from some known profile in the duct.

At the exit end of the open channel there was a different problem altogether. Here the gas phase has to be separated from the liquid phase, without any entrainment of the gas nor must the means of separation affect the open channel velocity upstream of the separating device. Initially a suitably inclined piece of material was tried, but this caused instabilities in the surface layers of the liquid in the open channel. The flat plate had therefore to be discarded in favour of a two dimensional nozzle, similar to the entrance nozzle. The design and manufacture of these nozzles is described in Appendix I.

(2.4) Measurement of the local turbulence properties of the stream.

As pointed out in Section 1.5, it appeared probable at the outset that the mass transfer rate is affected by local stream turbulence.

There are two ways of measuring the local hydrodynamic properties of a flowing liquid which seemed suitable in this case. Oneis to use a hot film wedge, similar to the hot wire anemometer used for gases, and the other method is to observe, by means of photography, foreign matter injected or suspended in the flowing liquid.

Each method has its disadvantages. In the case of the hot film wedge there are two. Firstly, the wedge can be fouled up by deposits from the liquid; secondly the presence of the wedge and its holder will alter the hydrodynamics of the situation. In the technique of observing foreign particles suspended in the liquid the disadvantages are, firstly that the record of their progress through the liquid may not be representative of the motion of the liquid itself (61,62,63,64,65,66,67,68,69), and secondly, there may be a problem in disposing of the foreign matter.

Both methods are very laborious. The hot film wedge has the limitation that each measurement gives information about a very limited region of the flow. Exploring the characteristics of even a small region, which is all that would be required in this work, can be a lengthy business. The time in the hot film wedge method is taken up with locating the wedge at each station and recording the data. On the other hand, with the cine film method of recording the motion of foreign particles in a liquid,

the data for the whole region is recorded instantaneously and the time is consumed extracting the data from the film record. The second method was chosen since all the disadvantages can be eliminated by the suitable choice of foreign matter.

Originally it was intended to use a fine stream of nitrogen bubbles as the foreign matter. To do this required the production of very small nitrogen bubbles so that the buoyancy effects of the bubble would be negligible compared with the frictional effects. Unfortunately it proved impossible to construct a nozzle giving a rapid stream of sufficiently small bubbles with the gas pressure available. Moreover, fine nozzles easily became blocked with liquid.

It was therefore decided to use a dark water soluble liquid. If this "dye" has the same density as water, it will move as if it were part of the water. Kalinske and Pien (70) used a similar technique but employed immiscible liquids having the same density as water viz. dark coloured mixtures of n - but yl phthalate and benzene, and also carbontetrachloride and benzene. The mixture used in this work was a solution of pyrogallolic acid, sodium carbonate, distilled water and methanol, exposed to the air to darken it.

By examining a cine film record of a "dye" trace frame by frame values can be obtained for the overall velocity; and parallel to the free surface and channel walls; and the scale of turbulence for a given depth. Three corrections were applied to the cine film records. These were a parallax correction, velocity distortion correction and a "dye" extinction correction.

These are discussed in Chapter 4.

(2.5) Gases which can be used in this work.

The choice of gas used depends on the ease of measuring the dissolved concentration of the gas in water or its rate of absorption. For many reasons it seemed desirable to consider only methods of analysis such that no liquid need be removed from the system.

Three gases appeared potentially suitable for this work. These were oxygen, 1,3 - butadiene and carbondioxide. Due to the fact that no liquid could be removed from the system the dissolved polarographic or electrochemical cell technique was chosen. An electrochemical cell was developed for this work because the commercially available cells were too large and velocity sensitive, and had long response times.

In the case of 1,3 - butadiene use may be made of the fact that this gas absorbs ultra violet light. The degree of absorption depends on the concentration of dissolved 1,3 - butadiene in water. Thus, by traversing the channel with a collimated beam from a stabilised ultra violet light source and measuring the intensity of the transmitted light by means of a suitable detector, the concentration of 1,3 - butadiene averaged across the channel width may be found. This method has the added advantage that there are no probes intruding into the liquid, and therefore enables measurements to be made very close to the free surface.

Carbon dioxide absorption measurements are usually made in a system in which the gas is in contact with an appreciable area

of liquid with the aid of a soap film meter or a pressure sensing device such as a micromanometer to measure the total amount absorbed. Such methods only give overall mass transfer coefficients. For local coefficients, the dissolved concentrations in water would have to be measured by some sensitive pH meter or conductivity cell.

In this work it was intended to use the gases oxygen and 1,3 -butadiene. Oxygen was used first of all so that the results obtained could be compared directly with those obtained from rivers before trying to compare results obtained from 1,3 - butadiene experiments. Unfortunately no time was available for experiments with 1,3 - butadiene.

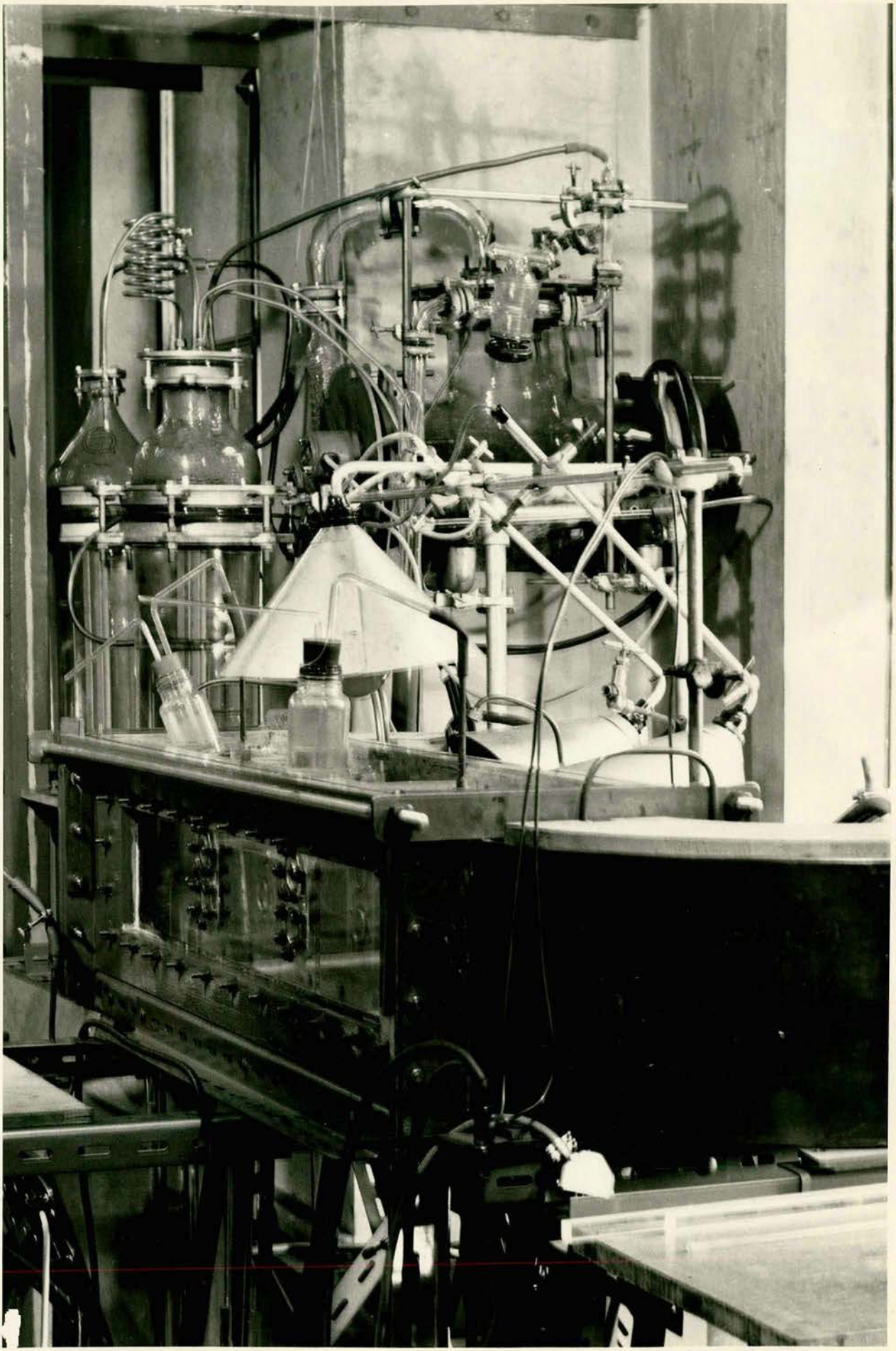

Chapter 3.

APPARATUS AND EXPERIMENTAL TECHNIQUE.

(3.1) General description of the apparatus.

The pump used was a 200 gal/min Harland Monoglide SNB4, located at ground level. 4 inch diameter P.V.C. pipes connected the pump with the channel on an upper floor. It was necessary to have the pump at least 7 feet below the free surface in the open channel. This was so that no release of dissolved gases from the water would occur in the pump.

The pipework terminated at the top in two 90° elbows. To these elbows were attached copper squinches whose shape varied from circular (4 inches diameter) to the rectangular section (6 inches by 8 inches) of the experimental duct within an 8 inch length. A copper cooling coil, composed of 10 feet of 0.25 inches o.d. tubing, was housed in the squinch attached to the outlet bend from the open channel. Between the two squinches and the open channel section were the semi-circular inlet and outlet copper bends. The dimensions of the supporting frame and apparatus are given in figures (ii) and (iii) and plate (ii) gives a general impression of the upper floor. The dimensions of part of the open section are given in figure (iv).

The brass blocks in figure (iv) served as locating stops for the perspex windows and narrowing sections which were fixed to the walls. The perspex windows were retained against the walls of the channel and the narrowing section by O.B.A. studs and nuts. Figure (v) shows how the stud was located in the perspex window. Each O.B.A. stud was set into the perspex with

Figure (ii) Supporting framework

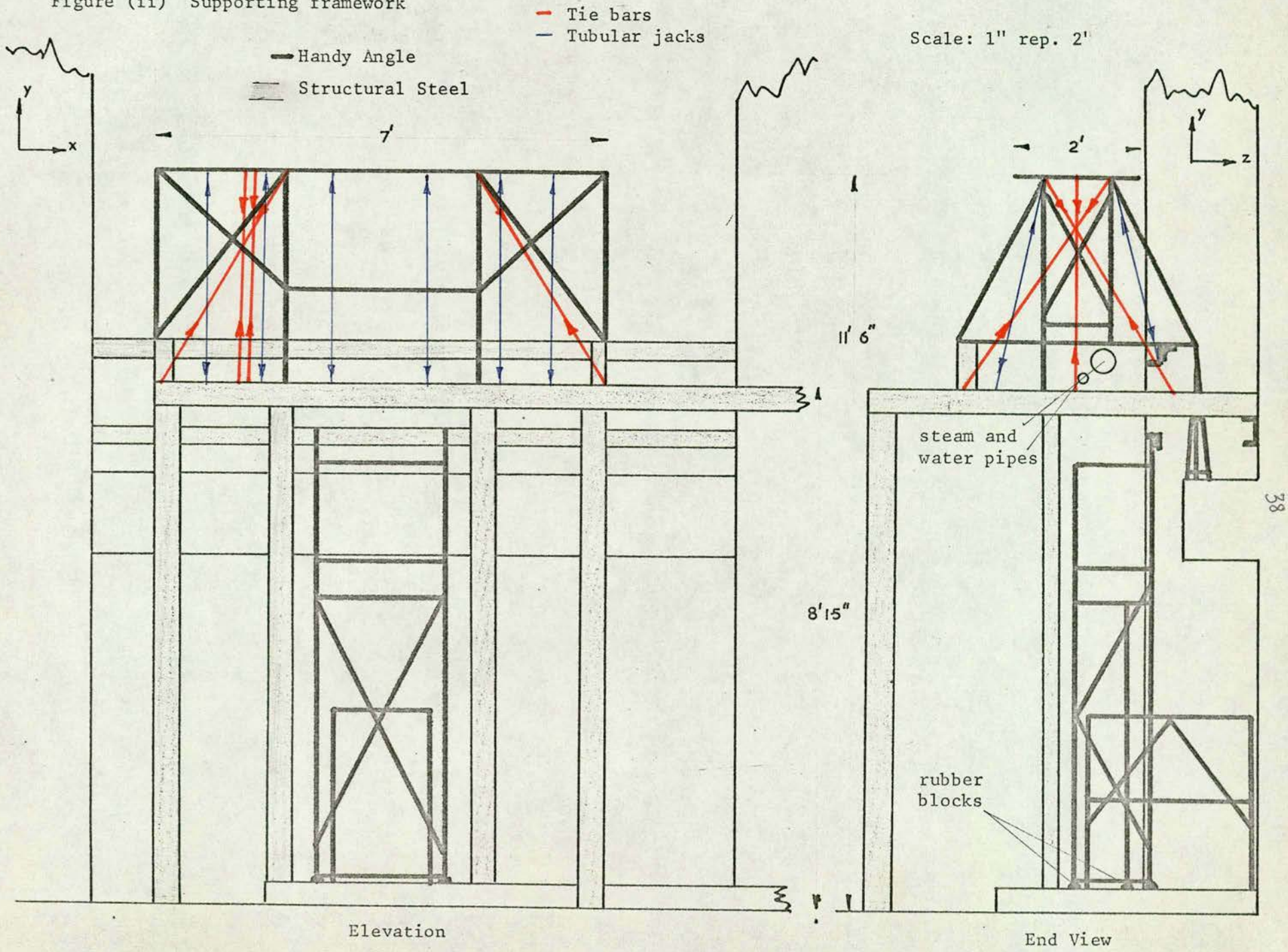

Figure (iii) Apparatus

Scale: 1" rep. 2'

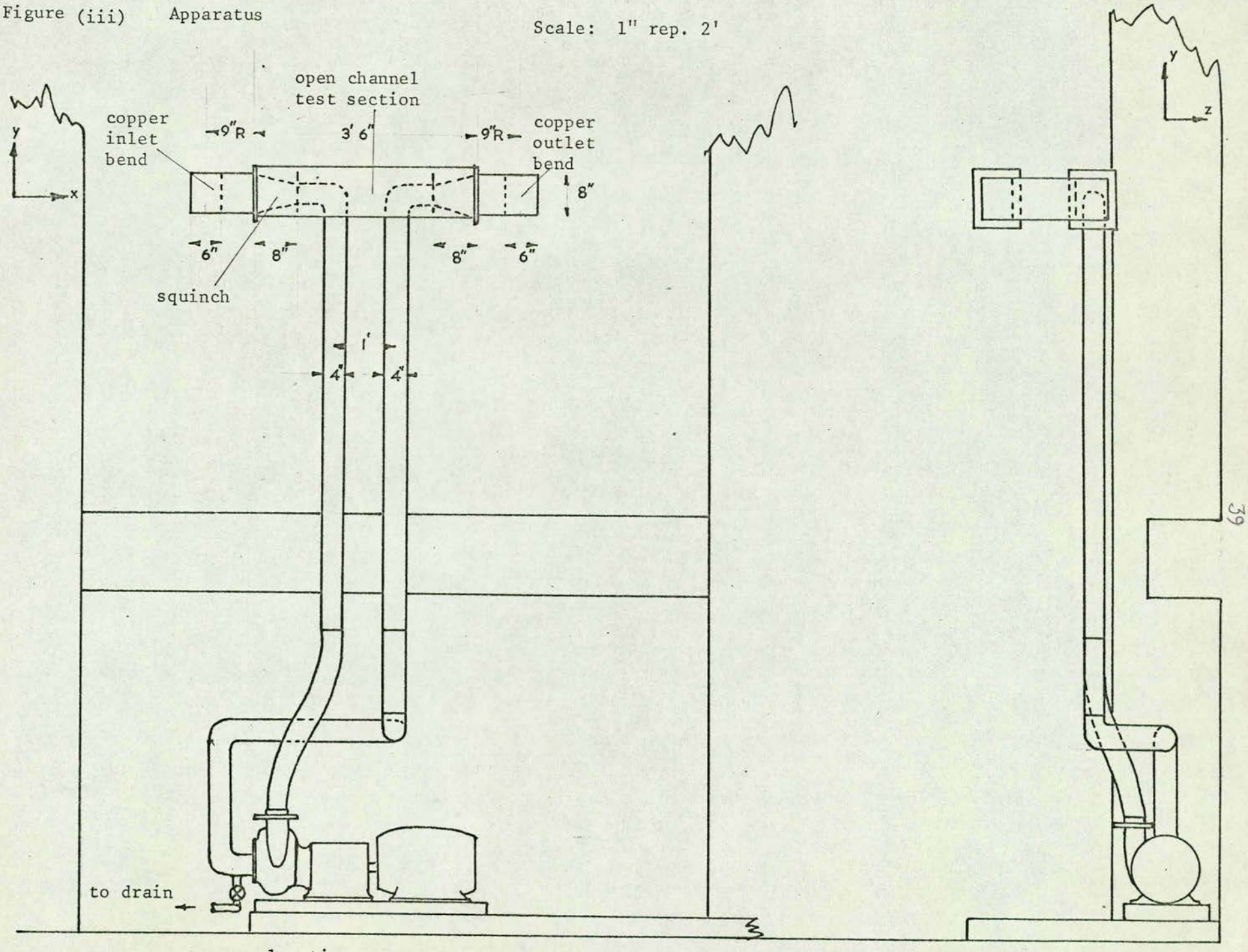

elevation

end view

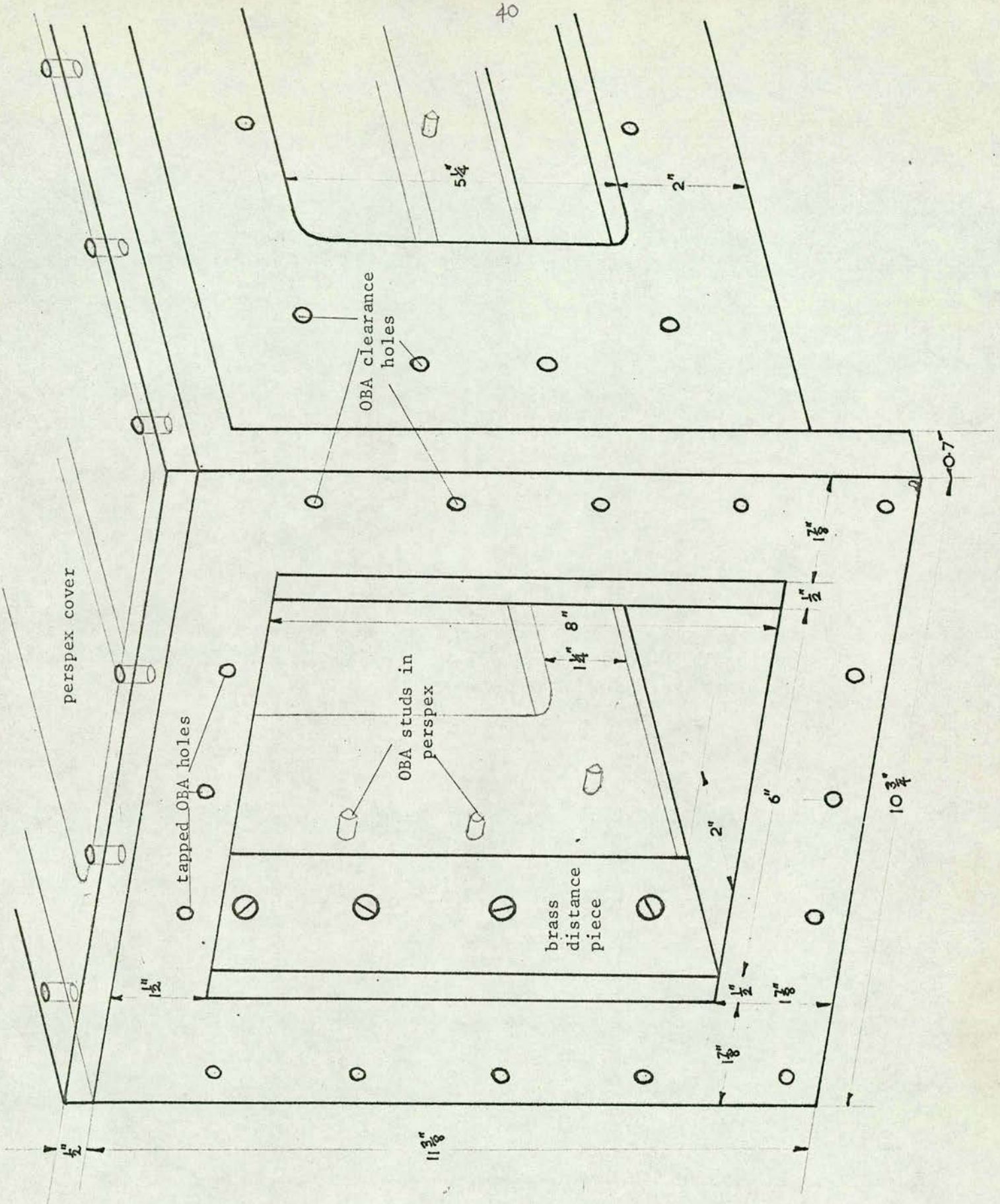

Figure (iv) Open channel test section Scale: 1" rep. 2"

Loctite 625. To ensure that the O.B.A. studs did not strip the perspex threads when the external nuts were being tightened up, the stud was first of all screwed fully into the blind hole in the perspex window and then slackened off one quarter of a turn. Finally the stud was locked in position with an O.B.A. nut.

Between the outer wall and the perspex window was a petrol resistant paper gasket (71). In the case of the narrowing sections 0.125 inches diameter neoprene rubber O-ring cord was used as the gasket. The choice of these two sealing methods was purely one of convenience when the apparatus was being assembled or dismantled.

At the other joins in the apparatus, neoprene rubber sheet was used as the gasket between the pump inlet and outlet and the P.V.C. pipes; 0.25 inches diameter neoprene rubber O-ring cord at the P.V.C. pipe - squinch joints; and between the squinch-bends - channel joints the gasket was a composition rubber/cork sheet (71).

(3.2) Fittings of the open channel section.

(a) The two nozzles. The first nozzles were made from paraffin wax but when these nozzles were tried out, air was found to be leaking into the region below the nozzles. Examination of the wax showed it to be porous. Changing over to perspex nozzles cured the air leak.

The design and manufacture of these nozzles is described in Appendix I. The outlet nozzle was set a few thou lower than the inlet nozzle to allow for the hydraulic gradient in the open channel. A vent was made on the inlet nozzle to remove trapped

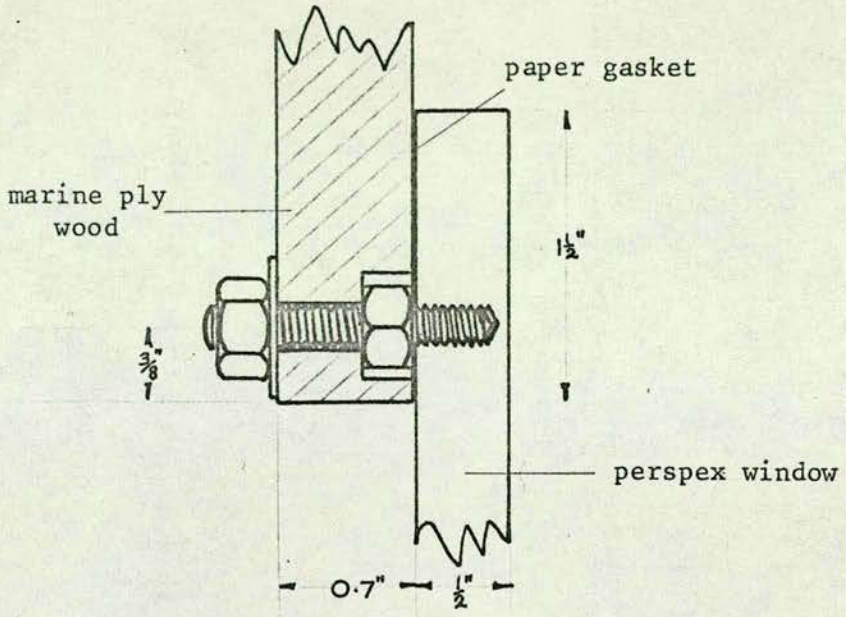

Figure (v) O.B.A. stud fixture

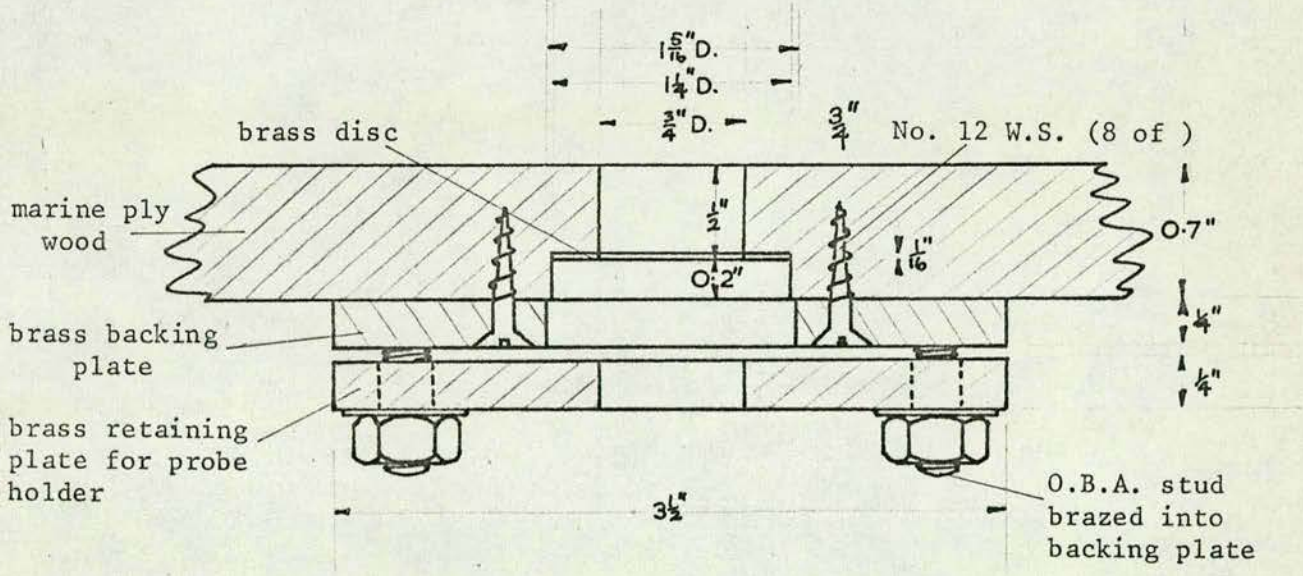

Figure (vi) Fixture for probe holders in channel bottom

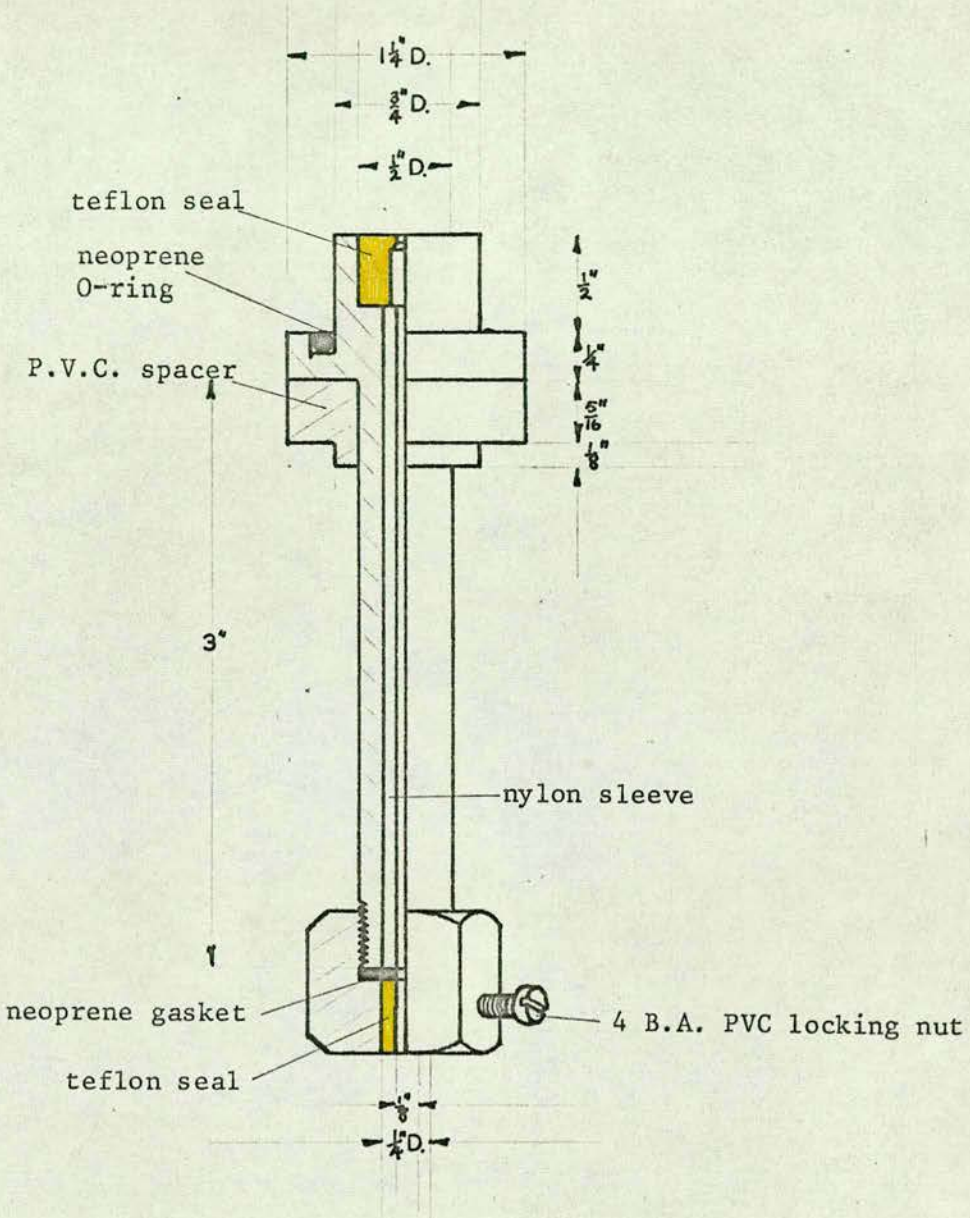

Figure (vii) Probe holder

air bubbles pushed out of the honeycomb section, at the inlet nozzle entrance, by the moving liquid. The exit nozzle had a similar vent. The seal for these vents was a water trap contained in a small bottle above the nozzles.

(b) Probe holders. Along the bottom of the channel were six suitably placed half inch diameter holes. These were to accommodate the probe holders for the three "dye" injector tubes, pitot tube and two oxygen analysing cell support tubes. Figure (vi) indicates how the holders were retained in position. Because the channel bottom was made from marine plywood it was impossible to machine a smooth recess for the holder's O-ring to seal against. A thin brass disc was therefore stuck onto the bare wood with Araldite and then finally sealed in with a coat of polyurethane paint thus providing a perfect surface for the O-ring.

The internal sealing of the holders is shown in figure (vii) and partly in plate (iii). Figure (vii) is complementary to plate (iv) indicating also how the two oxygen analysing cell holders were kept electrically separate from one another. Appendix III explains the reason why the insulation was necessary.

(c) The probes. All the probes were basically made from 0.1275 inches diameter stainless steel tubing. In the case of the "Dye" injector tubes, the stainless steel tube had a 9 inch length of stainless steel hypodermic tubing brazed on. The internal diameter was 20.5 thou. One of these injector tubes can be seen in plate (iii). The pitot tube was made in

Plate III

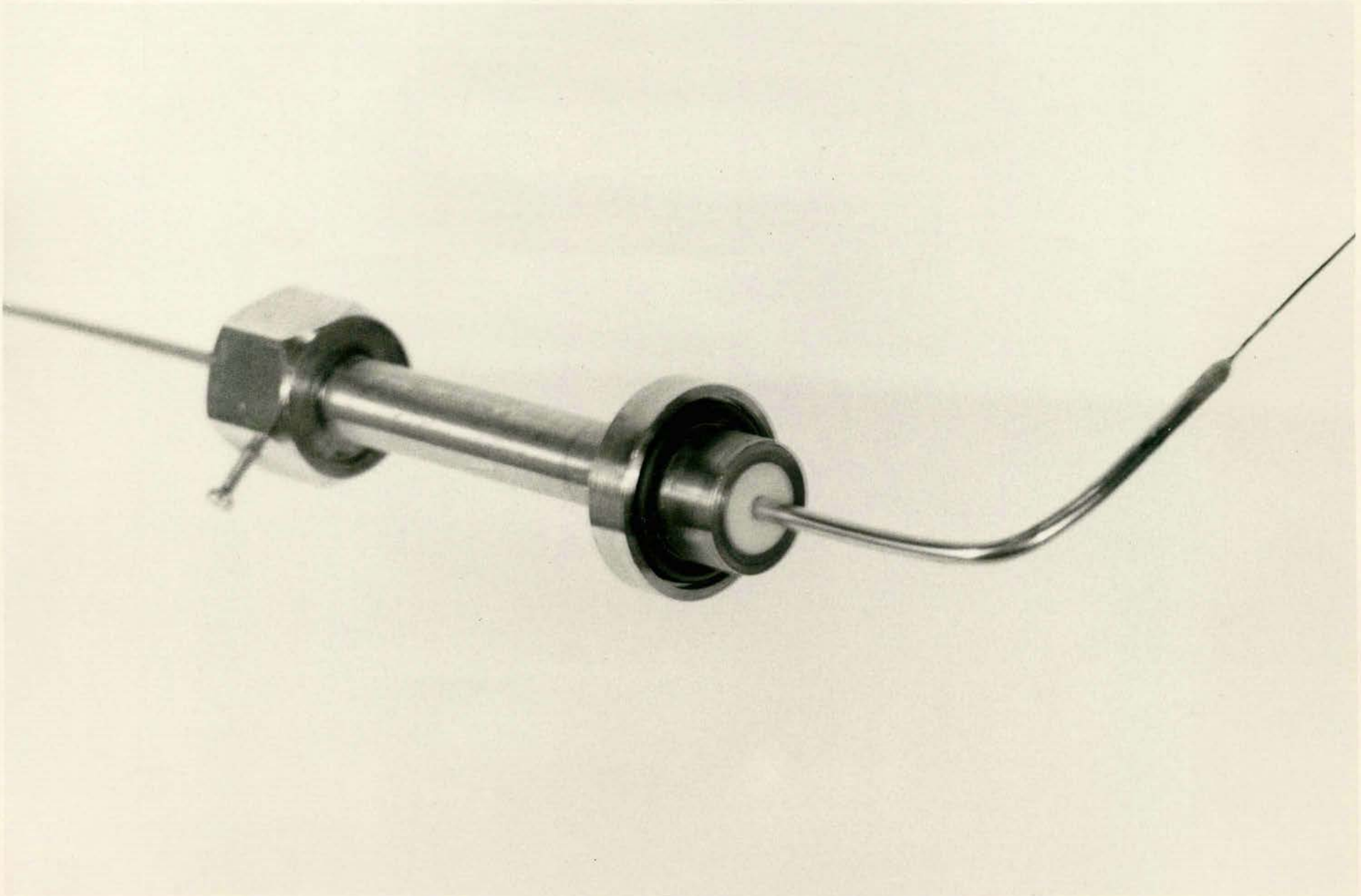

Plate IV

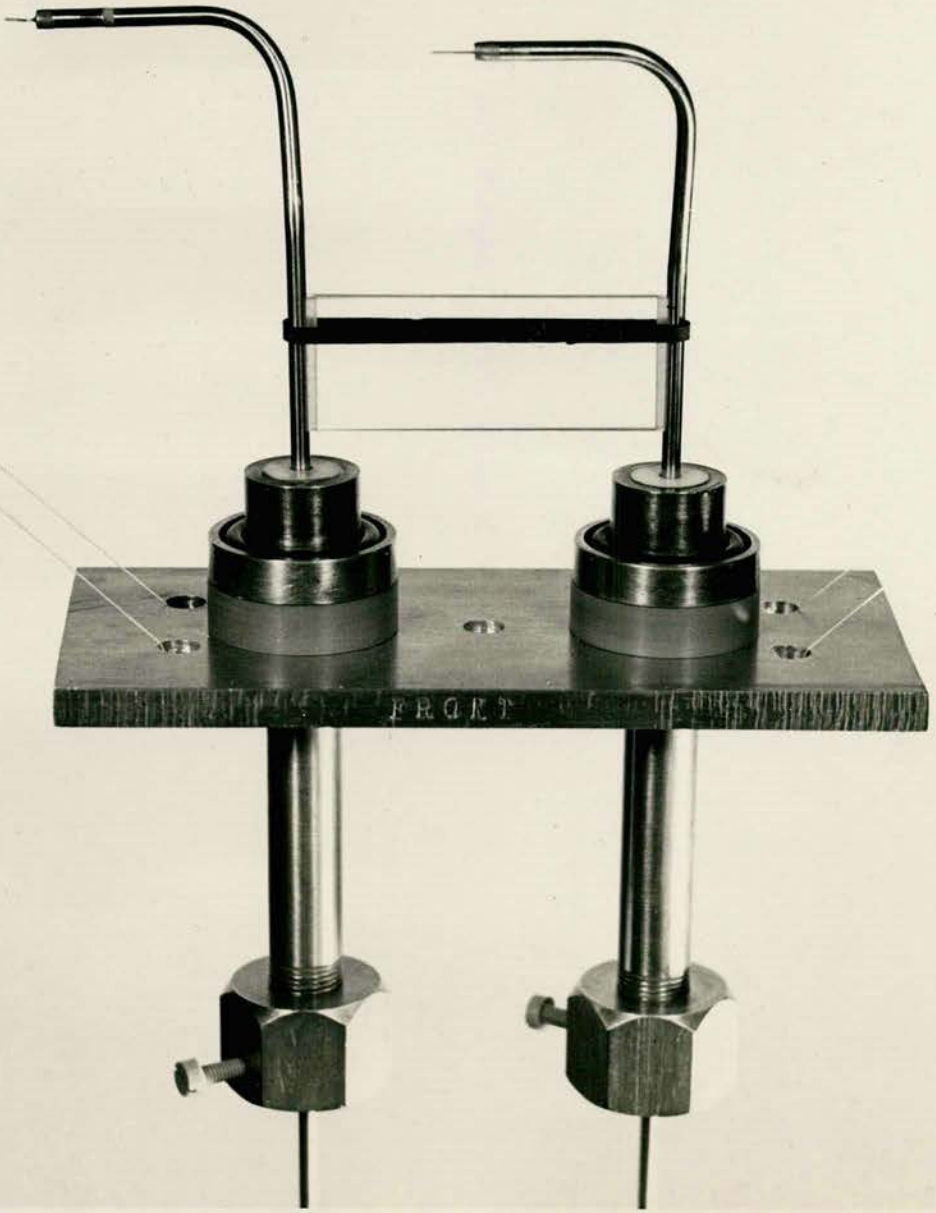

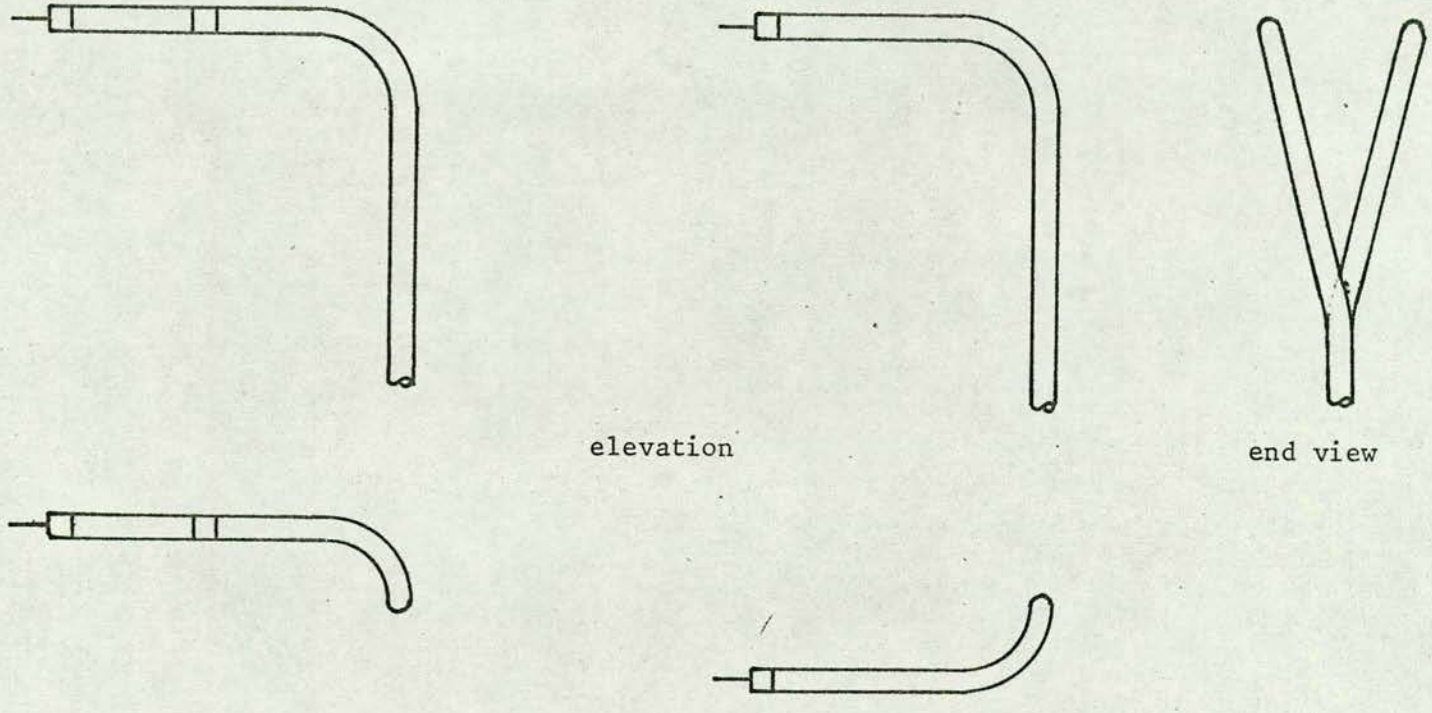

Figure (viii) Cranked O.A.C. stainless steel tubes (for plate IV)

accordance with B.S. 1041 specifications from 0.1275 inches diameter and 0.058 inches diameter stainless steel tubing.

Two oxygen analysing cells are shown in plate (iv) mounted in their holders. The one on the left was cranked to the back and the one on the right an equal amount to the front as in figure (viii). This was to maximise the distance between the two cells so that they would not "interfere" electrically with one anothers support tubes. A specially constructed jig was made to bend the tubes in an identical manner. The cell support tubes were kept at a constant distance apart by a distance piece made by machining parallel V-grooves at either end of 0.125 inch thick piece of perspex. The retaining spring for the constraint was an elastic band. The design and electrical circuits of the oxygen analysing cell are contained in Appendices II and III.

(d) The turbulence promoters. The first type of grid used was an interwoven copper wire with a mesh spacing of 0.25 inches. This type of grid was abandoned in favour of that shown in figure (ix) because of its ineffectiveness in promoting or suppressing turbulence.

The second grid was made by soldering together a set of number 9 gauge brass rods, machined to a length of 5.94 inches. In order to ensure that the mesh spacing was correct and square, a jig was made by carefully drilling a set of holes closely fitting the rods, 0.625 inches apart in four metal strips. These strips were then fitted together so that they formed a square. The rods were then put through the holes and the rod ends squared up to two of the jigs sides. The points at which

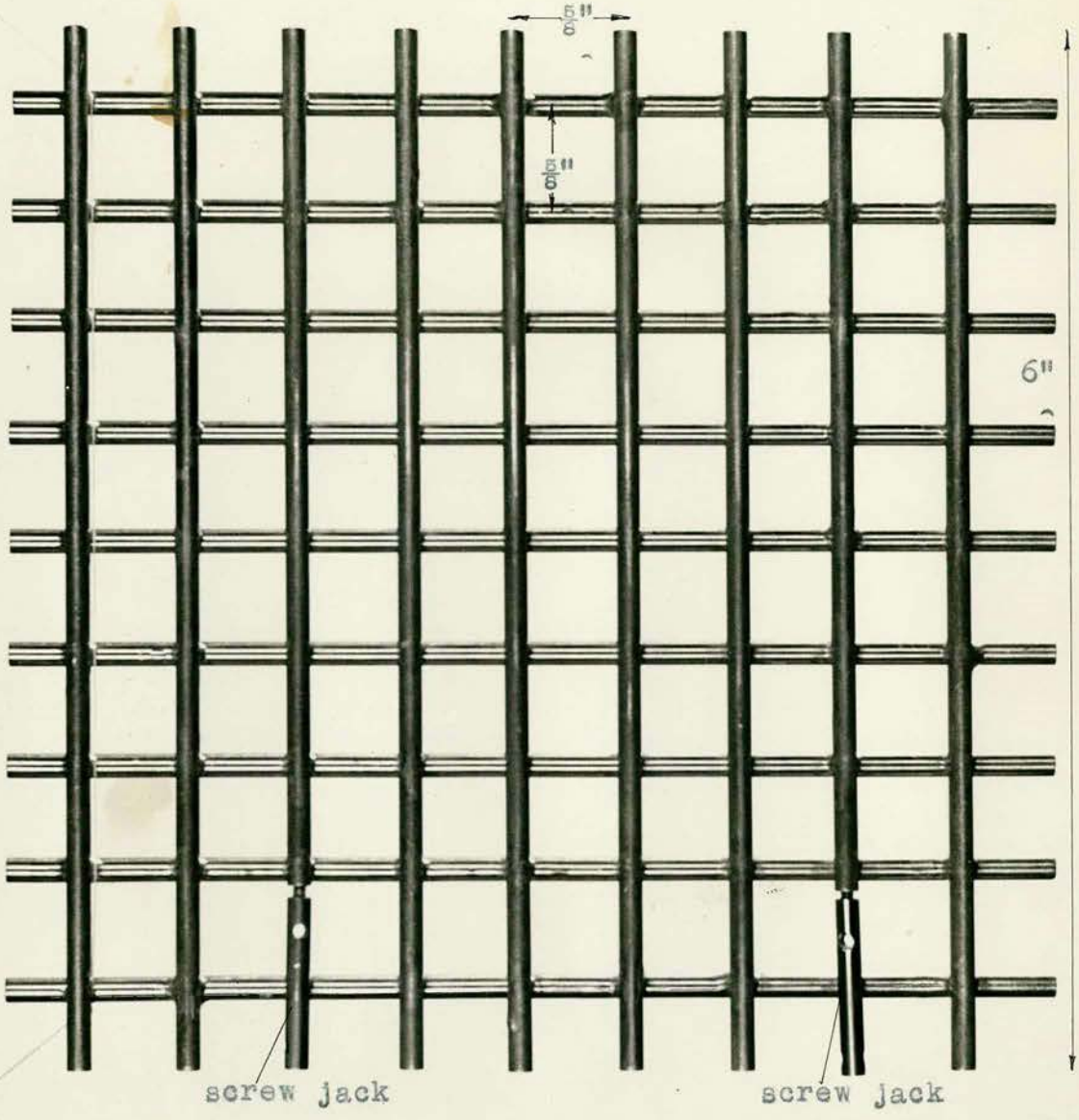

Figure (ix) No 9G Grid

the four perimeter rods touched the other rods were soldered. In order to fix this grid securely in the open channel, two small screwjacks were fitted to two of the rods spanning the width of the channel. This grid could thus be fixed anywhere in the open channel. Its correct position, square to the walls and floor, was achieved by using a machined rectangular metal block.

The other obstacles used are shown in plate (v). The large polished brass cylinder in the picture was used to represent a single boulder and as a comparison for the other objects in the picture. These objects were made from Handy Angle.

(3.3) Modifications made to the recirculation loop.

When the apparatus was first used the original Handy Angle frame work on the upper level was found insufficiently rigid and had to be reinforced. This reinforcement required the employment of four 0.5 inches diamter tie bars and a dozen jacks made from an inch diameter steel tubing and 0.5 inches B.S.W. nuts and bolts. Two tie bars anchored the frame across the width, with one anchoring it at either end. The jacks were spaced out equally on each side along the length of the frame.

The next modification was the insertion of two pieces of 4 inches diameter fire hose, just above the pump inlet and outlet, in place of two sections of the P.V.C. pipe. This was to stop vibrations from the pump travelling up the pipe to the open channel. Because of this modification the supporting frame for the pipes on the ground floor had to be split into two parts in such a way that the lower frame could vibrate while that supporting the pipework above the rubber hose remained free from

vibrations. The position of the Handy Angle framework is shown in relation to the surroundings in figure (ii).

The insertion of the rubber hose meant that the flow in the loop could now be regulated with greater ease than before, by simply clamping two lengths of round steel tube about the hose on the pump exit side. A set of marks were made on the tubing so that the "valve" could be altered to known positions by measuring the distance between both sets of marks. Previously the flow had been regulated by inserting one of a set of nine orifice plates into the inlet squinch - P.V.C. pipe joint.

Lastly, to suppress secondary flow in the bends and affecting the fluid motion in the channel, six sets of vanes were inserted into the 90° elbows and copper bends. The upper set of vanes in plate (vi) were used in the elbows and two like the lower one in each of the copper bends. Each set of vanes was made from HG brass sheets soldered together. The vanes in the exit side were primarily to stop disturbances being propagated back upstream into the open channel.

(3.4) Water supply for the channel.

The mains water supply to the whole building, in which the Laboratory was housed, was pressurised by air. This meant that the water was super-saturated with oxygen. To remove this excess oxygen and other dissolved salts, such as chlorides, from the water a 5KW distillation unit was used producing about 1.5 gallons of water per hour. The still and receiving vessels can be seen in the background of plate (ii).

To remove the remaining traces of oxygen from the water a

few drops of hydrazine hydrate were added to the moving water in the channel with the water sealed off from the atmosphere. The reaction which took place was as follows:

$$2\,N_2H_4 + O_2 = 2N_2 + 2H_2O \qquad (24)$$

The use of hydrazine was benificial in several ways. Firstly, there were no dissolved products in the water as there would have been if sodium sulphite had been used. Secondly, small bubbles of nitrogen produced in the reaction also remove some of the dissolved oxygen as they are carried along by the flowing water. These bubbles congregated at the two nozzles and were removed periodically via the vents. (The hydrazine also prevents any corrosion taking place in the pump since it renders the metal passive (72)).

Another way of removing the oxygen from the water, which was tried but without much success, was to pass a continuous stream of nitrogen bubbles through the water. This method has been successfully applied in a pulsed column (73) where the water was deoxygenated in about five minutes. The deoxygenation took about one and a half hours.

(3.5) Operating technique.

Prior to filling the channel up with water the required obstacle and/or oxygen analysing cells were correctly positioned in the open channel.

Starting with all valves shut, and with reference to figure (x), to fill up the channel with water the pressure in the nitrogen line was adjusted to 5 p.s.i.g. Valves 4V, 4W and 5W were opened and on opening valve 3N water was discharged from the

C.B. - control box
H. - hydrazine
M.M. - micro manometer
N. - nitrogen
O. - oxygen

R - recorder
S - switch
T - tracer "dye"
V - vent
W - water

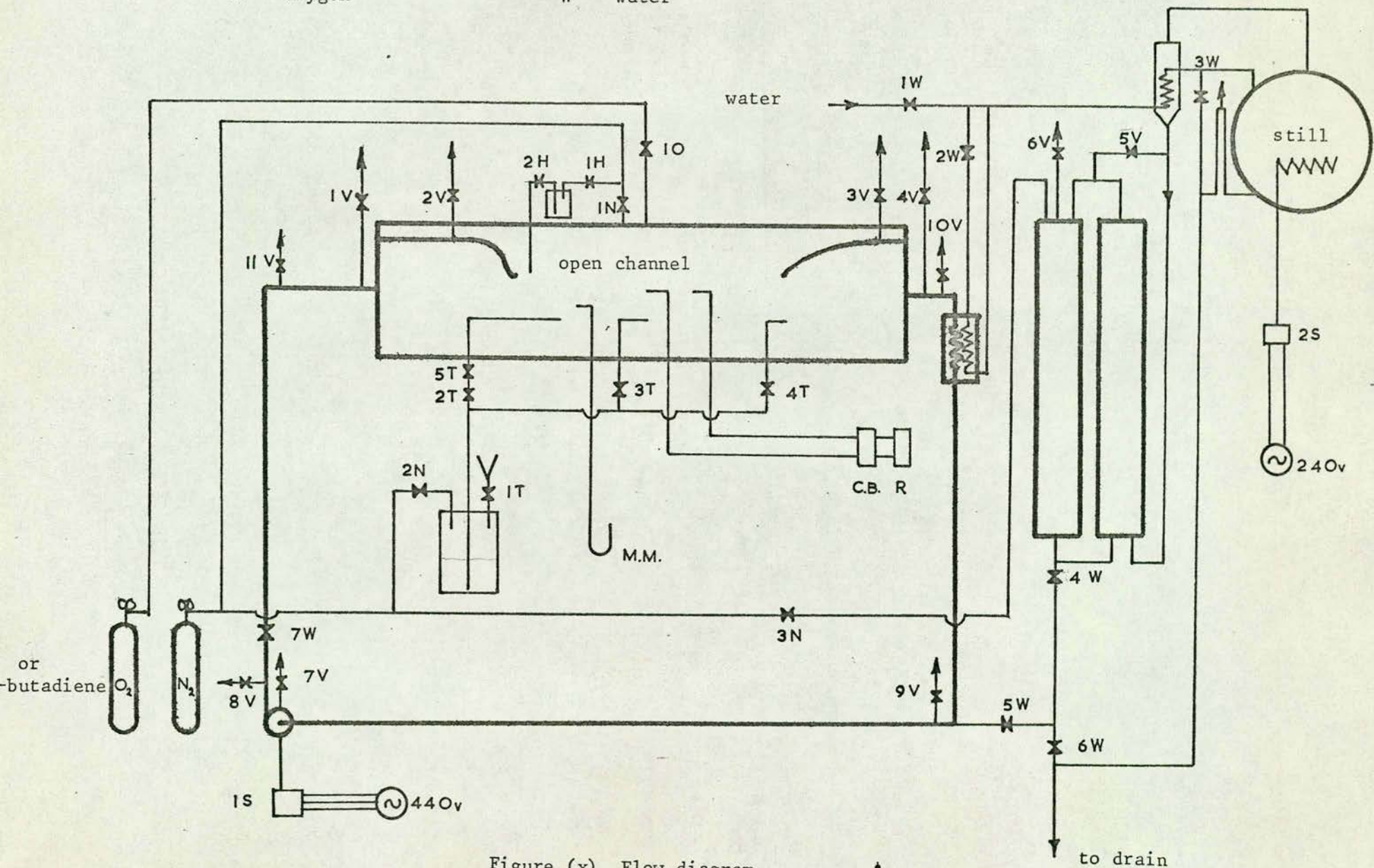

Figure (x) Flow diagram

still receiving vessels into the apparatus. Once the channel was completely full, including some of the gas space above the open channel, valves 4V, 5W, 4W and 3N were shut in that order. Valves 7V, 8V, 9V, 10V and 11V were each opened in turn till water issued from them; they were then shut. This action removed trapped air pockets from the pump and bends respectively. The pump was then switched on-off several times at 1S to push any air in the copper bends and honeycomb section out into the nozzles, where it was removed by suction through valves 2V and 3V. Once all the air had been removed the pump was switched on and the cooling water for the channel turned on at valves 1W and 2W. (Valve 1W was normally open since the distillation unit was working almost continuously). Valve 7W was then adjusted till the required velocity was attained in the open channel. The velocity was found from pitot tube measurements.

Any remaining water above the correct water level was then removed by syphoning it off through Valve 1V, till the correct depth was attained. Valve 1V was then shut.

(a) Technique for "dye" observations.

To carry out experiments with "dye" streams the cine camera was lined up to the centre line of the "dye" dispersion and the flood lighting switched on. The nitrogen line was then pressurised to 15 p.s.i.g. and valve 2N opened. Either valve 2T, 3T or 4T was opened. If a continuous dispersion was required then the valve opened was adjusted till the "dye" stream velocity was the same as that of the channel water at the point of injection. Then several ten second cine film shots were taken.

When valve 2T was being adjusted valve 5T was fully opened. To pass a puff of "dye" along the open channel valve 5T was shut till the "dye" injection had ceased, valve 2T still remaining set for the particular channel velocity at the point of injection. Valve 5T was then quickly opened and closed whilst at the same time firing the cine camera by remote control. Plate (vii) shows a typical trace at a hydraulic depth Reynolds number of 3800 with a three inch high Handy Angle obstacle and point of injection 6 cms. from the channel bottom.

This process was repeated using a different injection depth. The "dye" injector tube depth was set by lining up the hypodermic tube of the injector between two transparent scales fixed to the perspex windows at both sides of the channel. Once all the depths required were examined either a different obstacle or flow rate was used. To stop the "dye" concentration building up, the water in the apparatus was changed frequently.

The cine films were then developed and the results viewed frame by frame at a magnification of 1.5. The data from the cine film was then processed according to the method described in chapter 4.

(b) Technique for mass transfer measurements.

In the case of mass transfer experiments with oxygen, valve 1H was opened, to allow nitrogen at 5 p.s.i.g. to enter the hydrazine bottle, and then closed after a second. Valve 2H was carefully opened so that two of three drops of hydrazine hydrate entered directly into the flowing water. The free surface of the open channel was covered completely with a thin sheet of

perspex to exclude any oxygen and the atmosphere changed to nitrogen. When the deoxygenation was completed, the temperature of the water and the atmosphere, and barometric pressure were noted. The two potentiometer recorder chart speeds were set at thirty centimetres per minute. The thin perspex cover was then carefully removed and oxygen admitted to the system by opening valve 10, venting the displaced nitrogen atmosphere out through valves 1N, 2N and 1T. At the end of a run the two temperatures and the barometric pressures were noted. (In some experiments these conditions were noted several times during a run). The pump was then stopped and the apparatus drained out and the process started again with a new obstacle or flow rate.

Preliminary experiments has shown that if the laboratory air was used in place of oxygen there were no differences in the mass transfer coefficients, which is what would be expected in this situation. This simplified the operation since the top perspex cover could be left unbolted and used only as a dust cover.

The data obtained from the recorder charts were then broken down suitable for use with the mass transfer theory equations of chapter 4.

(3.6) Method of making the "dye".

1g of pyrogallolic acid was weighed into a 10ml beaker. To this was added 1g of sodium carbonate. This mixture was then dissolved in 90ml of distilled water. When all the solid particles had dissolved, 10ml of methanol was then added to

counteract the increase in density and viscosity caused by the acid and carbonate. The density of the resultant solution, after prolonged exposure to the air to darken it, was found to be the same as that of water but its viscosity, as measured with an Ostwald viscometer, was 4% less.

The "dye" was an intense brown colour. The solution was then diluted with ten parts distilled water to one part of solution so that the "dye" concentration could not build up too quickly in the apparatus during the filming experiments.

Chapter 4.

THEORY.

(4.1) The point concentration of matter dispersed continuously into a flowing fluid from a point source.

The equations previously used by other workers (74,76,77,81, 83,84,85,86) to describe the concentration of matter at any point in a continuous dispersion of matter from a point source were unsuitable for use in this work (apart from the fact that they all differed slightly from one another). Some of these equations will be discussed later in this section.

The assumptions in the derivation of an equation to describe the point concentration of matter were as follows:

(i) constant diffusivity

(ii) uniform velocity; i.e. the region of interest is near the axis of a uniform channel or in a stream of infinite cross section.

(iii) the net axial diffusion can be neglected compared with the radial diffusion in this case since the radial concentration gradients are much greater than the axial concentration gradients, particularly when x is large.

(iv) the radius of the injector tube, r_o, for injecting the matter is very small so that the source can be considered as a point. In this work r_o was 0.0105 inches.

(v) in this work the "outer" radius of the dispersion, r_a, is required. It is known that the concentration of matter in a dispersion is distributed according to a normal error law (74, 75,79,80,81) of the type:

$$C(xr) = C(x,o)\ e^{-\frac{r^2}{2\sigma^2}} \qquad (25)$$

where C(x,r) is the concentration in the yz plane at a point a distance r from the x-axis.

C(x,o) is the concentration at the x-axis.

r is the radial distance from the x-axis in the yz plane.

σ, which is a function of x, is the standard deviation of the concentration distribution about the x-axis and is a measure of the degree of dispersion.

Dispersions whose concentration distribution are described by a normal error law extend to infinity in the yz plane. r_a is therefore taken as the radius at which $C(x,r) \ll C(x,o)$. The inequality occurrs when equation (25) becomes

$$C(x,r_a) = C(x,o)\ e^{-6} \qquad (26)$$

(The value 6 has been arbitrarily chosen. Any number between 4.25 and ∞ will give the probability that at least 99% of the matter is within the area πr_a^2 in the yz plane). From equation (26), r_a is therefore the radius of the area in the yz plane which contains 99.858% of the matter in the yz plane being considered.

Comparing equations (25) and (26) when $r = r_a$

$$\text{i.e. } \frac{r_a^2}{2\sigma^2} = 6$$

$$\therefore \quad \sigma = \frac{r_a}{\sqrt{12}} = \left(\sqrt{\overline{r^2}}\right) \qquad (27)$$

Equation 25 therefore becomes:

$$C(xr) = C(x,o)\ e^{-\frac{6r^2}{r_a^2}} \qquad (28)$$

In order to show that equation 28 describes the point concentration of matter dispersed continuously from a point

source, a random walk procedure in two-dimensions was used. In this procedure the probability of particle, starting at r = o at time t = o, being at any other point in the yz plane at time t = t was evaluated.

Although diffusion takes place in three-dimensions, this situation can be considered as diffusion in "two"-dimensions as a consequence of assumptions (i) (ii) and (iii). The random walk was taken on a hexagonal grid in preference to a square grid, as this was found to give a quicker answer to the problem. The reason for this is that the square grid consists of two distinct sets of points viz. 4 neighbouring points which can be reached in one move from a central point and 4 neighbouring points which can be reached in two moves from a central point. Also, the square grid gives rise to a zero probability of the particle being at the x-axis at each odd step in the walk. There is a direct correspondence between the probability of a particle being at a point on the grid and the concentration of matter at the corresponding point in the dispersion.

Figure (xii) shows the probability of the particle being at different points on the hexagonal grid after one, two and three steps. The solution to further steps in the random walk on a hexagonal grid is given in Appendix VII. When the radial probabilities were plotted against radial distance, the result obtained was that shown in figure (xiii). The line in figure (xiii) represents the equation:

$$P(x,r) = P(x,o)\, e^{-\frac{6r^2}{ra^2}} \qquad (29)$$

where P(x,r) is the probability of the particle being at a

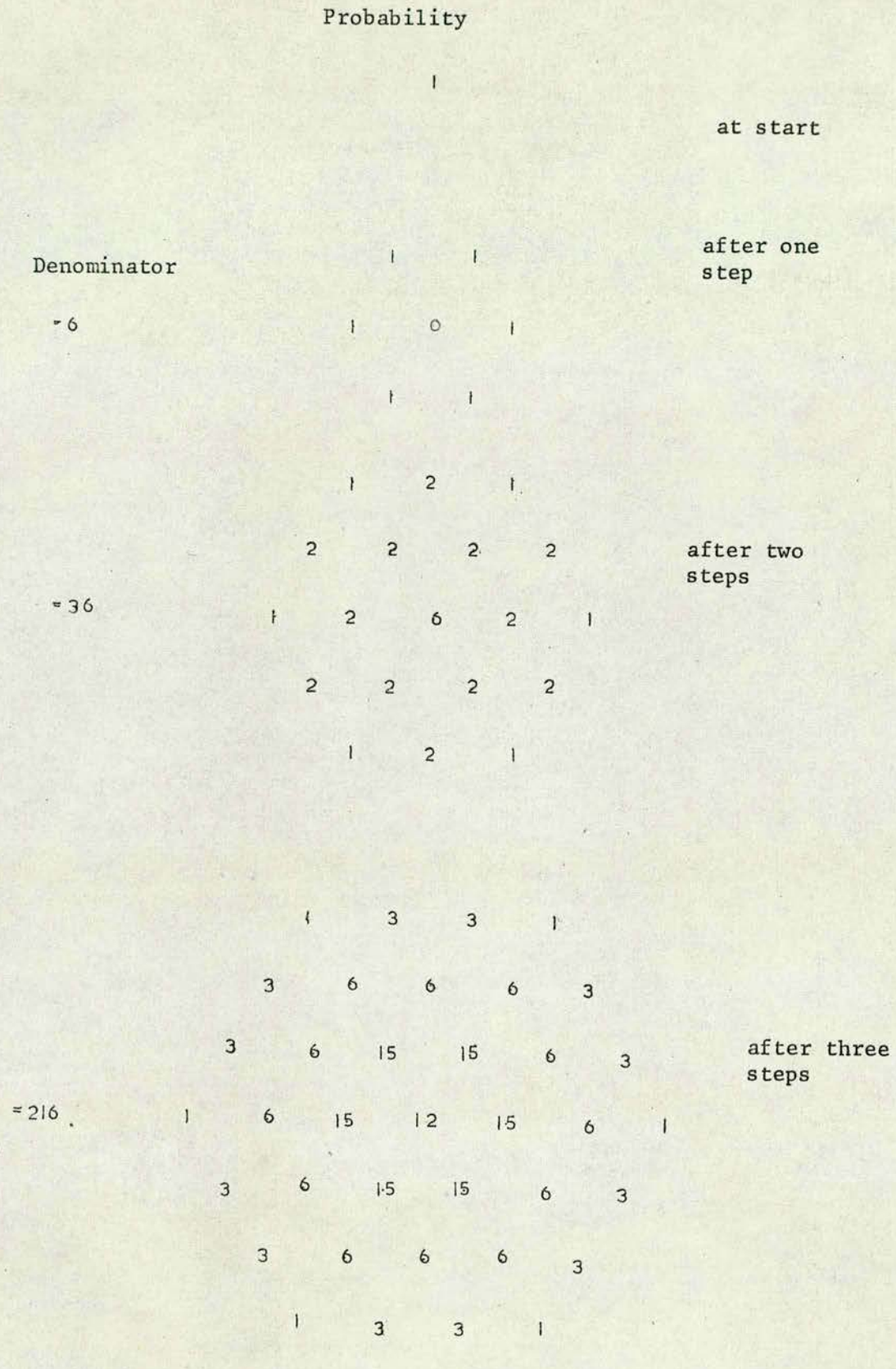

Figure (xii) Random walk in two-dimensions

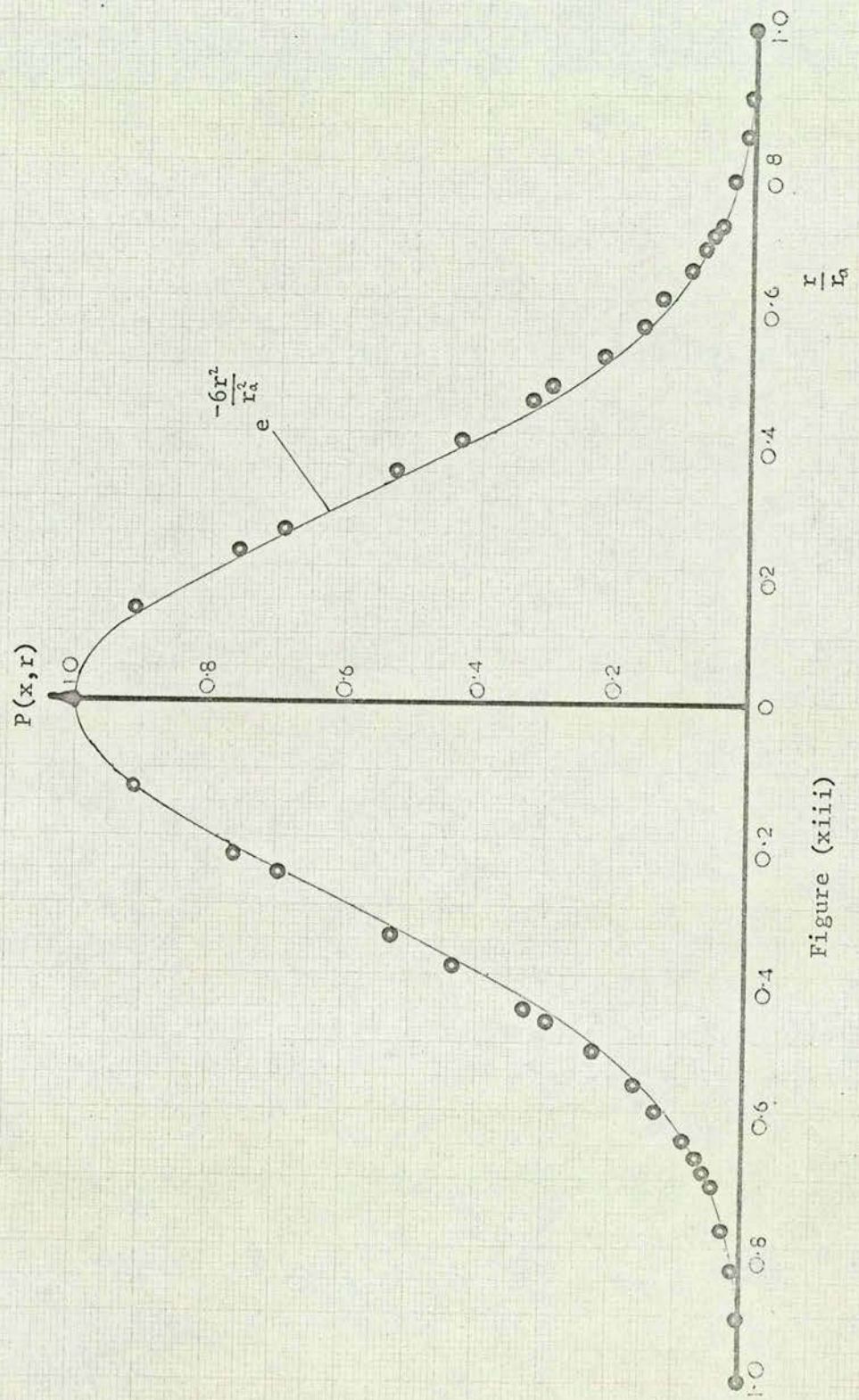
P(x,r)
1·0
0·8
0·6
0·4
0·2
0
0·2
0·4
0·6
0·8
1·0
1·0
0·8
0·6
0·4
0·2
0
0·2
0·4
0·6
0·8
1·0
$e^{-6\frac{r^2}{r_a^2}}$
$\frac{r}{r_a}$

Figure (xiii)

radial distance r from the x-axis

P(x,o) is the probability of the particle being at the x-axis.

The points on figure (xlii) were obtained from the hexagonal grid after ten steps. From the randon walk P(x,o) is proportional to $\frac{1}{r_a}$ after the first three steps. i.e. the radial probability distribution of the particle obeys a law of the form

$$P(x,r) = \frac{1}{\sigma\sqrt{2\pi}} \cdot e^{-\frac{r^2}{2\sigma^2}} \qquad (30)$$

where $= \frac{r_a}{\sqrt{12}}$

With reference to figure (xiv), the total probability under the curved surface is one, as shown in Appendix VII

$$\text{i.e.} \quad \int_0^\infty P(xr)\, dA = 1$$

$$\text{i.e.} \quad \int_0^\infty \frac{2\pi r\sqrt{6}}{r_a\sqrt{\pi}}\, e^{-\frac{6r^2}{r_a^2}}\, dr = 1$$

integrating the left hand side by parts

$$I_{LHS} = -\left[\frac{2\pi r\sqrt{6}}{r_a\sqrt{\pi}} \cdot \frac{r_a}{6.2r}\, e^{-\frac{6r^2}{r_a^2}}\right]_0^\infty + \int_0^\infty \frac{\pi r_a}{r\sqrt{6\pi}}\, e^{-\frac{6r^2}{r_a^2}}\, dr$$

$$= r_a \cdot \sqrt{\frac{\pi}{6}}$$

$$\neq 1$$

∴ Equation (30) has to be normalised

$$\text{i.e.} \quad P(x,r) = \frac{1}{\sigma^2 2\pi}\, e^{-\frac{r^2}{2\sigma^2}} \qquad (31)$$

If N particles are added at the origin at the beginning of the random walk, equation 31 becomes

$$P(x,r) = \frac{N}{\sigma^2 2\pi}\, e^{-\frac{r^2}{2\sigma^2}} \qquad (32)$$

The corresponding equation for the concentration of matter at any point in a dispersion is therefore:

$$C(x,r) = \frac{Q}{\sigma^2 2\pi} e^{-\frac{r^2}{2\sigma^2}} \qquad (33)$$

(where Q is the mass of dispersed matter in a region dx thick of indefinitely large area).

Substituting in equation (27) into equation (33)

$$C(x,r) = \frac{6Q}{\pi r_a^2} . e^{-\frac{6r^2}{r_a^2}} \qquad (34)$$

In the case of a dispersion near a free surface the corresponding equation is

$$C(xr) = \frac{12Q}{\pi r_a^2} . e^{-\frac{6r^2}{r_a^2}} \qquad (35)$$

since the random walk can be reflected about the surface giving rise to twice the probability at each point in the grid (see Appendix VII). This procedure of reflection and superposition is mathematically sound (85).

The theoretical equations used by other workers to describe the concentration of matter at any point for matter continuously dispersed from a point source will now be considered. These equations are based on the same assumptions used in the derivation of equation (34). The steps which were taken to obtain the published equations are not given in most cases and in others there is only a brief indication of the equations from which the published equations were derived.

For the purpose of discussion equation (33) will be divided up as follows:

$$C(xr) = (Q)\left(\frac{1}{\sigma^2 2\pi}\right)\left(e^{-\frac{r^2}{2\sigma^2}}\right) \qquad (33)$$

so that the parameters in the following theoretical equations will bear a relation to the three bracketed quantities on the right hand side of equation (33). Symbols not defined in the following equations have the same physical significance as when used previously.

Sutton (81) derived the following equation for use with dispersions in the atmosphere, such as smoke from chimneys:

$$C(xr) = (Q)\left(\frac{1}{\pi^{3/2} c^3 (Ut)^{\frac{3m}{2}}}\right)\left(e^{-\frac{r^2}{c^2(Ut)^m}}\right) \qquad (36)$$

where $c^2 = \dfrac{4a^n}{(1-n)(2-n)}$

and a and n are obtained from the Lagrangian correlation function, R_ξ, which behaves as $\left(\dfrac{a}{[u]\xi}\right)^n$ provided $|u\xi| > 1$

(where u is the local velocity and ξ is a time interval)

t is the time interval between the source and the yz plane a distance x from the source. $t = \dfrac{x}{\bar{U}}$

U is the overall fluid velocity

and $\sigma^2 = \frac{1}{2} c^2 (Ut)^{2-n}$ (37)

$(m = 2 - n)$

i.e. equation (36) is of the form:

$$C(xr) = (Q)\left(\frac{1}{c^3 (2\pi)^{3/2}}\right)\left(e^{-\frac{r^2}{2\sigma^2}}\right)$$

Towle and Sherwood (74) on the otherhand modified the Wilson (82) equation for diffusion of heat from a point source in an infinite medium to apply to diffusion of gases from a

point source inside circular ducts, 30.5 cms. and 15.24 cms. in diameter, to yield the following equation:

$$C(xr) = \frac{q}{4\pi D_\epsilon R} e^{-\frac{U(R-x)}{2D_\epsilon}} \qquad (38)$$

where D_E is the eddy diffusivity of the dispersed matter in the dispersing medium

$q = \frac{QR}{t}$ i.e. it is the rate at which matter is injected

R is the distance from the point of injection to the point under consideration, $R = \sqrt{x^2 + r^2}$

For their work $(R - x)$ can be taken as $\frac{r^2}{2x}$ and $\frac{U}{x}$ as $\frac{1}{t}$

Thus equation (38) becomes:

$$C(xr) = (Q)\left(\frac{1}{4\pi D_\epsilon t}\right)\left(e^{-\frac{r^2}{4D_\epsilon t}}\right) \qquad (39)$$

and if the molecular diffusivity, Dm, is very much less than D_E, then

$$\sigma^2 = 2D_\epsilon t \qquad (40)$$

i.e. equation (39) is of the form

$$C(xr) = (Q)\left(\frac{1}{\sigma^2 2\pi}\right)\left(e^{-\frac{r^2}{2\sigma^2}}\right)$$

Levich (76) developed an equation of the form:

$$C(xr) = (Q)\left(\frac{1}{\sqrt{2\pi}\, D_\epsilon t}\right) e^{-\frac{(x-Ut)^2}{4D_\epsilon t}} \qquad (41)$$

which is of the form:

$$C(xr) = (Q)\left(\frac{2}{\sigma^2\sqrt{2\pi}}\right)\left(e^{-\frac{r^2}{2\sigma^2}}\right)$$

Flint, Kada and Hanratty (83) developed one of the form:

$$C(xr) = \frac{q}{2\pi U \bar{r}^2} e^{-\frac{r^2}{2\bar{r}^2}} \qquad (42)$$

for dispersion inside pipes. In this case

$$\sqrt{\overline{r^2}} = \sigma$$

i.e. equation (42) is of the form:

$$C(xr) = (Q)\left(\frac{1}{2\pi\sigma^2}\right)\left(e^{-\frac{r^2}{2\sigma^2}}\right)$$

Prattle (84) based his equation on Crank's (85) equation describing diffusion from a point source into an infinite medium, when considering the case of a concentration dependent coefficient. Prattles equation was

$$C(x,r) = (Q)\left(\frac{1}{(4\pi D_e t)^{\frac{1}{2}s}}\right)\left(e^{-\frac{r^2}{4De t}}\right) \qquad (43)$$

(where s is the number of dimensions, in this case 2). i.e. equation 43 is of the form:

$$C(xr) = (Q)\left(\frac{1}{\sigma^2\ 2\pi}\right)\left(e^{-\frac{r^2}{2\sigma^2}}\right)$$

Kalinske and Pien (77) used the following equation for dispersions in an open channel.

$$C(x,r) = (Q)\left(\frac{1}{\sqrt{2\pi\overline{r^2}}}\right)\left(e^{-\frac{r^2}{2\overline{r^2}}}\right) \qquad (44)$$

i.e. it is of the form:

$$C(x,r) = Q\left(\frac{1}{\sigma\sqrt{2\pi}}\right)\left(e^{-\frac{r^2}{2\overline{r^2}}}\right)$$

or based on the concentration at the centre of the dispersion

$$C(xr) = C(x,o)\ e^{-\frac{r^2}{2\overline{r^2}}} \qquad (45)$$

The above equation was also used by Micklesen (86) when considering the continuous dispersion from a point source of helium and carbon dioxide in air.

Of the six equations considered i.e. (36) (38) (41) (42)

(43) and (44), only (38) (42) and (43) are of the same form as equation (33). Equation (44) is the unnormalised version of equation (33). In the case of equation (36) c has the dimensions of length to the power $\frac{n}{2}$, since a has the dimensions of length. Hence c in equation (37) will always have the dimension of length irrespective of the value of n. Thus the parameters in the middle bracket of equation (36) are inconsistent with the other equation describing the concentration of matter continuously dispersed from a point source.

Although equation (41) does not agree numerically with equations (38) (42) and (43) it will give the same result as these equations for the "dye" dispersion extinction correction described in section (4.2c).

(4.2) Corrections applied to the cine film record.

(a) Parallax correction.

The cine film record of the "dye" dispersion will be distorted towards the outer edges of the dispersion due to three media being between the "dye" and the camera viz. water, perspex and air. The degree of distortion can be calculated as follows:

With reference to figure (XV)

r_e is the value, of the observed outer edge of the dispersion's distance from the axis of the dispersion, measured from the cine film record

y_3 is the required value.

The refractive indices used were:

$$air/\mu_{perspex} = 1.495$$

$$air/\mu_{water} = 1.333$$

$$r_e = \frac{y_1 (Z_1 + Z_2 + Z_3)}{Z_1}$$

$$= 1.128\, y_1 \qquad (46)$$

From Snell's Laws of Refraction

$$\frac{y_1}{(Z_1^2 + y_1^2)^{1/2}} \cdot \frac{(Z_2^2 + (y_2 - y_1)^2)^{1/2}}{(y_2 - y_1)} = 1.495 \qquad (47)$$

and

$$\frac{(y_2 - y_1)}{(Z_2^2 + (Y_2 - y_1)^2)^{1/2}} \cdot \frac{(Z_3^2 + (y_3 - y_2)^2)^{1/2}}{(y_3 - y_2)} = \frac{1.333}{1.495} \qquad (48)$$

squaring both sides of equation (47):

$$\frac{y_1^2}{(Z_1^2 + y_1^2)} \cdot \frac{(Z_2^2 + (y_2 - y_1^2))}{(y_2 - y_1)^2} = 1.495^2$$

$$= \frac{A_o (Z_2^2 + (y_2 - y_1)^2)}{(y_2 - y_1)^2}$$

$$\text{i.e.} \quad (y_2 - y_1) = \left[\frac{A_o Z_2^2}{1.495^2 - A_o}\right]^{1/2}$$

$$\text{i.e.} \quad y_2 = \left[\frac{A_o Z_2^2}{1.495^2 - A_o}\right]^{1/2} + y_1 \qquad (49)$$

From equation (47)

$$\frac{y_2 - y_1}{(Z_2 + (y_2 - y_1)^2)^{1/2}} = \frac{A_o^{1/2}}{1.495} \qquad (50)$$

Substituting equation (50) in equation (48)

$$\frac{A_o^{1/2}}{1.495} \cdot \frac{(Z_3^2 + (y_3 - y_2)^2)^{1/2}}{(y_3 - y_2)} = \frac{1.333}{1.495} \qquad (51)$$

Substituting equation (49) in equation (51)

$$\text{i.e.} \quad \frac{A_o^{1/2} (Z_3^2 + (y_3 - A_1 - y_1)^2)^{1/2}}{(y_3 - A_1 - y_1)} = 1.333 \qquad .333 \qquad (52)$$

Squaring both sides of the above equation

$$A_o (Z_3^2 + (y_3 - A_1 - y_1)^2) = 1.333^3 (y_3 - A_1 - y_1)^2$$

*

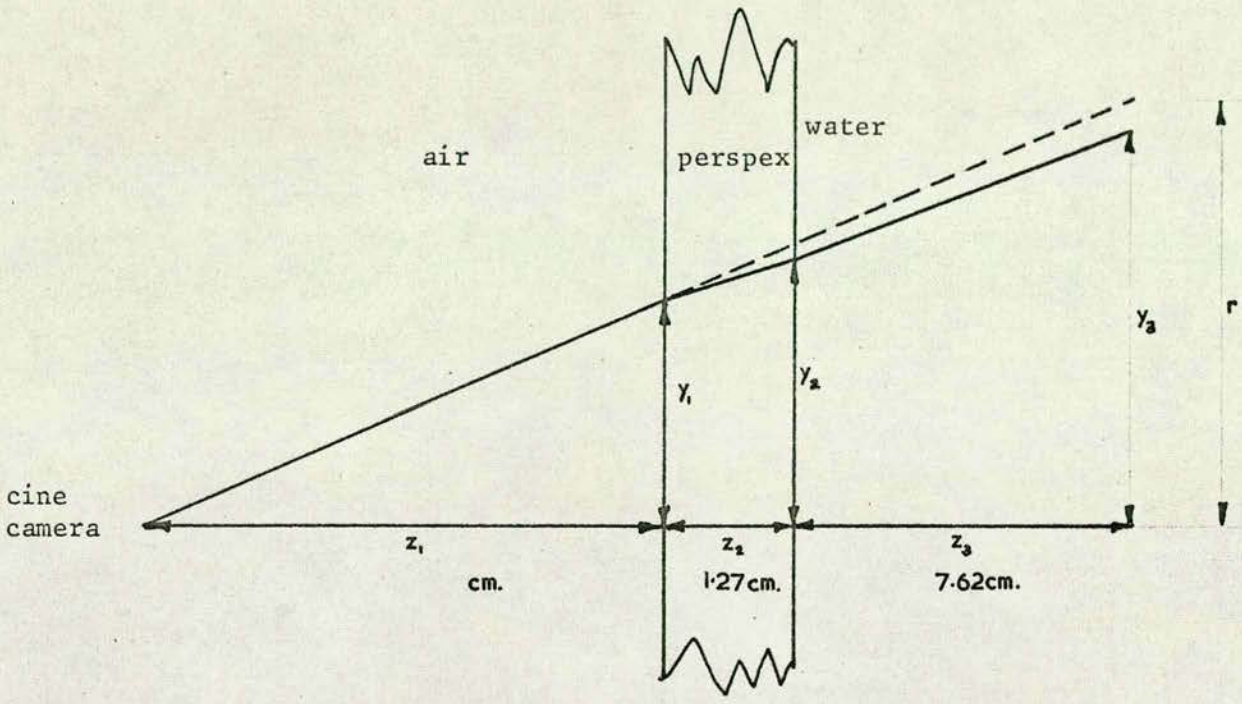

Figure (xv) Parallax correction

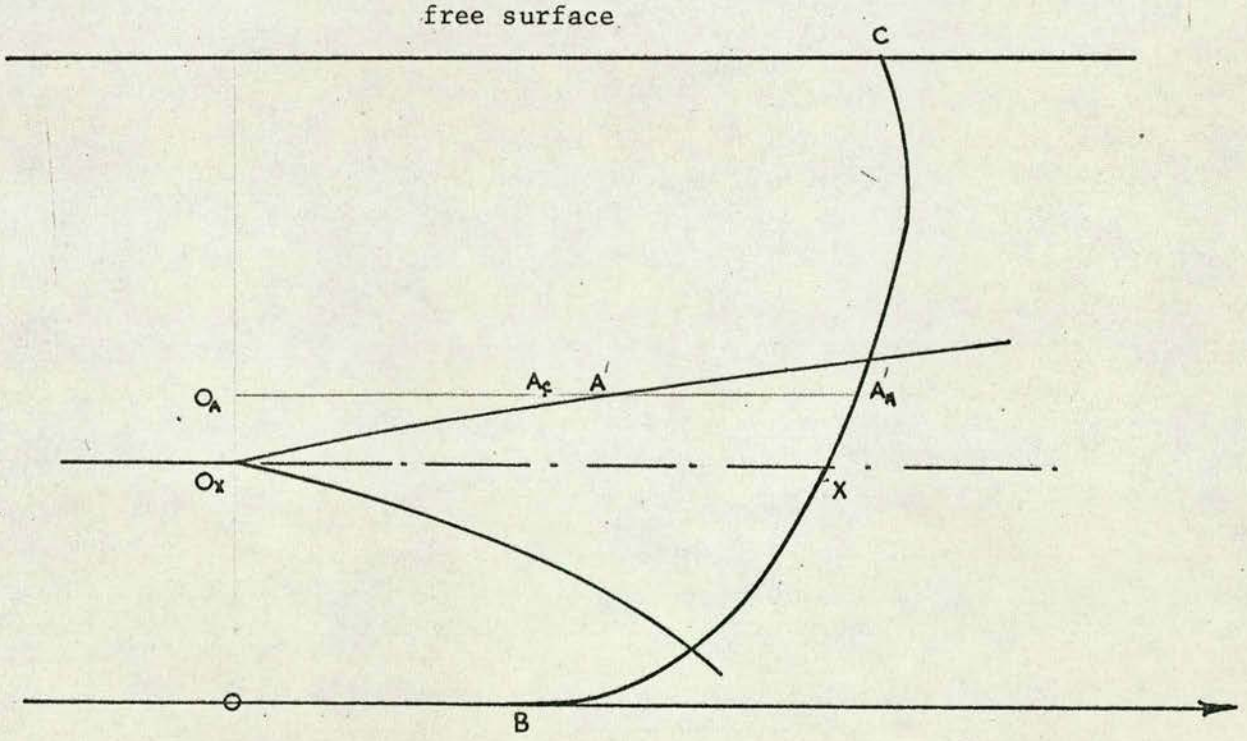

Figure (xvi) Velocity distortion correction

i.e. $(y_3 - A_1 - y_1)^2 (1.333^3 - A_0) = A_0 Z_3^2$

$$\text{i.e. } y_3 = \left[\frac{A_0 Z_3^2}{1.333^3 - A_0}\right]^{1/2} + A_1 + y_1 \qquad (53)$$

Substituting equation (46) in equation (53) for y_1

$$y_3 = \phi(r_e)$$

or
$$y_3 = A_2 + A_1 + 0.887 r_e \qquad (54)$$

where
$$A_2 = \left[\frac{\dfrac{(0.887)^2 r_e^2 Z_3^2}{(Z_1^2 + 0.887^2 r_e^2)}}{1.333^3 - \dfrac{(0.887)^2 r_e^2}{(Z_1^2 + 0.887^2 r_e^2)}}\right]^{1/2}$$

$$= \frac{0.887 r_e Z_3}{(1.778 Z_1^2 + 0.612 r_e^2)^{1/2}}$$

$$= \frac{6.7 r_e}{(8470 + 0.612 r_e^2)^{1/2}} \qquad (55)$$

(after substituting in the values of Z_1 and Z_3)

and
$$A_1 = \left[\frac{\dfrac{Z_2^2 (0.887)^2 r_e^2}{(Z_1^2 + (0.887)^2 r_e^2)}}{1.495^2 - \dfrac{(0.887)^2 r_e^2}{(Z_1^2 + (0.887)^2 r_e^2)}}\right]^{1/2}$$

$$= \frac{1.126 r_e}{(10650 + 1.096 r_e^2)^{1/2}} \qquad (56)$$

(after substituting in the values of Z_1 and Z_3)

Substituting in equations (55) and (56) to equation (54)

$$y_3 = \frac{6.7 r_e}{(8470 + 0.612 r_e)^{1/2}} + \frac{1.126 r_e}{(10650 + 1.096 r_e)^{1/2}} + 0.887 r_e \qquad (57)$$

Equation (57) was solved for various values of r_e and the corresponding values for y_3 are tabulated in table II of Appendix VI. This is only a minor correction to the observed dispersion.

(b) Velocity distortion correction.

As there was a slight variation of the overall velocity over the region in which the "dye" dispersion experiments were carried out, the dispersions at different depths were affected by the changes in the overall velocity as shown in figure (xvi).

In figure (xvi) the line BC represents the distance travelled in time t by fluid originally at plane Oy. The shaded area represents the observed "dye" dispersion after the parallax correction has been applied. The "dye" dispersion should be symmetrical about $O_X X$. $O_X X$ is the distance travelled from O_X by the fluid at the centre of the dispersion in time t. $O_A A'_A$ is the distance travelled from O_A by the fluid element a distance $O_X O_A$ above (or below) O_X in time t. $O_A A'$ is the observed distance from the plane Oy to the edge of the "dye" dispersion and $O_A A_C$ is the corrected distance to the edge of the dispersion. The distance $O_A A_C$ is given by:

$$O_A A_C = \frac{O_A A'}{O_A A'_A} (O_X X - O_A A'_A) + O_A A'$$

The velocity correction, like the parallax correction is only a minor one.

(c) <u>"Dye" dispersion extinction correction</u>.

In Appendix (iv) a correction is derived to account for the unseen portion of the "dye" dispersion. From the table in Appendix (iv), the solution to equation (xi) of Appendix IV i.e.

$$0.7779 - \beta \oint_2 (X_e) = \frac{2r_a^2}{13 r_{ax}^2} \quad 0.364$$

where r_{ax} is the outer radius of the dispersion at a distance x from the point of injection.

r_{ex} is the radius at which the "dye" disappears at a

distance x from the point of injection.

β is a function of r_{ax} and r_{ex}.

ϕ_2 (Xe) is a function of r_{ax} and r_{ox}.

at different extion radii, r_{ex}, for the outer radius, r_{ox}, of the dispersion were found. r_{ex} was found from the "dye" dispersion record after it had been corrected for velocity distortion. The complete picture of the "dye" dispersion was made from all the values of r_{ax} obtained from the solution of equation (xi). From this complete picture of the "dye" dispersion the root mean square velocities $\sqrt{u^2}$ and $\sqrt{v^2}$, and scale of turbulence were found.

(4.3) Calculation of the root mean square velocities and the scale of turbulence.

During the initial period of spread of injected matter into a stream, the effect of turbulence near the source will cause a linear rate of increase of $\sqrt{r^2}$ with x (24, 87) and that

$$\frac{\sqrt{r^2}}{x} = \frac{\sqrt{v^2}}{U}$$

or in terms of the angle of dispersion, , (in radians)

$$\frac{\sqrt{v^2}}{U} = \frac{\theta_1}{a_1} \qquad (58)$$

For this work the constant a_1 was found from eleven "dye" dispersion records in which the local velocities of the eddies were clearly measurable. The constant a_1 was found to be 2.02. Theoretically it should be between 1.862 and 2.243.

In the free surface layers of the fluid the relationship between $\sqrt{u^2}$ and $\sqrt{v^2}$ was found to be

$$\frac{\sqrt{\overline{u^2}}}{\sqrt{\overline{v^2}}} = 1.096 = a_2 \qquad (59)$$

Thus the turbulent intensities can be found from equations (58) and (59) for the x and y-directions in the channel.

In order to find the scale of turbulence, defined by

$$L = \sqrt{\overline{v^2}} \int_0^\infty R(\theta)\, d\theta \qquad (22)$$

for the y-direction, use was made of the fact that:

$$D_\epsilon = \overline{v^2} \int_0^\infty R(\theta)\, d\theta$$
$$= \sqrt{\overline{v^2}}\, L \qquad (60)$$

In order to use equation (60) the eddy diffusivity has to be related to $\sqrt{\overline{r^2}}$.

From the published equations relating the spread of matter in a fluid to the eddy diffusivity it is found that either the molecular diffusivity, D_M, is taken into account or ignored, the majority of workers preferring to take it into account.

According to Saffman (88) the interaction between molecular diffusion and turbulent motion reduces the dispersion from the value it would have had if the processes of molecular and turbulent diffusion were independent and additive. On the otherhand Townsend (89) maintains that interaction will increase the dispersion.

Townsend's equation is:

$$\overline{r^2} = 2D_\epsilon t + 2D_m t + \frac{28}{45} D_m \omega^2 t^3 \qquad (61)$$

while Saffman's equation is :

$$\overline{r^2} = 2D_\epsilon t + 2D_m t - \frac{1}{9} D_m \omega^2 t^3 \qquad (62)$$

(where ω is the vorticity of the fluid).

As Saffman himself points out, equation (62) will eventually lead to zero dispersion of matter, which will occur at time:

$$t = \frac{3}{\omega}\sqrt{2\left(\frac{D_e}{D_m} + 1\right)}$$

In an attempt to correct this anomaly he derives another equation:

$$\overline{r^2} = 2D_e t + 2D_m t - a_3 D_m \omega^2 t^2$$

which will still produce a zero dispersion of matter, but this time at

$$t = \frac{(D_e + D_m)}{a_3 \omega^2}$$

The constant a was found to be 0.23 from Micklesen's (86) work on continuous dispersion of helium and carbon dioxide in air from a point source.

Thus for this work Townsend's equation was used. Substituting equation (60) into equation (61) leads to:

$$\overline{r^2} = 2\sqrt{\overline{v^2}}\,Lt + 2D_m t + \frac{28}{45} D\omega^2 t^3 \qquad (63)$$

The vorticity, ω, can be taken as

$$\omega = \frac{2(\overline{u^2} + \overline{v^2})^{1/2}}{L} \qquad (64)$$

and $$t = \frac{x}{\bar{U}} \qquad (65)$$

Hence equation (63) becomes after substituting in equations (27)(58)(59)(64)(65) for $\sqrt{\overline{r^2}}$, $\sqrt{\overline{u^2}}$, $\sqrt{\overline{v^2}}$ ω and t respectively, and simplifying:

$$0.99\, x\, \theta_1 L^3 + L^2\left(\frac{2D_m x}{U} - \frac{r_{ax}^2}{\sqrt{12}}\right) + \frac{1.343\theta_1^2 D_m x^3}{U} = 0 \qquad (66)$$

Equation (66) was solved for L at the required point in the open

channel to describe the scale of turbulence in the fluid element between the two oxygen analysing cells.

For dispersions behind a grid of bars, was taken as $\tan^{-1} \frac{r_{ax}}{x}$ since the local velocities were not constant over the length of the channel. The equations of Batchelor and Townsend (90) describing the conditions downstream of a grid of bars can also be used to calculate u and L. Their equation relating u to the physical properties of the system is :

$$\frac{\sqrt{\overline{u^2}}}{U} = \frac{\alpha}{\left(\frac{x}{M} - 10\right)^{1/2}} \qquad (67)$$

and for the scale of turbulence L is

$$\frac{L}{M} = \left(\frac{10}{Re_M}\left(\frac{x}{M} - 10\right)\right)^{1/2} \qquad (68)$$

where $\alpha^2 = \frac{C_D}{105.5}$

C_D is a discharge coefficient for the grid given by:

$$C_D = \frac{\frac{d_R}{M}\left(2 - \frac{d_R}{M}\right)}{\left(1 - \frac{d_R}{M}\right)^4} = 1.105 \text{ (for this work)}$$

Re_M is the mesh Reynolds number = $\frac{UM\rho}{\mu}$

d_R is the diameter of the rods in the grid

and M is the mesh spacing

Since both $\sqrt{\overline{u^2}}$ and L varied along the length of the channel between the two oxygen analysing cells at $x = l_1$ and $x = l_2$ respectively, mean values of equations (67) and (68) were used to describe the conditions in the fluid between the cells, i.e.:

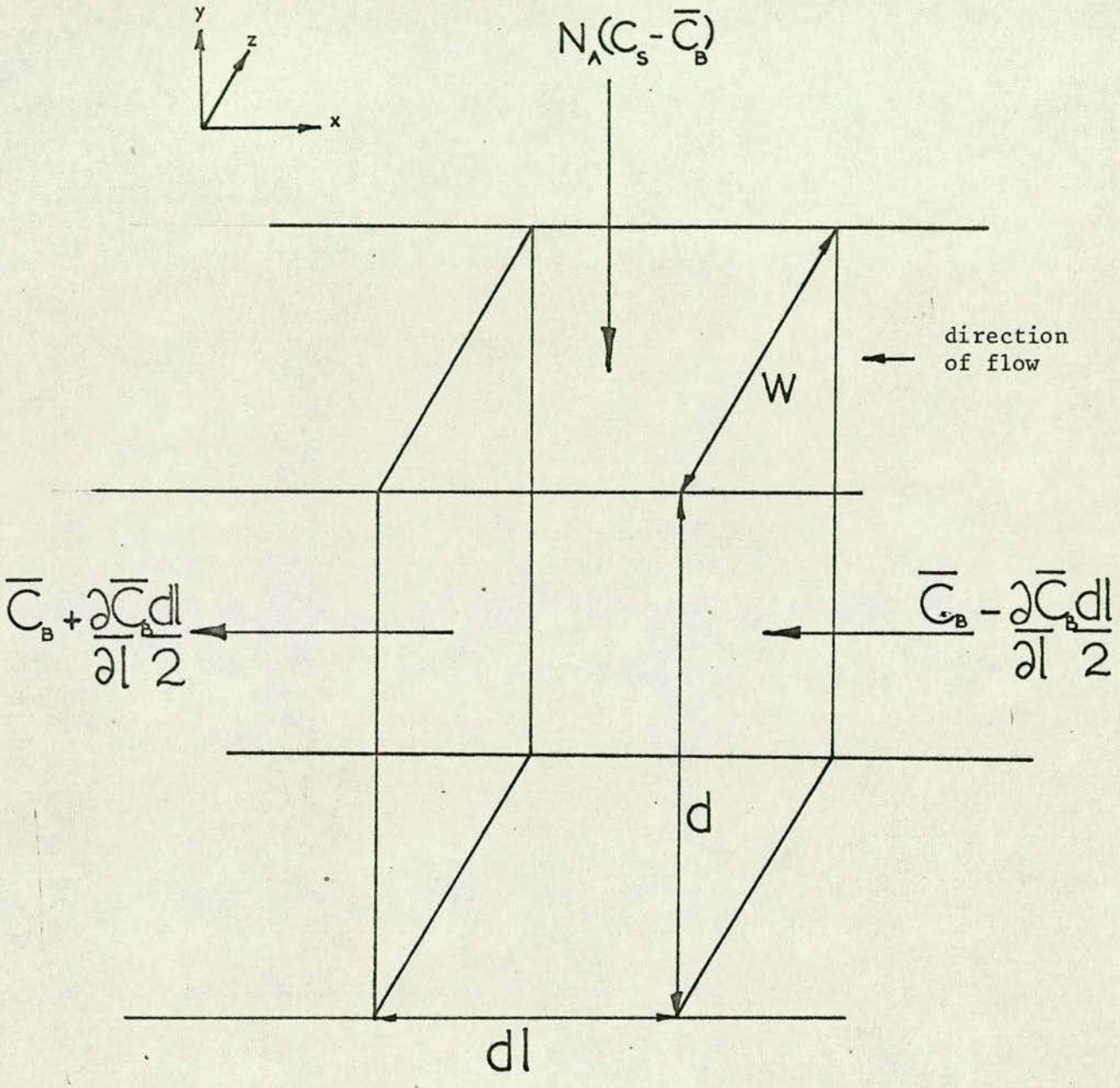

Figure (xvii) Control volume

$$\frac{\sqrt{\overline{u^2}}}{U} = \frac{1}{(l_2 - l_1)} \int_{l_1}^{l_2} \frac{\alpha \, dx}{\left(\frac{x}{M} - 10\right)^{1/2}} \qquad (69)$$

and:

$$L = \frac{M}{(l_2 - l_1)} \int_{l_1}^{l_2} \left(\frac{10}{Re_M} \left(\frac{x}{M} - 10 \right) \right)^{1/2} dx \qquad (70)$$

(4.4) Mass transfer coefficients.

Consider a control volume such as that shown in figure (xix). Taking a mass balance over the control volume:

$$w.d.dl \frac{\partial \bar{C}_B}{\partial t} = w.d.\, U(yz) \left(\bar{C}_S - \frac{\partial \bar{C}_S}{\partial l} \cdot \frac{dl}{2} - \left(\bar{C}_B + \frac{\partial C_B}{\partial l} \cdot \frac{dl}{2} \right) \right) + N_A (C_S - \bar{C}_B)$$

$$\text{i.e.} \quad \frac{\partial \bar{C}_B}{\partial t} = - U(yz) \frac{\partial \bar{C}_B}{\partial l} + \frac{k_L}{d} (C_S - \bar{C}_B) \qquad (71)$$

where $\bar{C}_B$ is the mixed average dissolved oxygen concentration throughout the depth.

C_S is the saturated dissolved oxygen concentration at the free surface.

d is the channel depth.

k_L is the mass transfer coefficient.

N_A is the flux of oxygen through the surface area of the control volume ($N_A = k_L$ w.dl.)

w is the channel width.

If there is a 1st order or a pseudo 1st order chemical reaction taking place, whose rate constant is k_1, then

$$\frac{\partial \bar{C}_B}{\partial t} = - U(yz) \frac{\partial \bar{C}_B}{\partial l} + \frac{k_L}{d} (C_S - \bar{C}_B) - k_1 \bar{C}_B \qquad (72)$$

Since the two oxygen analysing cells cannot be put an infinitesimal distance dl apart, equations (71) and (72) were

converted into finite difference equations:-

$$\frac{\Delta \bar{C}_B}{\Delta t} = - U(yz) \frac{\Delta \bar{C}_B}{\Delta l} + \frac{k_L}{d} (C_S - \bar{C}_{Bav}) \quad (73)$$

and

$$\frac{\Delta \bar{C}_B}{\Delta t} = - U(yz) \frac{\Delta \bar{C}_B}{\Delta l} + \frac{k_L}{d} (C_S - \bar{C}_{Bav}) - k_1 \bar{C}_{Bav} \quad (74)$$

k_L can be found from the above equations since all the other quantities are known or can be found from measurements. The velocity U(yz) used in equations (73) and (74) was that at the oxygen analysing cells.

If instead, the control volume is taken over the entire apparatus, a mass balance yields:

$$\frac{\partial \bar{C}_{Bav}}{\partial t} = \frac{k_L A}{V} (C_S - \bar{C}_{Bav}) \quad (75)$$

where A is the free surface area.

$\bar{C}_{Bav}$ is the mixed average concentration, $\bar{C}_B$, averaged over a length of the channel.

V is the volume being aerated.

Integration of equation (75) gives:

$$\frac{(C_S - \bar{C}_{Bav})}{C_S} = e^{-\frac{k_L A t}{V}} \quad (76)$$

A plot of $\ln \frac{(C_S - \bar{C}_{Bav})}{C_S}$ versus t will have a slope of $-\frac{k_L A}{V}$, from which k_L can be found, since $\frac{A}{V}$ is known. For a uniform channel $\frac{A}{V}$ will be the depth d.

A theoretical equation developed by Fortesque (59) was also used to find the mass transfer coefficient viz:

$$k_L = 1.33 \left(\frac{K D_m \sqrt{\overline{u^2}}}{L} \right)^{0.5} \qquad (77)$$

This equation is based on the hypothesis is that a set of contra-rotating roll cells exists at the free surface. These roll cells were supposed either two or three dimensional with no component of local velocity across the width of the channel. The local velocities in the x and y directions for the two dimensional model were assumed to be of the form

$$u' = A_2 \sin \left(\frac{\pi x}{L} \right) \cos \left(\frac{\pi y}{L} \right)$$

and $$v' = A_2 \cos \left(\frac{\pi x}{L} \right) \sin \left(\frac{\pi y}{L} \right)$$

(where $A_2 = \sqrt{6\ \overline{u^2}}$ ($\sqrt{2\ \overline{u^2}}$ for three dimensional model)).

The equation solved to obtain equation (77) was

$$u' \frac{\partial C_\beta}{\partial x} + v' \frac{\partial C_\beta}{\partial y} = D_m \left(\frac{\partial^2 C_\beta}{\partial x^2} + \frac{\partial^2 C_\beta}{\partial y^2} \right)$$

with the following conditions

(i) $C_\beta = 1$ at $y = 0$

$C_\beta = 0$ at $y = L$

$\frac{\partial C}{\partial x} = 0$ at $x = 0$ (origin of the coordinate system at the free surface).

and $$k_L = - \frac{D_m}{L} \int_0^L \frac{\partial C_\beta}{\partial y} \, dx$$

In equation (77) K is a constant dependent on the eddy model used. For the three dimensional roll cell K = 1, and for the two dimensional roll cell K = 1.233. The inclusion of equation (77) was to check how well the concept of a roll cell model would fit the case of reaeration in rivers.

In equations (73) (74) and (76) the quantities $\overline{C_\beta}$ and $\overline{C_{\beta_{out}}}$ have to be calculated. The method for doing this is given in Appendix V.

Chapter 5.

PRELIMINARY EXPERIMENTS.

(5.1) Object of the experiments.

These preliminary experiments were designed to determine the turbulent velocity profiles and other features of the flow in an open channel and in a river.

(5.2) Velocity profiles in open channels.

The turbulent velocity profiles in open channels are generally represented by (91,92,93,94,95)

$$U = U_s \left(\frac{y}{d} \right)^{1/n} \qquad (78)$$

(where n varies between 5 and 7)

or (96)

$$U = U_s + \frac{1}{\kappa} \ln \left(\frac{y}{d} \right) \qquad (79)$$

Ellison (97) postulates that near a free surface the velocity is given by:

$$U = U_{max} - \frac{2}{m} u_{*_o} \left(1 - \frac{y}{d} \right)^{1/2} \qquad (80)$$

where $u_{*_o} = \frac{\tau_o g_c}{\rho}$

From equation (80) he develops a profile which he claims satisfies both the conditions at the free surface and at the channel bottom, viz.

$$\frac{U - U_{av}}{u_{*_o}} = \left(\frac{b^2 - 1}{b} \right) \ln \left(\frac{b + 1}{b - 1} \right) - \ln \left(\frac{1 + q_1}{1 - q_1} \right) + \frac{1}{b} \ln \left(\frac{b + q_1}{b - q_1} \right) \qquad (81)$$

where

$$b = \left(\frac{m}{m - \kappa} \right) \qquad \text{and } m > \kappa$$

$$q_1 = \left(1 - \frac{y}{d} \right)^{1/2}$$

d is the channel depth

g_c is the gravitational constant

κ is von Karman's constant

m is a constant

U is the overall velocity at y

U_{av} is the average overall velocity in the channel

U_{max} is the maximum velocity

U_s is the velocity at the free surface

y is the distance measured from the bottom of the channel

τ_o is the shear stress at the channel bottom

ρ is the density of the fluid

The above equations (78), (79) and (81) all give a maximum velocity at the surface. This does not agree with observation. Binder (98) remarked in 1956 "The velocity distribution in an open channel is influenced by the walls and also by the free surface. The velocity is usually highest at the point or points least affected by the solid boundaries and the free surface. Experiments have shown that the maximum in a straight open channel may occur at a point below the water surface. No completely rational explanation of these observations has been established at the present time". It is clear that equations (78), (79), (81) only approximately describe flow in an open channel.

In turbulent vertical film flow the velocity profile has a maximum value below the free surface which, according to Lee (99), is due to an interfacial shear stress at the free surface acting caused by layers of fluid at the free surface moving slower than the layers of fluid in the bulk fluid. This may also

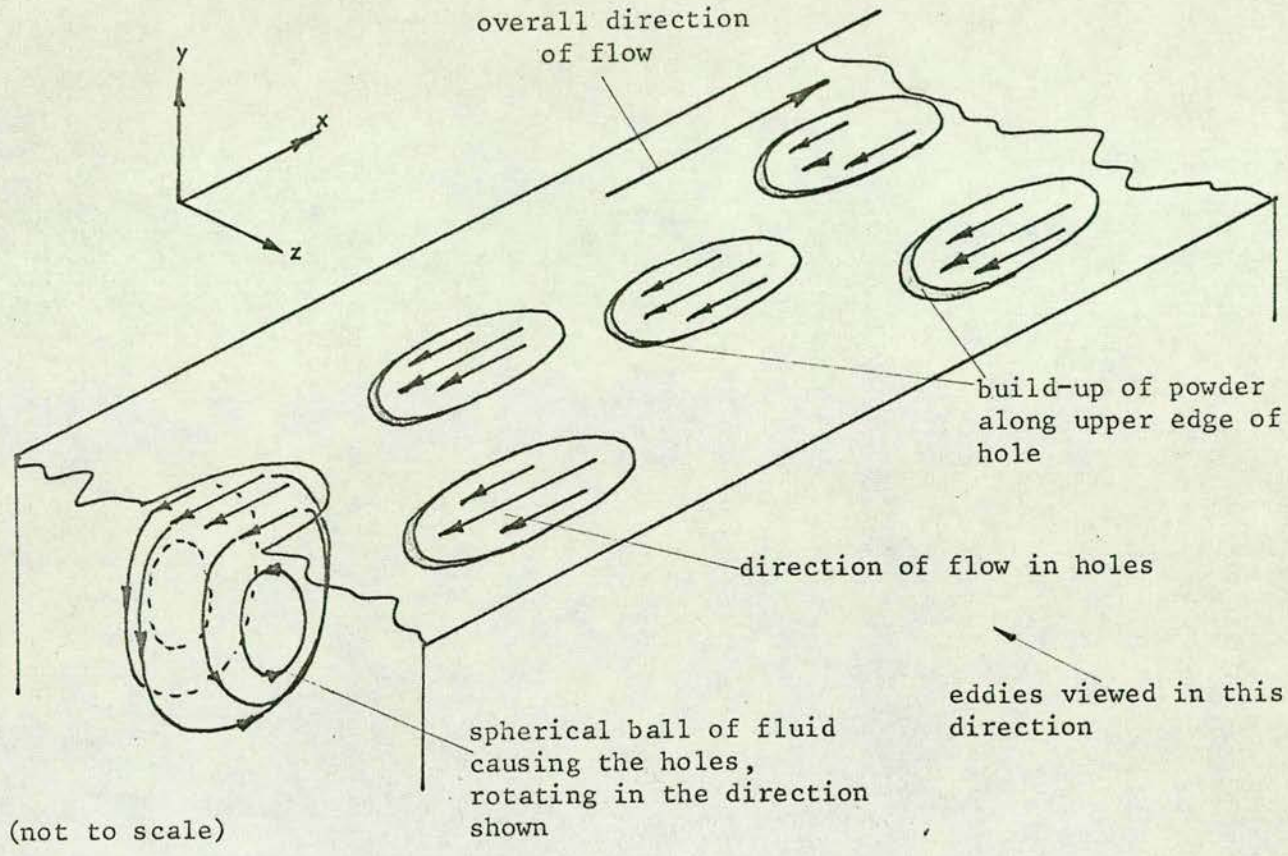

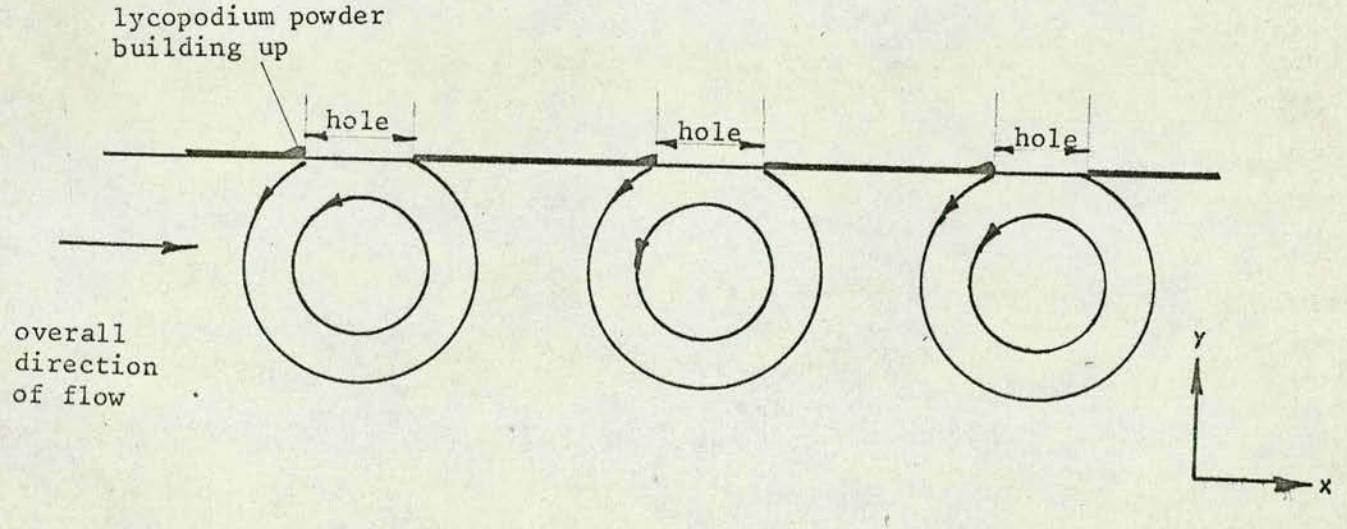

Figure (xix) Unidirectional roll cells at the free surface

be the reason in horizontal flows.

From experiments carried out in this work and from other work (70, 96) there would appear to be a relationship between the velocity at the free surface U_s, the maximum velocity U_{max} and the depth at which the maximum velocity occurs. When the ratios $\frac{U_s}{U_{max}}$ were plotted against $\frac{(d - y)}{d}$ the result was a straight line (see figure (xviii)).

It has been suggested in discussions that secondary flows in the free surface layers are responsible for the reduction in the free surface velocity. To check if secondary flows do occur at a freely moving liquid interface, experiments were carried out in which a thin layer of lycopodium powder was spread carefully over the free surfaces of three different channels (3.25" wide made from perspex; 5.5" wide rough concrete channel and the 6" wide test section).

The results of these experiments showed that there was secondary flow across the width of the channel and that the magnitude of this flow was very small compared with the overall flow in the channels. Secondary flow was also found to occur in the x-direction. Observation of a thin sheet of lycopodium powder as it travelled along revealed that though the sheet of powder moved forward as a whole, localised spots of powder were in fact moving backwards creating circular holes in the sheet of powder with an agglomeration of powder along the upstream edge of the holes (see figure (xix)).

These holes were caused by large eddies at the free surface rotating in an anticlockwise direction compared with the left to

right direction of flow, as in figure (XIX). The scale length of these eddies was comparable with the channel depth. In the Appendix of Ellison's (97) work he deduces that eddies of this size must exist near the free surface in an open channel, from his observations of the character of the surface motion.

In the experiments with the lycopodium powder when the whole free surface was covered near the walls of the open channels there were thin bands of powder moving up and down stream very rapidly and in a random manner as the sheet of powder moved along (see table III of Appendix VI). Between the walls and this randomly moving band the powder moved in the same direction as the fluid. The powder experiments are summarised in figure (XX). The arrows on this figure indicate the directions in which the local velocities in the x-direction were in relation to the overall flow in the channels.

From figure (XX) it will be seen that the local velocity in the x-direction over most of the channel width is against the overall direction of flow. Hence conditions exist where the free surface layers are moving slower than those in the bulk fluid. It is perhaps not this which causes the maximum velocity to be below the free surface but the large eddies at the free surface.

The eddies themselves are perhaps produced by a sinusoidal wave motion at the free surface. If there is an oscillatory "boundary layer" at the free surface of a fluid, Longuet-Higgins (101) has shown that it must generate a second order mean vorticity which diffuses inwards into the interior of the fluid.

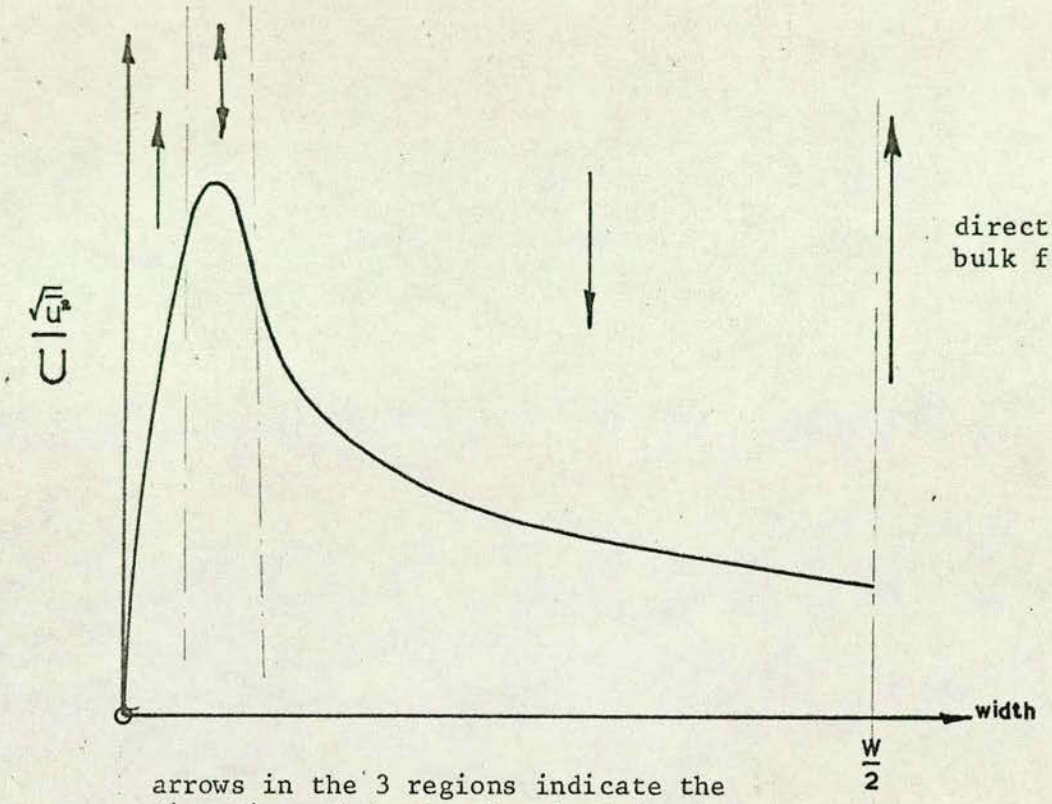

arrows in the 3 regions indicate the direction of the local velocities in relation to the overall velocity

Figure (xx)

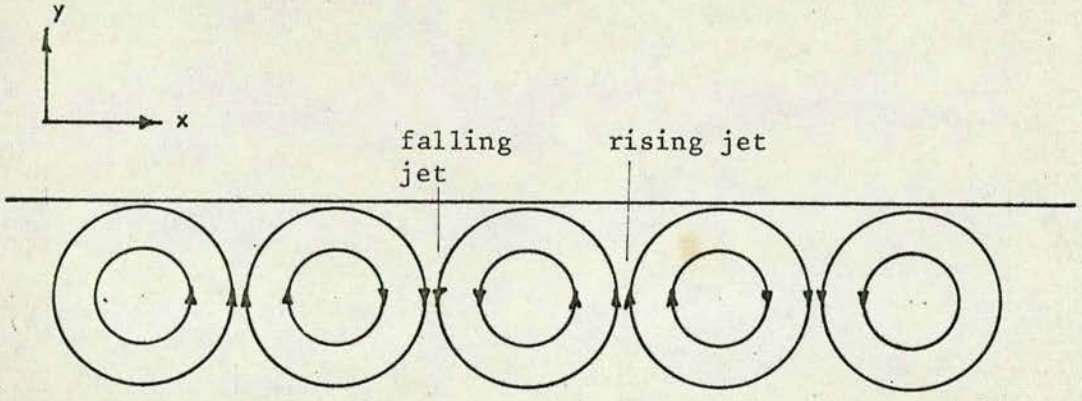

Figure (xxi) Fortesque & Pearson's roll cells

The velocity outside the "boundary layer" resulting from the waves is given by:

$$U_w = \frac{5}{4} \frac{a_4^2 \sigma_4 k_4}{\sinh^2 k_4(d-y)} \qquad (82)$$

where $\frac{2\pi}{k_4}$ is the wave length: $\frac{2\pi}{\sigma_4}$ is the period

and a_4 is the amplitude.

U_w decreases as the distance from the surface layers increases. If the amplitude of the waves in the open channel test section was taken as 1mm, then equation (82) gave velocites which when added to the velocity at y obtained from equation (78) (with n = 7) yielded a velocity profile similar to those obtained in the open channel test section.

The direction of the vorticity at the free surface in an open channel has been shown to be that indicated in figure (xix) at the free surface (102). This was confirmed in this work during the "dye" dispersion experiments. This unidirectional type of eddy system is contrary to what might be expected i.e. sets of contra-rotating eddies such as Fortesque and Pearson (60) assumed to exist at the free surface of channels and rivers. These eddies are characterised by a succession of rising and falling jets as in figure (xxi). The effects produced by the unidirectional eddies on the fluid between them are dispersed by a multitude of very small high frequency eddies and by the minute secondary flows in the direction.

(5.3) Velocity profiles in rivers.

Since there was no information available on river velocity profiles it was decided to repeat the lycopodium powder

experiments on a river along with experiments designed to find the maximum velocity and the depth at which it occurred.

The river chosen was the River Almond, Midlothian. Three different stretches were selected.

(i) 9.5" deep by 48' wide with disturbances a few yards upstream.

(ii) 1' deep by 35' wide and apparently "calm".

(iii) A narrow regular channel 4' deep and 8' wide cut in rocks. A hydraulic jump existed at the inlet to this channel at the time of the experiments.

In order to spread the lycopodium powder over a sufficiently large area of the water surface, the powder was first of all dispersed into the air 7 to 8' above the water so that it formed a large cloud. This cloud eventually settled on the water covering an area of about 200 square feet.

The results obtained from ten identical experiments at each of the three stretches were (a) "holes" appeared in the lycopodium layer similar to those in the open channel but much larger.

(b) periodically at some spots on the free surface, fluid from within a region of radius one foot converged, from three or four directions at the centre of the region, resulting in an annihilation of local momentum at the centre of the region.

(c) at sites (i) and (ii) over a 100 yard stretch, the overall path of the lycopodium powder on the free surface was a slightly zig-zag one, deviating about one foot to either side of a central axis and on average twice to either side within the

100 yards.

The effect of results (b) and (c) will be to cause a further reduction in the free surface velocity compared with the maximum velocity. Observations of suspended matter in the river such as tiny leaves, showed that the large eddies near the free surface in the x-y plane were moving in an anticlockwise direction in relation to the left to right overall motion of the river. The eddies were three dimensional but with no velocity component in the direction across the width of the river.

The overall velocities at different depths were measured by timing objects, floating at different depths, between two points. Ten sets of experiments were carried out at each depth. The results of the experiments are shown in figure (xviii). It will be seen that the predictions of the lycopodium powder experiments mentioned above are borne out i.e. that the free surface velocities are lower than the corresponding ones for open channels.

Also included in figure (xviii) are the results from the open channel test section. From the figure it will be seen that the open channel test section behaves like a river.

(5.4) <u>The effect of surfactants in the test section</u>.

Since there would always be surfactants present in the water used in this work (31,32,33) signs of the effects of surfactants on the flow pattern were sought. It has been shown (41) that surfactants retard the free surface velocities, which might explain why the surface velocities in the test section were lower than the corresponding ones in other open channels.

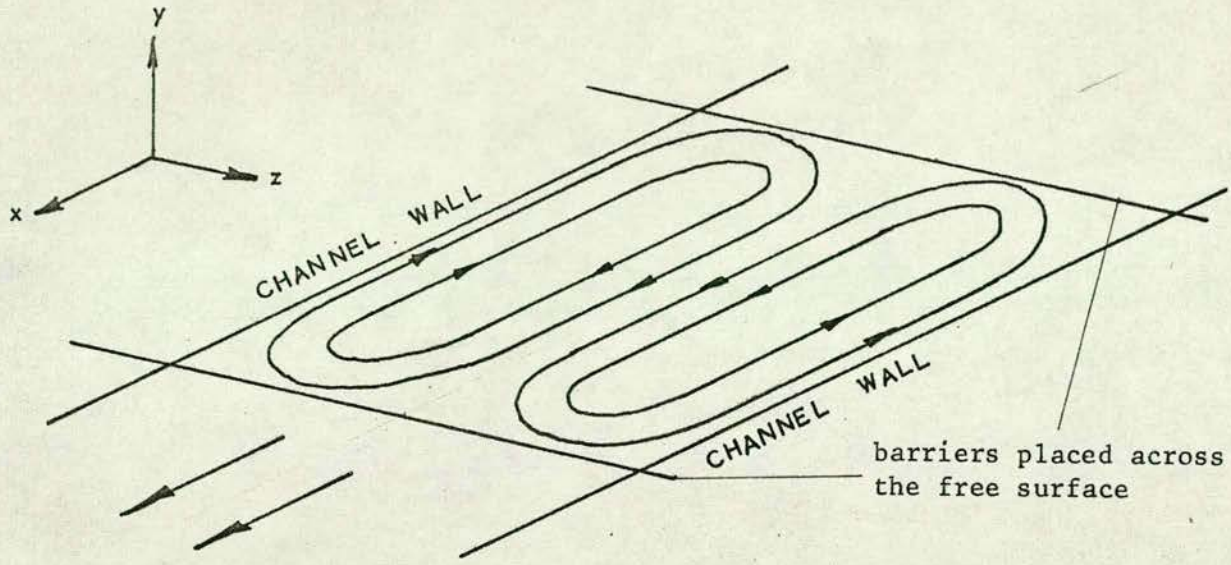

Figure (xxii) Interfacial circulation due to surfactants

The two nozzles at either end of the open channel can be considered as barriers across the free surface. Under such conditions, at the exit end a stagnant film would be expected to grow upstream (33) and there would be interfacial circulation (103) like that shown in figure (xxii).

No stagnant film or interfacial circulation was ever observed during the experiments with lycopodium powder. The reason why these effects were not observed was probably that there was continual free surface clearing by the large eddies.

Chapter 6.

EXPERIMENTAL RESULTS.

(6.1) Specimen Calculation.

Run 16: 1.75 FS

Quantities measured:

(a) From "dye" dispersions

distance over which a "puff" of "dye" was observed for overall local velocity = 20.5 cms.

Distance from channel bottom (cms)	No. of cine frames to record the motion of "dye" over 20.5 cms
15.24	17, 18, 17
14.5	16, 17, 16, 17, 17
14.0	16, 17, 16, 16
13.5	16, 17, 16, 17
13.0	17, 17, 17, 17
12.5	17, 17, 18
12.0	17, 18, 18, 17
11.0	18, 18, 17
10.0	18, 18, 18, 18
9.0	18, 18, 19, 18
8.0	18, 19, 18, 19
7.0	19, 19, 18
6.0	19, 19, 19, 19
5.0	19, 19, 20

θ_1 at free surface = 10.7°

r_{av} = 4.25 cms

x = 22.5 cms

(b) From the mass transfer experiment

Maximum output on recorder ($\equiv C_S$) = 32.22mV $\pm$ 0.005mV

Output used as C_{B1} ($= C_{B2}$ in this case) = 29.84mV

Outputs used to give $\Delta \bar{C}_B$ (at $\pm$5 mins. = 32.60mV

of the output used as C_{B1}) = 27.08mV

$\therefore \Delta \bar{C}_B$ measured output = 5.52mV

Temperature T = 23°C

l_1 = 18.5 cms

l_2 = 26.5 cms

Quantities taken from tables.

D_{m23} for oxygen in water (17) = $2.32.10^{-5}$ cm²/sec

D_{m23} for pyrogallotic acid in water (104) = $0.74.10^{-5}$ cm²/sec

D_{m23} for methanol in water (104) = $1.28.10^{-5}$ cm²/sec

C_{S23} saturated dissolved oxygen concentration in water (104) = 0.004087 gO_2/100g H_2O

The overall local velocity $U = \dfrac{20.5}{\frac{1}{16}(\text{No. of frames required})}$

and at y = 15.24 $U = \dfrac{20.5}{\frac{1}{16} \cdot 17.33}$

= 11.8 cm/sec

The other values for U are tabulated in table IV Appendix VI

From equation (58) the y intensity of turbulence in the sub-surface layers is:

$$\left(\frac{\sqrt{\overline{v}}}{U}\right)_{ss} = \frac{\theta_1}{2.02}$$

$$\left(\frac{\sqrt{\overline{v^2}}}{U}\right)_{ss} = \frac{10.7}{57 \cdot 296.2 \cdot 02}$$

$$= 0.0925$$

From table IV $U = 11.8$ cm/sec

$$\therefore \sqrt{\overline{v^2}} = 0 \cdot 0925 . \ 11 \cdot 8 \text{ cm/sec}$$

From Equation (59)

$$\sqrt{\overline{u^2}} = 0.0925 . \ 11.8 . 1.096$$

$$= 1.196 \text{ cm/sec}$$

From equation (66), for L:

$$0.99x\theta_1 L^3 + L^2 \left(\frac{2D_m x}{U} - \frac{r_{ax}}{\sqrt{12}}\right) + 1.343\ \theta_1 \frac{D_m}{U} x^3 = o$$

$$D_m = \left(0.92 . 0 \cdot 74 + 0.08 . \ 1 \cdot 28\ \right) . 10^{-5} \text{ cm}^2/\text{sec}$$

$$= 0 \cdot 78 \ . 10^{-5} \text{ cm}^2/\text{sec}$$

$$U = 11.8 \text{ cm/sec}$$

i.e. $L^3 - L^2\ 1 \cdot 257 + 4 \cdot 625 . 10^{-4} = 0$

$$L = 1.256 \text{ cms}$$

Calculation of k_L from equation (73)

(i) $\Delta \bar{C}_B = 0.0000701\ g\theta_2 / 100g\ H_2O$

$\Delta t = 10 \times 60$ secs.

$\frac{\Delta \bar{C}_B}{\Delta l_1} = 0$ i.e. $C_{Bl_1} = C_{Bl_2} = C_B$

$C = 0.003787\ g\theta_2 / 100g\ H_2O$

From equation (xii) of Appendix (V)

$$C = \left(\frac{C_{Bl_2} + C_{Bl_1}}{2}\right) - \frac{(C_B - C_{Bl_1})(y_{Bl_1} - d)(l_2 + l_1)}{4\ dl_1}$$

$$+ \frac{(C_{Bl_2} - C_{Bl_1})(y_{Bl_1} - d)(2l_2 + l_1)}{12\ dl_1}$$

$$= C_B - \frac{(C - C)(y_{Bl_1} - d)(l_2 + l_1)}{4\ dl_1}$$

$$= 0.003787 - \frac{(0.0003)(14.4 - 15.24)(26.5 - 18.5)}{4\ 15.24.\ 18.5}$$

y_{α_1} is obtained from table VIII, Appendix VI.

l_1 is the distance between the leading oxygen analysing cell and the entrance to the open channel.

l_2 is the distance between the second oxygen analysing cell and the channel entrance.

$$\bar{C}_{Bav} = 0.003787 + 0.00001$$

$$= 0.003797\ gO_2/100gH_2O$$

From equation (73)

$$k_L = \frac{\Delta \bar{C}_B}{\Delta t} \frac{d}{(C_s - \bar{C}_{Bav})}$$

$$= \frac{0.0000701\ \ 15.24}{10.\ 60\ \ \ (0.0004087 - 0.003797)}$$

$$= 0.0061\ cm/sec$$

k_L calculated from equations (77)(59) and (66)

$$k_L = 1.33. \left(\frac{K\ D_m \sqrt{\bar{u}^2}}{L} \right)^{0.5}$$

K = 1 since three dimensional eddies exist at the free surface

$$k_L = 1.33. \left(\frac{2.32.\ 10^5\ .\ 1.196}{1.256} \right)^{0.5}$$

$$= 0.0063\ cm/sec$$

$$\bar{U}_{av} = \frac{7}{8d} \sum_{y=0}^{d} \bar{U}(y)$$

$$= 0.875.\ 10.81$$

$$= 9.46\ cm/sec$$

$$d_{HD} = \frac{dw}{(2d + w)} \qquad (d=w=15.24\ cms)$$

$$= 5.08\ cms$$

$$\therefore \quad Re_{HD} \text{ at } 23^{\circ}C = \frac{U_{av}\, d_{HD}\, \rho}{\mu}$$

$$= \frac{9.46.\ 5.08.\ 0.9976}{0.009358}$$

$$= 5130$$

$$(Re_{HD})^{0.5} = 71.6$$

From these values of k_L, $\frac{k_L}{U_{av}}$ values were calculated i.e.

$$\frac{0.0061}{9.46} = 0.00065$$

$$\frac{0.0063}{9.46} = 0.00066$$

The above figures were then multiplied by $(Re_{HD})^{0.5}$

$$0.00065.\ 71.6 = 0.0465$$

$$0.00066.\ 71.6 = 0.0473$$

(6.2) Results obtained from the "dye" dispersion experiments.

(a) No obstacles in the test section.

The velocities at different depths were obtained by counting the number of cine frames required to record the motion of a puff of "dye" between two points. These measurements were not affected by the presence of the eddies as was the case with the pitot tube. The time interval between each frame was 1/16th of a second, measured by filming a clock with a seconds hand over a period of two minutes and then counting the number of frames required to record the motion of the hand.
The velocities were measured at the inlet and at the exit. No difference was found between these velocities. Thus there were uniform conditions along the open channel.

The velocities obtained for five settings of the valve on

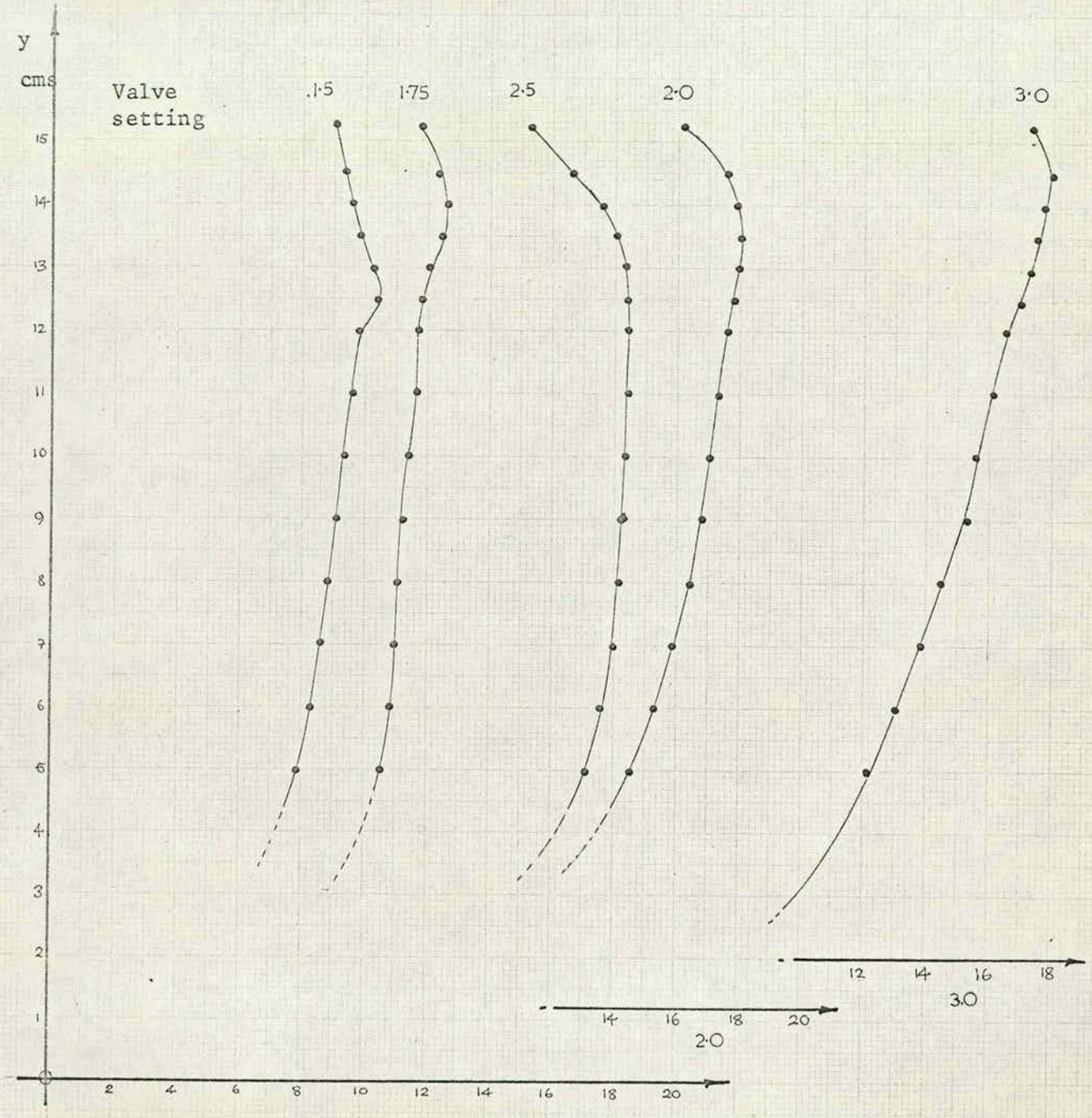

Figure (xxiii) Velocity profiles in open channel at different valve settings

obtained from the "dye" dispersions. In the surface layers however, the values obtained from Batchelor and Townsend's equations were about a third of those obtained from the "dye" dispersions via equations (59) and (66). These results were not surprising since Batchelor and Townsend's equations were derived from experiments in a closed duct. The fact that the equations were obtained with a gaseous medium does not affect the results obtained in this work since Batchelor and Townsend's results have been shown to hold for a liquid medium (105).

Since the two methods agree over 80% of the depth it can be inferred that the values of $\sqrt{u^2}$, $\sqrt{v^2}$ and L obtained from the "dye" dispersion records in the free surface region are in fact correct.

(c) Handy Angle obstacles in the test section.

The first experiments were carried out to find the effect on the "dye" dispersion of varying distances between these obstacles and the channel inlet. The obstacles were placed at 1", 3" and 6" from the end of the inlet nozzle and all three "dye" injectors were used at a fixed distance from the obstacle. The corresponding "dye" dispersions were compared, No difference was found between the corresponding "dye" dispersions downstream of the obstacles. All subsequent experiments were therefore carried out with the Handy Angle obstacles placed 1" downstream from the end of the inlet nozzle. The Handy Angle obstacles are hereafter referred to as H.A.O. with a number after the initials indicating the height of the obstacle in inches.

When the cine film was being analysed it was noticed that at some depths the "dye" did not start to disperse until some

the rubber hose are tabulated in Appendix VI, table IV. The numbers for the valve settings represent the distance, in inches, between the two marks on the clamp tubing. The data is plotted in figure (xxiii). The velocities are the averages of three or more results at each depth and valve setting.

The angles from which the turbulent intensities were calculated are tabulated in Appendix VI table V. The dispersion shapes were obtained by recording the projected images from a whole series of frames on top of one another till a solid outline of the observed dispersion was made. The three corrections were then applied to the observed dispersion record. The angle measured was that between the tangent to the dispersion at the origin and the x-axis of the dispersion.

(Although a pitot tube was incorporated in the apparatus it could not be used to find the overall velocities in the surface layers. This was due to the effect of the large eddies at the impact tube of the pitot tube, resulting in a fluctuating pressure difference. The pitot tube was only used as a check in lower depths of the channel).

(b) 9G Grid in the test section.

The object of these experiments was to check the validity of the methods used to find $\sqrt{u^2}$, $\sqrt{v^2}$, and L by comparing the results with those obtained from Batchelor and Townsend's equations (67) and (68).

The results obtained (see Appendix VI table VI) showed that over 80% of the depth the agreement was good between the values of $\sqrt{u^2}$ and L obtained from equations (67) and (68) and those

distance downstream of the obstacle. These distances along with the local overall velocities, U, and the dispersion angles, θ_1, are given in Appendix VI, table VII. Only three valve settings were used in these experiments. The data for the cylindrical brass obstacle is also given at the end of table VII. h_o in the right hand column of table VII, H.A.O. height in centimetres.

Table VII is shown graphically in figures (XXIV) and (XXV). Figure (XXIV) shows how the y-direction intensity of turbulence at different depths varies with the height of the obstacle. Although a definite trend in the data is evident only approximate values for the y-direction turbulent intensity can be obtained from figure (XXIV). Figure (XXV) indicates the extent of a non-diffusing region above a submerged obstacle.

From the "dye" dispersion records, governed by the conditions marked with an asterisk in tables IV, V and VII, the relationships between $\sqrt{\overline{u^2}}$ and $\sqrt{\overline{v^2}}$, and $\sqrt{\overline{v^2}}/U$ and the angle θ_1, were found. These relationships are given in section (4) equations (58) and (59). In the depths of the liquid in the experiments with the 9G grid, the ratio between $\sqrt{\overline{u^2}}$ and $\sqrt{\overline{v^2}}$ was found to be $\sqrt{\overline{u^2}}/\sqrt{\overline{v^2}} = 1.4$ which is the ratio normally found in closed ducts (106).

(6.3) Discussion of the "dye" dispersion results.

It is observed that the DC - and - y-direction turbulent intensities with no obstacles in the test section are two to three times as large in the free surface regions of the fluid as those in the bulk of the water. The scale of turbulence, L, is larger to a similar degree. Thus the apparent eddy diffusivity at the free surface is four to nine times as large as that in the lower

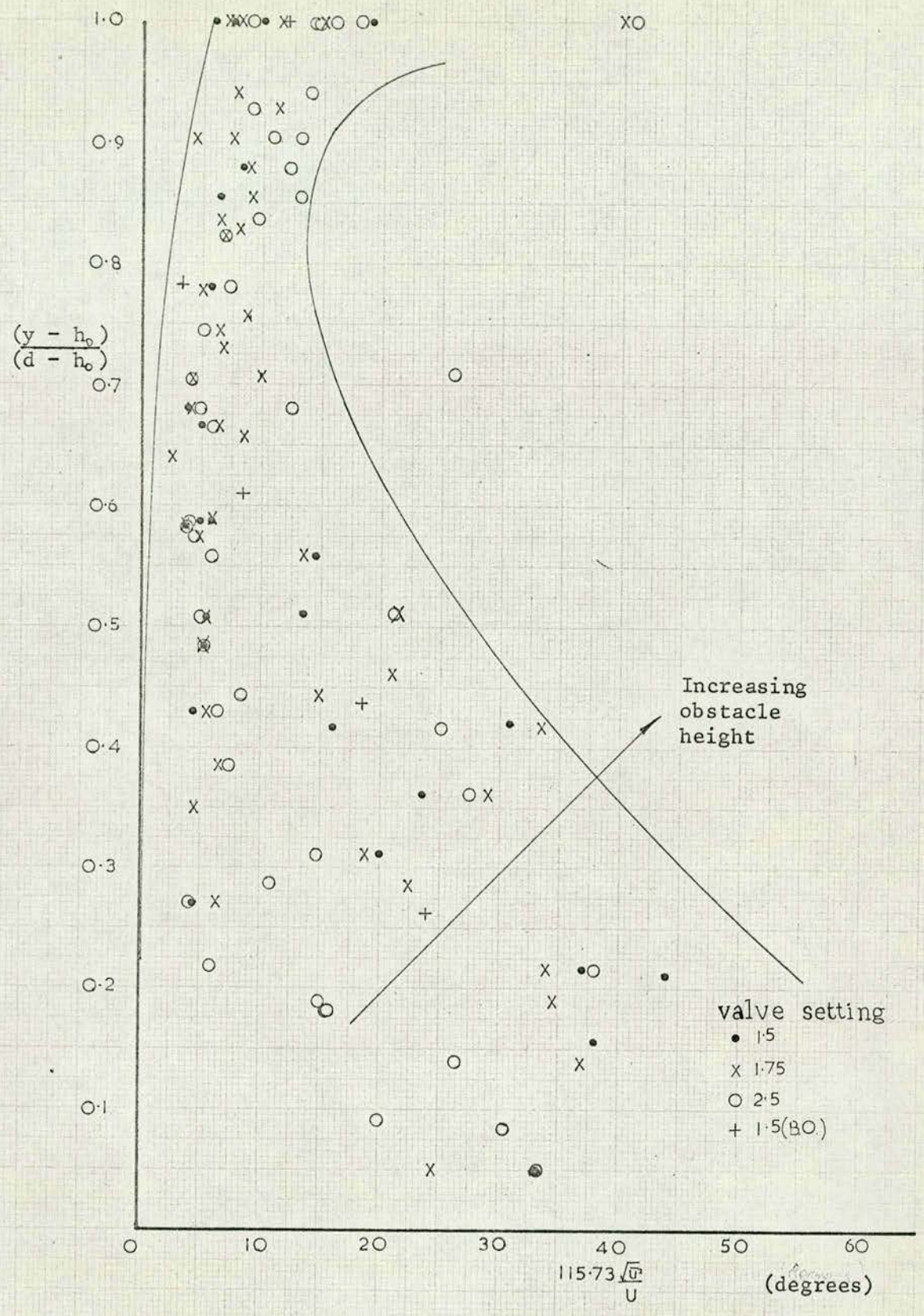
1·0
0·9
0·8
(y - h₀)
(d - h₀)
0·7
0·6
0·5
0·4
0·3
0·2
0·1
0
10
20
30
40
50
60
115·73 √ū / U
(degrees)
Increasing obstacle height
valve setting
• 1·5
X 1·75
O 2·5
+ 1·5(BO.)

Figure (xxiv)

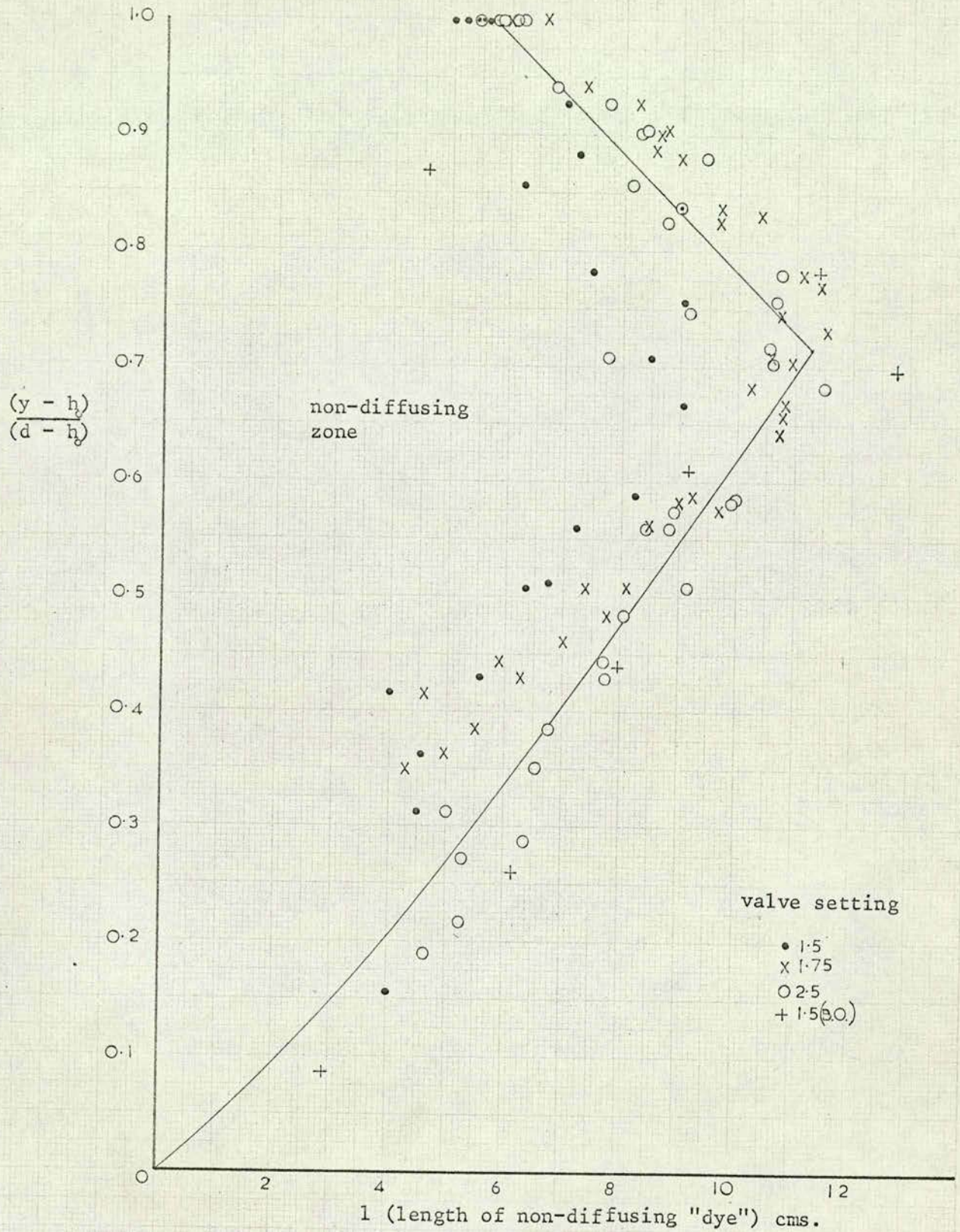
1·0
0·9
0·8
0·7
0·6
0·5
0·4
0·3
0·2
0·1
0
(y - h)/(d - h)
non-diffusing zone
valve setting
• 1·5
X 1·75
O 2·5
+ 1·5(B.O.)
2
4
6
8
10
12
l (length of non-diffusing "dye") cms.

Figure (x_{xv})

depths. This is contrary to the reports of Kalinske and Pien (70), who found that the eddy diffusivity was a maximum at approximately half the depth. Although Kalinske and Pien used the wrong equation to evaluate the eddy diffusivity, the eddy diffusivity variation found here does follow the pattern of their results in the bulk of the fluid. But at a point of 20% of the depth below the free surface the preseht experiments show that the eddy diffusivity starts to increase rapidly to a maximum at or near the free surface.

The implications of figure (XXV) are that the large eddies which dominate the free surface regions in the case of an unobstructed channel are altered by the presence of obstacles. The results are summarised in figure (XXVI). With the high obstacles, the direction of rotation of the large eddies was changed and the size of the eddy increased. With obstacles whose height is about two thirds the channel depth, the effect was to remove the large eddies completely. With smaller obstacles the eddies rotated in the same direction as the large eddies in an obstacle free channel but were reduced in size.

By placeing five of the H.A.O. 4.0 obstacles behind one another, a distance of 2.5" apart, it was possible to eliminate the large eddies from the whole open channel test section. This multiple obstacle was therefore a suppressor of secondary flow.

"Dye" dispersion experiments were carried out in the River Almond to find out if stones and boulders in a river produced the same sort of non-diffusing region as in figure (XXV). No records of the "dye" traces were taken and only visual observations were

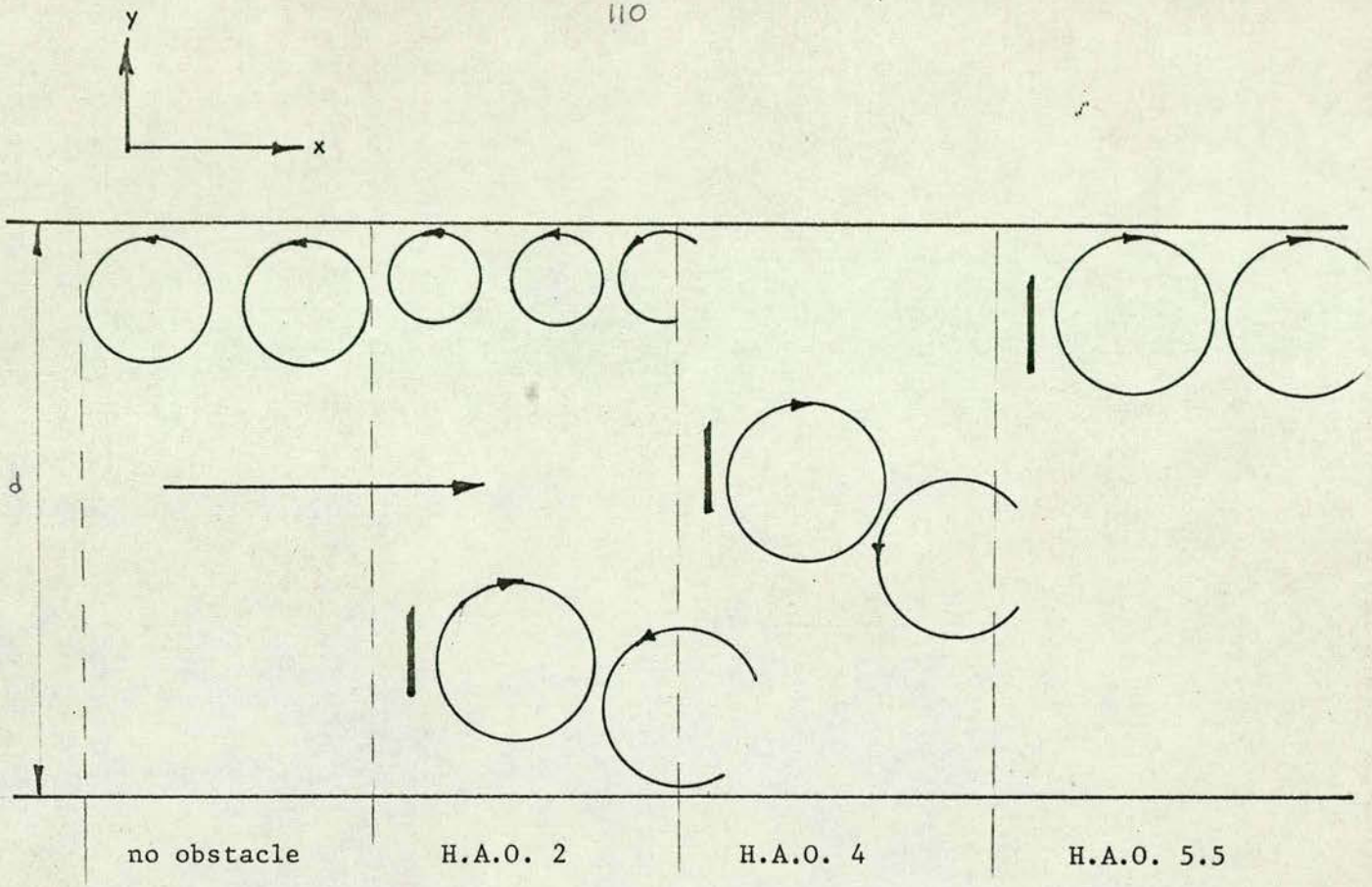

Figure (xxvi) Effect of H.A.O. height on eddy rotation at the free surface

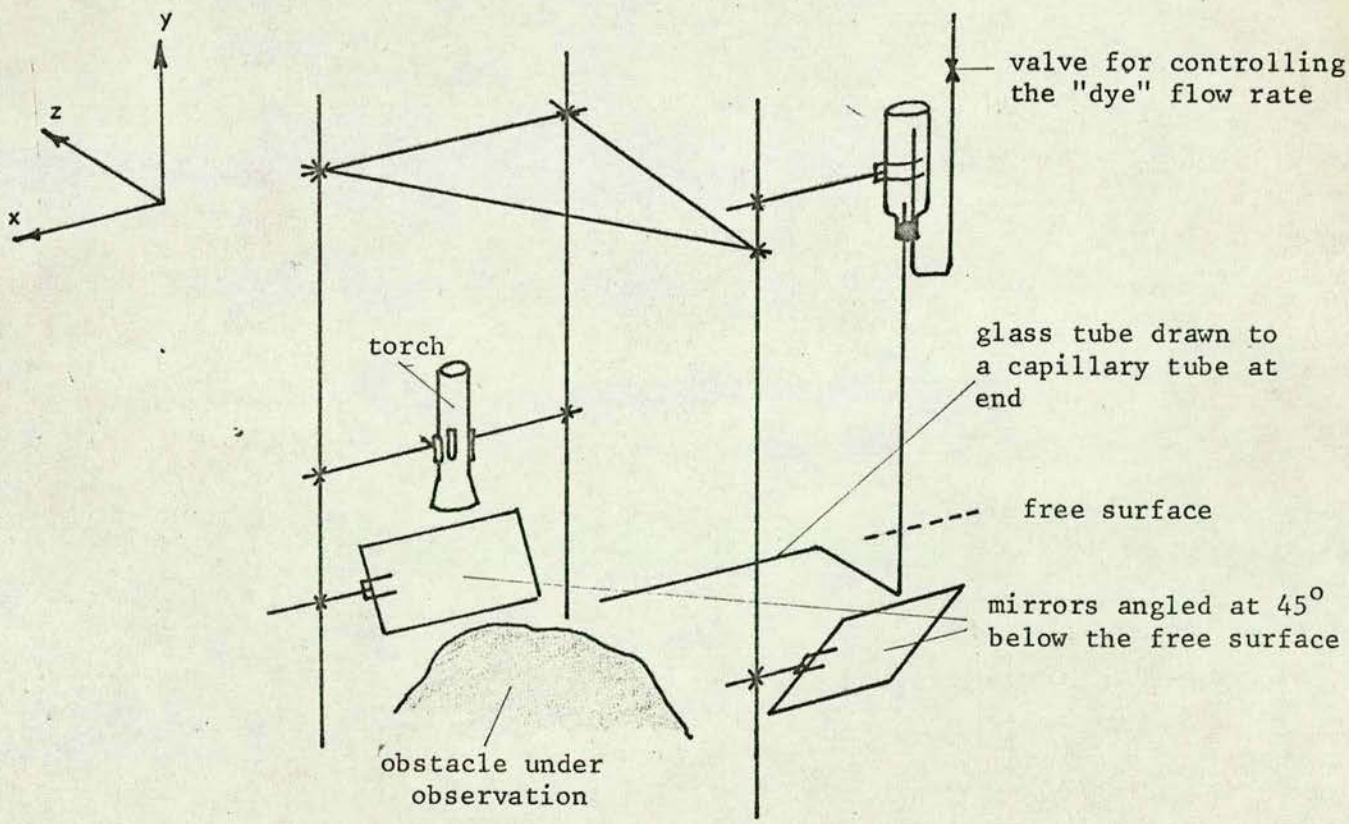

Figure (xxvii) Apparatus for "dye" dispersions in rivers.

made. The apparatus used is shown in figure (XXVII). The dispersions obtained showed a very marked similarity to those obtained with the obstacles in the open channel. Moreover the results found with the cylindrical brass obstacle in the channel were similar to those obtained with the Handy Angle obstacles. Thus the multiple obstacle can be considered as a group of boulders whose sizes are such that they will suppress turbulence.

When turbulence is promoted in an open channel or river it was observed in these experiments that the effect persists for a considerable distance downstream, but when the turbulence is suppressed the calming effect suddenly ceases within a predictable distance. When two obstacles were placed in close proximity (about 2.5" apart) the length of the non-diffusing portion of the "dye" dispersion at the second obstacle was increased by 50%.

(6.4) Mass Transfer experiments.

(a) Distance, $y_B(x)$, over which the bulk concentration C_B, extends.

The experiments to find $y_B(x)$ for different conditions in the channel were executed in the same manner as the mass transfer experiments described in sections (3.5b). The experiments were carried out with the oxygen analysing cells at 5,7,9,11,13,13.7, 14.3,14.7 and 15 cms. from the channel bottom in each case. Experiments carried out at different distances from the channel entrance confirmed that $y_B(x)$ was a linear function in x, the distance along the channel from the inlet nozzle outlet. The values of y_{BL}, used in equation (xii) of Appendix V are summarised in table (VIII).

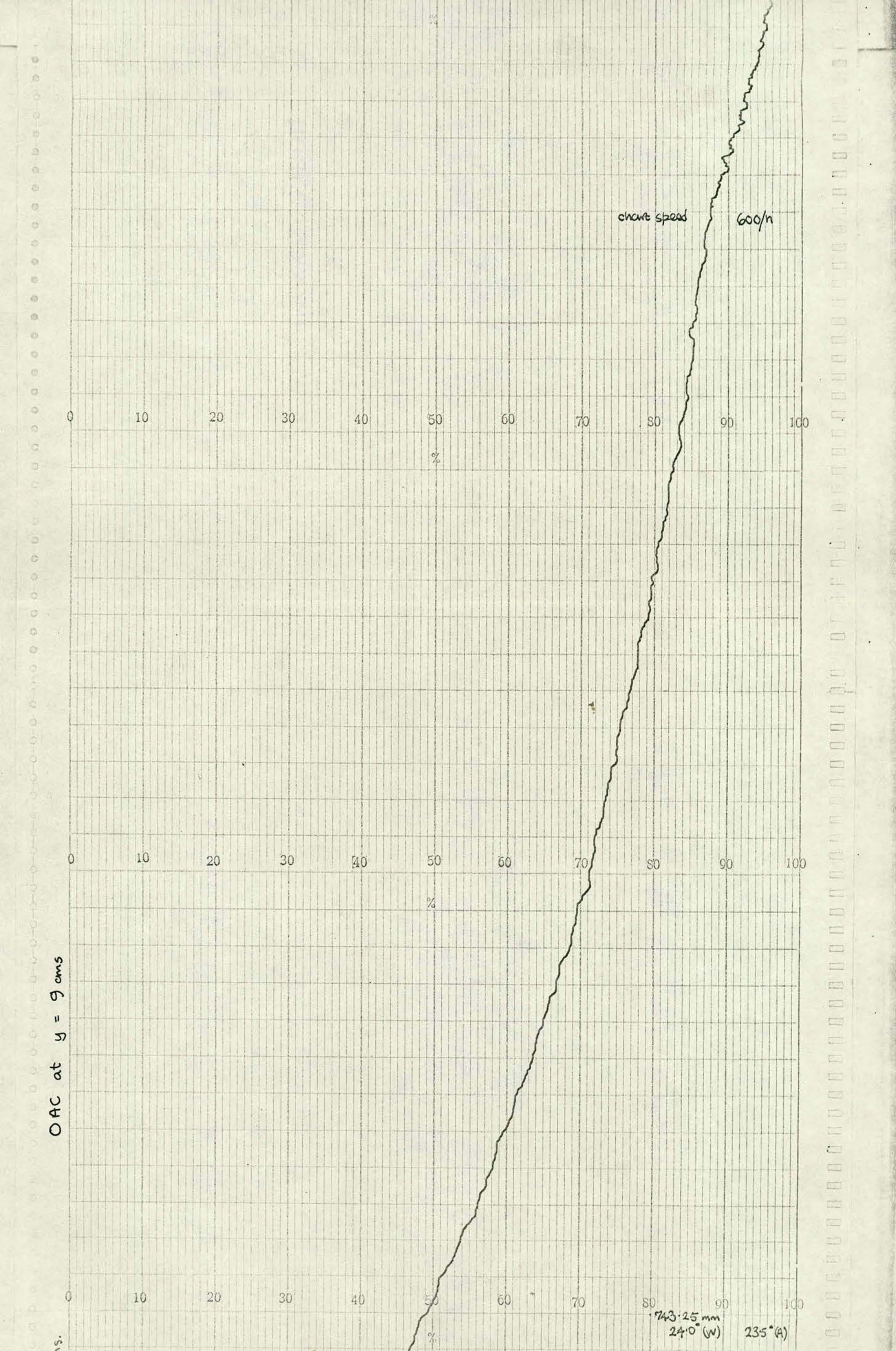
chart speed 600/h
0 10 20 30 40 50 60 70 80 90 100
%
OAC at y = 9 ams
743·25 mm
24·0° (W)
235° (A)

figure xxviii

O.AC. at y = 13 cms

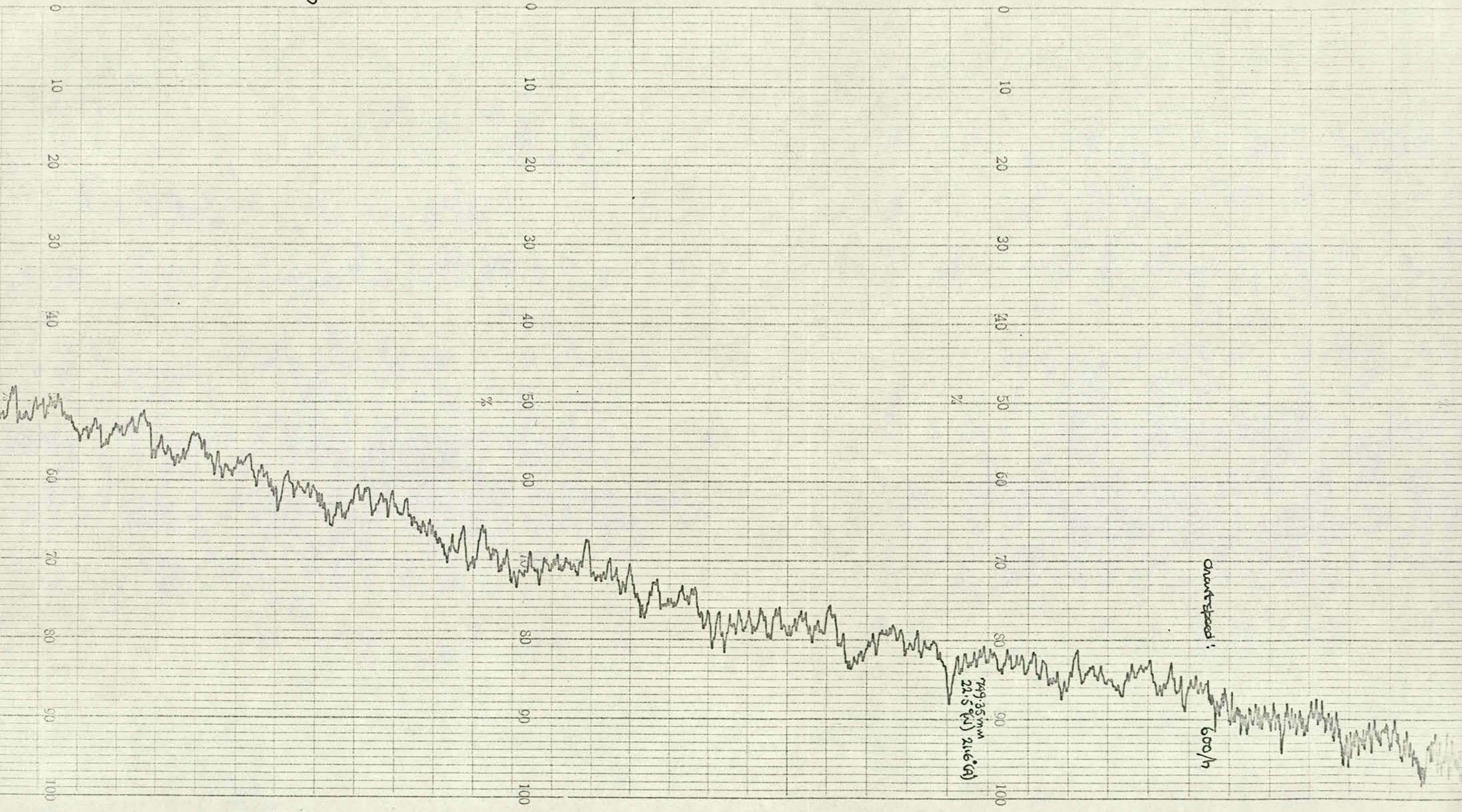

The function $C_B(x)$ was found to be an almost linear function in x over the whole channel length and the function can be considered linear between l_1 and l_2 a distance 8 cms. apart.

Figure (xxviii) is two chart records for the case 1.75 with no obstacles present. The oxygen analysing cells were at y = 9 and 13 cms. respectively. This figure gives an indication of the reproducibility of the above experiments. It also gives the impression that the observed fluctuations indicate the rate at which the large eddies in the free surface region bring in fluid with a higher oxygen concentration from the free surface.

(b) Reaeration results.

The mass transfer coefficients calculated from equations (59)(66)(69)(70)(73)(74)(76) and (77) are listed in Appendix VI table (IX). For the experiments with no obstacles, 9G grid and H.A.O. 5.5, the oxygen analysing cells were situated at 10 cms. from the channel bottom and for the multiple object runs at 13 cms. Another set of runs were carried out with the cells at 7 cms. from the channel bottom in all cases. In both sets of experiments the distance from the end of the inlet nozzle to the leading oxygen analysing cell was 18.5 cms.

The value of K used in equation (77) for the H.A.O. 5.5 case was that for a two-dimensional eddy, and for the 9G grid and the obstacle free cases the three-dimensional value was used.

(6.5) Discussion of the mass transfer coefficient results.

There is little or no difference, in some cases, between the mass transfer coefficient obtained via equations (73) and (74), and equation (76) even though equation (76) will only give overall

mass transfer coefficients. The explanation for such good agreement could be either that the position chosen to measure the local mass transfer coefficient in the channel was that corresponding to the average mass transfer coefficient for the whole channel, or that the mass transfer coefficient was almost constant over the entire length of the open channel.

The work of Watson and Thomson (107) agrees with the results obtained in this work for the mass transfer coefficients with turbulence promoters present in an open channel. In their work they were investigating forced convective mass transfer of a ferro-ferricyanide redox system in a channel 2.5" deep by 0.49" wide. Their turbulence promoters were 0.0625" diameter and 0.09375" diameter cylinders placed near the free surface with their axes across the width of the channel. These obstacles were equivalent to 5.75" high Handy Andy obstacles in a 6" deep open channel. With one cylinder in the open channel the mass transfer coefficients were double that with no cylinders present, which is the same increase as that found in this work between no obstacle present and H.A.O. 5.5 for all the valve settings used.

The theoretical equation of Fortesque (59) equation (77), agrees with the results obtained from equations (73)(74) and (76) for all cases except those for the multiple obstacle. This was expected since Fortesque has pointed out that equation (77) does not hold for small values of $\sqrt{u^2}$ and L.

The above observation can be explained in another way. Models for mass transfer work are normally described by (1) a system of eddies within which matter is transferred by molecular

diffusion or (ii) a system which can be described by a true eddy diffusivity. In this work from the "dye" dispersion observations the obstacle free and H.A.O. 5.5 cases are described by both systems but mainly by the large eddies. In the multiple obstacle case, only system (ii) describes the conditions that exist. Hence as equation (77) was derived from a model described by system (i), it will not hold for a system described by a true eddy diffusivity. An apparent eddy diffusivity can be used to describe system (i).

In the case 1.5, 9G grid, the last mass transfer coefficient, which is about 20% lower than the others in this group, was obtained by using Fortesque's own equation for L in equation (77). The equation Fortesque used was:

$$L = M\left(\frac{x}{160M} + 0.1\right)^{\frac{1}{2}} \qquad (82)$$

which is of the form

$$L = M\left[\frac{10}{1600}\left(\frac{x}{M} + 16\right)\right]^{\frac{1}{2}} \qquad (83)$$

and comparing the above equation with equation (68) i.e.

$$L = M\left[\frac{10}{Re_M}\left(\frac{x}{M} - 10\right)\right]^{\frac{1}{2}} \qquad (68)$$

equation (83) will give larger values for L than equation (68) for the corresponding x. Hence the mass transfer coefficients calculated from equations (77), (69) and (83) will be lower than those calculated from equations (77) (69) (70). This is one explanation why Fortesque's experimental results are lower than the theoretical prediction between Re_{HD} of 1000 and 2500 (see the group of lines on the left hand side of figure (xxix)).

Another cause could have been that the value of u^2 calculated from equation (69) was wrong for his situation. Fortesque placed his grids inside a closed duct some distance upstream of the channel entrance. In most cases there was a sudden enlargement of the fluid at the free surface where the duct opened out into the open channel. Uberoi and Wallis (106) have shown that when enlargements and contractions take place downstream of a grid, the turbulent intensity, in all three directions of space, is altered. Hence equation (69) will cease to apply in Fortesque's case after the enlargement. Furthermore the results of this work show that the turbulent intensity at a free surface behind a grid is increased by a factor of about three. There is also the fact that in some cases the grids were ineffective since the flow in the entrance duct was laminar. The lowest Reynolds number (based on an equivalent pipe diameter) attained in the duct during his "turbulent" runs was 1710 and the highest 4270.

In the open channel it appears that the conditions for Fortesque's experiments were those in the laminar/turbulent transition region. The fluid in an open channel changes from turbulent motion to laminar motion at a hydraulic depth Reynolds number of 300 (144) but the change in the other direction from laminar to turbulent motion is not fully attained till much higher Reynolds numbers are reached. The value of the hydraulic depth Reynolds number for this transition was found to be 3000 in this work, from the "dye" dispersion experiments, and 2400 in the work of Watson and Thomson (107). This means that all

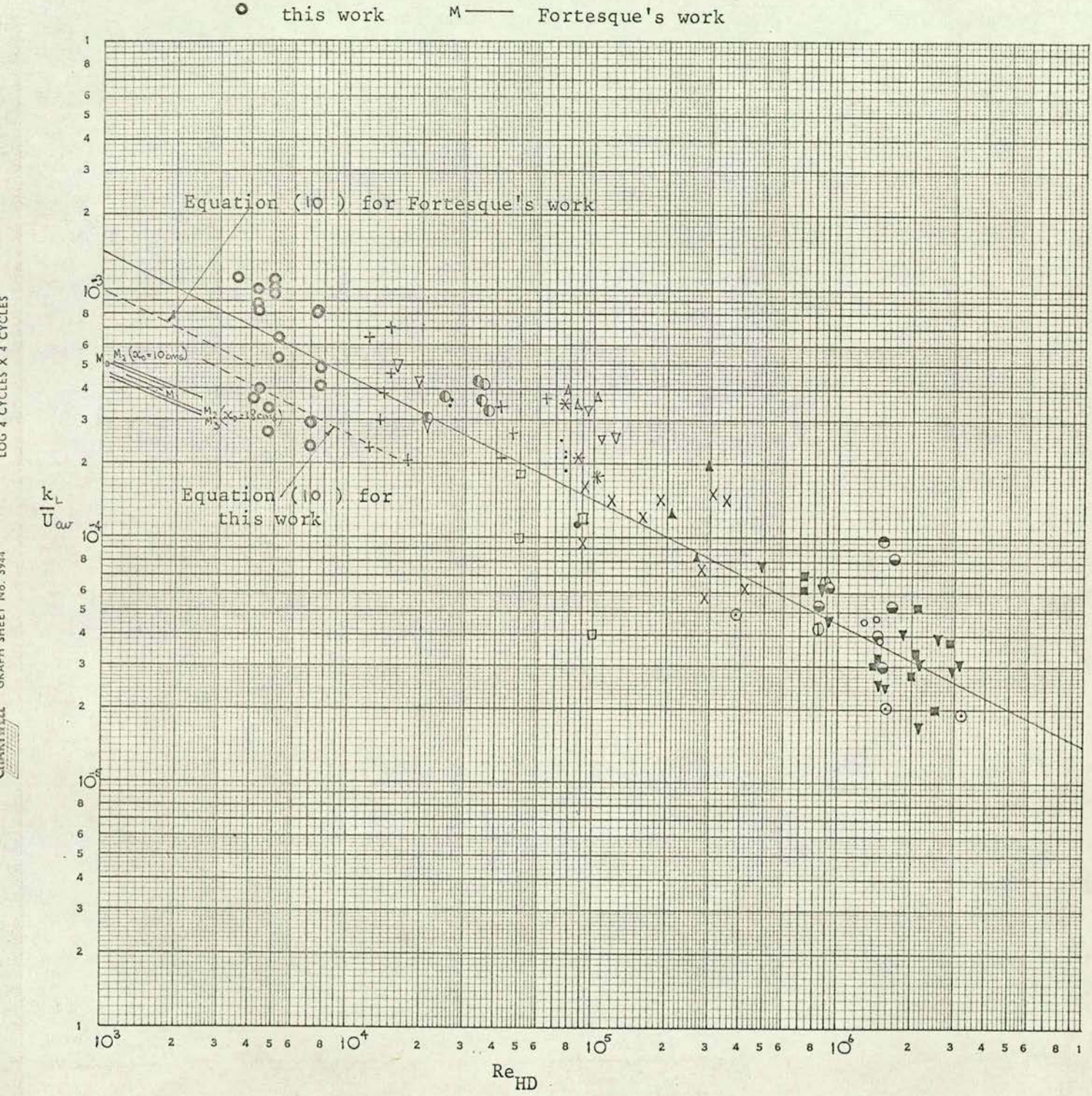
this work
Fortesque's work
Equation (10) for Fortesque's work
Equation (10) for this work
$\frac{k_f}{U_{\omega}}$
Re_{HD}

Figure (xxix)

Fortesque's results lie within the laminar/turbulent transition region and as a consequence his experimental results would not be expected to agree with his theory which was developed from fully turbulent flow assumptions.

The mass transfer coefficients obtained in this work are plotted in figure (xxix). The data used is contained in Appendix VI table X. From figure (xxix) it can be seen that the scatter of the experimental results obtained in this work was of the same magnitude as that of other workers in rivers. The values of $\frac{k_i}{\bar{U}_{av}}$ obtained were multiplied by the square root of the corresponding hydraulic depth Reynolds number and plotted against the y-direction turbulent intensities, as in figure (xxx). The data used is tabulated in Appendix VI table X. Because of the possible difference between the apparent and true eddy diffusivity, the eddy diffusivity was not used to correlate $\frac{k_i}{\bar{U}_{av}} \cdot (Re_{HD})^{0.5}$.

In figure (xxx), the experimental errors associated with the data are shown by the shaded areas surrounding the points. In figure (xxix) the agreement between the experimental results and the theoretical prediction is to within 250%. In figure (xxx) the discrepancy between the experimental results and the theoretical prediction is 10%, which it is reasonable to suppose corresponds to the limits of experimental accuracy. It appears likely that the omission of a variable viz. the turbulence intensity, accounts for the large discrepancy recorded in figure (xxix).

The apparent "eddy diffusivity" is one which is used to characterise the conditions of a mixture of laminar eddies and diffusion in a fluid. In this work the laminar eddies and the diffusion appeared to be, from the "dye" experiments, present to an equal extent.

It would probably be better to refer to the apparent "eddy diffusivity" as a dispersivity.

Chapter 7.

CONCLUSIONS.

The correltaion relating the mass transfer of atmospheric oxygen into flowing water to the hydrodynamic variables of the situation is of the from described by equation (23) in chapter 1 viz.

$$\frac{k_L}{\bar{U}_{av}} = A_1 \left(\frac{D_m \rho}{\mu}\right)^{0.5} \left(\frac{U_{av} d_{HD} \rho}{\mu}\right)^{-0.5} \left(\frac{\sqrt{\overline{v^2}}}{\bar{U}}\right)_{ss}^{\alpha} \qquad (23)$$

From figure (XXX), A_1 is ~~0.13~~ 2.65 and α is 0.5 and equation (23) therefore becomes:

$$\frac{ki}{\bar{U}} = \text{~~0.13~~ } 2.65 \left(\frac{D_m \rho}{\mu}\right)^{0.5} \left(\frac{U_{av} d_{HD} \rho}{\mu}\right)^{-0.5} \left(\frac{\sqrt{\overline{v^2}}}{\bar{U}}\right)_{ss}^{0.5} \qquad (84)$$

In order to apply equation (84) to rivers, the quantity $\left(\frac{\sqrt{\overline{v^2}}}{\bar{U}}\right)_{ss}$ has first of all to be evaluated.

It would be ideal if figure (XXiV) could be used to provide this information since it is easier to measure the heights of obstacles and the corresponding depths in rivers than it is to measure the y-direction turbulent intensities.

The way in which equation (84) would be used to control river pollution is as follows:

(i) The dissolved oxygen concentration in the river at some fixed point downstream is set at a specific value, and it is specified that the dissolved oxygen concentration between the effluent discharge point and the fixed point must remain above a certain level.

(ii) The river reach downstream of the effluent discharge point is divided into areas within which the y-direction turbulent intensities are the same.

(iii) From equation (84), the mass transfer coefficient is calculated for the area at the point of effluent discharge.

(iv) Using this mass transfer coefficient in equation (74), the dissolved oxygen concentration of the water flowing out of the discharge area is found.

(v) Repeat (iii) and (iv) for the next area downstream and so on till the area in which (a) the chemical reaction has ceased, in which case equation (73) is then used, or (b) the required dissolved oxygen concentration is obtained at the fixed point.

(vi) If the dissolved oxygen concentration falls below the minimum value set for the stretch of river before the fixed point is reached, then the value of k_1, the reaction rate constant, used in equation (74) has to be changed by altering the amount and/or quality of the effluent discharged.

(vii) The correct solution is reached when the two conditions in (i) are met.

It is possible that when a river level rises the mass transfer coefficient decreases. This would occur if obstacles present in the river were of the H.A.O. 5.5 type which would become the H.A.O. 4.0 type when the river level rose. Or the mass transfer coefficient would increase when the level rises i.e. when obstacles of the type H.A.O. 4.0 become H.A.O. 2.0 and H.A.O. 1.0 type obstacles. The implication of this is that the amount and quality of effluent which could safely be dumped into a river would vary from month to month (or even week to week) as the river conditions varied. Hence for complete control of effluent disposal agreement would have to be reached between

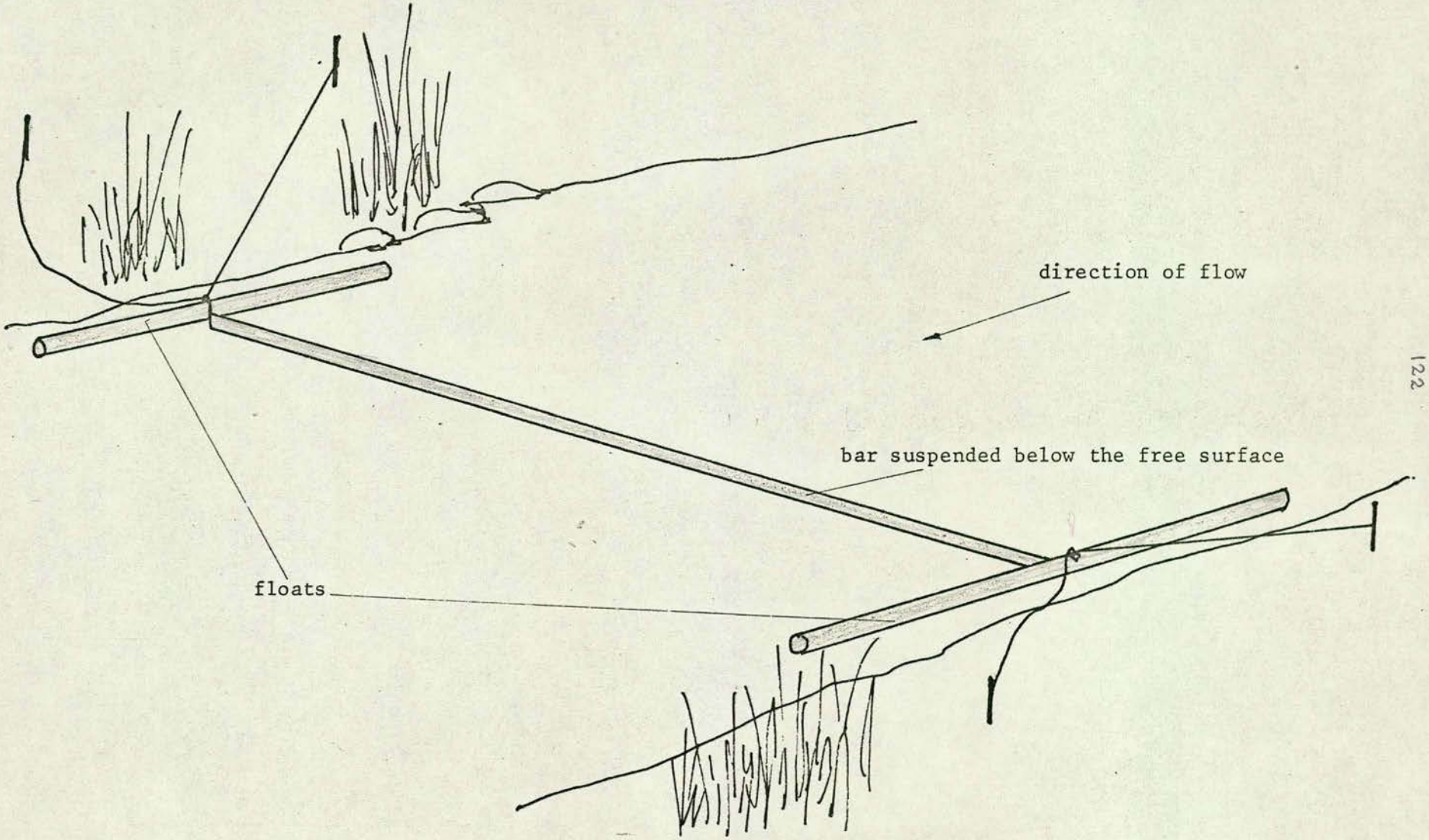

Figure (xxxi) Apparatus for increasing turbulence intensity in rivers.

River Boards and industry as to an acceptable seasonal rate of effluent discharge.

It should be possible to increase the effluent load which a river can safely accommodate by increasing the mass transfer rates in stretches of the river where the rate would be low. Figure (XXXi) shows a device which could be used to promote turbulence in rivers. This device is based on H.A.O. 5.5 and is made to float at a set distance below the water level. Just how far apart these turbulence promoters should be spaced would have to be determined from future work in a longer open channel.

Future work in this field should include also

(a) Similar experiments to those carried out in this work but at hydraulic depth Reynolds numbers of the order of 10^6, since equation (84) is only valid for Reynolds number range 3000 to 8000.

(b) Determination of the effect of several different obstacles in an open channel at one time. This experiment would require a much longer open channel.

(c) An attempt to clarify figure (XXiV) so that it can be used for rivers.

(d) Using 1,3 - Butadiene as the gas phase under the same experimental conditions as those used in this work.

If the same conclusions are reached at the high Reynolds numbers as in this work, then the correlation of equation (84) will hold over all turbulent ranges found in rivers. The results from the experiments where there were several obstacles present could lead to a simplification in the pollution control problem

by doing away with the need to divide a river into areas of similar y-direction turbulent intensities. The use of 1,3 - Butadiene would provide a check on this work and confirm the exponent of 0.5 on the Schmidt number in equation (84).

Fortesque and Pearson's (60) hypothesis of roll cells with rising and falling jets, figure (XXi), certainly does not hold in rivers and open channels at the free surface. The mechanism is one of unidirectional roll cells at the free surface and the direction of rotation of these cells, when they exist, is the dominant factor governing the mass transfer rates. These roll cells have been observed in rivers and open channels.

Those roll cells which rotate in a clockwise direction, in the x-y plane, compared to the left to right overall motion of the water, i.e. those produced by H.A.O. 5.5 type obstacles, tend to increase the mass transfer rates above "normal" which is produced by anticlockwise rotating cells. When the size of the roll cell diminishes or the roll cell ceases to exist (i.e. when the system is described by a true eddy diffusivity) then the mass transfer rate decreases to a low value.

Because of the wide variation in $\sqrt{\overline{u}^2}$ and L from place to place in rivers, $\sqrt{\overline{u}^2}$ and L cannot be taken as one tenth the overall average velocity and depth respectively as O'Connor and Dobbins (17), and Fortesque (59) have done when comparing the calculated mass transfer coefficients from equations (8) and (77) respectively with the observed values from rivers.

Despite the setbacks encountered, this work has achieved what it set out to do, namely to shed some light on the process

of reaeration in rivers and to suggest a way of calculating and increasing the rate of oxygen uptake of a given river.

NOMENCLATURE.

a	area of silver electrode or constant
a_{123}	constants
a_q	wave amplitude
A	area of free surface being aerated or thermistor constant.
A_1	constant
$-A_G$	amplifier gain
b	constant
B	thermistor constant
c	constant
C	dissolved oxygen concentration
C_B	dissolved oxygen concentration in the bulk of the fluid
C_D	coefficient of discharge for a grid of bars
C_S	saturated dissolved oxygen concentration
$\bar{C}_s$	mean dissolved oxygen concentration in yz plane
$\bar{C}_{Saw}$	mean $\bar{C}_B$ over distance x
$C(x,o)$	"dye" concentration at axis of dispersion
$C(x,r)$	"dye" concentration at a distance $\sqrt{x^2 + r^2}$ from the origin
d_{12}	channel depth
d_{HD}	hydraulic depth
d_R	diameter of rods in grid
D_e	eddy diffussivity
D_M	molecular diffussivity
F	Faraday (96500 coulombs)
g_c	gravitational constant
h_D	height of obstacle in the channel

ΔH_s	heat of solution
i	maximum current available from cell on short circuit
I_{out}	output current from amplifier
J	cell constant
k	constant
k_1	reaction rate constant
k_2	reaeration coefficient
$\frac{2\pi}{k_4}$	wavelength
k_L	mass transfer coefficient
K	constant or cell constant
l	half the length of a chord or the length of the non-dispersing part of the dispersion or the membrane thickness
l_1	distance from channel entrance to first O.A.C.
l_2	distance from channel entrance to second O.A.C.
L	scale of turbulence
m	constant
M	mesh length
n	constant or number of electrons taking part in cell reaction
N	total number of particles at the origin at t = o
N_A	flux of oxygen through the surface area of the control volume
P	permeability coefficient of the membrane
P(x,o)	probability that the particle is on the x-axis
P(x,r)	probability that the particle is a distance $\sqrt{x^2 + r^2}$ from the origin

q	rate at which matter is injected
q_1	constant
Q	total matter between two yz planes a distance δx apart
r	radial distance from the x-axis
$\sqrt{\overline{r^2}}$	root mean square radial distance
r_{ax}	radial distance at which $C(xr_a) = 0.00248\ C(x,o)$
r_{ex}	radius at which the "dye" disappears on the cine film record at a distance x from the point of injection
r_o	radius of injector tube
R	distance from the point of injection to the point under consideration or resistance
R_{1-8}	cell load resistances
$R_{23456789}$	network resistances
R_{av}	average value of R_{1-8} over temperature range
R_c	universal gas constant
R_{Th}	thermistor resistance
Re	Reynolds number based on the depth
Re_{HD}	Reynolds number based on hydraulic depth
Re_M	Reynolds number based on mesh spacing
$R(\theta)$	correlation coefficient (Lagrangian)
s	number of dimensions or rate of surface renewal
ss	sub-surface layers of fluid
S	solubility parameter
S_o	solubility parameter at $T = T_o$
t	time
T	temperature
T_1	lower limit of temperature range
T_N	upper limit of temperature range

T_*	mid point of temperature range
u_w	velocity caused by waves
u'	local velocity in x-direction
u_{*o}	friction velocity at channel bottom
$\sqrt{\overline{u^2}}$	root mean square local velocity in x-direction
U	overall velocity in x-direction
U_{av}	average overall velocity
U_{max}	maximum overall velocity
U_s	free surface overall velocity
v_i	maximum overall velocity at nozzle inlet
v'	local velocity in y-direction
$\sqrt{\overline{v^2}}$	root mean square local velocity in y-direction
V	voltage
V_{AB}	voltage across AB
V^*_{AB}	voltage across AB at $T = T_*$
$(V_{AB})_{av}$	average voltage across AB
w	channel width
x	direction along the length of the channel
X_a	function of r_{ax}
X_e	function of r_{ax} and r_{ex}
y_{i23n}	direction or distance measured from channel bottom
y_B	distance over which C_B extends
Z_{123}	distance across the width of the channel
α	constants
β	constant or function of r_{ax} and r_{ex}
∇	operator
θ	time interval

θ_1 half angle of dispersion

κ von Karman's constant

μ viscosity or refractive index

ξ time interval

ρ density

σ standard deviation, which is a function x, and is a measure of the dispersion

$\frac{2\pi}{\sigma_4}$ period of oscillation

τ_o shear stress at channel bottom

ϕ potential function or function

ψ stream function

ω vorticity

$\phi_1(X_a)$ function of X_a

$\phi_2(X_e)$ function of X_e

References.

1. W.P.R.L. "Effects of polluting discharges on the Thames Estuary". Water Research Tech. Paper No.11.

2. H.M.S.O. "Methods of Chemical Analysis as Applied to Sewage and Effluents". London (1956)

3. Soc. for Anal.Chem. "Recommended methods for the Analysis of Trade Effluents". London (1958).

4. Clough G.F.G. & Abson J.W.: The Chem.Eng. No.177 CE58 (1964).

5. Kirby A.W.W.: ibid No.177 CE76 (1964).

6. Franklin J.S., Colville J.E., & Bowes E.: ibid No.177 C.E.68 (1964).

7. Downing A.L. & Wheatland A.B.: Trans. I.Ch.E. 40 91 (1962)

8. Downing A.L. & Bayley R.W.: Trans. I.Ch.E. 39 A53 (1961).

9. Private Communication - source John Brown (Contractors).

10. Private Communication - source D.C.L. Distilleries. Cambus. Stiringshire.

11. Clough G.F.G.: The Chem.Eng. No.202 C.E.228 (1966).

12. Gameson A.L.H. & Truesdale C.A.: T. Inst. Water Eng. 13 No.2 (1959).

13. _____ & Downing A.L.: ibid 9 571, (1955).

14. _____ & Varley R.A.: The Water & San. Eng. Aug. (1956).

15. Ogden C.G., Gibbs J.W. & Gameson A.L.H., The Water & Waste Treatment Jr. Oct. (1959).

16. Owens M., Edwards R.W. & Gibbs J.W., Int. J. of Air-Water Pollution 8 469 (1964).

17. O'Connor D.J. & Dobbins W.E.: Proc. Amer.Soc.Civ.Eng. 82 546 paper 115 (1956).

18. Churchill, Elmore & Buckingham; Int. J. of Air-Water Pollution 6 467 (1962).

19. W.P.R.L. "Surface Aeration"; report (1965).

20. Streeter H.W., Wright C.T. & Kehr R.W.: Sewage Works Journal VIII No.2 (March 1936).

21. Lewis W.K. & Whitman: Ind. Eng. Chem. 16 1215, (1924).

22. Higbie R.: Trans.Am.I.Ch.E. 31 365 (1935).

23. Danckwerts: Ind.Eng.Chem. 43 1460 (1951).

24. Taylor G.I.: Proc.Roy.Soc. 151A 428 (1935).

25. Toor H.L. & Marchello J.M.: A.I.Ch.E.Jl. 4 97 (1958).

26. Harriot P.: Chem.Eng.Sci. 17 149 (1962).

27. King C.J.: I. & E.C. Fund 5 1 (1966).

28. Krenkel P.A., & Orlob G.T.: Proc.Am.Soc.Civ.Eng., San.Eng. Div.

29. D.S.I.R. "Notes on Water Pollution" No. 26 Sept. (1964).

30. Yagi S. & Inoue H.: Chem.Eng.Sci, 17 441 (1962).

31. Hickmann K.C.D.: Ind.Eng.Chem. 44 1892 (1952).

32. Hickmann K.C.D. & Torpey W.A.: Ind.Eng.Chem. 46 1446 (1954)

33. Merson & Quinn: A.I.Ch.E.Jl. 11 391 (1965).

34. Scriven L.E. & Pigford R.L.: ibid 4 434 (1958).

35. Ruckenstein, E.: Chem.Eng.Sci. 20 853 (1965).

36. Ternovskaia A.N. & Belopolski B.P.: Zhur.Fiz.Khim. 24 43 (1950).

37. Emmert E.E. & Pigford R.L.: Chem.Eng.Prog. 50 87 (1954).

38. Tailby S.R. & Portalski: Trans.I.Chem.Eng. 39 328 (1961).

39. Chiang S.H. & Toor H.L.: A.I.Ch.E.Jl. 5 165 (1959).

40. Duda J.L. & Vrentas J.S.: Chem.Eng.Sci. 22 27 (1967).

41. Farley R.W. & Schechter R.S.: ibid 21 1079, (1966).

42. Brow, Zazuhiro, Sato & Sage.: Ind.Eng.Chem. Eng.Data Series 3 263 (1958).

43. Batchelor G.K.: The Theory of Homogeneous Turbulence Cambridge Univ. Press (1953).

44. Hanratty T.J. & Engen J.N.: A.I.Ch.E.Jl. 3 299 (1957).

45. Cohen L.S. & Hanratty T.J.: ibid 11 138 (1958).

46. _____ : J. of Fluid Mech. 31 499 (1968)

47. Smith T.N. & Tait R.W.F.: ChemEng.Sci. 21 63 (1966).

48. Chou C.H. & Charles M.E.: Can.J.Chem.Eng. 46 143 (1968).

49. Hanratty T.J. & Hershman, A. .: A.I.Ch.E.Jl. 7 488 (1961).

50. Lilleht, L.U. & Hanratty T.J.: ibid. 7 548 (1961).

51. Charles M.E, & Lilleht, L.U.: J.Fluid Mch. 22 217 (1965).

52. Miles J.W.: ibid. 6 583 (1959).

53. Boyd D.P. & Marchello J.M.: ibid. 21 769 (1966).

54. Banerjee S., Rhodes E., & Scott D.S.: ibid 22 43 (1967).

55. Stainthrop F.P. & Wild G.J.: ibid 22 701 (1967).

56. Ruckenstein E. & Berbente.: ibid 20 795 (1965).

57. _____ : Int.J. Heat & Mass Transfer 11 743 (1968).

58. Makers D. Grant, Westfield, Edinburgh.

59. Fortesque G.E.: Ph.D. Thesis Cambridge (1965).

60. _____ & Pearson J.A.R.: ChemEng.Sci. 22 (1967).

61. Daily J.W. & Chu T.K.: M.I.T. Hydrodynamics Lab. Tech. Report No. 48.

62. _____ & Hardison R.L.: ibid No. 67.

63. _____ & Shen C.L.: ibid No. 68.

64. _____ & Roberts C.P.R.: ibid No. 69.

65. Elata C. & Ippen A.T.: ibid No. 45.

66. Robertson A.A.: T.A.P.P.I.

67. Elata C: Bull.Res.Council of Israel 10C 93 (1961).

68. Kada H. & Hanratty T.J.: A.I.Ch.E.Jl. 6 624 (1960).

69. Bobkowiez A.J. & Gauvin W.I.T.: Can.J.Chem.Eng. 43 2,87 (1965).

70. Kalinske A.A. & Pien C.L.: Ind.Eng.Chem. 36 220 (1944).

71. Jas. Walker Co.Ltd.,: Lion Works, Woking, Surrey.

72. Notes: C.P.E. 49 21 (1968).

73. Garstang J.: Ph.D. Thesis Edinburgh (1968).

74. Towle W.L. & Sherwood T.K.: I. & E.C. 31 457 (1939).

75. Topping J.: "Errors of Observation and their Treatment". The Institute of Physics & the Physical Soc. Monograph for Students. Chapman Hall, London, (1962).

76. Levich V.G.: "Physiochemical Hydrodynamics" Prentice Hall, N.J. 1962.

77. Kalinske A.A. & Pien C.L.: I. & E.C. 36 220 (1944).

78. Baldwin L.W. & Walsh T.J.: A.I.Ch.E.Jl. 7 53 (1961).

79. Mickelsen W.R.: N.A.C.A. Tech. Note 3570 (1955).

80. Uberoi M.S. & Corrsins.: N.A.C.A. Tech.Rep. 1142 (1953).

81. Sutton O.G.: Proc.Roy.Soc. A135 143 (1932).

82. Wilson H.A.: Proc. Cambridge PhilSoc. 12 406 (1904).

83. Flint C.L., Kada H. & Hanratty T.L.: A.I.Ch.E.Jl. 6 325 (1960).

84. Prattle R.E.: Quart.J.Mech.Appl.Math. 12 407 (1959).

85. Crank, J.: Mathematics of Diffusion Oxford Univ.Press(1956)

86. Mickelsen W.R.: J. of Fluid Mech. 7 397 (1960).

87. Schubauer G.B.: N.A.C.A. Tech.Rep. 524 (1935).

88. Saffman P.G.: J. Fluid Mech. 8 273 (1960).

89. Townsend A.A.: Proc.Roy.Soc. A224 487 (1954).

90. Batchelor G.K. & Townsend A.A.: ibid A194 527 (1948).

91. Falkner V.M.: Aircraft Eng. 15 65 (1943).

92. von Karman.: N.A.C.A. Tech. Memo 1092 (1946).

93. van der Hegge-Zijnen B.G.: Thesis Delft 1924.

94. Hansen M.: N.A.C.A. Tech. 585 (1930).

95. Burgess J.M.: Proc.Intern.Cong. Appl.Mech. 1st Cong. Deftt. 113 (1924).

96. Vanoni V.A.: Civil Engineering 11 356 (1941).

97. Ellison T.H.: J.Fluid Mech. 8 33 (1960).

98. Binder R.C.: "Fluid Mechanics" Prentice Hall N.Y. 1956.

99. Lee J.: Chem.Eng.Sci. 20 533 (1965).

100. Laufer J.: N.A.C.A. Tech. Note 2123 (1950); Tech. Report 1053 (1951).

101. Longuet-Higgins M.S.: J.Fluid Mech. 8 293 (1960).

102. Southhampton Hydraulic Lab. Rep. No. 1 (1967).

103. Kenning D.B.R. & Couper M.G.: J. of Fluid Mech. 24 293 (1966).

104. Perry R.H.: Chem.Eng. Handbook 4th ed.

105. Gibson C.H. & Schwarz W.H.: J.Fluid Mech. 16 365 (1963).

106. Uberoi M.S. & Wallis S.: ibid 8 539 (1960).

107. Watson J.S. & Thomas D.G.: A.I.Ch.E.Jl. 14 676 (1967).

108. Waner N.S. & Soroka W.W.: Proc.Soc.Expt.Anal. 9 19 (1953).

109. Acheson Colloids Ltd., Plymouth, England.

110. Hotchkiss G.: Western Union Tech. Rev. 2 176 (1948).

111. Mancy K.H. & Okun D.A.: Anal.Chem. 32 108 (1960).

112. Lynn, W.R. & Okun D.A.: Sewage and Industrial Wastes 27 (1) 4 (1955).

113. "Standard Methods for the Examination of water and waste water" 11th ed. Amer.Public Health Ass. N.Y.(1960)

114. Rand M.C. & Heukelekian H.: Sewage & Industrial Waste 23 (9) 1141 (1951).

115. Clark L.C., Weld R.C. & Taylor E.: J.Appl.Physiol 6 189 (1953).

116. Carritt,D.E. & Kanwisher J.W.: Anal.Chem. 31 5 (1959).

117. Precision Scientific Co.: J.Electroanal Chem. April (1962).

118. Baker J.W., Combs F.J., Linn T.L., Worting A.N., & Wall R.F.: Ind.Eng.Chem. 51 727 (1959).

119. Mackereth F.J.H.: J.Sci. Instrum. 41 38 (1964).

120. Hersch P.A.: Anal.Chem. 32 1030 (1960).

121. Keidel E.A., Ind.Eng.Chem. 52 490 (1960).

122. Protech: Technical Literature Manual Data Sheet SM28.

123. Charlton G.: Australian Patents 237805 March 1962.

124. Khaidarov I. Sh.: Vestn.Mosk.Univ.Ser. VI Biol, Pochuoued, 20 (4) 59 (1965) (Russ).

125. Heldenbrand J.L.: U.S. patent 3239444 (1966).

126. Keyser A.H., & Anderson R.L.: U.A. patent 3235477 (1966).

127. C.E.B.G. Brit. Patent 1026071; 1026072.

128. Lingane J.J.: J. Electroanal Chem. 2 296 (1961).

129. Sawyer D.T. & Interrante L.V.: J. Electroanal.Chem. 3 Rec (1962).

130. Mancy K.A. & Okun D.A.: Report Dept. of San.Eng. & School of Public Health Univ. of North Carolina.

131. Kinsey D.W. & Bottomley R.A.: J.Inst.Brew. 69 164 (1963).

132. Rickles R.N.: I. & E.C. 58 19 (1967).

133. Amerongen G.J. van: J.Appl.Phys. 17 972 (1946).

134. Michaels A.S. & Bixler H.J.: J.Polymer Sci. 50 393 (1961)

135. J. & G. Cox, Gorgie Mills, Edinburgh.11.

136. McKeown J.J., Brown L.C. & Grove G.W.: J. Water Poll.Cont. Fed. 39 1323 (1967).

137. Precision Scientific Co.: Bulletin 638 T - 9.

138. Private Communication - M. Murphy, MacMaster Univ. Canada.

139. Mancy K.H. & Westgarth W.C.: J. Water Poll.Cont.Fed. 34 1037 (1962).

140. Standard Telephone Cables Ltd.,: Technical Data Sheets.

141. Briggs R. & Viney M.: J.Sci.Instrum. 41 78 (1964).

142. Perry R.H.: Chem.Eng. Handbook 4th ed. 14 6.

143. Water Pollution Research: H.M.S.O. 198 (1965).

144. Allen: Phil Mag. XVII 1081 (1934).

ACKNOWLEDGMENT.

I wish to thank (i) Dr. N. MacLeod for his guidance and encouragement throughout this work.

(ii) Mr. C. McLeod for the freedom of his workshop in the Heriot-Watt University and to the workshop technicians for their assistance.

(iii) the S.R.C. and C.S.I.R.O. for their financial assistance in making this work possible, and lastly

(iv) other members of the University of Edinburgh staff for their advice and interest in this work.

APPENDIX 1.

DESIGN AND MANUFACTURE OF THE ENTRANCE AND EXIT NOZZLES FOR THE OPEN CHANNEL.

1. Introduction.

The method used to design the nozzles was an electrostatic plotting technique. There is an analogue between the potential fields of electrostatics and ideal irrotational fluid flow since both obey the Laplace Equation:

$$\nabla^2 \phi = 0 \qquad \text{(i)}$$

2. Methods for solving the Laplace Equation.

(The assumption in this work is that there is irrotational steady state flow).

For a two-dimensional electrostatic field the Laplace Equation is

$$\frac{\partial^2 V}{\partial x^2} + \frac{\partial^2 V}{\partial y^2} = 0 \qquad \text{(ii)}$$

and for flow in two directions

$$\frac{\partial^2 \phi}{\partial x^2} + \frac{\partial^2 \phi}{dy^2} = 0 \qquad \text{(iii)}$$

where V is the electric potential and ϕ the velocity potential. For fluid flow there is also an equation expressing the condition of irrotational flow:

$$\frac{\partial^2 \psi}{\partial x^2} + \frac{\partial^2 \psi}{\partial y^2} = 0 \qquad \text{(iv)}$$

where is a stream function and is constant along a streamline in the fluid. The functions ϕ and ψ are orthogonal functions i.e. lines representing them intersect at right angles.

Because there is a momentum boundary layer within the

nozzle at the bottom of the channel, the flow in the region of fluid adjacent to the channel bottom will be rotational. Hence the analogue between potential fields of electrostatic and ideal irrotational flow can only be used in the region of fluid adjacent to the nozzle.

The electrostatic technique will only produce an approximate solution to the Laplace Equation for the nozzle shape. A theoretical nozzle shape was found from the equation which would produce a velocity profile like that shown in figure (1). Such a profile was chosen so that the skin friction of the nozzle could be allowed for.

The simulation of the Laplace Equation can be accomplished with any one of the three electrical parameters, resistance, capacitance or inductance. Invariably it is resistance which is used, since it is very hard to obtain pure inductance or capacitance without any of the other two parameters.

Electrical analogues are classified under

(i) conductive sheet and solid analogues

(ii) conductive liquid analogues and

(iii) lumped electrical analogues.

3. CHOICE OF ELECTRICAL ANALOGUE.

Of the three analogue systems considered in the last section, conducting liquid analogues were neglected since there were better and cheaper conducting sheet analogues. Out of the conducting sheet analogues teledeltos paper was chosen as the most practicable form of conducting sheet analogue.

Comparing the possible use of a resistance network and the

teledeltos paper, the latter gives an instantaneous record of the electric field, whereas the values of the potentials obtained at the nodes of the network would have to be plotted. Furthermore having set up the network it might be found that the network is too coarse in some areas, and so a new netwrok must be added into the existing one. It would appear that a teledeltos paper plot is necessary first of all to give a rough idea of how the network spacing should be arranged. For this reason teledeltos paper was used as the electrical analogue despite its error of about 10% in the solution of the Laplace Equation compared with a possible maximum error of 1.0% from the lumped electrical analogue.

4. Teledeltos Paper.

This paper is made by adding carbon black to paper pulp in the pulp beating stage of the paper manufacturing process, resulting in a high quality paper stock with a uniform dispersion of carbon. During the final process in the paper making, care is taken to give the paper a uniform thickness and a smooth surface. The conductive paper is then coated with a lacquer on one side which acts as an insulator, and on the other side with a layer of aluminium paint which is reported to consist of micron sized particles (108). Figure (ii) shows a cross section through the paper.

During the manufacture of the paper no control is exercised over the resistivity and so the resistivity varies from roll to roll. Besides this variation there is a variation in the sheet resistivity of about $\pm$ 10%, and the resistivity measured along

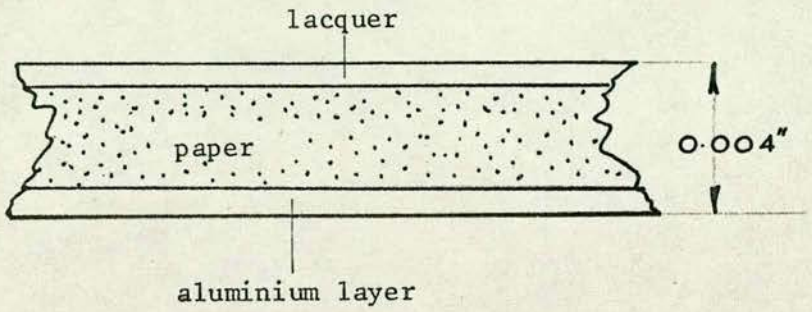

Figure (ii) Section through Teledeltos paper

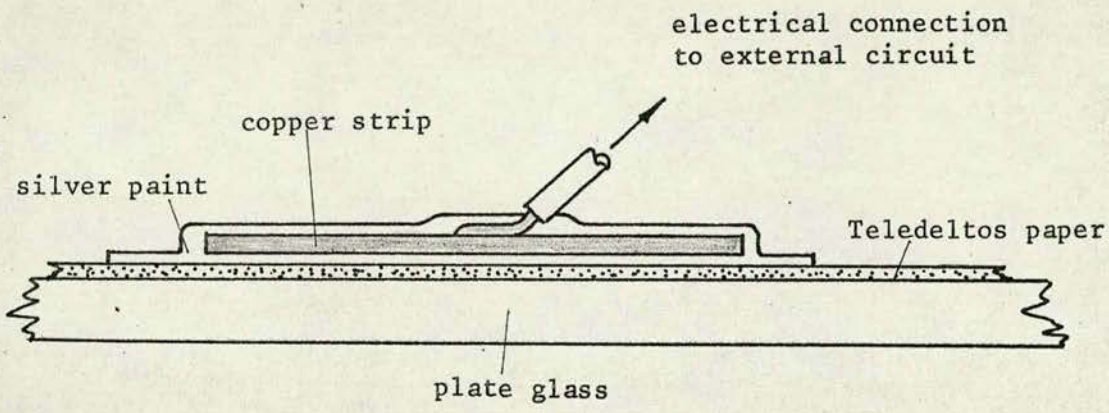

Figure (iii) Section through electrode

the length of the roll is generally about 10% lower than that across the width of the roll.

The physical properties of the paper with respect to temperature and humidity are as follows:

(a) the temperature coefficient of resistance is - 0.2 per cent per degree centigrade, i.e. the resistance is relatively insensitive to ambient temperature changes. Even so it is recommended that the maximum power dissipation be 1/3 rd watt per square inch to minimise heating errors.

(b) the humidity - resistance characteristics are such that it is advisable not to touch the teledeltos paper with moist hands when carrying out an electrostatic plot.

5. Apparatus used to solve the Laplace Equation.

The apparatus consists of the teledeltos paper mounted on a plate glass sheet with cellotape. The electrical connections to the paper were strips of copper 2.5" x 0.5" x 0.0525", which were stuck to the paper with silver paint (Dispersion 915, situer in M.I.B.K. obtainable from Acheson Colloids Ltd. (109)), the paint being extended over the paper to define the boundaries of the inlet and outlet copper bends and the depth in the open channel. Figure (iii) shows a cross section through an electrode. A resistance box (11000) and an Ever Ready PP9 Power Pack were connected in parallel across the electrodes. The null point was found using an Airmec Galvamp Type 391 as the galvanometer along with a brass probe which tapered gradually to a fine, but rounded point to prevent puncturing the teledeltos paper. Figure (iv) shows the electrical circuit with the

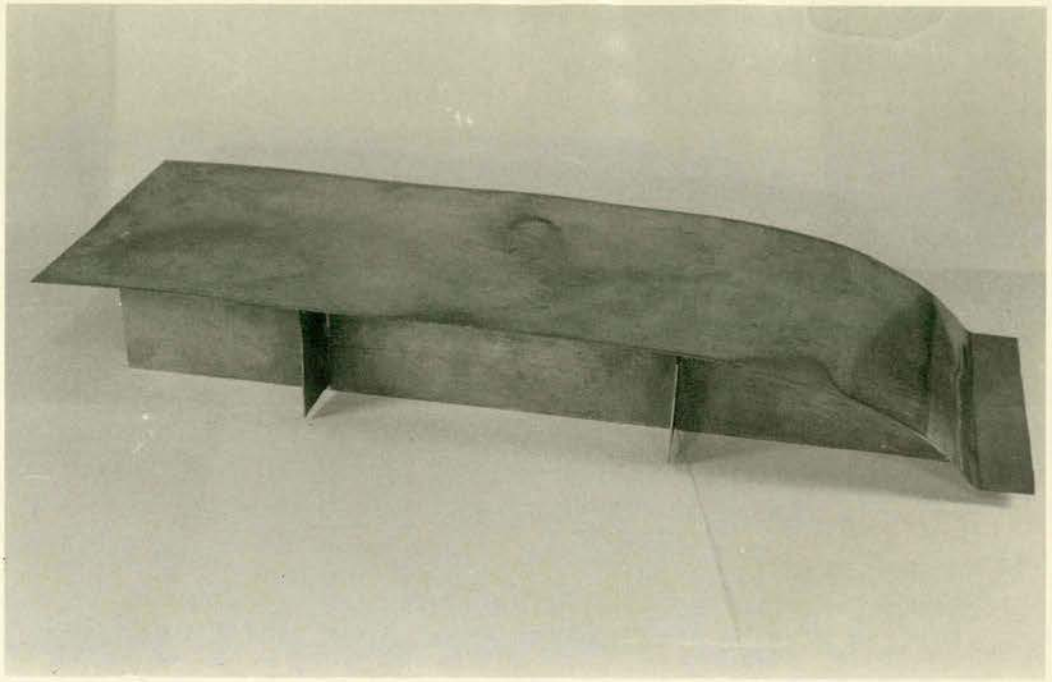

Plate I

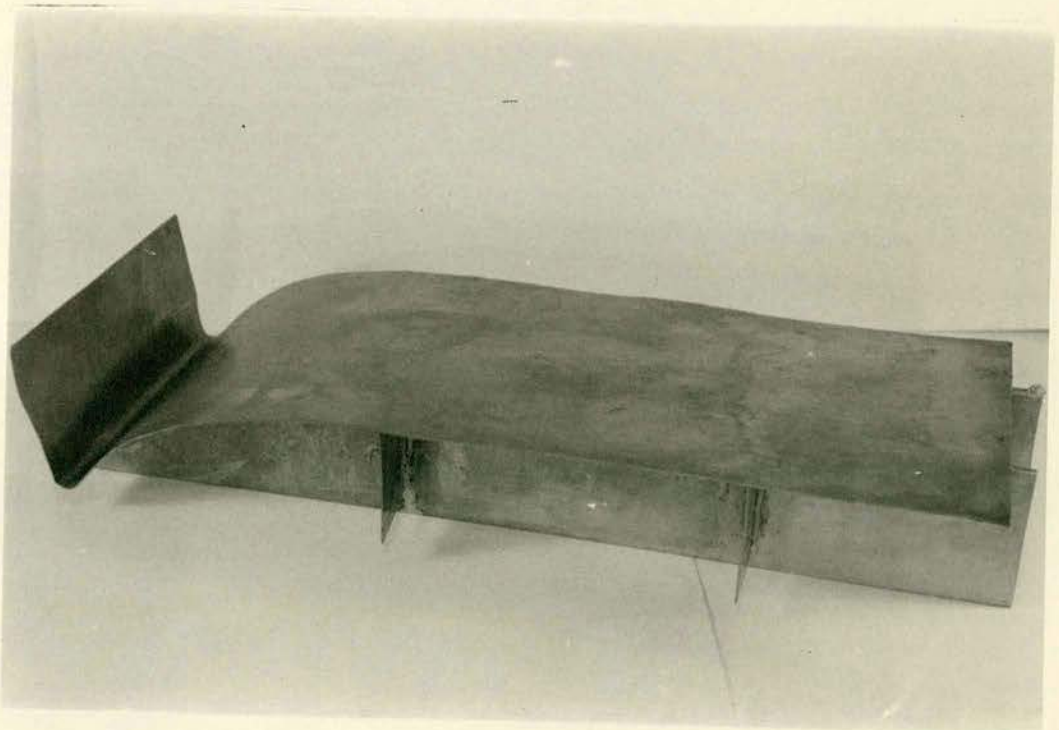

electrodes indicated on the paper.

6. Manufacture of the Nozzles.

The streamlines connecting the corners of the silver paint electrodes (see figure (v) for the inlet nozzle shape) were used for the nozzle shapes. A correction was made in the dimensions perpendicular to the electrodes i.e. along the direction of flow, to allow for the difference in resistivity in the teledeltos paper mentioned in section 4.

A set of templates were then cut out of 0.125 inch thick brass plate to fit the corrected streamline, allowing for a sheet of brass 14G thick which was later soldered on to the templates. The resultant moulds formed from the templates and brass sheets are shown in plate I. The lower mould is for the inlet nozzle and the upper one for the exit nozzle. Each mould was so constructed that when hot it took up a smooth shape along its length and no hollows across its width. These moulds will make nozzles any width up to 6 inches wide for a 6 inches deep channel. Moulds for other depths can be constructed from scaled down sizes in figure (v).

The nozzles themselves were made from 0.125 inch thick perspex sheet. To mould the perspex, a film of 3 in 1 oil was spread over the mould and the perspex sheet then placed on top. The whole lot was then placed in an oven at 140°C and left for eight hours by which time the perspex was soft enough to be finally pressed into the mould by weights. If the perspex is left longer than eight hours in the oven, a brittle perspex is obtained which cracks very easily.

The presence of the oil is to preserve the perspex and prevent it sticking to the mould. When the perspex nozzle was taken from the mould it was cut to the required length. Two half inch square pieces of perspex, the length of the nozzle and drilled with 4 B.A. clearance holes every 2 inches along their lengths, were then stuck to the sides of the 0.125 inch thick perspex sheet with Tensol No. 6 cement. Perspex bracing struts were then attached to the 0.125 inch perspex sheet and the half inch square pieces of perspex, to keep the nozzle rigid when in position in the test section. The half inch square pieces of perspex were used to anchor the nozzles down on to the top of the side windows of the open channel. An airtight seal was effected by using Dow Corning sealant. This sealant is a silicone rubber and has the property of setting with a tough pliable outer skin with a soft inside, and it does not age.

7. Velocity distribution obtained from the inlet nozzle at the entrance to the open channel.

The velocity distribution was found from cine film records for the "dye" dispersions. The resultant velocity profile is compared with the 1/7th power law velocity profile and the velocity profile predicted by the teledeltos paper plot in figure (vi), the data for which is contained in table II in section 8.

Before the velocity profile can be found from the teledeltos paper plot, a relationship between the surface velocity at the nozzle outlet , and the maximum velocity at the nozzle inlet, , must first be established.

From figure (vii) for continuity at the inlet and outlet,

$$\bar{v}_{av}\, d_1 = U_{av}\, d_2 \qquad (v)$$

and $$\bar{v}_{av} = \frac{1}{\bar{d}_1}\left[2 \int_0^1 v_1 (y)^{1/7}\, dy + \int_1^7 v_1\, dy \right]$$

i.e. $$\bar{v}_{av} = 0.9685 v_1$$

and $$U_{av} = \frac{1}{\bar{d}_2} \int_0^{d_2} U_S \left(\frac{y}{\bar{d}}\right)^{1/7} dy$$

i.e. $$U_{av} = 0.875\, U_S$$

Hence equation (v) becomes

$$v_1 = \frac{U_S}{1.476} \qquad (vi)$$

To findthe velocity distribution at the outlet, consider two streamlines at distance y_n and y_{n+1} from the channel bottom. By continuity the average velocity at the inlet nozzle outlet between these streamlines is

$$U_{av}\Big]_{y_n}^{y_{n+1}} = \bar{v}_{av}\Big]_{y_n}^{y_{n+1}} \frac{(y_{n+1} - y_n)\ \text{entrance}}{(\bar{y}_{n+1} - \bar{y}_n)\ \text{outlet}} \qquad (vii)$$

and $\bar{v}_{av}$ is a function of v_1 of the form

$$\bar{v} = K_1 v_1 \qquad (viii)$$

where K_1 is a constant lying between 0.9685 and 1. Thus from equation (vi), equation (viii) becomes

$$v_{av} = K_2 U_S \qquad (ix)$$

Substituting equation (ix) in equation (vii)

$$U_{av}\Big]_{y_n}^{y_{n+1}} = K_2 U_S \frac{(y_{n+1} - y_n)\ \text{entrance}}{(\bar{y}_{n+1} - \bar{y}_n)\ \text{outlet}} \qquad (x)$$

(y_n (entrance) are shown in figure (v) and y_n outlet in table I)

It will be seen from figure (vi) that the actual profile obtained is similar to the 1/7th power law velocity distribution over most of the depth. The predicted profile from equation (x)

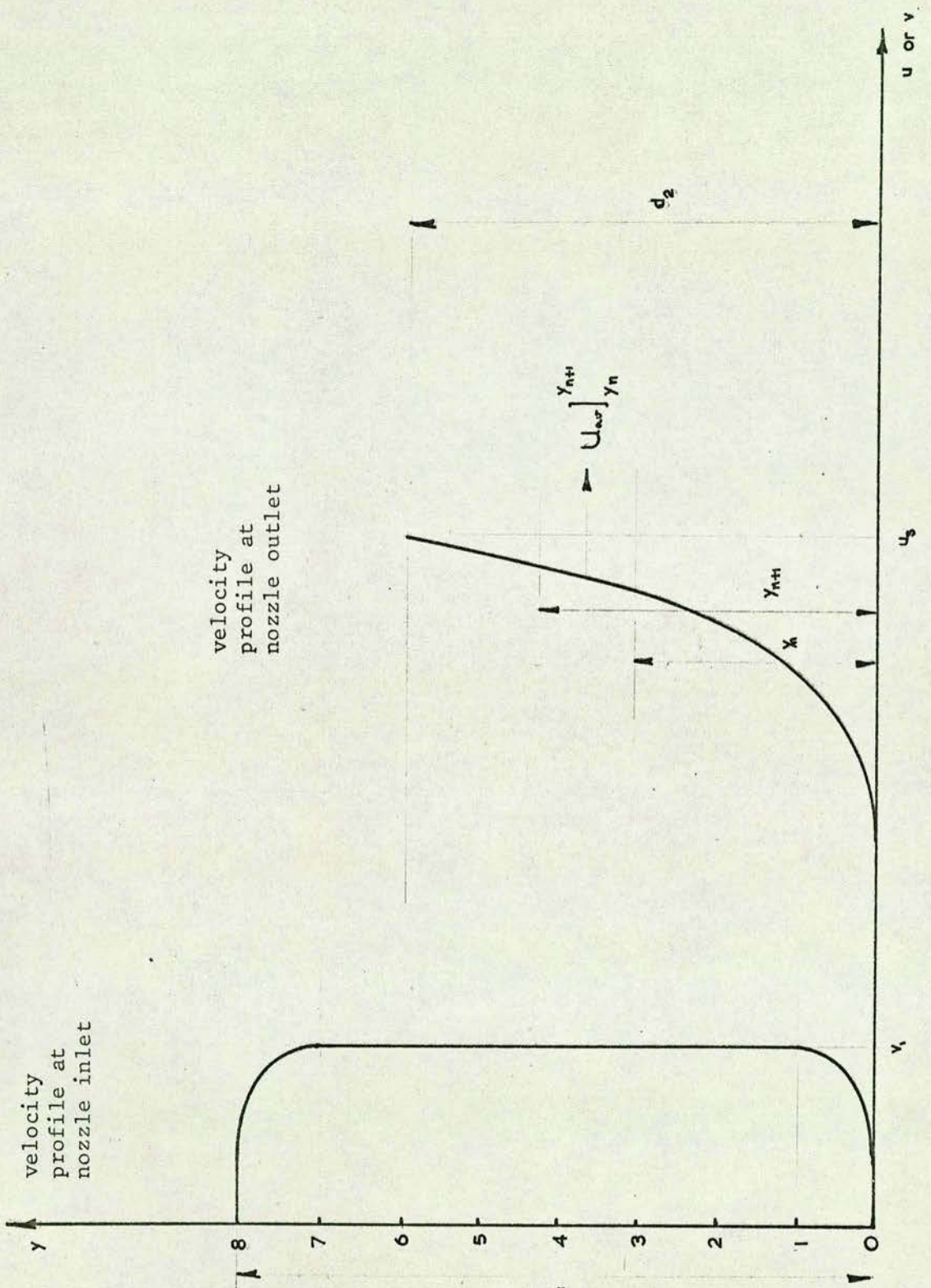

Figure (vii) Assumed velocity profiles at nozzle inlet and outlet

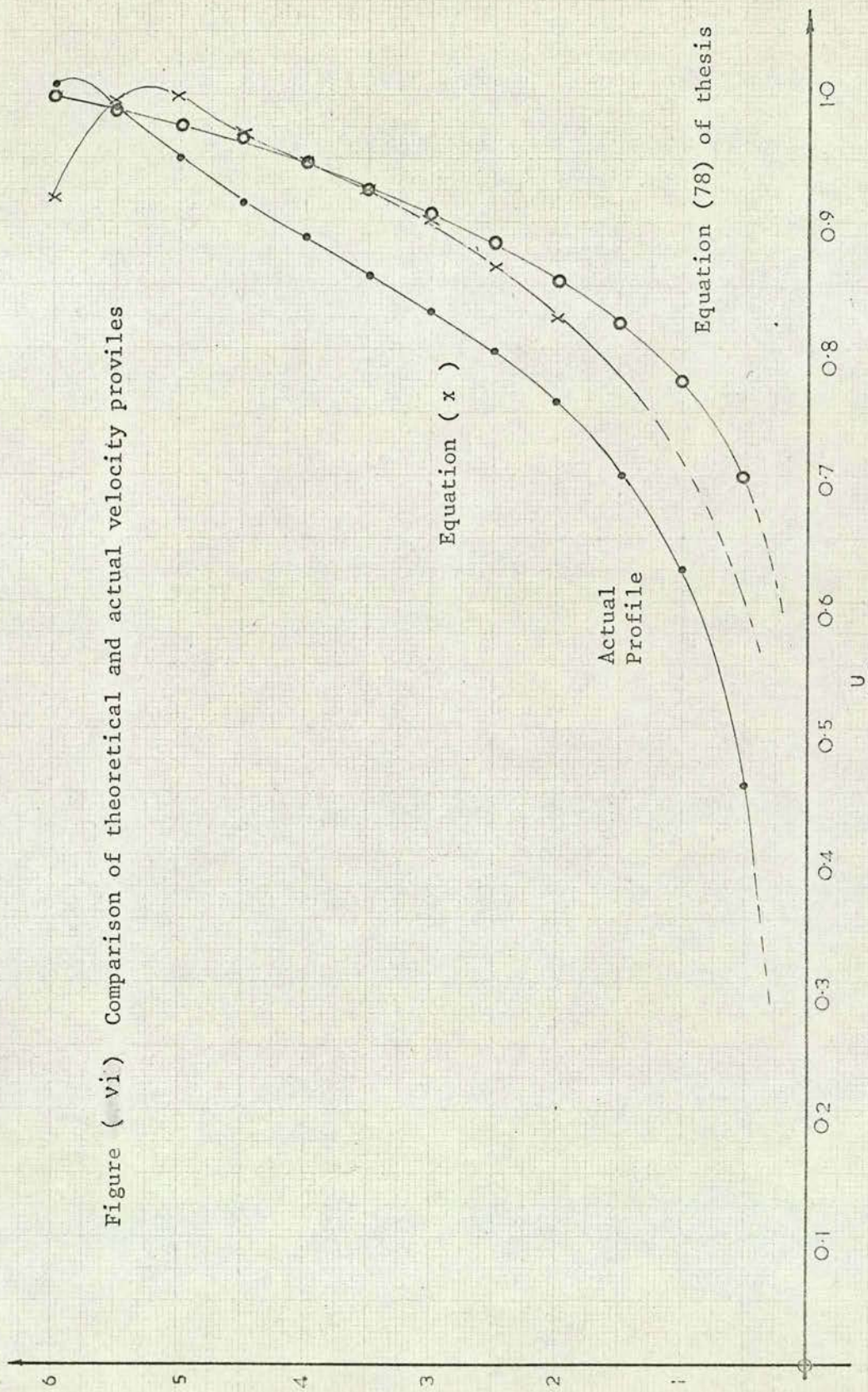

Figure (vi) Comparison of theoretical and actual velocity proviles

does not in fact occur. In section 5.3 of the thesis, it is seen that the velocity profile obtained from the inlet nozzle was of the correct shape for river flow.

No mention has so far been made of the velocity profile in the outlet nozzle. It appeared that the shape of the velocity profile in this part of the apparatus does not matter, so long as the change over from open channel flow to flow in a duct is achieved smoothly, with no gases being entrained in the out going liquid at the leading edge of the outlet nozzle.

TABLE I.

Position of the streamlines at the inlet nozzle outlet.

Streamline No. (numbered from channel bottom)	Position obtained from electrostatic plot y_n ins (outlet)
0	0
1	0.57
2	1.03
3	1.48
4	1.93
5	2.38
6	2.80
7	3.20
8	3.60
9	3.96
10	4.34
11	4.68
12	5.02
13	5.32
14	5.62
15	5.86
16	6.0

TABLE II.

Velocity distribution with depth.

Depth y ins	$\frac{\bar{U}}{\bar{U}_s}$ or $\frac{\bar{U}}{\bar{U}max}$		
	Actual @	1/7th Law	via Equa. (x)
0	-	0	0
0.5	-	0.701	0.455
1.0	-	0.774	0.625
1.5	-	0.820	0.700
2.0	0.824	0.855	0.758
2.5	0.860	0.882	0.798
3.0	0.898	0.906	0.830
3.5	0.927	0.926	0.857
4.0	0.944	0.944	0.889
4.5	0.965	0.960	0.915
5.0	0.994	0.974	0.950
5.5	0.992	0.988	0.990
6.0	0.918	1.0	1.030

(@ average of all the velocity profiles obtained in the open channel)

APPENDIX II.

DEVELOPMENT OF A DEVICE TO MEASURE THE DISSOLVED OXYGEN CONCENTRATION IN FLOWING WATER.

1. Choice of methods for analysing the dissolved oxygen concentration.

The following conditions must be met by the chosen system:-

(i) None of the oxygenated water must be removed from the system, since this would cause entrainment of the air at the entrance to the exit nozzle from the open channel.

(ii) The free surface of the open channel must not be disturbed.

(iii) The cross-sectional area available for flow must not be cut down too much by the presence of an analysing device otherwise the turbulence intensity in the open channel will be altered locally.

It can be seen from condition (i) that the chemical and photo chemical methods, which all involve withdrawing samples are not acceptable here. Since electrochemical cells are the only alternative, the question arises as to which type of cell can be used.

The commercially available cells from both Britain and America are too large in diameter and hence conflicted with condition (iii) and possibly (ii). It was therefore decided to develop an oxygen analysing cell to suit the open channel.

2. Electrochemical methods for analysing oxygen concentrations in liquids.

Electrochemical methods are based mainly on polarography

or the principles of galvanic cells. In polarography a voltage is applied across the cell but a galvanic cell produces the E.M.F. for the external circuit. The cell is a selective device for the reduction of dissolved oxygen and has the same mechanism in both cases. One of the first polarographic types was the dropping mercury electrode (111). but it was very sensitive to turbulence and vibrations, and was soon superseded by solid electrodes. The first of these was a rotating platinum electrode (112).

Then came a proliferation of stationary electrode systems (both polarographic and galvanic) which were membrane covered, the membrane acting as a selective barrier to dissolved gases other than oxygen and also stopping the electrodes from becoming poisoned (113,114,115). Thus solid systems appeared in the following order, those with (p) after the number being cells used in polarographic methods.

(i) Platinum cathode with a silver/silver oxide anode (116)

(ii) Silver cathode with a lead anode and either potassium hydroxide (117,118) or potassium bicarbonate (119) or sodium hydroxide (120) as the electrolyte.

(iii) Silver cathode with cadmium anode (121).

(iv) Carbon cathode with silver anode and a proprietary electrolyte Protech 9 X (122).

(v) (p) Gold cathode with a silver anode and potassium chloride as the electrolyte (123)

(vi) (p) Platinum cathode with silver anode and sodium chloride/silver chloride mixture as the electrolyte (124).

(vii) Gold foil cathode with cadmium anode and sodium chloride as the electrolyte (125).

(viii) (p) Platinum cathode with a silver anode coil (126).

All but (viii) are polyethylene covered cells; no membrane details are given for (viii). Where the electrolyte is not given, no data about its nature is available. Lack of suitable commercial cells is the reason for sugh a large number of experimental cells being developed.

It can be seen that there is a choice in the type of electrode and electrolyte system which can be used. The basic design factors for oxygen analysing cells are:-

(i) The anodematerial must consist of a relatively basic metal of reasonable stability that has no tendency toward passivation.

(ii) The supporting electrolyte must consist of a good conducting electrolytic solution which does not dissolve the anode metal at any significant rate when the cell is in open circuit.

(iii) The cathode must be relatively noble, so that when the cell is in closed circuit, the cathode potential is sufficient for the reduction of molecular oxygen.

(iv) The membrane must serve as a selective diffusion barrier i.e. be sufficiently permeable to oxygen but practically impermeable to ionic species and water molecules from the test solution. Furthermore the membrane permeability characteristics should not change with time, and there should be no interaction between the membrane material and the diffusing oxygen molecules or ionic species present in the test solution or the electrolyte.

Polyethylene, teflon, polypropylene and rubber (natural or synthetic) have been found suitable (127), polyethylene being the best.

For condition (iii) silver has been found more stable than platinum as the cathode material because

(i) it has better ageing characteristics. It has been shown by Lingane (128) as well as by Sawyer and Interrante (129) that the reaction mechanism of oxygen reduction at the platinum electrodes is complex due to an oxide film on the platinum surface which accumulates there and interferes with the electrode process.

(ii) Studies with membrane systems of various designs composed of platinum cathodes and silver-silver oxide anodes showed inconsistency of response and low stability.

Silver cathodes showed none of these effects when used with lead anodes.

In lead-silver cells, the cell reactions are assumed to be:- at the cathode

$$O_2 + 2H_2O + 4\epsilon = 4OH^- \qquad (1)$$

at the anode

$$Pb + 4OH^- = PbO_2^{2-} + 2H_2O + 2\epsilon \qquad (2)$$

or $$2Pb + 4OH^- = 2Pb(OH)_2 + 4\epsilon \qquad (3)$$

or $$Pb + PbO_2^{2-} + 2H_2O = 2Pb(OH)_2 + 2\epsilon \qquad (4)$$

probably all three reactions at the anode take place at the same time.

The maximum cell current which can be developed on short circuit is given by the following equation (130, 131).

$$i = \frac{n F a P C}{l} \qquad (5)$$

where C is the dissolved oxygen concentration (moles/ml)

F is the Faraday (96500 coulombs)

P is the permeability coefficient of the membrane(cm^2/sec)

a is the area of the silver electrode (cm^2)

l is the thickness of the plastic membrane (cm)

n is the number of electrons taking part in the electrode reaction per mole of electroactive species.

The internal resistance of most cells is greater than 1MΩ. In the external circuit the load resistance of the cell is normally of the order of 750Ω so that the current drawn from the cell is almost the maximum available.

This current, i, is temperature dependant and varies according to the law:

$$i = K e^{-J/T} \qquad (6)$$

where K and J are cell constants and T is the absolute temperature (^{o}K).

This type of law is due to the permeability characteristics of the membrane and the effect of temperature on the chemical reaction rates of equations (1), (2), (3) and (4). The diffusion of material through membranes follows three distinct steps:

(i) Solution of the penetrant(s) in the membrane to equilibrium state.

(ii) Subsequent diffusion of the penetrant(s) in the direction of minimised free energy, and

(iii) Equilibrium at the second boundary is established.

The temperature dependence of the solubility of the material in the membrane (i) follows an Arrhenius type law similar to that of the chemical reaction viz (132)

$$S = So \, e^{\frac{-\Delta Hs}{RcT}} \qquad (7)$$

where S is a solubility parameter

So is a solubility parameter @ To

ΔHs is the heat of solution

Rc is the gas constant

T is the Absolute temperature

For oxygen dissolving in natural rubber ΔHs is 0.75 Kcal/gmole (133) and in polyethylene is 0.4 to 0.6 Kcal/gmole (134).

Steps (ii) and (iii) are also temperature dependent but their contributions to the overall effect of temperature is small compared with that of step (i).

In the gold cadmium cell, the cell reaction is assumed to be (125)

at the cathode

$$2H_2O + O_2 + 4\epsilon = 4OH^-$$

at the anode

(i) $2Cd = 2Cd^{2+} + 4\epsilon$

and (11) $2Cd^{2+} + 4OH^- = 2Cd(OH)_2$

In both the silver-lead and the gold cadmium cells the reaction products, $Pb(OH)_2$ and $Cd(OH)_2$, have to be periodically removed from the lead and cadmium anodes respectively.

3. <u>Development of the oxygen analysing cell</u>.

From part 2, it was seen that the best electrode system was

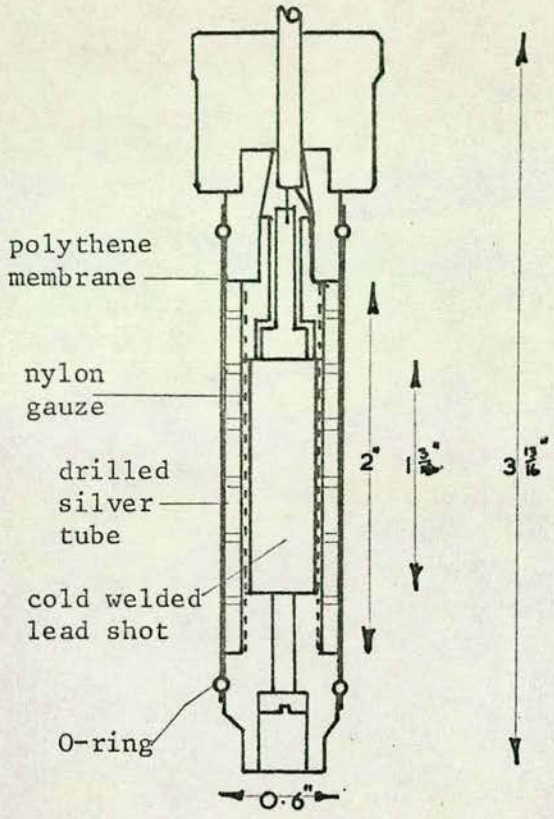

Figure (i) Mackereth (119)

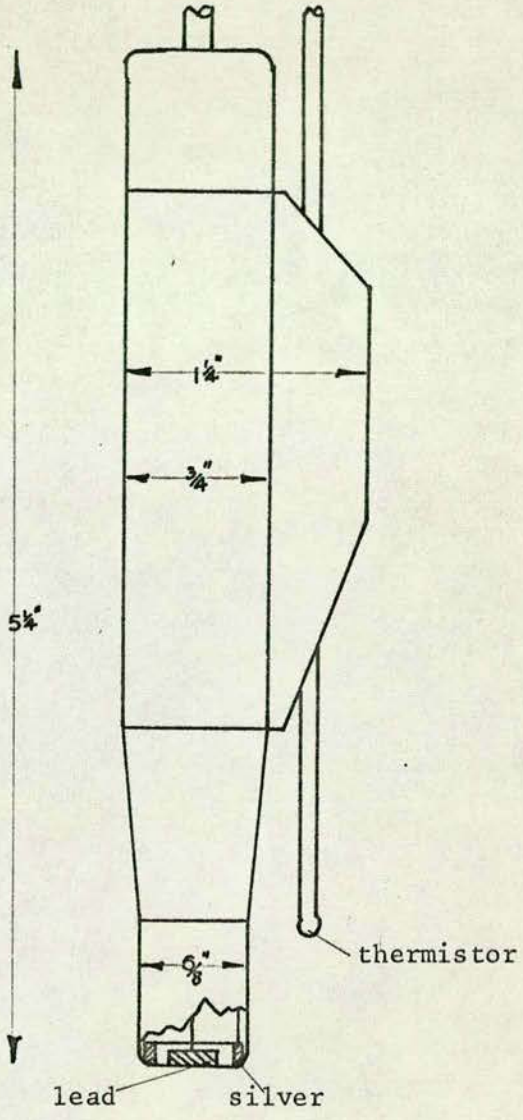

Figure (ii)b Precision Scientific Co. (117)

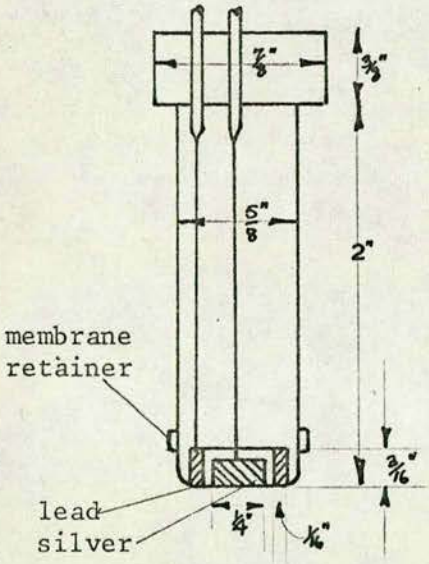

Figure (ii)a Mancy & Westgarth (117)

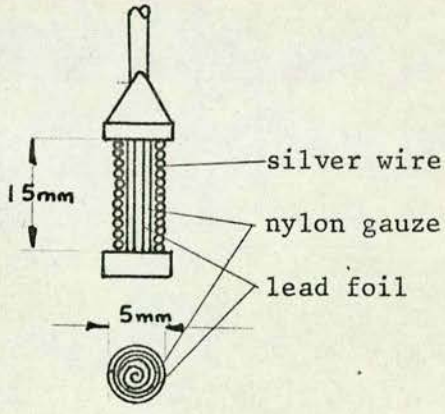

Figure (iii) W.P.R.L. (143)

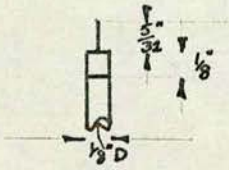

Figure (viii)a on the same scale as above figures

the silver-lead cell, and there are several ways in which the electrodes can be arranged in their holders, see figures (i), (iia) and (iib) and (iii).

When the first electrode system was made it was decided to cast the lead electrode directly on to the holder which in this case was 0.125" diameter copper tubing. In order to carry out the casting a brass block was made (figure iv) then some lead chips were placed in the hole and the block heated up. When the lead had melted, the copper tube was placed in the molten pool quickly (to stop oxidation taking place). A jet of cold water was then aimed at the copper tube just above the molten lead, to solidify the lead in the neighbourhood of the copper tube. By continuing the cold water treatment and at the same time rotating the tube, the lead electrode was built up to the required size and then withdrawn from the brass block.

The silver electrode was made from 0.025" diameter silver wire forced into a five strand insulated cable until a third of the silver wire was covered. A paper disc 0.0625" diameter and 0.003" thick was placed over the silver wire flush with the insulated cable. The paper disc was then covered in Araldite and the silver wire and cable fitted into the lead electrode, (the paper disc holding the silver electrode concentric with the lead electrode), and the system left until the Araldite had set, (figure (v)).

The electrolyte used was a sodium hydroxide/paper tissue mixture which was applied to the electrodes as a gummy paste and then left to harden before the membrane was put on.

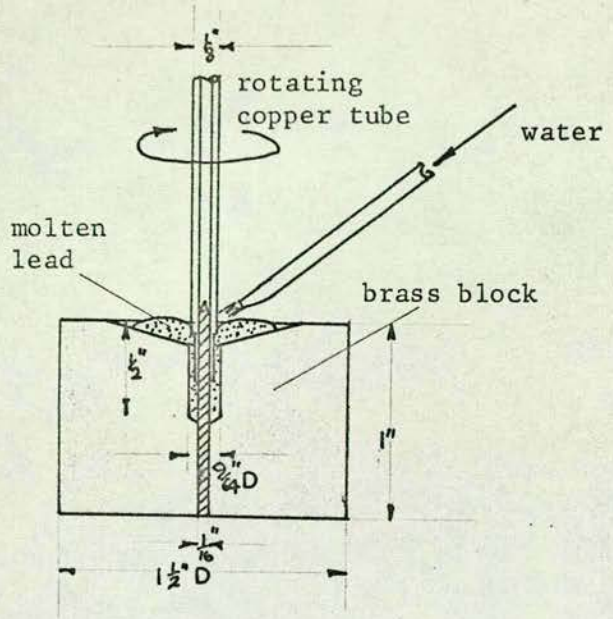

Figure (iv)

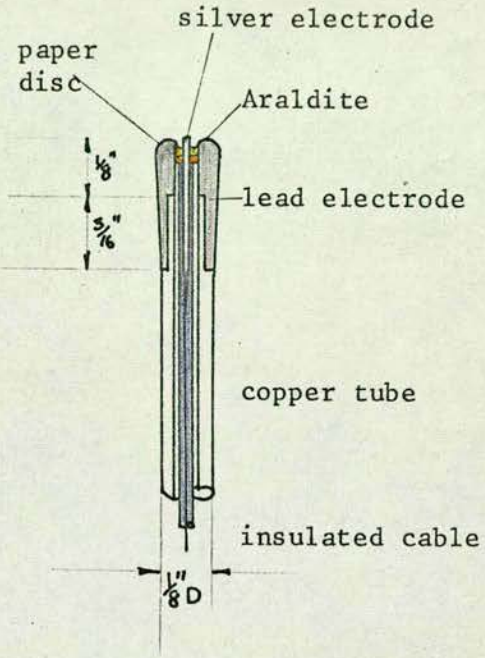

Figure (v)

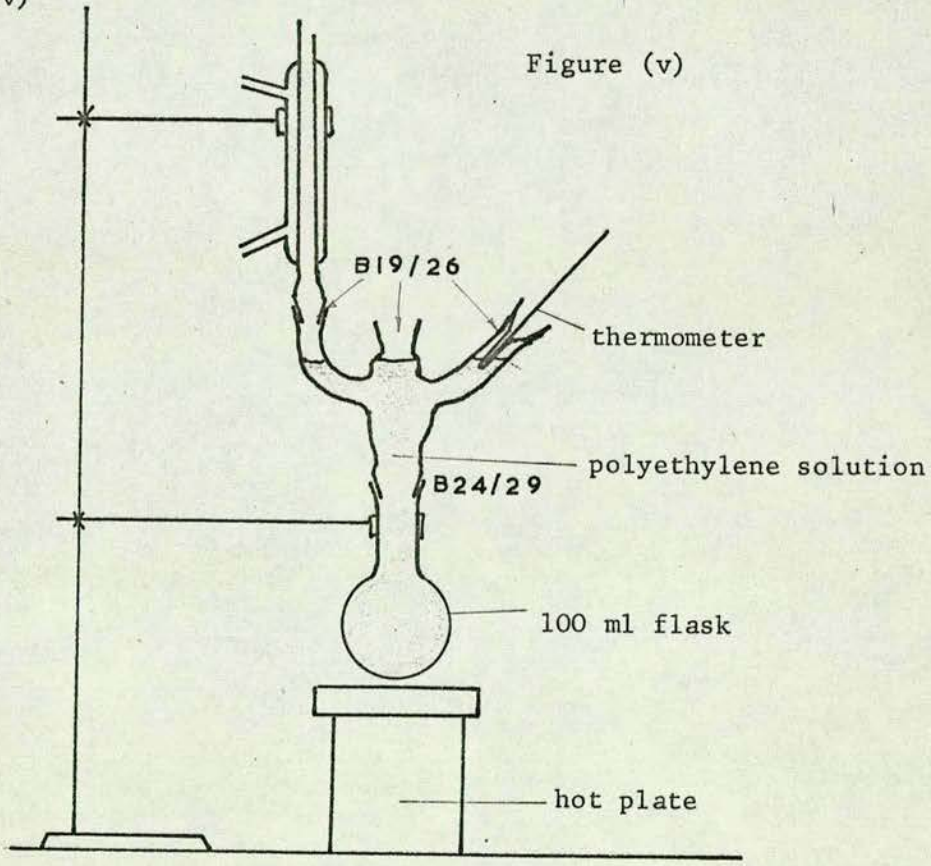

Figure (vi) Apparatus for applying polyethylene membranes

Polythene was chosen for the membrane. The first membranes were made from sheets of 0.0025" thick polyethylene sheeting stretched over the silver and lead electrodes, but these membranes fractured from the strain exerted on them by the edges of the two electrodes. To overcome this problem, the cell was dipped into a solution of polyethylene, which besides being self sealing, gave thin films of polyethylene very much less than 0.001" thick.

This polyethylene solution was made by dissolving 5g of clear 0.0025" thick polyethylene sheeting in 100ml of toluene (xylene will serve, but toluene gives a better quality polyethylene film). This 1:20 ratio of polyethylene to toluene gave far better results than the 1:4 ratio of polyethylene to xylene used by Charlton (123). The polyethylene films from the latter solution tended to break down into powdery deposits on the electrodes. The polyethylene solution was kept at a temperature of 115°C. The electrode assembly was then quickly dipped into the solution and withdrawn, then air dried at a temperature of about 100°C. When dry, the cell was again dipped in and out of the polyethylene solution quickly. (The apparatus for coating the cell with polyethylene solution is shown in figure (vi)).

When the membrane was cool, it was tested for holes by immersing the cell in a beaker of still water and noting the appearance of the water immediately below the electrodes. In each case of a cell made by the above method, it was found that electrolyte flowed out of the cell into the water i.e. there were holes in the membrane.

At this stage it was decided to lengthen the silver electrode from that shown in figure (v) to that shown in figure (vii). Because the polythene membrane was deposited from solution, it was no longer necessary to leave the silver electrode flush with the lead electrode. This change in the silver electrode length resulted in an increase in the current from the cell. The comparative tests between the two electrode systems, figures (v) and (vii) were carried out using distilled water with pure oxygen dissolved in it. As a consequence the holes in the membrane did not affect the outcome of the tests since the membrane is only present to stop species other than oxygen molecules from reaching the electrodes.

In an attempt to solve the problem of holes in the membrane, a piece of polyethylene sheet was cut so that, when placed over the silver electrode, it covered the electrolyte as in figure (vii) and then the cell was dipped in and out of the polyethylene solution. When the membrane was now tested for holes, it was found that they were still present but confined to the edge of the lead electrode where it met the electrolyte.

The holes were due to moisture in the electrolyte being boiled off by the hot polyethylene solution and the escaping water vapour caused the "blow holes". This problem was overcome after further modifications to the cell.

It was found that the copper tubing used to carry the electrodes became annealed due to heat received from the boiling polyethylene solution. As a result of this the tubing became insufficiently stiff to stand up to the water flowing past it in

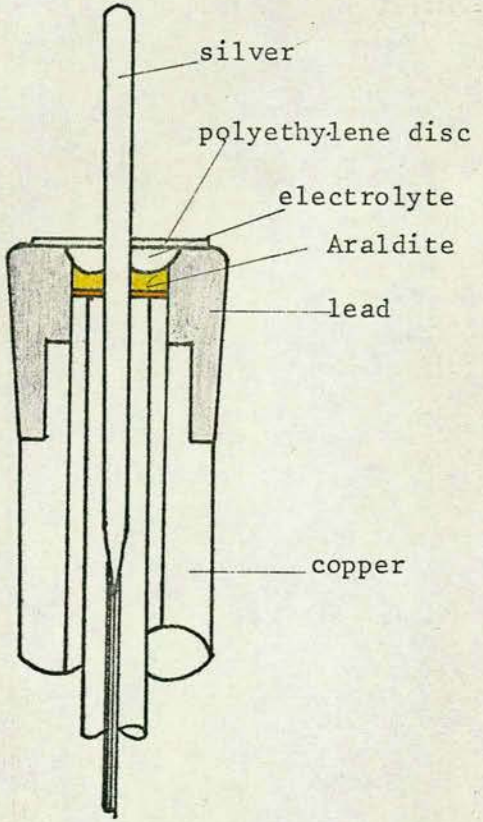

Figure (vii)

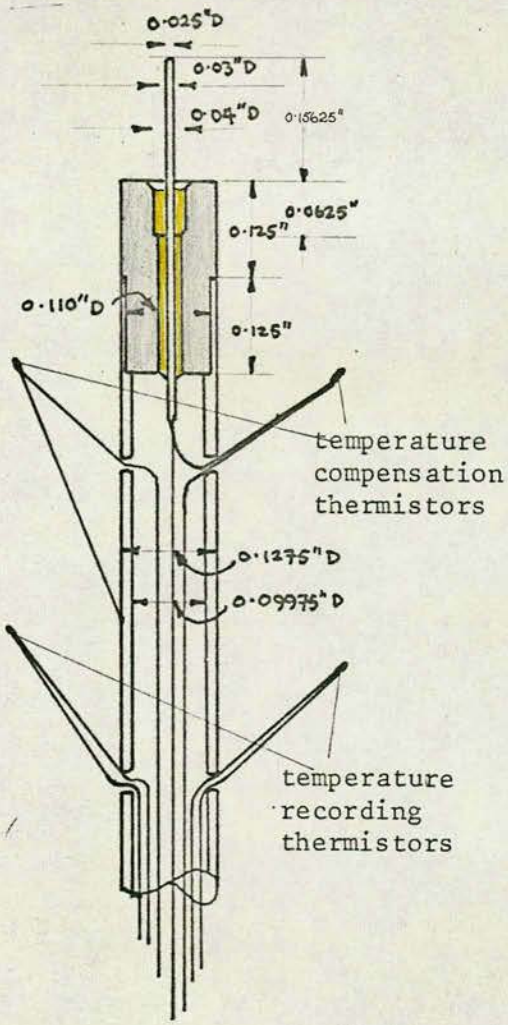

Figure (viii)a

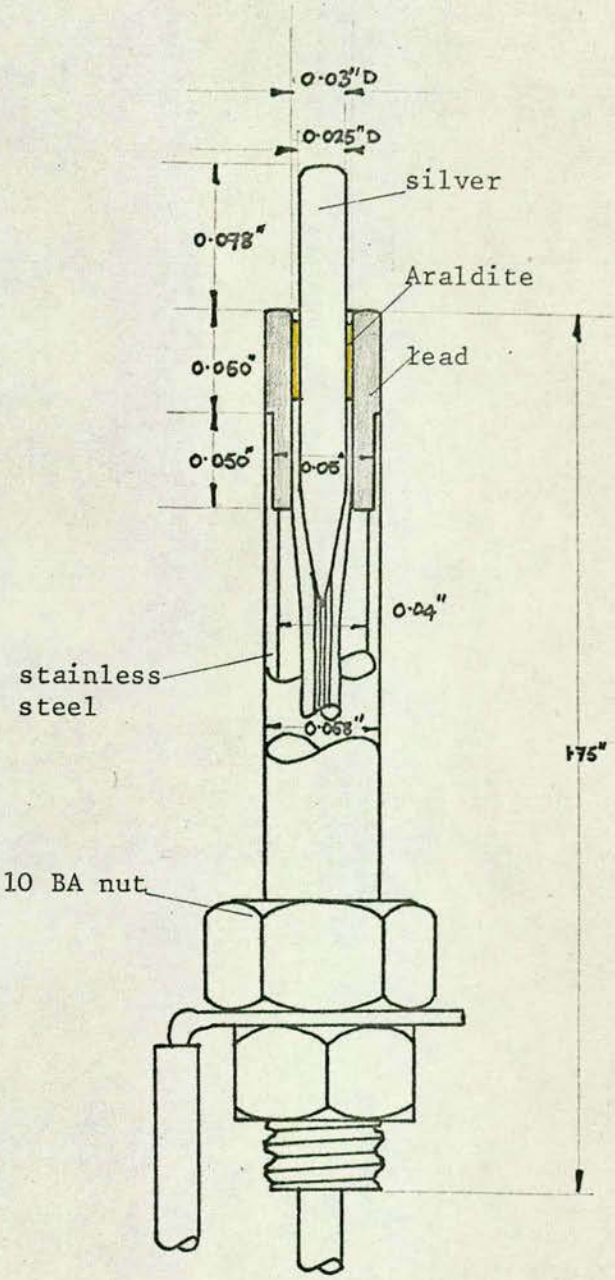

Figure (viii)b

the open channel. The copper tubing was therefore replaced by stainless steel tubing 0.1275" diameter and this stood up to the flowing water without deflecting significantly.

The anode was made from pure lead rod 0.15" diameter. The end of the rod was tapered to a diameter of 0.09975" over a 0.125" length. The lead rod was forced into a stainless steel tube (about 2" long, 0.1275" O.D and 0.09975" I.D) the end of which was drilled to a depth of 0.125" with a No. 37 drill. The lead was then turned down to size and a hole was drilled right through the centre of the lead rod using a No. 60 drill. Then a No. 52 drill was used to drill to a depth of 0.0625". The finished lead electrode was carefully knocked out of the stainless steel tube.

The silver electrode was then fitted as before but without the paper disc. During this operation it was necessary to check the electrical continuity of the cell. There should be no resistance between the silver wire and its external cable; and there should be an infinite resistance between the lead and silver electrodes. A recheck of the above resistances was also necessary after the Araldite had set.

The lead and silver electrodes were then coupled to the appropriate temperature compensating thermiestors (see figure (viiia) and section 5) before the lead electrode was force fitted into the cell holder. The cell holder was a stainless steel tube one foot long, 0.1275" O.D and 0.09975" I.D. The end of this tube was drilled to a depth of 0.125" with a No. 38 drill, thus ensuring that the lead-steel join was a tight fit.

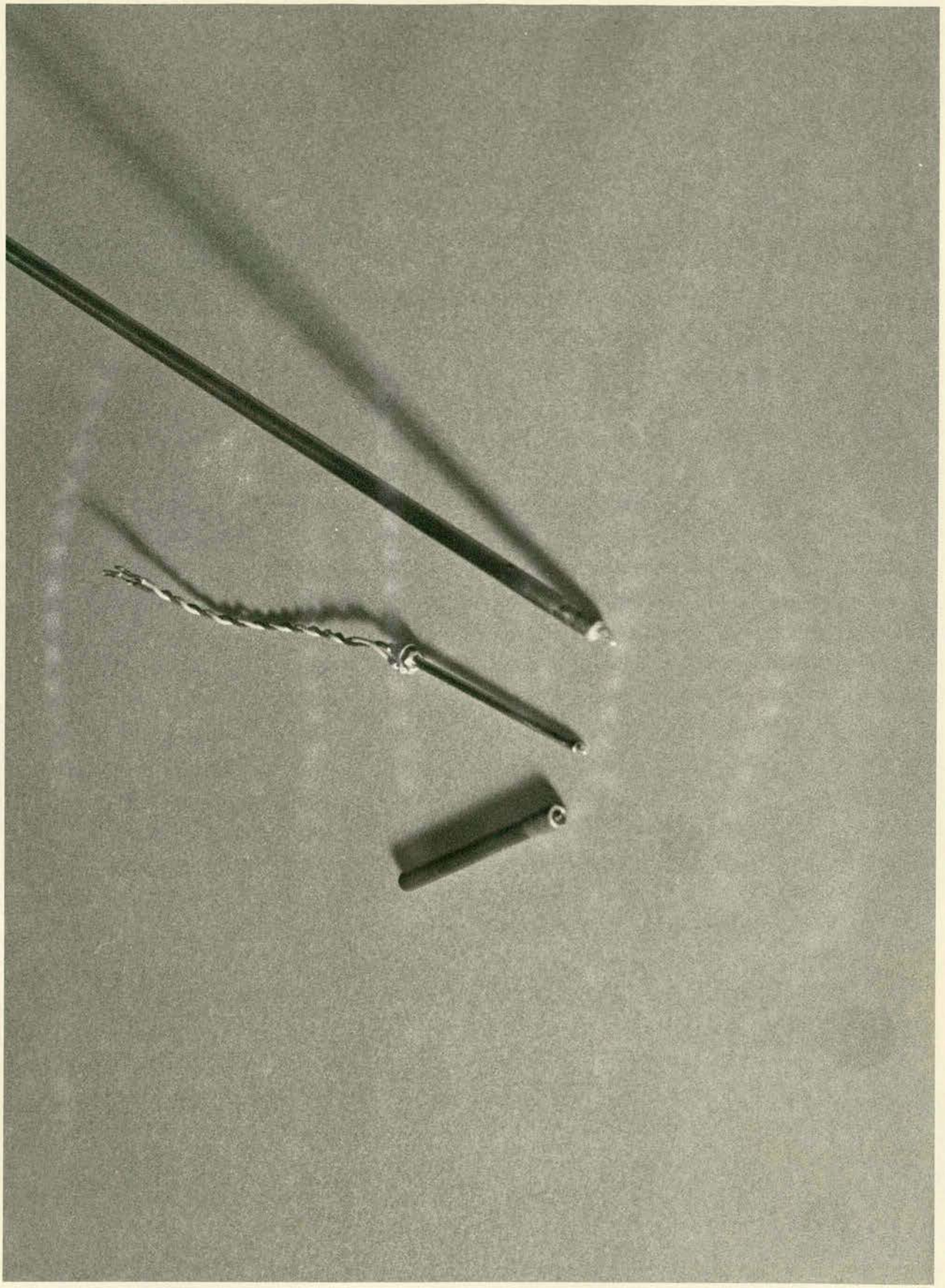

Plate I

Figure (viiia) shows the dimensions of the cell, while figure (viiib) shows the dimensions of a smaller cell, probably the minimum size of cell which can be made by this method due to difficulties encountered in turning lead. This small cell could be used to measure dissolved oxygen concentrations in very small spaces. Plate I shows the copper holder cell (of figure (v)) on the left, the small cell (of figure (viiib)) in the middle, and one of the completed cells used in this work, (Magnification of plate I is 1.25).

As well as changing the cell holder to stainless steel, the electrolyte composition was also altered. The electrolyte was made from Cox's gelatine and sodium hydroxide in the following manner. A saturated solution of sodium hydroxide was heated until its temperature was above 90°C (the melting point of gelatine) and then powdered gelatine was added very slowly, so that each addition dissolved before adding any more. Periodically the mixture was tested for its setting properties by dipping in a glass rod and withdrawing it. If the solution remained "runny" on the glass rod a while after it had been withdrawn, more gelatine was required. The correct consistency was reached when a long strand could be pulled out of the molten solution, setting within five seconds. The electrolyte was then put on to the cell which had been previously warmed to above 40°C (the setting point of gelatine), to prevent the electrolyte carrier from setting as it was being pressed into shape. Any excess electrolyte around the lead electrode was cut away.

Gelatines other than the "instant" variety manufactured by

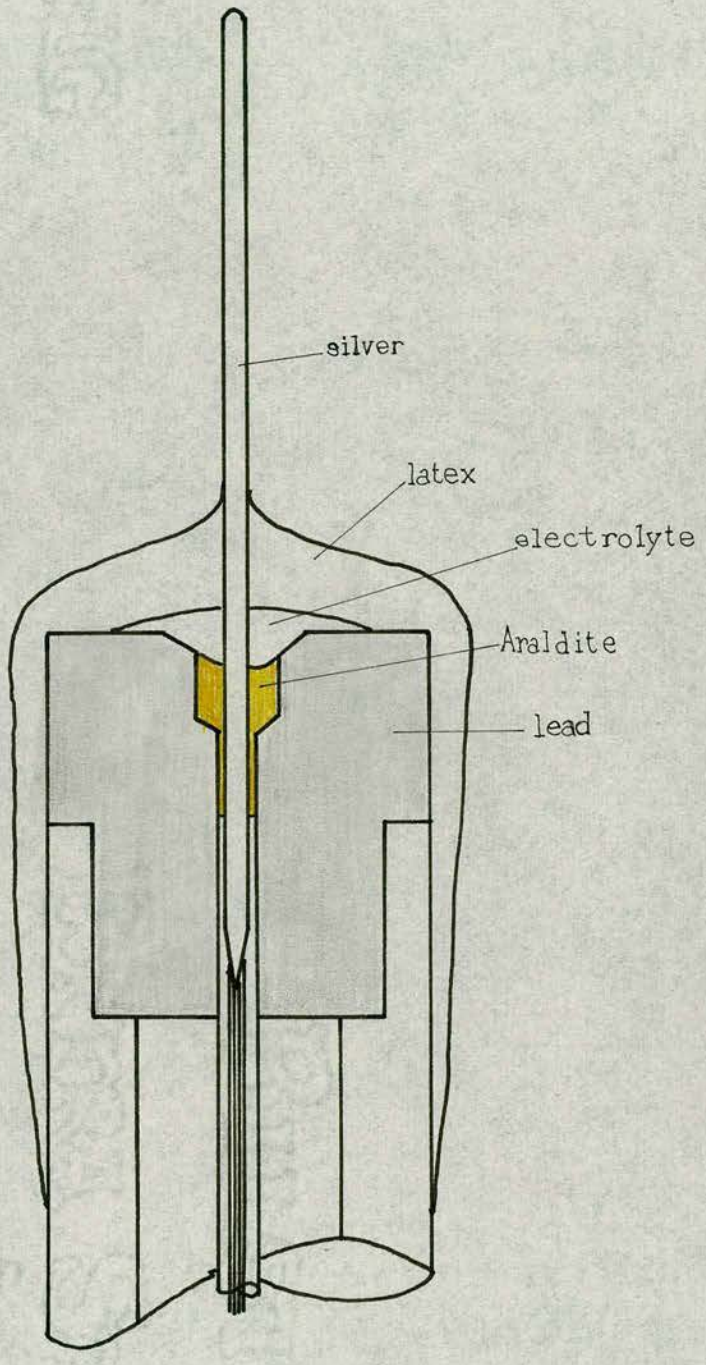

figure (ix)

Cox (135) were found unsatisfactory for the electrolyte carrier as they either made crystalline electrolytes which were very difficult to put on, or they were deliquescent which rendered them useless.

When the polyethylene membrane was applied to this system, by the method described previously, the result was a bubbly mass of polyethylene and electrolyte formed by the rapid escape of water vapour from the gel. This problem was solved by sealing in the electrolyte with a layer of ammonia-stabilised latex, (as in figure (ix)), which was air-dried since the usual curing agent, formaldehyde, reacted with the silver and lead electrodes and so could not be used.

On applying a polyethylene film to this system, the results appeared good i.e. there were no apparent leaks in the membrane when the cell was immersed in a beaker of still water. A further check was then made using an ohmmeter. With the oxygen analysing cell still in the water, one terminal of the ohmmeter was connected to the stainless steel tube and the other immersed in the water. An infinite resistance was found, indicating that the membrane had no holes in it. Thus a satisfactory membrane hade been produced.

4. Performance of the oxygen analysing cell.

Since the electrode system was small compared with the manufactured cells and the thickness of the membranes was probably less than 0.0005", its response time was very rapid compared with that of the manufactured cells which ranged from 20 seconds for a 65% change from maximum to zero to 90 seconds

for a 99% change from maximum to zero.

The response time was measured by recording the time taken for the output from the electrodes to change from its maximum value to its minimum value. The minimum value (zero) was achieved by adding cobalt catalysed sodium sulphite solution to a beaker of oxygen saturated water in which the oxygen analysing cell was immersed. The catalysed sodium sulphite solution removes the dissolved oxygen from the water almost immediately. There was an almost instantaneous change from maximum to zero of the output voltage reading in the recorder as soon as the sodium sulphite solution entered the oxygen saturated water. The time taken for a 100% change from maximum to zero was 0.4 sec, measured on a high speed chart recorder. It would appear that the response time of the cell is linked directly to the cell's capacitance.

Besides the quick response time, this oxygen analysing cell was found to be superior to existing cells in other ways. Its main advantage is that it is not velocity sensitive (compare previously mentioned cells, (122, 124,136,137,138,139)). (It has been said that some cells make excellent velocity measuring devices (138)).

The cell was not found to be affected by strong alkalis or weak acids, i.e. it was stable over a pH range from 3 to 14. With strong acids however there was a slight change in the output, probably due to the presence of some hydrogen ions at the silver electrode. Other dissolved ions such as Cu^{2+}, Co^{2+}, Na^{+}, Cl^{-}, SO_3^{2-} and SO_4^{2-} did not affect the output from the oxygen

analysing cell.

The electrical life span of the cell was 48 hours continuous use at maximum voltage output, before any change was noticed in the output voltage valve. The decrease in output that ultimately appeared was due to a gradual build up of lead hydroxide on the lead electrode. The hydroxide was removed with very fine carborundum paper. The minimum mechanical life of the cell was 2 years continuous use before an electrode, usually the silver one, needed replacing. For their size and shape the cells were very robust. The silver electrodes of the cells were accidentally bent on many occasions during their lifetime without any impairment to the cell performance.

5. Temperature compensation of the oxygen analysing cell.

Since the output current from the cell is dependent on the temperature according to the law

$$i = K e^{-J/T} \qquad (6)$$

the cell has to be compensated so that the resultant output from the cell does not vary with temperature.

By using a thermistor it is possible to counteract the temperature variation of the cell since a thermistor resistance, R_{Th}, varies with temperature according to the law.

$$R_{Th} = A e^{B/T} \qquad (7)$$

(where A and B are thermistor constants). There are three known ways of utilising thermistors for temperature compensation:

(i) The first method uses a specially selected thermistor as the oxygen analysing cell load resistance and the voltage developed across the thermistor is measured using a high

impedance voltmeter.

$$\text{i.e. } V = i R_{th} \qquad (8)$$

and substituting for i and R_{th} in equation (8).

$$V = AKe^{\left(\frac{B-J}{T}\right)} \qquad (9)$$

and since the voltage is to be temperature independent, B is required to equal J exactly in equation (9).

In order for equation (6) to be valid, Rth must be very much less than the internal resistance of the cell. J usually has a value in the 3500 to 6000 ^{o}K range. It is only possible to obtain thermistors with a B value in this range whose resistance at 20^{o}C is 20K or greater. Consequently this method can only be used with oxygen analysing cells having a very high internal resistance and a very small output current.

(ii) To overcome the limitations of the method above, the thermistor is used as the feed back resistor of a directly coupled amplifier of high input impedance and gain ($-A_G$). It is then only necessary to select a thermistor with B equal to J to achieve compensation. The thermistor resistance is unimportant because the required output can be obtained by selecting a suitable value for R1, the output load resistance, and choosing the cell load resistance to be much less than the minimum internal resistance of the cell. See figure (x) for the circuit diagram. Figures (xi) and (xii) show other amplifier circuits which could be used.

Thus for figure (x) the output current, I out, is given by

$$I_{out} = i \frac{R_{th}}{R_1} \qquad (10)$$

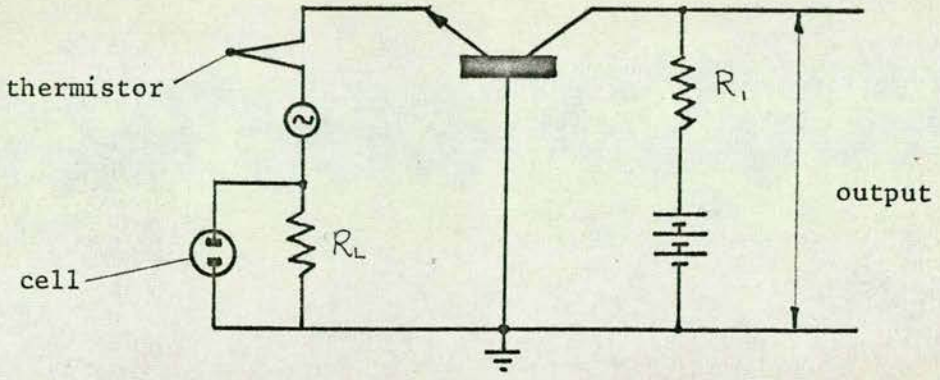

Figure (x) Transistorized amplifier

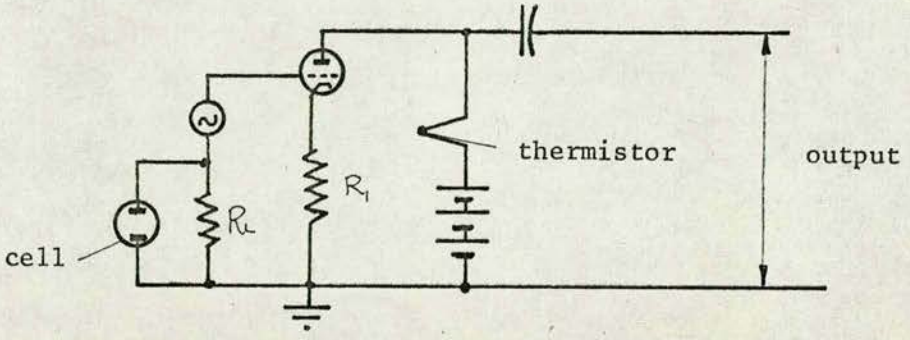

Figure (xi) Current feedback amplifier

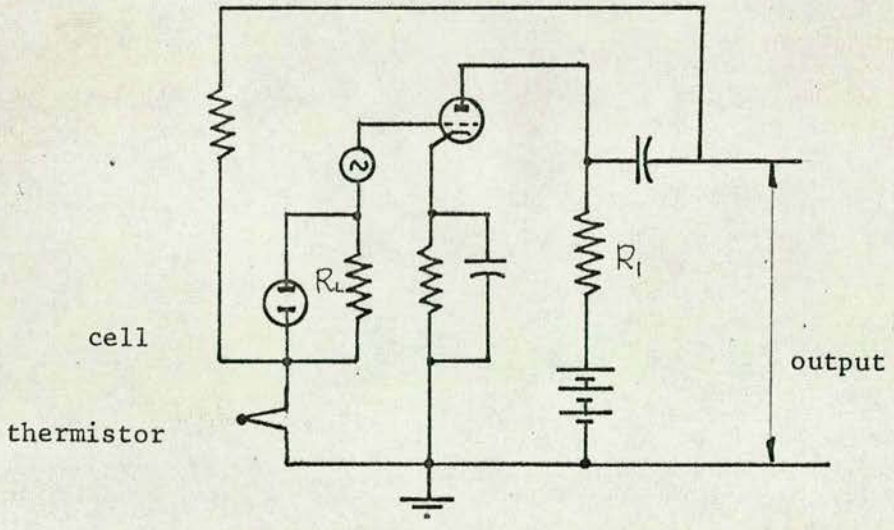

Figure (xii) Voltage feedback amplifier

and substituting for i and R_{Th} from equation (6) and (7), equation (10) becomes:

$$I_{out} = \frac{AK}{R_1} e^{\left(\frac{B-J}{T}\right)} \qquad (11)$$

and for temperature compensation

$$\frac{dI_{out}}{dT} = 0$$

$$\text{i.e.} \quad B = J. \qquad (12)$$

The only disadvantage of this method is that any difference between B and J becomes the temperature coefficient of the system e.g. if there was a 2% difference the system would have a temperature coefficient of about 0.1% per K.

If the J value for a particular cell varies appreciably each time a new membrane is put on, then a very wide range of thermistors would be required to cover all the possible values of J. Since there is only a limited range of thermistors available (150), methods (i) and (ii) are no use in this case.

(iii) This third method gives a limited temperature compensation over a small temperature range of about 7 °K.

A Wheatstone Bridge is used as the oxygen analysing cell load, the bridge consisting of two matched thermistors and two matched resistors, figure (xiii). The value of the resistance, R, can be calculated so that V_{AB}, the off-balance voltage between A and B, remains substantially independent of temperature over, say, a 10 °K temperature range.

The off-balance voltage is given by:

$$V_{AB} = \frac{i}{2} (R_{Th} - R) \qquad (13)$$

(Thus if the temperature increases by dT, say

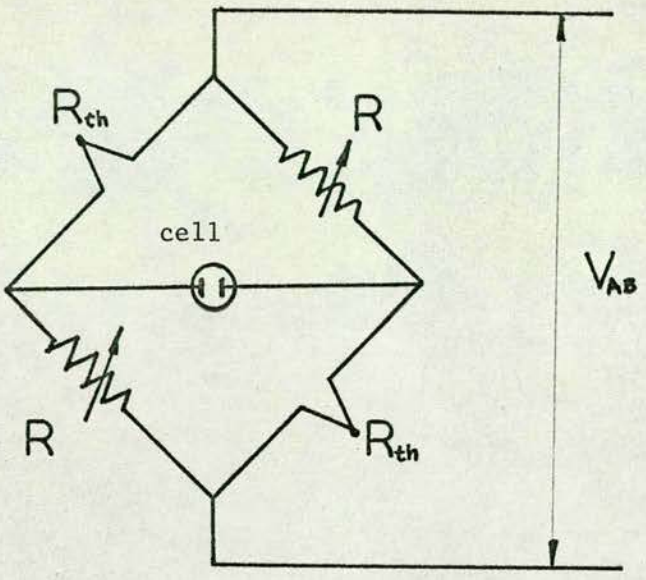

Figure (xiii) Wheatstone bridge network

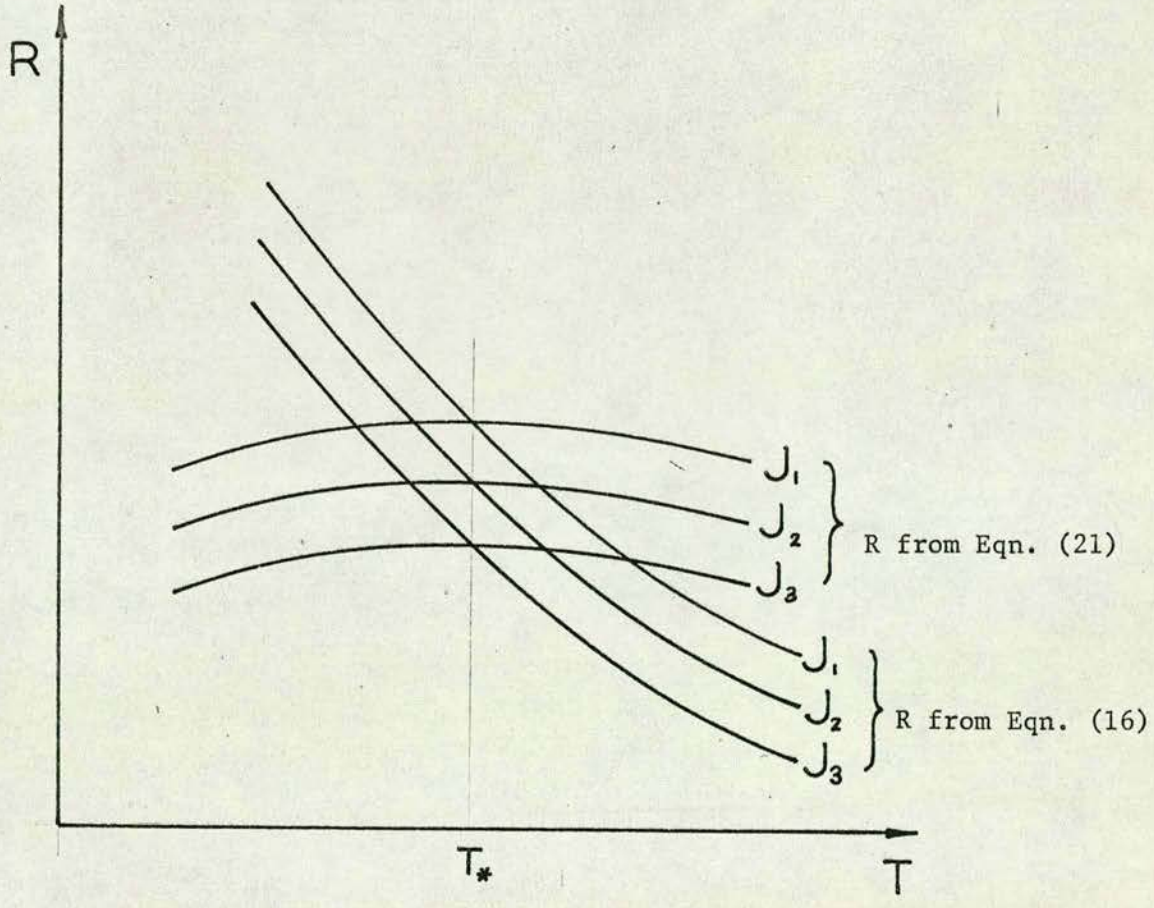

Figure (xiv)

$$V_{AB} = \frac{1}{2} (i + di) (R_{Th} - dR_{Th} - R - dR)$$

where V_{AB} has the same value as at temperature T).

Substituting in equation (13) for i and R_{Th}

$$V_{AB} = \frac{1}{2} K e^{-J/T} (Ae^{B/T} - R) \qquad (14)$$

and for temperature compensation

$$\frac{dV_{AB}}{dT} = 0$$

i.e. from equation (14)

$$\frac{JKe^{-J/T}}{2T^2} (Ae^{B/T} - R) + \frac{Ke^{-J/T}}{2} \left\{ \frac{-B}{T^2} Ae^{B/T} - \frac{dR}{dT} \right\} = 0 \qquad (15)$$

rearranging equation (15)

$$\frac{JAe^{B/T}}{T^2} - \frac{BAe^{B/T}}{T^2} - \frac{JR}{T^2} - \frac{dR}{dT} = 0$$

i.e. $$R = Ae^{B/T} \left(1 - \frac{B}{J}\right) - \frac{T^2}{J} \cdot \frac{dR}{dT} \qquad (16)$$

Neglecting the term $\frac{T^2}{J} \cdot \frac{dR}{dT}$

introduces a small error into the computations - in a typical case (Briggs and Viney's data) about 3%.

If the resistor is kept in a thermostatic box then $\frac{dR}{dT} = 0$. But in this work, when the water in the channel settled down to "steady state" conditions, any changes in the air temperature in the vicinity of the apparatus resulted in a corresponding change in the water temperature, and hence $\frac{dR}{dT} \neq 0$.

From equation (16) it can be seen that R is a function of temperature (see figure (xiv)). Over a temperature range of say ΔT with

$$T_N - T_1 = \Delta T \qquad (17)$$

(where T_N is the upper limit of the temperature range and T_1 is the lower limit of the temperature range) an average value for R can be found without neglecting the term $\frac{T^2}{J}\frac{dR}{dT}$

$$R_{av} = \frac{\sum_{T=T_1}^{T_N}\left[Ae^{B/T}\left(1-\frac{B}{J}\right)-\frac{T^2}{J}\frac{dR}{dT}\right]}{N} \qquad (18)$$

If instead of using Rav found from equation (18), Rav is taken as

$$R_{av} = Ae^{B/T_*} - (1 - B/J) - \frac{T_*^2}{J}\frac{dR}{dT} \qquad (19)$$

(which Briggs and Viney (141) used in their calculations). (T_* is the mean temperature of the range ΔT), then there would be an error of about 0.68% in the value of R_{av} used in the next part of the calculation.

Using Rav computed from equation (18), a value for V_{AB} can be found using equation (14) with the temperature at T_* i.e.

$$V_{AB}^{*} = \frac{Ke}{2}^{-J/T_*}\left(Ae^{B/T_*} - \frac{\sum_{T_1}^{T_N}\left[Ae^{B/T}\left(1-\frac{B}{J}\right)-\frac{T^2}{J}\frac{dR}{dT}\right]}{N}\right) \qquad (20)$$

This value of V_{AB}^{*} is now used to calculate a more accurate value for R using equation (14) i.e.

$$\frac{Ke}{2}^{-J/T_*}\left(Ae^{B/T_*} - \frac{\sum_{T_1}^{T_N}\left[Ae^{B/T}\left(1-\frac{B}{J}\right)-\frac{T^2}{J}\frac{dR}{dT}\right]}{N}\right)$$

$$= \frac{K}{2}e^{-J/T}\left(Ae^{B/T} - R\right)$$

$$\text{i.e. } R = Ae^{B/T} - \frac{e^{-J/T_*}}{e^{-J/T}}\left(Ae^{B/T_*} - \frac{\sum_{T_1}^{T_N}\left[Ae^{B/T}\left(1-B/J\right)-\frac{T^2}{J}\frac{dR}{dT}\right]}{N}\right) \qquad (21)$$

R is still a function of temperature, see figure (xiv)

From equation (21)

$$R_{aw} = \frac{\sum_{T_1}^{T_N}\left[Ae^{B/T} - \frac{e^{-J/T_*}}{e^{-J/T}}\left(Ae^{B/T_*} - \sum_{T_1}^{T_N}\left[\frac{Ae^{B/T}\left(1 - B/J\right) - \frac{T^2}{J}\frac{dR}{dT}}{N}\right]\right)\right]}{N}$$

Using this new value for R_{aw}, the variation of voltage with temperature can be calculated using equations (14) and (22)

i.e. $$V_{AB} = \frac{Ke^{-J/T}}{2}\left[Ae^{B/T} - \frac{\sum_{T_1}^{T_N}\left[Ae^{B/T} - \frac{e^{-J/T_*}}{e^{-J/T}}\left(Ae^{B/T_*} - \sum_{T_1}^{T_N}\left[\frac{Ae^{B/T}\left(1-\frac{B}{J}\right) - \frac{T^2}{J}\frac{dR}{dT}}{N}\right]\right)\right]}{N}\right] \quad (23)$$

and

$$(V_{AB})_{aw} = \frac{\sum_{T_1}^{T_N}\left[\frac{Ke^{-J/T}}{2}\left[Ae^{B/T} - \frac{\sum_{T_1}^{T_N}\left[Ae^{B/T} - \frac{e^{-J/T_*}}{e^{-J/T}}\left(Ae^{B/T_*} - \sum_{T_1}^{T_N}\left[\frac{Ae^{B/T}\left(1-\frac{B}{J}\right) - \frac{T^2}{J}\frac{dR}{dT}}{N}\right]\right)\right]}{N}\right]\right]}{N} \quad (24)$$

Using equations (23) and (24) the % error in V_{AB} can be calculated as a function of J and B, figure (xv).

This method still gives a temperature coefficient when J is altered but it is considerably smaller than that shown by method (ii).

An unsuccessful attempt was made to obtain an even better temperature compensation for the oxygen analysing cell by shunting a suitable resistor across the thermistor.

Going back to equation (16), it can be seen that before R can be calculated for a particular cell, A, B and J must be known. The first two can be found from thermistor manufacturer's (140) specifications, but the latter must be calculated from experimental data.

Figure (xvi) shows the apparatus used to determine J. The cell was immersed in a stirred beaker of oxygen saturated water, and the temperature of the water and the current through the cell

fig.(xv)

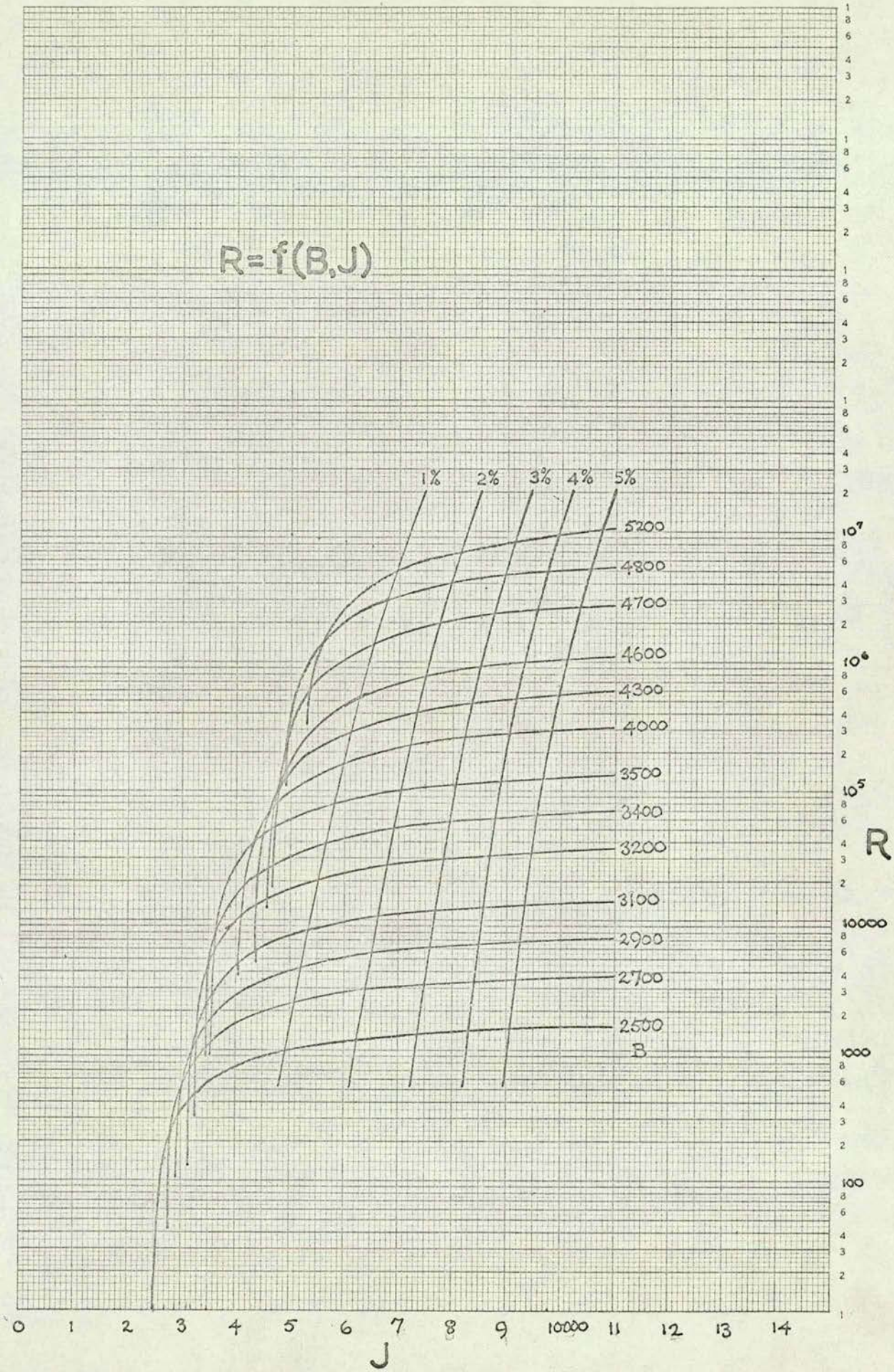

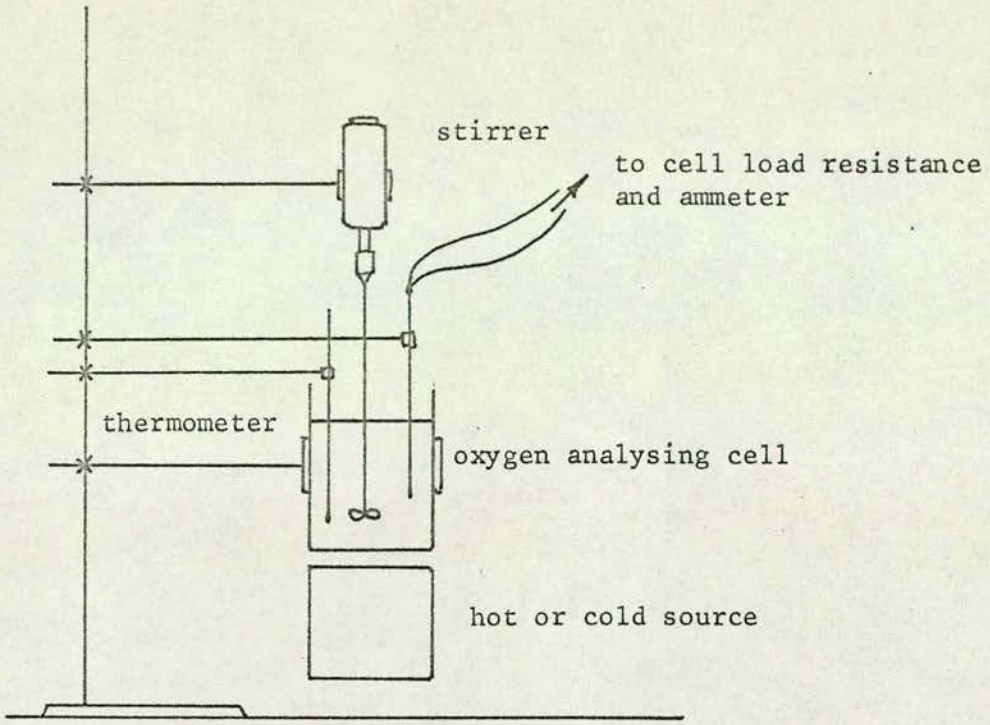

Figure (xvi) Apparatus to determine J

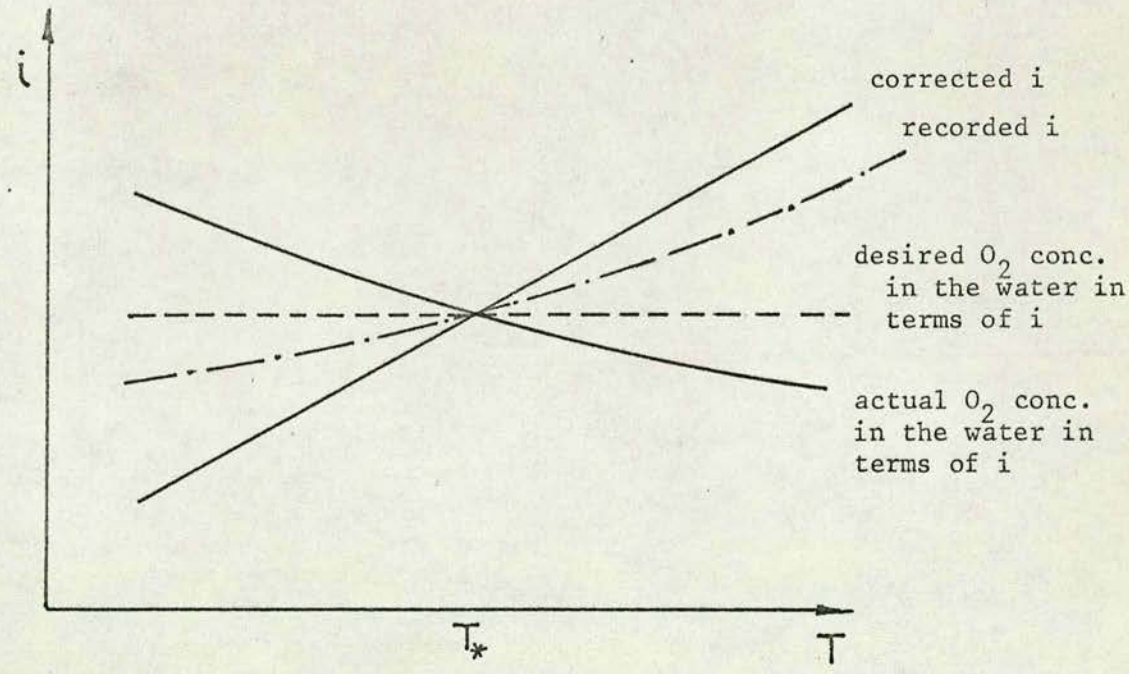

Figure (xvii)

Figure (xviii)

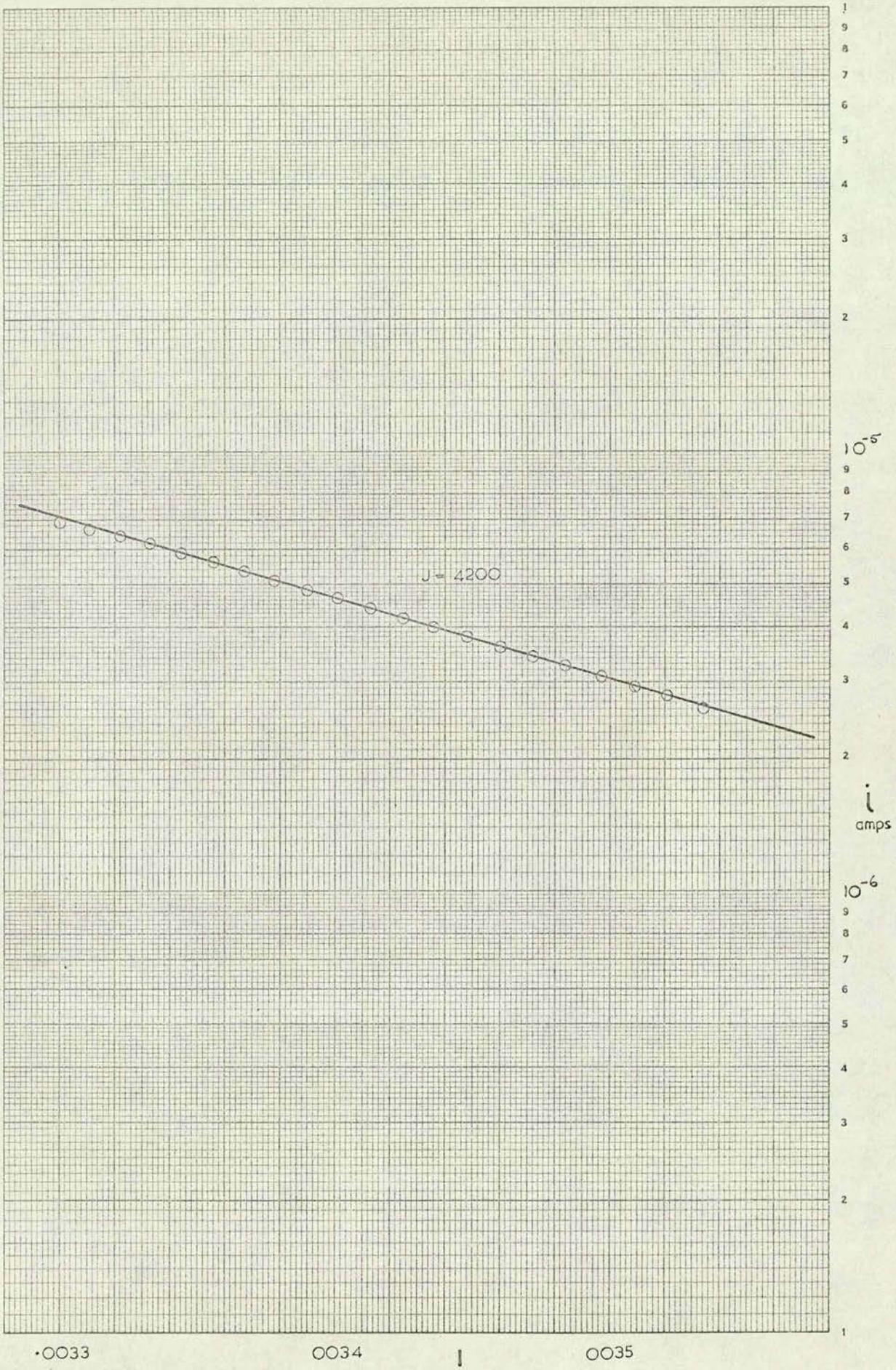

noted. The temperature was then changed, using either a freezing mixture or a hot plate applied to the outside of the beaker, and the new temperature and current recorded. Since the saturated dissolved oxygen concentration in water changes with temperature (142) the recorded current must be corrected for changes in the saturated oxygen concentration in the water as the temperature changes (see Figure xvii). From equation (5), the current through the cell is proportional to the oxygen concentration in the water. Using this fact a relationship between the oxygen concentration and the current can be found and figure (xvii) can be altered to read the current that would be expected a saturated dissolved oxygen concentration is in water. This is done by multiplying the observed current by the ratio of the saturated oxygen concentration at T to the saturated oxygen concentration at T.

Figure (xvii), the log of the corrected current was plotted against the reciprocal of the absolute temperature (figure xviii) and the slope of the resultant graph gave the value of J. The values obtained lay mainly in the 4000 to 4500 range.

Once J was found for a particular oxygen analysing cell, R, and hence the percentage error in V_{AB}, were calculated for a particular temperature from equations (22) (23) and (24). Experiments showed that the channel water in this work normally attained a value of about 23°C when the water was flowing under steady state conditions, and so for this work T_* was taken as 298°K. Figure (xix) shows the general solution of equation (22) along with the percentage error in V_{AB} over 10°K range for

fig.(xix)

$R = f(J.T_*)$

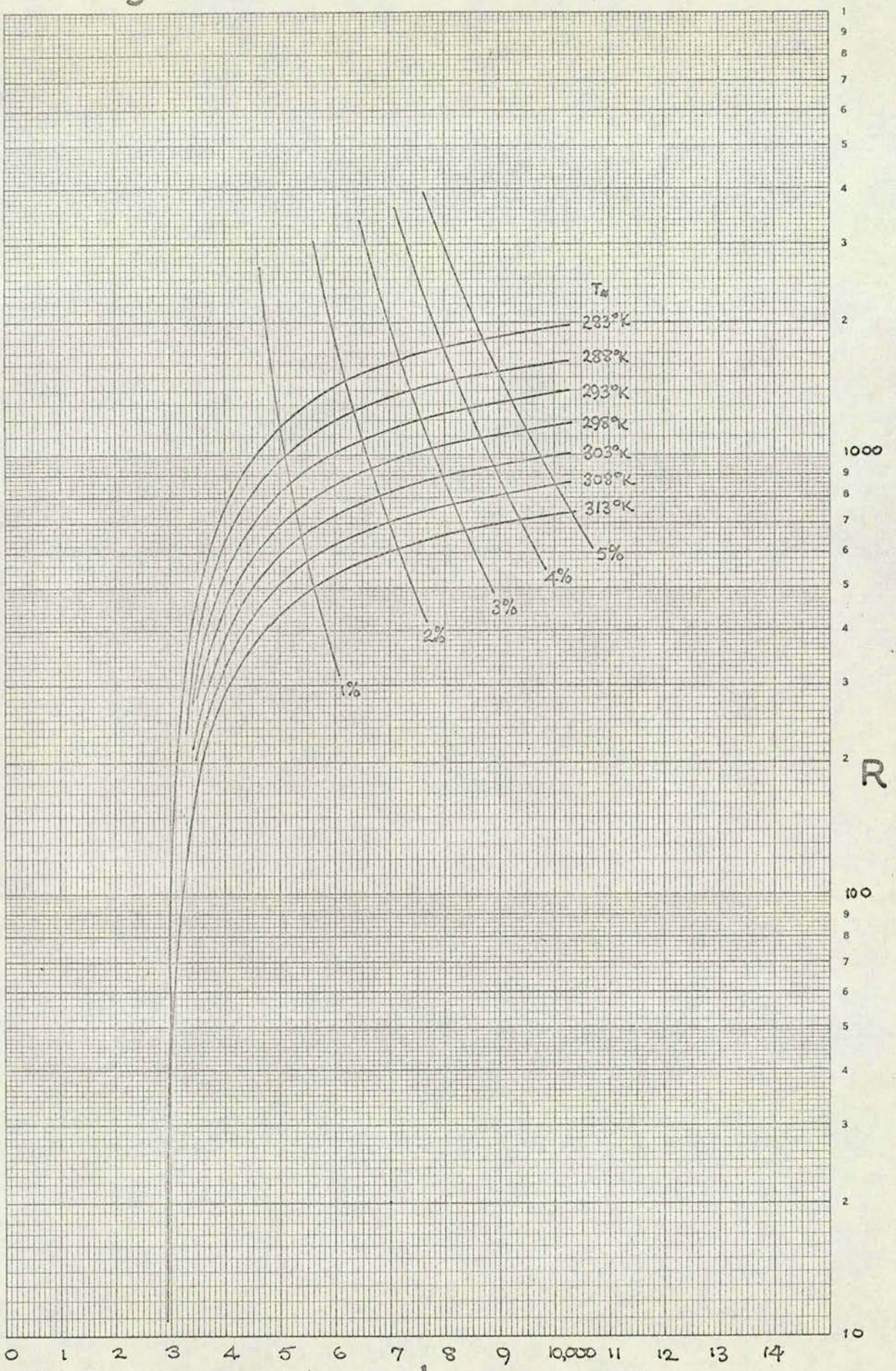

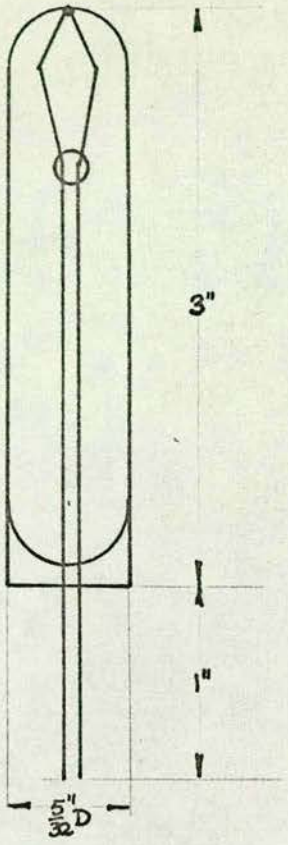

type F

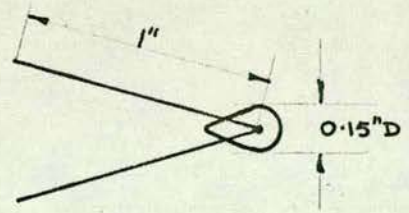

type G

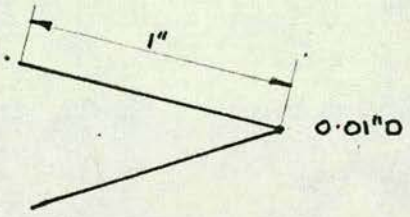

type U23 US

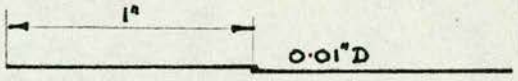

type U23 UD

Figure (xx) S.T.C. Thermistors

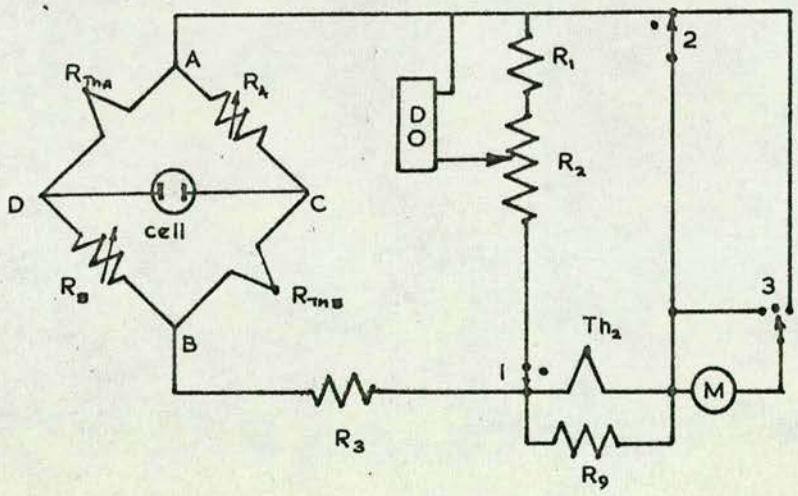

D.O. Dissolved oxygen recorder

Figure (xxi) Cricuit diagram for oxygen analysing cell

different values of J and $T_{\neq}$.

6. Choice of components for the temperature compensation and the circuit diagrams for the components.

Three types of thermistors were available from Standard Telephones and Cables Ltd. for temperature compensation, viz. type F, type G and type U. The dimensions and shapes are given in figure (xx)

Since, in section 1, condition (ii), a restriction was placed on the geometry of the oxygen analysing cell, the size of the thermistors was therefore likewise restricted as they were mounted on the stainless steel tube next to the cell. Hence from figure (xx) types F and G were ruled out leaving only type U, the US thermistor being preferred to the UD type.

In other cases where disturbances of the fluid in which the dissolved oxygen concentration is to be measured do not matter, then type G thermistors should be used since there is a reasonable variety of B values which are available to cover most of the possible values of J which may arise each time the membrane is changed. The nearer B is to J the better the compensation is for temperature fluctuations.

The circuit diagram for one oxygen analysing cell is shown in figure (xxi). This shows that a shunted thermistor was connected in series with a meter acting either as voltmeter or ammeter depending on how switches 1, 2 and 3 were placed. The meter had a positive temperature coefficient of 2% per ^{o}C which was compensated for by using the thermistor. The required degree of compensation was achieved by shunting the thermistor

with a resistor R_9. The value of R_9 was found as follows:

$$\frac{d}{dT}\left(\frac{Ae^{B/T} R_9}{Ae^{B/T}+R_9}\right) = \frac{Ae^{B/T} R}{(Ae^{B/T}+R)^2}\cdot\left(\frac{B}{T^2} Ae^{B/T} - \frac{dR_9}{dT}\right) + \frac{Ae^{B/T}}{(Ae^{B/T}+R_9)} \cdot \frac{dR_9}{dT}$$

$$- \frac{B}{T^2}\cdot\frac{Ae^{B/T} R_9}{(Ae^{B/T} + R_9)}$$

$$= -0.02 \quad \frac{Ae^{B/T} R_9}{(Ae^{B/T} + R_9)} \qquad (25)$$

The solution to equation (25) for R_9 when the temperature was 293°K (ambient room temperature) was

$$R_9 = 570\ \Omega$$

R (R_4 and R_8) varies between 0 and 850 Ω for the range of J normally encountered and T_* equals 298°K (see figure (xix)) and hence a wirewound potentiometer can be used in preference to a moulded carbon track potentiometer, having a lower temperature coefficient of resistance than the latter. Thus Rav as calculated from equation (22), remains the same or nearly at the same value as R calculated from equation (21), over the lower end of the temperature range. This was the reason why T_* was taken as 298°K and not the channel water of 296°K in this work.

Since there were two oxygen analysing cells, the final circuit made use of common components along with a temperature recording circuit which worked on the same principle as the cell circuit, except that the current supplied across CD was now kept constant by using a battery. Figure (xxii) shows the completed circuit and figure (xxiii) the wiring diagram for the control box. Plate II shows the outside of the control box panel with the various items labelled. Plate III shows the inside of the

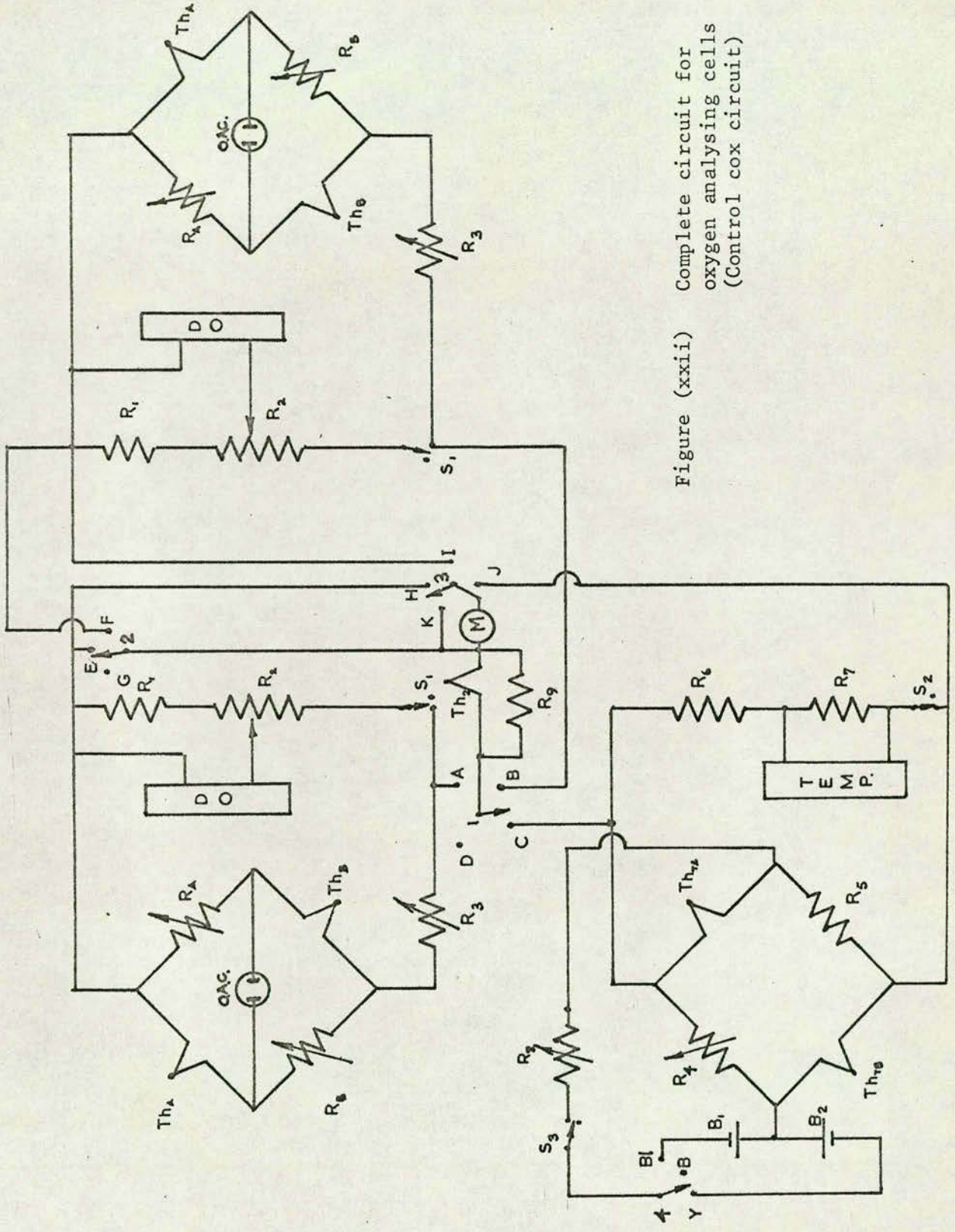

Figure (xxii) Complete circuit for oxygen analysing cells (Control cox circuit)

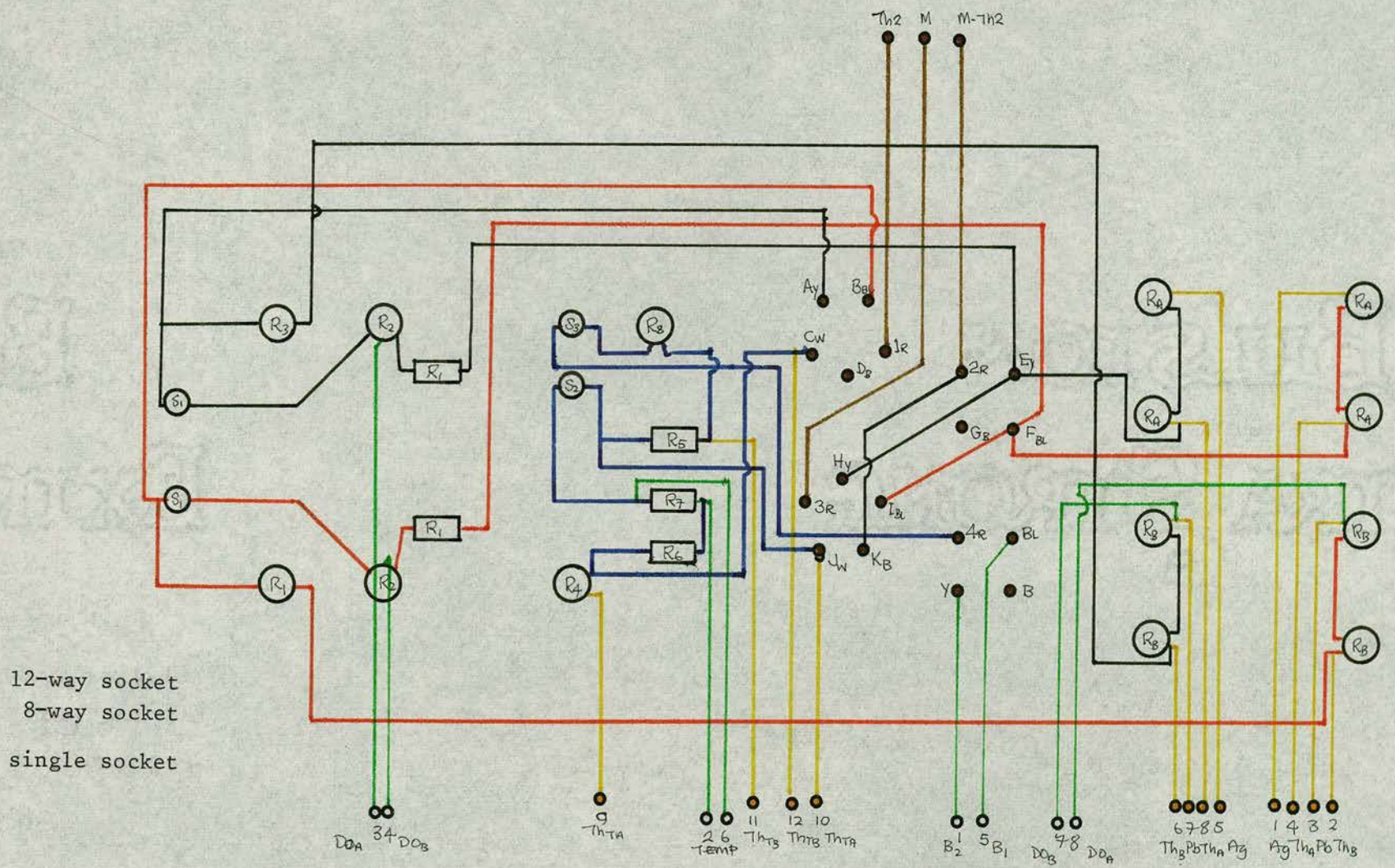

12-way socket
8-way socket
single socket

B - black Bl - blue R - red W - white Y - yellow

Figure (xxiii) Wiring diagram for the control box

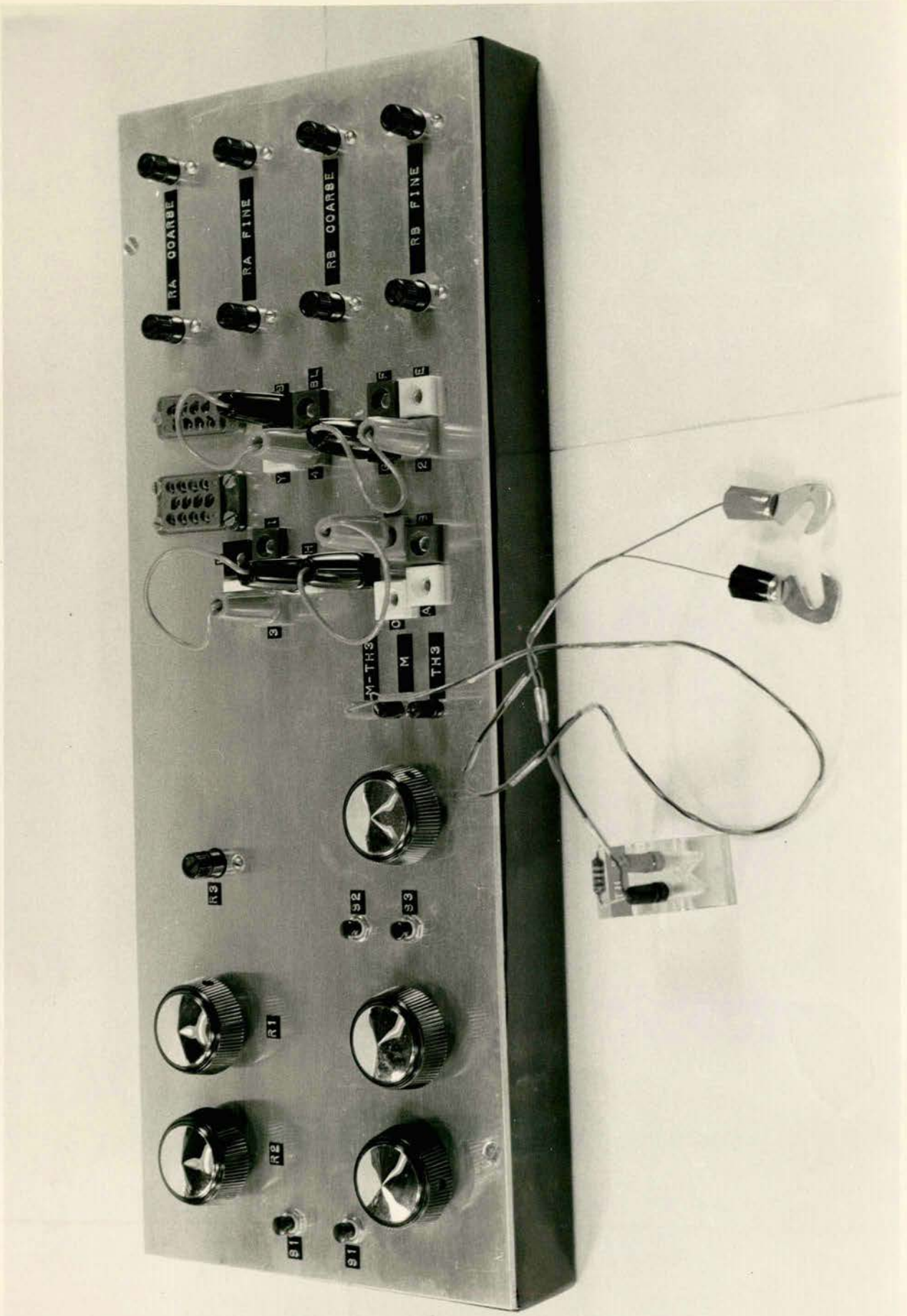
RA COARSE
RA FINE
RB COARSE
RB FINE
M-TH3
M
TH3
R3
S2
S3
R1
R2
S1
S1

Plate II

Plate III

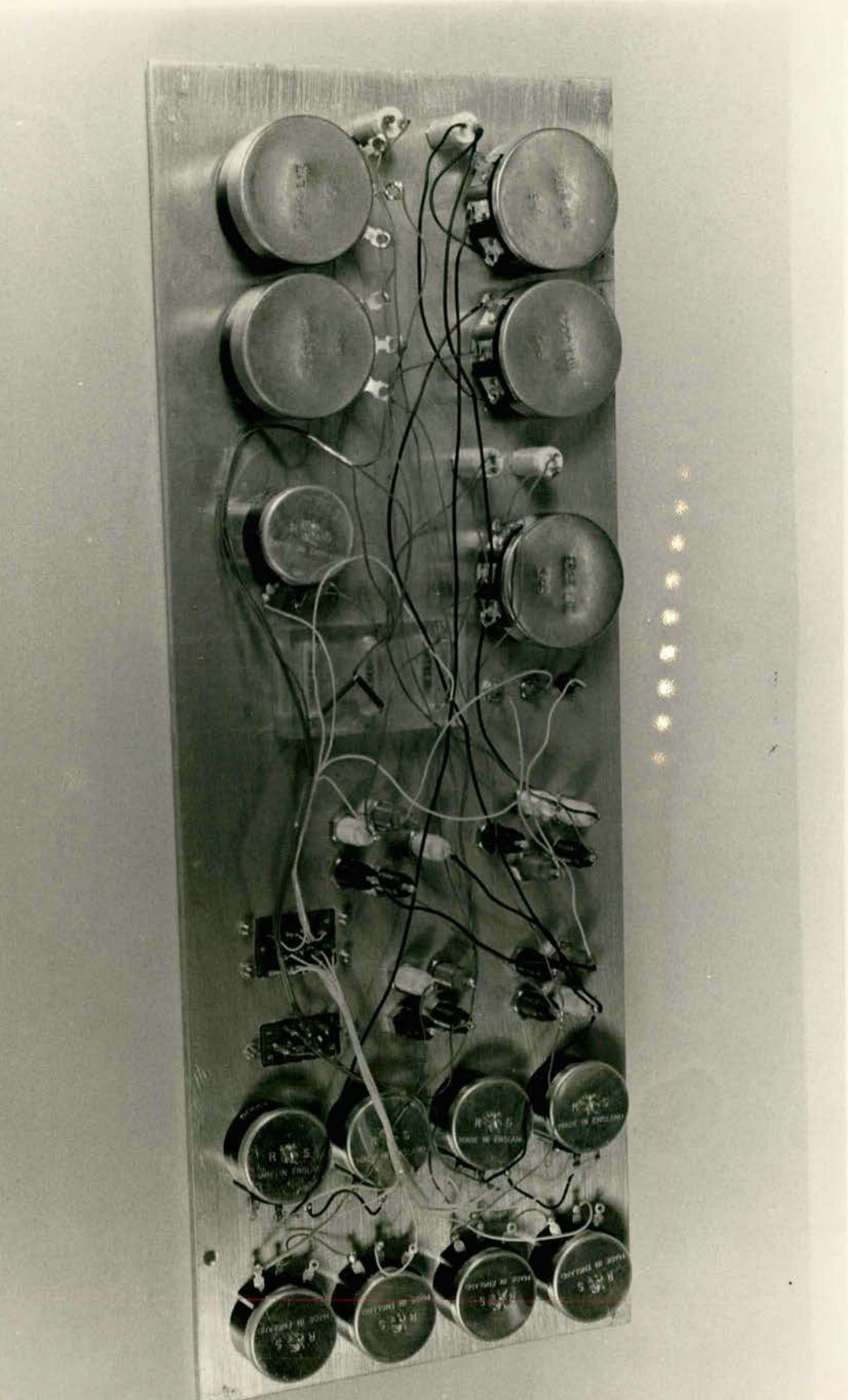

control box with the position of all the parts indicated. Table I contains the list of components and their source.

The connecting up of all the various parts was straightforward except when joining the thermistors on to their copper lead wires and to the stainless steel tube which was connected to the lead electrode.

Thermistor wires in this case were made of a platinum alloy, and the usual way of connecting them into a circuit is to use a "silver solder" (140) in a paint form and complete the soldering by applying heat using a non luminous gas flame with the added precaution of having a heat shunt across the thermistor. Since one of the thermistor wires was fixed to the stainless steel tube another method had to be found. This was simply to paint the wire into position using silver paint of the same type used for making the electrodes in the electrostatic plotting technique described in Appendix I. A small depression was drilled in the side of the stainless steel tube, and a drop of paint put into the depression along with the thermistor wire. More silver paint was added as each application dried, until the depression was full.

The other thermistor wires were also connected to the copper lead wires using the silver paint as it proved so successful. The thermistors were then set in position on the stainless steel tube with clear polyurethane paint and the lead electrode force fitted home (see figure (viiia)).

Once the polyurethane paint had dried the oxygen analysing cell was ready to receive its electrolyte, latex cap and membrane

as described in section 3. When this was completed, and J had been found and the required value of R (R_A and R_B) as found from figure (xix) had been set in the control box, the cell was ready for use.

7. Temperature Compensation Achieved.

The apparatus used was that shown in figure (xvii) with a water bath to alter the temperature of the air inside the control box artificially, so that the air - water temperature relationship of the channel could be simulated.

The temperature range over which the results were taken was 293°K to 303°K. The results for one cell are given in Table II. Similar results were obtained for the other cells. The error in the voltage V_{AB} over the 10°K range was 0.6%.

8. Tables. Table I. List of components.

Circuit Code		Source
B_1	1.5 bell cell	Ever Ready
B_2	Flag cell (1.5v)	Ever Ready
$R(R_A, R_B)$	750 ohm 3w potentiometer	Radio Spares Ltd.
R_1	10000 ohm 0.5w Hystab resistor	Radio Spares Ltd.
R_2, R_3, R_4	500 ohm 3w potentiometer	Radio Spares Ltd.
R_5, R_6	330 ohm 0.5w Hystab resistor	Radio Spares Ltd.
R_7	1400 ohm " " "	Radio Spares Ltd.
R_8	10000 ohm 3w potentiometer	Radio Spares Ltd.
R_9	570 ohm 0.5w Hystab resistor	Radio Spares Ltd.
S_1, S_2, S_3	Push to break switches	Radio Spares Ltd.
1 A B C D	5 x 4 mm sockets & banana plugs	Radio Spares Ltd.
2 E F G	4 x 4 mm " " " "	Radio Spares Ltd.
3 H.I J K	5 x 4 mm " " " "	Radio Spares Ltd.
4 BL BY	4 x 4 mm " " " "	Radio Spares Ltd.
M	Galvamp Type 391	Airmec
Th_A Th_B Th_{TA} Th_{TB}	U23US Matched Pair Thermistors	S.T.C
Th_2	U23US Thermistor	S.T.C

Table II. Voltage Obtained Across the Wheatstone Bridge.

$T^{c}K$	V_{AB} /mV)
293	42.7
294	42.4
295	42.6
296	42.1
297	41.4
298	41.8
299	42.2
300	42.2
301	42.1
302	41.9
303	42.1

T_{*}

Error in V_{AB} = 0.606%

Theoretical error in V_{AB} = 0.58%

APPENDIX III

METHOD OF USING OXYGEN ANALYSING CELLS TO MEASURE THE DISSOLVED OXYGEN CONCENTRATION DIFFERENCE, BETWEEN TWO POINTS A SHORT DISTANCE APART, IN AN OPEN CHANNEL.

1. Introduction.

From equation (73) and (74) of chapter 4 the term $\frac{\Delta \bar{C}_B}{\Delta l}$ is is required in the calculation of k_L. This therefore requires the measurement of the bulk dissolved oxygen concentration at two points a distance Δl apart.

In this work three methods for measuring the concentration difference were evaluated:

(i) "joined O.A.C.": In this method the outputs from two cells are added to give the difference between the outputs directly.

(ii) "separate O.A.C.": Two cells were used in separate circuits and the bulk concentrations at each point recorded continuously.

(iii) "moving O.A.C.": This method used only one cell which was moved from one fixed point to the other a distance away.

2. Choice of Method.

Method (i) gives $\Delta \bar{C}_B$, (which is small) directly, without the need for a difference calculation between two large numbers as in method (ii) and (iii). Method (iii) can be discarded since assumptions have to be made as to the dissolved oxygen concentration at one of the fixed points while the cell is measuring the dissolved oxygen concentration at the other fixed

point. During the operation of moving the O.A.C. from one point to the other, the presence of the operator's hand greatly increased the cell output.

Before a final decision was taken on what method to use, some experiments were carried out with the "joined O.A.C." and "separate O.A.C." methods.

3. Results of the two methods.

(a) "Joined O.A.C."

The initial experiments were made in a large beaker of water which was continuously stirred. The result obtained on the chart recorder was a d.c. signal with a superimposed a.c. signal.

Investigation of the a.c. part of the signal, using a high gain ascilliscope, showed that besides a 50 c/s pick up from the stirrer motor, the combined cells were acting as a V.H.F. aerial. The a.c. components of the output signal were removed by shorting the input to the recorder with a suitable capacitor ($4\mu F$) so that the response time of the recorder was not affected.

The d.c. signal was made up of other parts besides that produced by the dissolved oxygen. Part was due to a $10\mu A$ leak from the stirrer motor via the stainless steel impeller shaft. The rest was due to the formation of "voltaic cells" between the O.A.C. stainless steel holders and the stirrer shaft. The equivalent circuit is shown in figure (i). To overcome these d.c. signals, the stainless steel stirrer was replaced by a glass one and the lead electrodes were left unearthed.

Under conditions of zero dissolved oxygen concentration

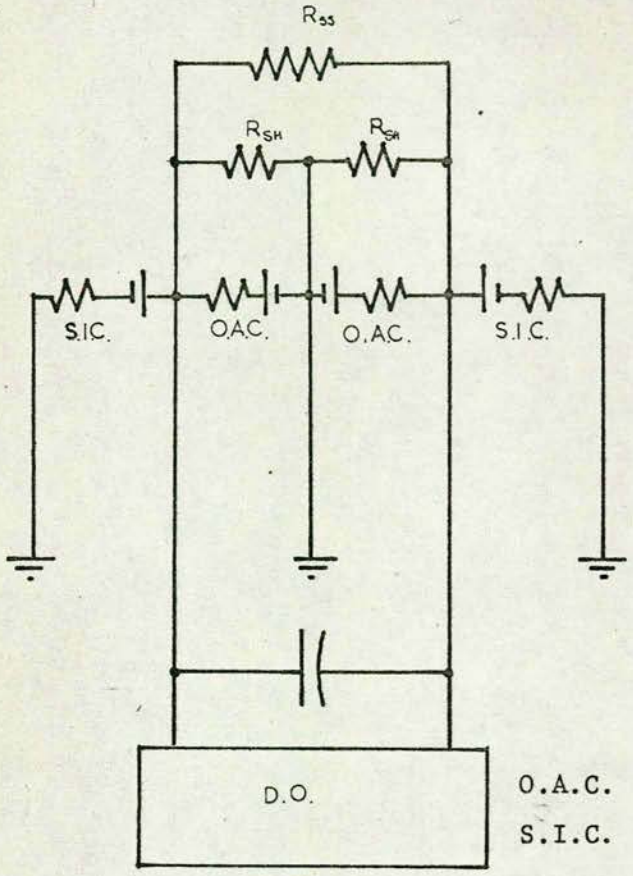

O.A.C. oxygen analysing cell

S.I.C. cell formed between stainless steel holder and impeller shaft

R_{ss} resistance between the stainless steel holders

R_{sh} resistance between the Ag electrode and the stainless steel holders

Figure (i) Equivalent circuit

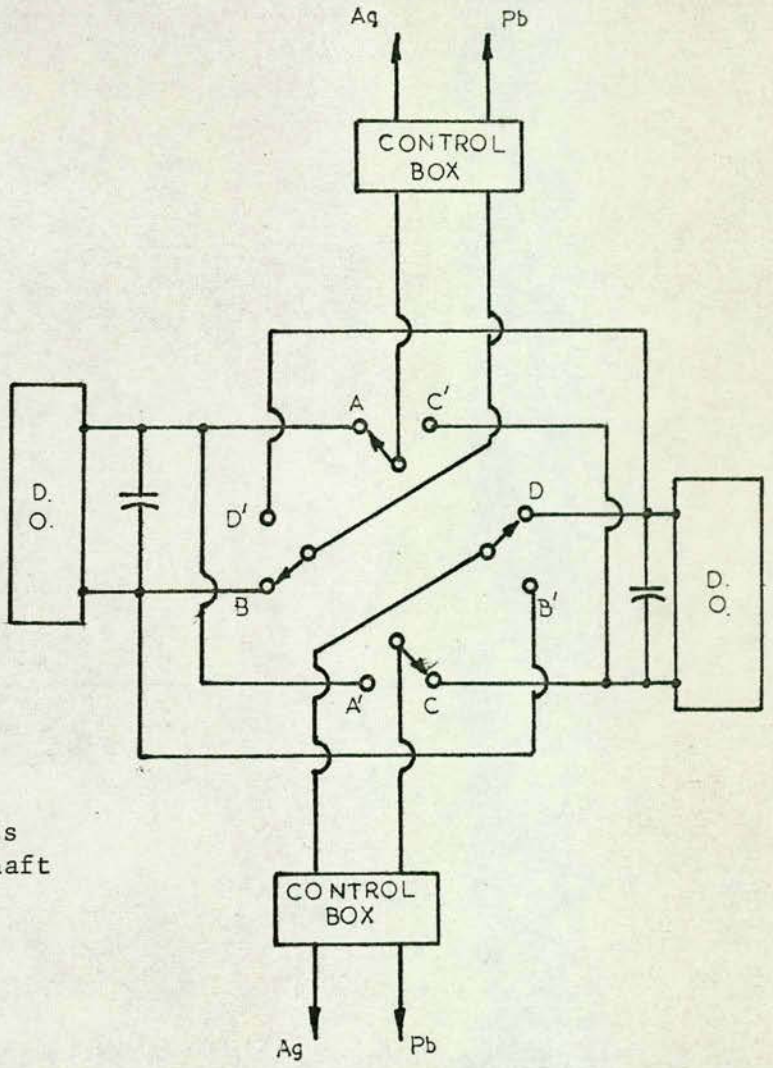

Figure (ii) Switching circuit

there was no a.c. or d.c. signal left now. The significance of the latter signal meant that any junction potentials in the external circuit were balancing each other. When this circuit was used with the two cells in the open channel, the result was that one of the oxygen analysing cell's output started to decrease rapidly at a regular rate. Briggs and Viney (141) have advised that on no account should two oxygen cells be used in the same circuit since, for Mackereth cells, there is a "leakage" resistance between them of about 20kΩ. No full explanation has yet been given as to why two oxygen analysing cells (O.A.C.) can't be used in the same circuit. When this cell was stripped down afterwards, the silver electrode was brown due to the following reaction taking place:

$$2\,Ag + O_2 \quad 2\,AgO$$

This reaction was promoted by the O.A.C. in the higher dissolved oxygen concentration region producing a higher output current than the other O.A.C. in the lower concentration region. Hence the higher current from the former cell was able to reverse the direction of current flow within the O.A.C. in the lower concentration region. This is the reason why two cells can't be used in the same circuit. It appeared that the only way to solve this problem was to use the "separate O.A.C." method.

(b) <u>The "separate O.A.C." method</u>.

The circuit used for the "separate O.A.C." was that shown in Appendix II, figure (xxiv), with a reversing switch between the two outputs from the control box to the chart recorders. This allowed any differences in the two recorder outputs to be

accounted for and provided a means of putting a time base on the two charts. This circuit is shown in figure (ii).

Initial tests with the "separated O.A.C." gave results similar to the "joined O.A.C." i.e. "burning out" of one of the cells. This was because there was a low "leakage" resistance of 1500 ohms between the two stainless steel holders i.e. between the lead electrodes. The "burn out" rate in this case was about 1 hour compared with 2 minutes for the "joined O.A.C.". The solution to this problem was to increase the resistance between the two lead electrodes till it is infinite or as near infinite as is practicable.

There were two possible methods of creating an infinite resistance between these electrodes. The first method tried was to completely cover the stainless steel holders with polyurethane paint. This proved impracticable since the paint was scraped off when the stainless steel holders were put into their probe holders in the base of the channel.

The alternative method was to cut from the stainless steel holder a piece of tubing about 0.75" long containing the cell and to insert a small tufnol spacer, as in figure (iii), between this and the rest of the stainless steel holder, and reassemble as in figure (iv). The tufnol spacer was held in position with Araldite. A coating of polyurethane paint was put over the 0.75" length piece of tubing, part of the lead electrode and the tufnol spacer.

Because of the extra wire now inside the stainless steel holder, connecting the lead electrode to the external circuit,

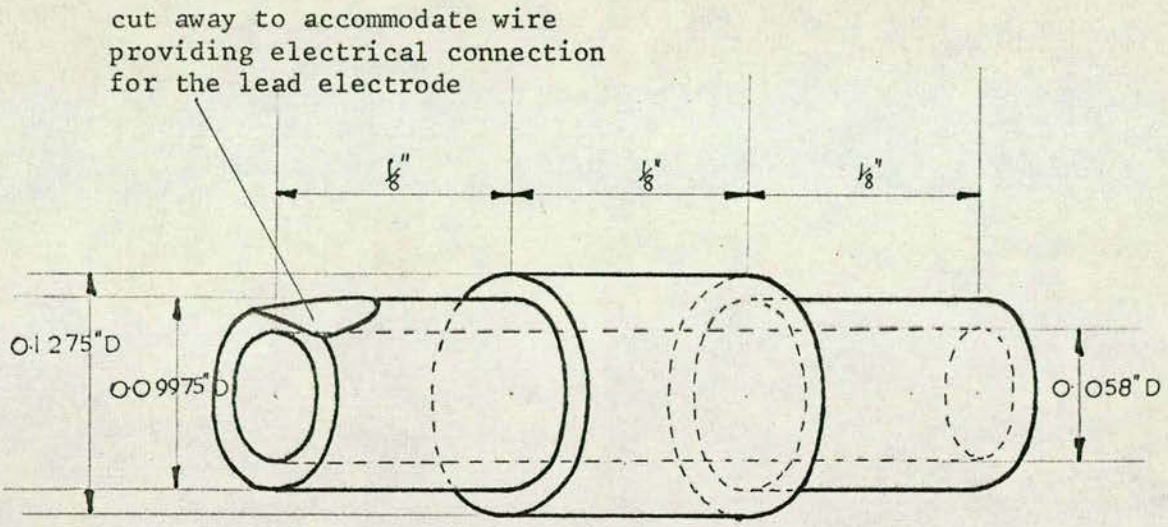

Figure (iii) Tufnol insulator

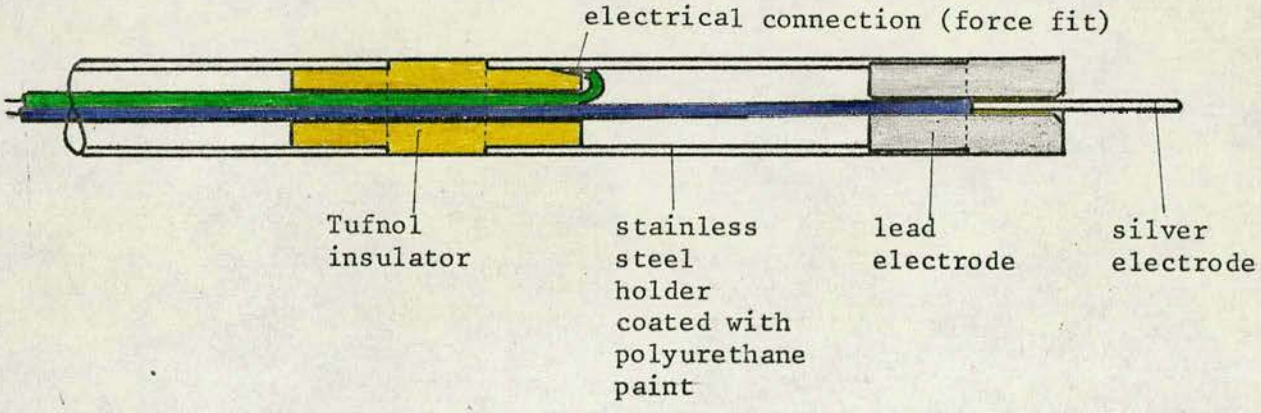

Figure (iv) Insulated oxygen analysing cell

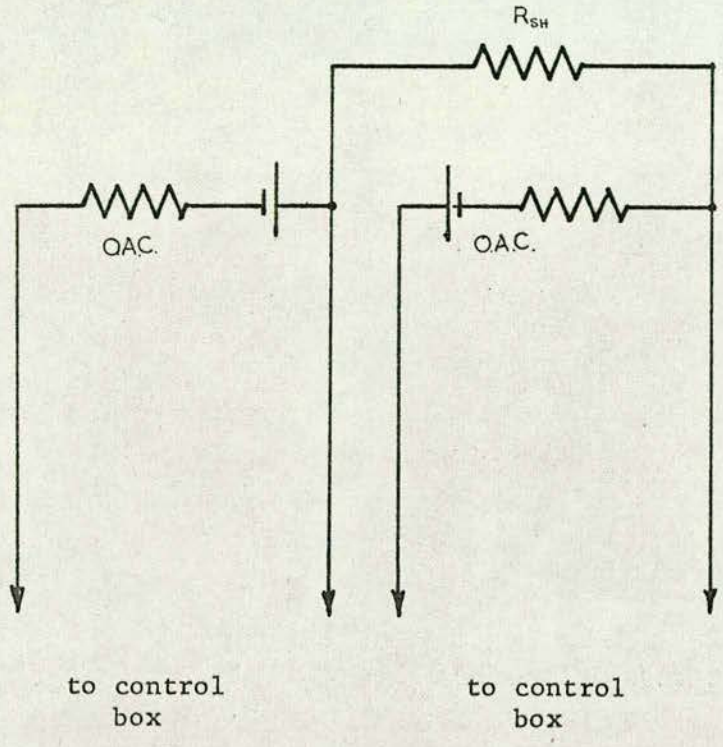

Figure (v) Equivalent circuit of insulated oxygen analysing cells

there was no room to accommodate the thermistors' wires internally. The thermistors were therefore mounted on a separate stainless steel holder.

The resultant assembly of the two oxygen analysing cells proved satisfactory. There was no zero drift in the recorder outputs due to the room temperature changes over a period of 48 hours. None of the oxygen analysing cells showed any signs of "burn out" after the tufnol spacer was inserted.

The reason for cranking the stainless steel holder tubes was to maximise the "leakage" resistances, Rss, and Rsh, between the silver electrodes and stainless steel holders. If this is not done "burn out" could still take place, although the rate would be very slow, since the "leakage" resistance in the uncranked case are much lower and approach that of the cell load resistances. The equivalent circuit is shown in figure (v).

APPENDIX IV

Dye dispersion extinction correction.

The cine film (Kodachrome II 8 m.m.) only records a certain minimum "dye" concentration in the water due to the composition of the film emulsion and the lighting conditions used. It is imperative, therefore, that this extinction concentration be known for the results from the cine film record to be meaningful. The experiments required to obtain data for the calculation of the "extinction" concentration were straight forward.

Two "dye" solutions were made up to known strengths. These two different "dyes" were then injected into the flowing water under identical hydrodynamic and lighting conditions. A condition governing one of the "dye" solutions was that it should "disappear" on the cine film record before the dispersion reached the exit end of the open channel.

The "extinction radius" r_e, can be found as follows:

Consider a plane perpendicular to the axis of the "dye" streams, at a distance x from the point of injection of the "dyes", where one of the "dye" dispersions becomes extinct with respect to the cine film. With reference to figure (i), and examining the quantity of matter which is not seen by the cine film in the volumes AB and CD, both quantities of "dye" matter in AB and CD will be equal.

Thus from equation (34) of the thesis

$$C(xr) = \frac{6N}{\pi r_a^2} e^{-\frac{6r^2}{r_a^2}} \qquad (i)$$

The total matter in volume AB

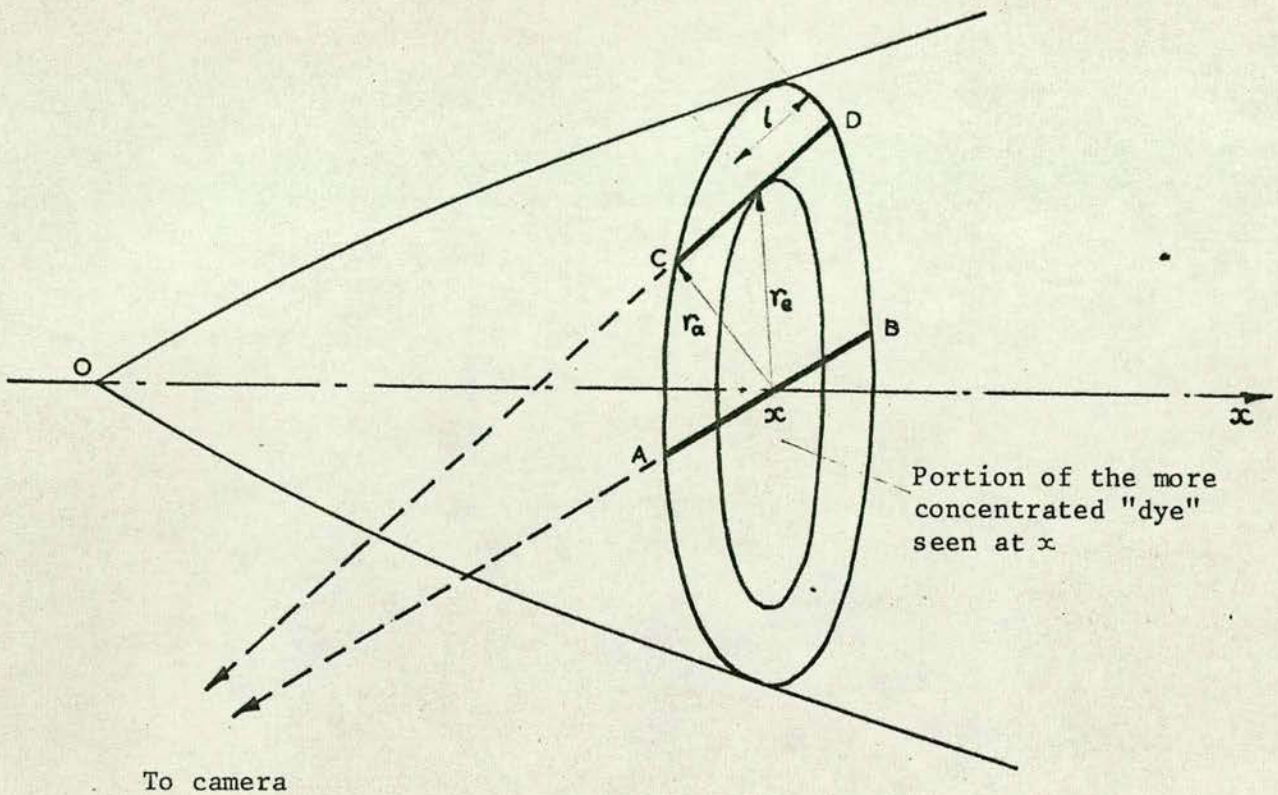
O
C
D
l
r_a
r_e
B
A
x
x
Portion of the more concentrated "dye" seen at x
To camera

$$= 2\int_0^{r_a} C_1(x,r)\,dr$$

$$= 2\int_0^{r_a} \frac{6N_1}{\pi r_a^2}\, e^{-\frac{6r^2}{r_a^2}}\, dr \qquad \text{(ii)}$$

The total matter in volume CD

$$= 2\int_0^{l} C_2(x,r)\,dl \qquad \text{(iii)}$$

where 2l is the length of a chord

and $dl = -r\,(r_a^2 - r^2)^{-\frac{1}{2}}\,dr$ (iv)

$l = l$ at $r = r_e$

$l = 0$ at $r = r_a$

substituting equation (iv) in equation (iii)

$$(\text{Total matter})_{CD} = 2\int_{r_e}^{r_a} \frac{6N_2}{\pi r_a^2}\, r(r_a^2 - r^2)^{-\frac{1}{2}}\, e^{-\frac{6r^2}{r_a^2}}\, dr \qquad \text{(v)}$$

In the experiments carried out to find the "extinction" radius r_e

$$N_2 = 13\,N_1 \qquad \text{(vi)}$$

Hence, equating equations (ii) and (v), substituting equation (vi) and simplifying yields:

$$\int_0^{r_a} e^{-\frac{6r^2}{r_a^2}}\, dr = \int_{r_e}^{r_a} 13r\,(r_a^2 - r^2)^{-\frac{1}{2}}\, e^{-\frac{6r^2}{r_a^2}}\, dr \qquad \text{(vii)}$$

Solving the integral on the left hand side of equation (vii) first

$$I_{LHS} = \int_0^{r_a} e^{-\frac{6r^2}{r_a^2}}\, dr$$

Put $X = \frac{6r^2}{r_a^2}$; $dr = \frac{r_a^2}{12r}\,dX$

$$I_{LHS} = \frac{n}{2\sqrt{6}} \int_0^{X_a} X^{-\frac{1}{2}} e^{-X}\, dX$$

Successive integration by parts yields:

$$I_{LHS} = \frac{r_a}{2\sqrt{6}}\left[\left[2X^{\frac{1}{2}}\ e^{-X}\right]_0^{X_a} + \int_0^{X_a} 2X^{\frac{1}{2}}\ e^{-X}\,dX\right]$$

$$= \frac{r_a}{2\sqrt{6}}\left[\left[2X^{\frac{1}{2}}\ e^{-X}\right]_0^{X_a} + \left[\frac{2X}{3}^{\frac{3}{2}} e^{-X}\right]_0^{X_a} + \int_0^{X_a} 2.\frac{2X}{3}^{\frac{3}{2}}\ e^{-X}\,dX\right]$$

etc.

$$= \frac{r_a}{\sqrt{6}}\left[X^{\frac{1}{2}}\ e^{-X}\left(1 + \frac{2X}{3} + \frac{(2X)^2}{3.5} + \frac{(2X)^3}{3.57} + \ldots.\right)\right]_0^{X_a}$$

Expanding e^{-X} as a series and muliplying out yields

$$I_{LHS} = \frac{r_a}{\sqrt{6}}\left[X^{\frac{1}{2}} \sum_{n=0}^{\infty} \frac{(-1)^n}{(2n-1)n!}\ X^n\right]_0^{X_a}$$

$$= \frac{r_a}{\sqrt{6}}\left[\sqrt{6}.\ 0.364\right]$$

$$= 0.364\ r_a \qquad \text{(viii)}$$

Solving the integral on the right hand side of equation (vii)

$$I_{RHS} = 13\int_{re}^{ra} r(r_a^2 - r^2)^{-1/2}\ e^{-\frac{6r^2}{r_a^2}}\,dr$$

as before put $X = \frac{6r^2}{r_a^2}$

$$I_{RHS} = \frac{13r_a}{12}\int_{X_e}^{X_a}\left(1 - \frac{X}{6}\right)^{-\frac{1}{2}}\ e^{-X}\,dX$$

Expanding $\left(1 - \frac{X}{6}\right)^{-\frac{1}{2}}$ as a power series

$$I_{RHS} = \frac{13r_a}{12}\int_{X_e}^{X_a}\left(1 + \frac{X}{6}\frac{1}{2} + \frac{X^2}{2!6^2}\frac{1}{2}\frac{3}{2} + \frac{X^3}{3!6^3}\frac{1}{2}\frac{3}{2}\frac{5}{2} + ..\right)e^{-X}dX$$

Expanding e^{-X} as a series and multiplying out the two series yields:

$$I = \frac{13r_a}{12}\int_{X_e}^{X_a}\left[\sum_{n=0}^{\infty}\left[\sum_{m=0}^{n}\frac{(-1)^m\ 6^m\ k(k+1)(k+2)(...)}{(n-m)!\ m!(k+n-m)(k+n-1-m)(.)}\right]\left(\frac{X}{6}\right)^n\right]dX$$

$$= \frac{13r_a}{12}\left[\sum_{n=0}^{\infty}\left[\frac{1}{(n+1)}\left[\sum_{m=0}^{n}\frac{(-1)^m\ 6^m\ k(k+1)(k+2)(...)}{(n-m)!\ m!(k+n-m)(k+n-1-m)(.)}\right]\frac{X^{n+1}}{6^n}\right]\right]_{X_e}^{X_a}$$

where m = 0,1,2,3,4 ... n

n = 0,1,2,3,4,5,6 .....

k = 0.5

$$I_{RHS} = \frac{13r_a}{12}\left[X_a\left[\left(1 - \frac{X_a}{2.1!} + \frac{X_a}{3.2!} - \frac{X_a}{4.3!} + \frac{X_a}{5.4!} - \frac{X_a}{6.5!} + \ldots\right)\right.\right.$$

$$+ \frac{1}{2}\left(\frac{1}{2} - \frac{X_a}{3.1!} + \frac{X_a}{4.2!} - \frac{X_a}{5.3!} + \frac{X_a}{6.4!} - \frac{X_a}{7.5!} + \ldots\right)$$

$$+ \frac{3}{8}\left(\frac{1}{3} - \frac{X_a}{4} + \frac{X_a}{5.2!} - \frac{X_a}{6.3!} + \frac{X_a}{7.4!} - \frac{X_a}{8.5!} + \ldots\right)$$

$$\left.+ \frac{5}{16}\left(\text{etc.}\right)\right]$$

$$- X_e\left[\left(1 - \frac{X_e}{2.1!} + \frac{X_e}{3.2!} - \frac{X_e}{4.3!} + \frac{X_e}{5.4!} - \frac{X_e}{6.5!} + \ldots\right)\right.$$

$$+ \frac{1}{2}\beta\left(\frac{1}{2} - \frac{X_e}{3.1!} + \frac{X_e}{4.2!} - \frac{X_e}{5.3!} + \frac{X_e}{6.4!} - \frac{X_e}{7.5!} + \ldots\right)$$

$$+ \frac{3}{8}\beta^2\left(\frac{1}{3} - \frac{X_e}{4.1!} + \frac{X_e}{5.2!} - \frac{X_e}{6.3!} + \frac{X_e}{7.4!} - \frac{X_e}{8.5!} + \ldots\right)$$

$$\left.\left.+ \frac{5}{16}\beta^3\left(\text{etc.}\right)\right]\right]$$

i.e. $I_{RHS} = \frac{13r_a}{2}\left(\phi_1(X_a) - \beta\phi_2(X_e)\right)$

(since $X_e = \beta X_a$ and $X = 6$)

i.e. $I_{RHS} = \frac{13r_a}{2}\left(0.7779 - \beta\phi_2(X_e)\right)$ (ix)

Equating equation (viii) and (ix)

$$0.364 = \frac{13}{2}.\left(0.7779 - \beta\phi_2(X_e)\right) \quad (x)$$

The solution to equation (x)

$$\frac{r_e}{r_a} = 0.9923$$

r_a was measured from the "dye" dispersion, hence r_a was found.

For other "outer" radial values, r_e , along the dispersion, equation (x) is modified to

$$0.364 = \frac{13 r_{ax}^2}{2 r_a^2} \left(0.7779 - \beta \phi_2 (X_{ex})\right) \qquad \text{(xi)}$$

From other "extinction" radii r_{ex}, the corresponding r_{ax} were found. Equation (xi) was also used to find r_a for other dispersions at different depths. In this case r_{ax} is the required value of r_a for the dispersion at a different depth but at the same distance from the injector tube at which r_e was measured. For dispersions near the free surface equation (xi) becomes

$$0.364 = \frac{13 r_{ax}^2}{r_a^2} \left(0.7779 - \beta \phi_2 (X_{ex})\right).$$

Values of $\beta \phi_2 (X_e)$ and $\frac{r_e}{r_a}$ are tabulated below.

$\frac{r_e}{r_a}$	$\beta \phi_2 (X_e)$
0.51	0.1449
0.52	0.1482
0.53	0.1515
0.54	0.1548
0.55	0.1580
0.56	0.1613
0.57	0.1647
0.58	0.1680
0.59	0.1714
0.60	0.1749

$\frac{r_e}{r_a}$	$\beta \oint_2 (X_e)$
0.61	0.1784
0.62	0.1819
0.63	0.1856
0.64	0.1893
0.65	0.1932
0.66	0.1972
0.67	0.2013
0.68	0.2055
0.69	0.2106
0.70	0.2146
0.71	0.2194
0.72	0.2245
0.73	0.2298
0.74	0.2354
0.75	0.2413
0.76	0.2475
0.77	0.2541
0.78	0.2611
0.79	0.2685
0.80	0.2764

$\frac{r_e}{r_a}$	$\beta \phi_2 (x_e)$
0.81	0.2849
0.82	0.2939
0.83	0.3036
0.84	0.3141
0.85	0.3253
0.86	0.3375
0.87	0.3508
0.88	0.3652
0.89	0.3809
0.90	0.3983
0.91	0.4175
0.92	0.4388
0.93	0.4627
0.94	0.4897
0.95	0.5205
0.96	0.5560
0.97	0.5975
0.98	0.6467
0.99	0.7057
1.00	0.7779

APPENDIX V

Calculation of $\bar{C}_{Bav}$

Although the bulk of the fluid was mixed through its depth, there was a thin layer of fluid at the surface whose dissolved oxygen concentration varied somewhere between that of saturation on the surface, C_S , and that of the bulk liquid, C_B . Thus in the calculation of the mass transfer coefficient, the effect of this tin layer of varying concentration has to be taken into account through a mean concentration.

At any point ys, the bulk concentration, C_B, averaged over the plane is given by:

$$\bar{C}_B = \frac{1}{d}\left[\int_0^{y_B} C_B(y)dy + \int_{y_B}^{d} C(y)\,dy\right] \qquad (i)$$

where it will be assumed that

$$C(y) = \left(\frac{C_S - C_B}{d - y_B}\right)(y - y_B) + C_B \qquad (ii)$$

and d is total depth

and y is distance from the channel bottom.

y_B is the distance over which C_B extends

i.e. $C_B(y) = C_B$ (iii)

i.e. it is assumed that the variation of concentration within the thin layer at the surface in linear in y.

Substituting (ii) and (iii) in equation (i) gives:

$$\bar{C}_B = \frac{1}{d}\left[C_B y_B + \left[\left(\frac{C_S - C_B}{d - y_B}\right)\left(\frac{y^2}{2} - y_B y\right)\right]_{y_B}^{d} + C_B d - C_B y_B\right]$$

$$= \frac{1}{d}\left[\left(\frac{C_S - C_B}{d - y_B}\right)\left(\frac{d^2}{2} - y_B\, d - \frac{y_B^2}{2} + y_B^2\right) + C_B d\right]$$

$$= \frac{1}{d}\left[\left(\frac{C_S - C_B}{d - y_B}\right)\left(\frac{d - y_B}{2}\right)^2 + C_B d\right]$$

$$\bar{C}_B = \frac{1}{d}\left[\frac{C_S d}{2} - \frac{C_S y_B}{2} - \frac{C_B d}{2} + \frac{C_B y_B}{2} + C_B d\right]$$

$$= \frac{(C_S + C_B)}{2} - \frac{(C_S - C_B)}{2d}\, y_B \qquad \text{(iv)}$$

To find the bulk concentration between two planes at l_1 and l_2 at a given instant, we have to take into account that y_B is a function of x, the distance along the channel, and C_B a function of time t which can be converted into a function of x for the given instant. In this case

$$C_B = C_S\,(1 - e^{-\alpha_1 t})$$

or

$$C_B = C_S\,(1 - e^{-\beta_1 t}) \qquad \text{(v)}$$

where β_1 depends on C_{Bl_1}, C_{Bl_2} and the velocity. y_B has a linear relationship with x, viz:

$$y_B = (y_{Bl_1} - d)\frac{x}{l_1} + d \qquad \text{(vi)}$$

The bulk average concentration between ys planes at l_1 and l_2, see figure (i) is given by integrating equation (iv) with respect to x, i.e.:

$$\bar{C}_{Bav} = \frac{1}{(l_2 - l_1)} \int_{l_1}^{l_2} \left(\frac{(C_S + C_B(x))}{2} - \frac{(C_S - C_B(x))y_B(x)}{2d} \right) dx \qquad \text{(vii)}$$

Substituting equation (v) and (vi) in equation (vii) gives

$$\bar{C}_{Bav} = \frac{1}{(l_2 - l_1)} \int_{l_1}^{l_2} \left(\frac{(C_S + C_S(1 - e^{-\beta_1 x}))}{2} - \frac{(C_S - C_S(1 - e^{-\beta_1 x}))}{2d} \cdot \left((y_{Bl_1} - d)\frac{x}{l_1} + d\right) \right) dx$$

$$= \frac{1}{(l_2 - l_1)} \int_{l_1}^{l_2} \left(\frac{C_S + C_S\,(1 - e^{-\beta_1 x})}{2} - \frac{C_S(y_{Bl_1} - d)x}{2dl_1} - \frac{C_S}{2} + \frac{C_S\,(y_{Bl_1} - d)x}{2dl_1} - \frac{C_S\,(y_{Bl_1} - d)x e^{-\beta_1 x}}{2dl_1} + C_S(1 - e^{\beta_1 x}) \right) dx \qquad \text{(viii)}$$

Integration of equation (viii) yields

$$\bar{C}_{Bav} = \frac{1}{(l_2 - l_1)} \left[C_S \left(x + \frac{e^{-\beta_1 x}}{\beta_1}\right) - \frac{C_S (y_{Bl_1} - d)x^2}{4dl_1} \right.$$
$$\left. + \frac{C_S (y_{Bl_1} - d)x^2}{4dl_1} + \frac{C_S (y_{Bl_1} - d)e^{-\beta_1 x}}{2dl_1} \left(x + \frac{1}{\beta_1}\right) \right]_{l_1}^{l_2}$$
$$= C_S + \left(\frac{e^{-\beta_1 l_2} - e^{-\beta_1 l_1}}{\beta_1 (l_2 - l_1)}\right)$$
$$+ \frac{C_S (y_{Bl_1} - d)}{2d\, l_1 \beta_1 (l_2 - l_1)} \left[e^{-\beta l_2} \left(l_2 + \frac{1}{\beta_1}\right) - e^{-\beta l_1} \left(l_1 + \frac{1}{\beta_1}\right) \right] \quad \text{(ix)}$$

If $C_B(x)$ is taken as a linear function of x instead of an exponental function, then

$$C_B(x) = \frac{(C_{Bl_2} - C_{Bl_1})(x - l_1)}{(l_2 - l_1)} + C_{Bl_1}$$
$$= K(x - l_1) + C_{Bl_1} \quad \text{(x)}$$

Substituting equations (vi) and (x) into equation (iv) and integrating with respect to x yields:

$$\bar{C}_{Bav} = \frac{1}{(l_2 - l_1)} \int_{l_1}^{l_2} \left(\frac{(C_S + K(x - l_1) + C_{Bl_1})}{2} \right.$$
$$- \frac{(C_S - K(x - l_1) - C_{Bl_1})(y_{Bl_1} - d)x}{2dl_1}$$
$$\left. - \left(\frac{C_S - K(x - l_1) - C_{Bl_1}}{2}\right) \right) dx$$

i.e. $$\bar{C}_{Bav} = \frac{1}{(l_2 - l_1)} \int_{l_1}^{l_2} \left(K(x - l_1) + C_{Bl_1} - \frac{(C_S - C_{Bl_1})(y_{Bl_1} - d)x}{2dl_1} \right.$$
$$\left. + K\frac{(y_{Bl_1} - d)(x^2 - l_1 x)}{2dl_1} \right) dx$$

Integrating

$$\bar{C}_{Bav} = \frac{1}{(l_2 - l_1)} \left[K\left(\frac{l_2^2}{2} - l_1 l_2 - \frac{l_1^2}{2} + l_1^2\right) + C_{Bl_1}(l_2 - l_1) \right.$$
$$- \frac{(C_S - C_{Bl_1})(y_{Bl_1} - d)(l_2 - l_1)(l_2 + l_1)}{4dl_1}$$
$$\left. + K\frac{(y_{Bl_1} - d)}{2dl_1}\left(\frac{l_2^3}{3} - \frac{l_1 l_2^2}{2} - \frac{l_1^3}{3} + \frac{l_1^3}{2}\right) \right]$$

$$\bar{C}_{Bav} = \frac{1}{(l_2 - l_1)} K \frac{(l_2 - l_1)^2}{2} + C_{Bl_1}(l_2 - l_1)$$

$$- \frac{(C_S - C_{Bl_1})(y_{Bl_1} - d)(l_2 - l_1)(l_2 + l_1)}{4dl_1}$$

$$+ \frac{K(y_{Bl_1} - d)(l_2 - l_1)^2 (2l_2 + l_1)}{12\, dl_1}$$

$$= \frac{K}{2}(l_2 - l_1) + C_{Bl_1} - \frac{(C_S - C_{Bl_1})(y_{Bl_1} - d)(l_2 + l_1)}{4dl_1}$$

$$+ K \frac{(y_{Bl_1} - d)(l_2 - l_1)(2l_2 + l_1)}{12\, dl_1} \qquad \text{(xi)}$$

Substituting for K in equation (xi) yields

$$\bar{C}_{Bav} = \frac{(C_{Bl_2} + C_{Bl_1})}{2} - \frac{(C_S - C_{Bl_1})(y_{Bl_1} - d)(l_2 + l_1)}{4dl_1}$$

$$+ \frac{(C_{Bl_2} - C_{Bl_1})(y_{Bl_1} - d)(2l_2 + l_1)}{12\, dl_1} \qquad \text{(xii)}$$

The difference between the value of $\bar{C}_{Bav}$ found from equation (ix) and that found from equation (xii) was so small that equation (xii) was accurate enough for this work.

APPENDIX VI.

Table I: data for figure (i)

British Rivers.

River	Re_{HD}	$\frac{k_L}{U_{av}}$	$\frac{w}{d}$
Ivel River	14540	4.620	23.71
	13750	3.840	22.41
+	12200	6.300	25.06
	17250	2.018	18.50
	14920	7.000	26.04
	12690	3.095	28.81
	12470	2.310	23.73
	46700	2.634	19.01
	62950	3.623	19.09
	41600	2.097	7.35
	40730	3.353	11.11
Lark River	39240	1.027	12.91
□	51100	1.891	13.68
	89750	1.176	21.86
	98100	0.398	14.49
Derwent River	86150	3.518	30.41
△	102200	3.780	23.98
	78950	4.095	27.94
Black Beck	15570	5.070	38.35
▽	19520	4.325	30.13
	20900	3.508	28.18
	95100	3.433	26.87
	105900	2.530	20.54

River	Re_{HD}	$\frac{k_L}{U_{av}}$	$\frac{W}{d}$
▽	122000	2.578	11.49
St.Sunday Beck	75900	3.505	26.55
*	85300	2.166	24.72
Yewdale Beck	25470	3.623	27.07
	25400	3.505	36.89
·	72700	2.528	28.77
	75450	2.188	30.32
	75900	1.885	29.65
	75150	2.273	29.07
Colthouse River	34710	4.275	13.96
	37000	3.293	12.96
◐	33650	4.490	13.34
	34520	3.617	12.95
	24980	3.830	14.21
	21000	3.138	17.53
Tennessee Rivers.			
Clinch River	907000	0.646	70.03
	1676000	0.531	47.54
◒	842500	0.552	77.83
	1477500	0.303	58.31
	1463000	0.404	66.43
	1684000	0.820	43.65
Holston River	2886000	0.293	27.34
▾	483500	0.771	291.04
	858000	0.636	216.72

River	Re_{HD}	$\frac{k_L}{U_{av}}$	$\frac{w}{d}$
▼	1728000	0.409	146.92
	2479000	0.392	39.37
	1425000	0.261	65.82
	2127000	0.172	58.91
	2104000	0.315	63.65
	1523000	0.254	60.66
	3067000	0.304	42.93
	907500	0.476	23.20
Fr.Broad River	2009000	0.281	57.87
■	2495000	0.200	53.88
	725000	0.689	158.05
	1499000	0.308	112.87
	2094000	0.336	94.76
	2848000	0.376	79.14
	727000	0.617	120.51
	1502000	0.320	88.35
	2091000	0.522	75.28
	2842000	0.154	64.55
Watanga River	1533000	1.015	53.22
◓ Hiwassee River	817000	0.433	41.06
◑	880000	0.694	40.64

Channel	Re_{HD}	$\frac{k_L}{U_{av}}$	$\frac{w}{d}$
	900	0.889	23.80
	1360	1.385	16.68
⊖	1791	1.603	13.29
	2200	1.406	12.56
	2873	1.395	10.63
	4260	1.346	9.38
	5770	1.397	7.43

Ohio Rivers	Re_{HD}	$\frac{k_L}{U_{av}}$
Ohio River	91000	0.934
	92000	1.620
X	117000	1.430
	155000	1.211
	185000	1.412
	273000	0.756
	282000	0.574
	303000	1.476
	343000	1.439
	412000	0.601
Illinois River	1260000	0.464
○	1420000	0.474
	1460000	0.387
Elk River •	87000	1.184
Clarion River *	103000	1.766
San Diego Bay	381000	0.480
⊙	1580000	0.307
	3220000	0.293
Tennessee River	203000	1.247
▲	262000	0.810
	292000	2.003

Table II.

Solution to equation (57).

r_e cms	y_3 cm
0	0
0.5	0.485
1.0	0.971
1.5	1.456
2.0	1.941
2.5	2.427
3.0	2.912
3.5	3.397
4.0	3.883
4.5	4.638
5.0	4.853
5.5	5.338
6.0	5.824
6.5	6.309
7.0	6.793

Table III

Channel	Position of $\sqrt{\bar{u}^2}$ from the wall
Laufer	0.0100w
3.25" wide	0.0195w
5.5" wide	0.0115w
6" wide	0.0155w

Table IV.

Distance from channel floor in cms.	Velocity cm/sec				
	Valve setting				
	1.5	1.75	2.0	2.5	3.0
15.24	9.08	11.80	*16.13	15.27	17.35
14.5	9.45	12.37	17.60	16.60	17.98
14.0	9.60	12.61	*17.90	17.60	17.75
13.5	*9.85	12.42	18.00	18.00	17.50
13.0	10.33	12.00	17.95	18.35	*17.35
12.5	10.45	11.80	17.80	18.40	*17.00
12.0	9.82	11.70	17.60	18.40	16.50
11.0	9.60	11.61	17.37	18.40	16.13
10.0	9.40	11.40	17.05	18.35	15.55
9.0	9.13	11.25	16.80	18.20	15.40
8.0	8.82	11.10	16.42	18.13	14.50
7.0	8.60	10.98	15.90	18.00	13.88
6.0	8.33	10.84	15.27	17.60	13.07
5.0	7.90	10.60	14.60	17.10	12.18

Table V.

Distance from channel floor cms.	θ, degrees				
	Valve setting				
	1.5	1.75	2.0	2.5	3.0
15.24	5.0	10.7	*19.3	10.0	20.0
14.5	7.7	11.6	15.2	9.0	5.7
14.0	6.8	8.0	*15.2	7.8	5.3
13.5	*5.8	8.0	6.8	-	-
13.0	5.0	8.0	-	6.8	*3.5
12.5	4.3	6.8	4.7	-	-
12.0	3.8	4.5	4.5	4.3	3.5
11.0	3.8	3.5	4.3	3.9	3.0
10.0	3.5	3.5	4.2	3.8	3.0
9.0	3.3	3.5	3.6	3.3	3.0
8.0	2.9	3.3	3.6	3.3	3.0
7.0	2.9	3.3	3.5	3.3	3.0
6.0	2.9	2.8	3.0	3.3	3.0
5.0	2.9	2.8	2.5	3.3	2.5

TABLE VI. Comparison of "dye" dispersion results for u and L and those obtained from Batchelor and Townsends equations

y cms	$\sqrt{\frac{\overline{u^2}}{U}}$ (dye dispersion x = 18.5 cms)	$\sqrt{\frac{\overline{u^2}}{U}}$ (Batchelor & Townsends eqn.)
15.24	0.3840 cm/sec	0.0886 cm/sec
14	0.1920	
13	0.1396	
12	0.0873	
11	0.0873	
10.	0.0873	
9	0.0873	
8	0.0873	
7	0.0873	
	x = 26.5 cms	
15.24	0.3840 cm/sec	0.0405 cm/sec
14	0.1920	
13	0.0758	
12	0.0427	
11	0.0427	
10	0.0427	
9	0.0427	
8	0.0427	
7	0.0427	

(grid placed 0.5 cms from channel entrance)

at x = 18.5 cms		
y cms	L(from dye dispersion) cms	L(from Batchelor and Townsends eqn) cms
15.24	1.344	0.330
14	0.938	0.321
13	0.512	0.309
12	0.512	0.317
11	0.512	0.321
10	0.512	0.325
9	0.512	0.329
8	0.512	0.335
7	0.512	0.339
at x = 26.5		
15.24	1.302	0.722
14	0.911	0.702
13	0.494	0.676
12	0.494	0.694
11	0.494	0.702
10	0.494	0.708
9	0.494	0.720
8	0.494	0.732
7	0.494	0.742

Table VII.

Results from cine film record with obstacles in the channel.

Valve Setting	Object	Depth y (cms)	Velocity (cm/sec)	θ_1	l (cms)	$\frac{y-h_o}{d-h_o}$
1.5	HAO 5.5	15.24	11.61	19.0	5.178	1.0
		14.5	11.86	16.0	4.0	0.417
	HAO 5.0	15.24	13.20	6.0	4.997	1.0
		14.5	15.27	10.0	8.525	0.709
		14.0	12.62	13.5	6.725	0.512
		13.1	12.43	38.0	4.060	0.158
	HAO 4.0	15.24	15.02	6.0	5.36	1.0
		14.5	17.07	6.5	6.23	0.855
		14.0	16.98	9.0	9.03	0.756
	"	13.0	15.09	14.5	7.18	0.559
		12.0	14.51	33.5	4.93	0.362
		11.0	10.37	37.0	-	0.216
		10.8	10.01	44.0	-	0.212
	HAO 3.0	15.24	17.47	7.5	5.46	1.0
		10.0	11.61	20.0	4.51	0.312
	HAO 2.0	15.24	14.51	10.0	5.59	1.0
		14.5	15.28	9.5	7.00	0.928
		14.0	15.69	8.3	7.18	0.879
		13.0	15.28	5.8	7.46	0.780
		12.0	15.28	3.8	-	0.681
		11.0	15.28	3.8	-	0.583
		10.0	15.28	5.3	-	0.484

Valve Setting	Object	Depth y (cms)	Velocity (cm/sec)	θ_1	l (cms)	$\frac{y-h_o}{d-h_o}$
1.5	HAO 1.0	11.0	13.51	5.0	9.01	0.666
		10.0	13.51	5.0	8.27	0.588
		9.0	13.83	5.5	6.34	0.509
		8.0	13.83	4.5	5.59	0.430
		7.0	13.21	4.5	-	0.351
		6.0	12.93	4.5	-	0.272
* 1.75	HAO 5.5	15.24	16.13	40.0	-	1.0
		14.5	13.51	33.5	4.54	0.417
	HAO 5.0	15.24	19.36	15.0	-	1.0
		14.5	17.60	10.0	10.62	0.709
*		14.0	16.69	21.5	7.40	0.512
		13.05	14.88	37.0	-	0.138
	HAO 4.0	15.24	18.15	7.5	-	1.0
		14.5	19.67	9.0	8.89	0.855
		14.0	19.63	8.8	11.57	0.756
		13.5	18.95	8.5	10.81	0.658
		13.0	18.73	13.5	8.54	0.559
		12.5	18.51	21.0	7.01	0.461
		12.0	18.51	29.0	4.94	0.362
		11.0	16.13	34.0	-	0.216

Valve Setting	Object	Depth y (cms)	Velocity (cm/sec)	θ_1	l (cms)	$\frac{y-h_o}{d-h_o}$
1.75	HAO 3.0	15.24	22.33	7.0	-	1.0
		14.5	20.75	4.5	8.78	0.903
		14.0	24.20	6.5	9.68	0.837
		13.5	20.75	4.9	11.48	0.771
		13.0	22.33	4.5	10.99	0.706
		12.5	22.33	2.6	10.74	0.640
		12.0	24.20	4.8	9.70	0.575
		11.0	22.33	14.8	5.92	0.444
		9.0	19.36	18.8	-	0.312
		8.0	15.69	24.5	-	0.050
	HAO 2.0	15.24	18.15	11.5	6.65	1.0
		14.5	19.36	11.2	8.25	0.928
		14.0	20.75	8.8	9.01	0.879
		13.5	20.75	8.0	10.41	0.829
		13.0	20.75	6.7	11.14	0.780
		12.0	22.33	4.0	10.21	0.681
		11.0	22.33	3.7	9.00	0.583
		10.0	20.75	5.3	7.79	0.484
		9.0	20.75	6.5	6.49	0.386
		8.0	19.36	22.5	-	0.287
		7.0	18.15	34.5	-	0.189

Valve Setting	Object	Depth y (cms)	Velocity (cm/sec)	θ_1	l (cms)	$\frac{y-h_o}{d-h_o}$
1.75	HAO 1.0	15.24	20.75	8.0	6.01	1.0
		14.5	19.69	7.8	7.33	0.941
		14.0	19.36	7.3	8.69	0.902
		13.0	19.36	6.8	9.67	0.824
		12.0	19.36	6.5	10.72	0.745
		11.0	18.15	6.3	10.81	0.666
		10.0	18.74	6.0	9.23	0.588
		9.0	20.75	5.5	7.90	0.509
		8.0	18.15	5.5	6.27	0.430
		7.0	19.36	4.5	4.33	0.351
		6.0	16.13	6.5	-	0.272
2.5	HAO 5.5	15.24	19.36	41.0	6.07	1.0
		14.5	19.36	25.0	-	0.417
	HAO 5.0	15.24	24.20	18.0	6.07	1.0
		14.5	22.76	26.0	7.78	0.709
		14.0	22.33	21.0	8.87	0.512
		13.05	19.36	26.5	-	0.138
*2.5	HAO 4.0	15.24	22.33	14.0	5.89	1.0
		14.5	26.42	13.1	8.16	0.855
		14.0	27.65	12.5	10.66	0.756
		13.0	24.20	6.0	8.43	0.559
		12.0	21.52	27.6	-	0.362
		11.0	18.73	38.0	-	0.216

Valve Setting	Object	Depth y (cms)	Velocity (cm/sec)	θ_1	l (cms)	$\frac{y-h_o}{d-h_o}$
2.5	HAO 3.0	15.24	24.20	9.0	5.73	1.0
		14.5	23.25	10.8	8.39	0.903
		14.0	23.25	9.8	9.01	0.837
		13.0	29.06	4.3	10.63	0.706
		12.0	32.27	4.3	8.92	0.575
		11.0	26.42	8.5	7.74	0.444
		10.0	22.33	14.9	5.02	0.312
		9.0	19.36	16.0	-	0.181
		8.0	19.36	33.5	-	0.050
	HAO 2.0	15.24	24.20	16.0	6.11	1.0
		14.5	26.42	9.0	7.74	0.928
		14.0	24.20	12.3	9.43	0.879
		13.0	26.42	7.3	10.74	0.780
		12.0	26.42	4.8	11.49	0.681
		11.0	26.42	3.8	9.90	0.583
		10.0	26.42	5.5	8.03	0.484
		9.0	26.42	7.5	7.25	0.386
*		8.0	26.42	10.8	6.34	0.287
*		7.0	23.33	10.0	4.65	0.189
		6.0	18.15	20.1	-	0.091
		5.3	15.27	31.0	-	0.022

Valve Setting	Object	Depth y (cms)	Velocity (cm/sec)	θ_1	l (cms)	$\frac{y-h_o}{d-h_o}$
2.5	HAO 1.0	15.24	18.73	14.5	5.41	1.0
		14.5	22.33	14.1	6.81	0.941
		14.0	22.33	13.1	8.25	0.902
		13.0	20.75	6.1	8.78	0.824
		12.0	22.33	5.0	9.14	0.745
		11.0	22.33	6.0	10.56	0.666
		10.0	22.33	3.8	10.08	0.588
		9.0	22.33	4.9	9.14	0.509
		8.0	22.33	6.3	7.77	0.430
		7.0	22.33	6.1	6.56	0.351
		6.0	19.36	4.0	5.33	0.272
		5.0	16.13	6.0	5.23	0.217
1.5	Brass	15.24	-	12.0	-	1.0
	Object	14.0	-	3.25	11.39	0.784
		13.0	-	13.5	9.12	0.610
		12.0	-	18.5	7.36	0.436
		11.0	-	24.0	6.15	0.261
		14.5	-	-	4.55	0.871
		13.5	-	-	12.76	0.697
		10.0	-	-	2.95	0.087

TABLE VIII

Position of y_{BL1} in the open channel.

y_{BL1} (cms)	Valve Setting	Obstacle
14.5	1.5	None
14.2		9G grid
14.0		HAO 5.5
14.8		MO4
14.1	1.6	9G grid
14.4	1.75	None
13.8		HAO 5.5
15.0		MO4
14.4	2.5	None
13.6		HAO 5.5
15.0		MO4

(l_1 = 18.5 cms)

TABLE IX Mass Transfer Results.

Temperature 23°C

Valve setting	Obstacle	Mass transfer coefficient k_L (cm/sec)	Source Eqn.
1.5 (3500)	No 9G Grid	0.0068	(73)
		0.0070	
		0.0073	(74)
		0.0072	(76)
		0.0072	(77)(69)(70)
		0.0070	(77)(59)(66)
		0.0057	(77)(69)(82)
1.5 (4370)	None	0.0033	(73)
		0.0032	
		0.0032	
		0.0031	(76)
		0.0031	(77)(59)(66)
1.5 (4300)	H.A.O. 5.5	0.0062	(73)
		0.0069	(76)
		0.0069	(77)(59)(66)
1.5 (4080)	MO 4	0.0028	(73)
		0.0027	
		0.0028	(76)
		0.0068	(77)(59)(66)
1.6 (4370)	No 9G Grid	0.0072	(73)
		0.0067	(76)
		0.0079	
		0.0083	(77)(69)(70)
		0.0083	(77)(59)(66)
1.75 (5130)	None	0.0061	(73)
		0.0050	
		0.0063	(77)(59)(66)
		0.0062	

Valve setting	Obstacle	Mass transfer coefficient k_L (cm/sec)	Source Eqn.
1.75 (5000)	H.A.O. 5.5	0.0089	(73)
		0.0105	(76)
		0.0094	(77)(59)(66)
1.75 (4730)	M.O. 4	0.0023	(73)
		0.0023	
		0.0024	
		0.0022	(76)
		0.0029	
		0.0074	(77)(59)(69)
2.5 (7700)	None	0.0068	(74) at $\frac{\partial \bar{C}_B}{\partial t} = 0$
		0.0075	(73)
		0.0065	(76)
		0.0059	
		0.0067	(77)(59)(66)
2.5 (7450)	H.A.O. 5.5	0.0111	(73)
		0.0119	
		0.0111	(76)
		0.0116	
		0.0107	(77)(59)(66)
2.5 (7060)	M.O. 4	0.0030	(73)
		0.0031	
		0.0031	(76)
		0.0037	
		0.0082	(77)(59)(66)

The figures in brackets in the left hand column are the hydraulic depth Reynolds numbers.

TABLE X Data for figures (XXIX) and (XXX).

U_{av} cm/sec	Re_{HD}	$\frac{k_L}{U_{av}}$	$\frac{k_L}{U_{av}} (Re_{HD})^{0.5}$	$\left(\frac{\sqrt{v^2}}{U}\right)_{ss}$
6.45	3500	0.00106	0.0627	0.199
		0.00109	0.0645	
		0.00113	0.0668	
		0.00112	0.0663	
		0.00112	0.0663	
		0.00108	0.0639	
8.06	4370	0.000412	0.0272	0.0518
		0.000397	0.0262	
		0.000395	0.0261	
		0.000386	0.0255	
		0.000386	0.0255	
7.94	4300	0.000781	0.0512	0.164
		0.000870	0.0571	
		0.000870	0.0571	
7.45	4080	0.000370	0.0236	0.0346
		0.000356	0.0228	
		0.000370	0.0236	
8.06	4370	0.000895	0.0592	0.216
		0.000836	0.0553	
		0.000993	0.0657	
		0.00104	0.0688	
		0.00104	0.0688	
9.46	5130	0.000649	0.0465	0.0918
		0.000530	0.0379	
		0.000661	0.0473	
		0.000654	0.0468	

U_{av} cm/sec	Re_{HD}	$\frac{k_L}{U_{av}}$	$\frac{k_L}{U_{av}} (Re_{HD})^{0.5}$	$\left(\frac{\sqrt{\overline{v^2}}}{U}\right)_{ss}$
9.23	5000	0.000964	0.0682	0.346
		0.00114	0.0806	
		0.00102	0.0721	
8.74	4730	0.000262	0.0180	0.0173
		0.000263	0.0181	
		0.000275	0.0189	
		0.000252	0.0173	
		0.000332	0.0228	
14.20	7700	0.000476	0.0417	0.0864
		0.000493	0.0433	
		0.000457	0.0401	
		0.000415	0.0364	
		0.000472	0.0414	
13.72	7450	0.000803	0.0693	0.354
		0.000867	0.0748	
		0.000803	0.0693	
		0.000845	0.0729	
		0.000780	0.0674	
13.02	7060	0.000227	0.0191	0.0216
		0.000237	0.0199	
		0.000239	0.0201	
		0.000289	0.0243	

APPENDIX VII.

Two-dimensional random walk of a particle on a hexagonal grid.

at start .1

one step 1 1

n = 1 1 0 1 probability at each point is $\frac{a}{6}$ (where a is any whole number)

1 1

two steps 1 2 1

n = 2 2 2 2 2

1 2 6 2 1 $\frac{a}{36}$

2 2 2 2

1 2 1

total of all the numbers in the grid is 6^n where n is the number of the step.

Total = 6 (total in triangle) + number at the origin

Total = 6 . 5 . + 6

= 36

= 6^2

i.e. the total probability of the particle being on the grid is 1.

For further steps only one sixth of the grid will be shown, since the grid is symmetrical.

n = 3 12

15 15 probability = $\frac{a}{216}$

6 6 6

1 3 3 1

Total = 6.34 + 12

= 216

= 6^3

i.e. probability of the particle being on the grid is 1

n = 4

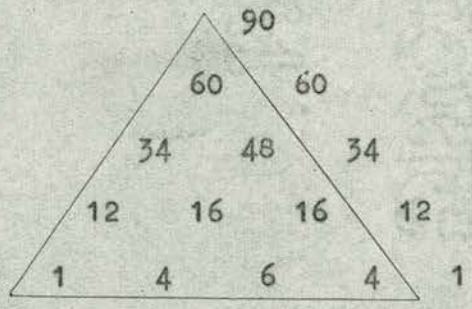

probability = $\frac{a}{1296}$

Total = 6.201 + 90

= 1296

= 6^4

n = 5

360

340 340

200 220 200

75 120 120 75

20 35 40 35 20

1 5 10 10 5 1

probability = $\frac{a}{7776}$

n = 6

2040

1680 1680

1095 1320 1095

530 690 690 530

156 270 330 270 156

30 66 90 90 66 30

1 6 15 20 15 6 1

probability = $\frac{a}{46656}$

n = 7

10080

9135 9135 probability = $\frac{a}{179936}$

6230 6930 6230

3171 4235 4235 3171

1232 1862 2100 1862 1232

301 567 791 791 567 301

42 112 182 210 182 112 42

1 7 21 35 35 21 7 1

n = 8

54810 probability = $\frac{a}{1,679,616}$

48440 48440

34636 39200 34636

19656 24528 24528 19656

8330 12096 13776 12096 8330

2632 4480 5712 5712 4480 2632

540 1120 1736 2016 1736 1120 540

56 176 336 448 448 336 176 56

1 8 28 56 70 56 28 8 1

n = 9

290640 probability = $\frac{a}{10,077,696}$

264726 264726

195552 215208 195552

116214 143892 143892 116214

55440 76482 84672 76482 55440

20070 31626 39816 39816 31626 20070

5280 9900 14112 15792 14112 9900 5280

909 2088 3654 4662 4662 3564 2088 909

72 261 576 882 1008 882 576 261 72

1 9 36 84 126 126 84 36 9 1

n = 10

1588356 probability = $\frac{a}{60,466,176}$

1446060 1446060

1099140 1208340 1099140

691740 832020 832020 691740

352500 471660 520380 471660 352500

143772 215820 262500 262500 215820 143772

44955 76740 105360 117180 105360 76740 44955

10050 20490 32220 (40020) 40020 32220 20490 10050

1450 3690 6915 10020 11340 10020 6915 3690 1450

90 370 930 1620 2100 2100 1620 930 370 90

1 10 45 120 210 252 210 120 45 10 1

Each number in a new network is obtained by adding the 6 neighbouring numbers about the corresponding point in the (n - 1) network

e.g. for n = 10 and the point ringed

number = sum of 6 ringed numbers in the ninth network.

The data taken from the tenth network for figure (xii) of the thesis is tabulated below.

r_a = 7.75 step units

$\frac{r}{r_a}$	$\frac{P(xr)}{P(x,o)}$
0	1.0
0.129	0.910
0.226	.760
0.258	.691
0.343	.524
0.388	.432

$\frac{r}{r_\alpha}$	$\frac{P(xr)}{P(x,o)}$
0.451	.328
0.473	.297
0.516	.222
0.560	.165
0.601	.135
0.645	.0905
0.678	.0738
0.692	.0666
0.710	.0483
0.775	.0283
0.838	.0129
0.903	.0063
1.0	.0025

By reflecting a random walk about a surface it can be shown that equation (35) should be twice equation (34).

at start - - - - - - - 1 - - - - - - surface

probability

n = 1 - - - - 1 - - 0 - - 1 - - - - $\frac{a}{6}$

2 2

n = 2 - - - - 1 - - 2 - - 6 - - 2 - - 1 - - $\frac{a}{36}$

4 4 4 4

2 2 2

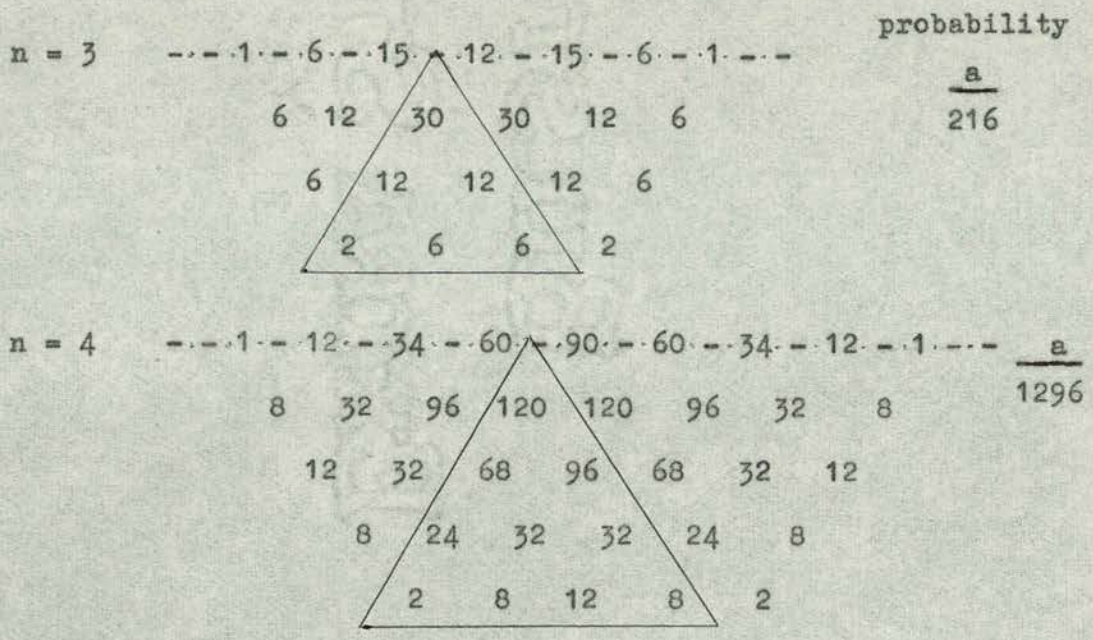

Comparing the figures within the triangles for both random walks, it will be seen that the probability of a particle being at a point in the second walk is twice the probability of it being at the corresponding point in the first walk.